Real-Time Drug Discovery: Characterization of the Myelin-associated Glycoprotein/Ligand Interaction

Inauguraldissertation zur Erlangung der Würde eines Doktors der Philosophie
vorgelegt der Philosophisch-Naturwissenschaftlichen Fakultät der Universität Basel

von

Daniel Strasser
aus Gottlieben, Schweiz

Referent: Prof. Dr. Beat Ernst
Korreferent: Dr. Walter Huber

Basel, 2008

Genehmigt von der Philosophisch-Naturwissenschaftlichen Fakultät auf Antrag von:

Prof. Dr. Beat Ernst, Institut für Molekulare Pharmazie, Universität Basel
Dr. Walter Huber, Pharmaceutical Research, F. Hoffmann-La Roche Ltd., Basel

Basel, den 26. Juni 2007

Prof. Dr. Hans-Peter Hauri
Dekan

Fortschritt ist noch keine Leistung –
es kommt auf die Richtung an.
(Jean Giono, 1895–1970)

ACKNOWLEDGEMENT

I would like to especially thank Prof. Dr. Beat Ernst, who gave me the opportunity to work in a challenging, international and multidisciplinary environment. I enjoyed developing and pursuing my own ideas, which were only possible in such a stimulating atmosphere.

I would like to express my gratitude to Dr. Walter Huber, who accepted to become co-referee of my thesis. His review as a surface plasmon resonance and pharmaceutical research expert was a great honor for me.

For the help on scientific and project-related questions, my gratefulness goes to many researchers and co-workers. Out of these I would like to specifically name Dr. Daniel Ricklin for introduction into the surface plasmon resonance technology and Steven Knecht for his support throughout the thesis.

Furthermore, I would like to accentuate Dr. Said Rabbani, Dr. Oliver Schwardt and Dr. Brian Cutting for assistance within their scientific area of expertise.

An important part of the thesis was possible due to the support of Prof. Dr. Kelm and Dr. Frank Dietz to whom I'm especially grateful.

Finally, I want to thank all members of the Institute for Molecular Pharmacy for the establishment of an encouraging working atmosphere.

SUMMARY

The challenge of drug discovery is the finding of potent molecules against relevant targets that exhibit no or, in comparison to the benefit, tolerable adverse effects on the health of patients. Costs for a new drug can be approximated to US$1 billion and the overall process can last up to 12 years. For such a long-term investment, early elimination of compounds with a poor outlook contributes significantly to cost and time efficiency. Hence, it is fundamental to understand and predict pharmacological as well as toxicological properties of potential drug candidates at early steps during development.

After implementation of high-throughput screening in the 1990s the amount of screened compounds per validated pharmacological target increased dramatically. But higher throughput did not automatically result in larger numbers of new molecular entities. A possible explanation is that current thinking and the methodologies used in drug discovery mainly focus on equilibrium aspects of drug binding (K_D, IC_{50},…). In contrast, many successful drugs act in a non-equilibrium way caused by very slow complex dissociation, covalent bond formation or based on biochemical target properties *e.g.* a two-state model prolonging the binary complex residence time. Whereas target properties are preset, the complex dissociation time based on ligand properties is modifiable and drawing increasing interest among drug researchers.

Despite the emerging use of techniques to determine interaction kinetics, no consistent correlation between structural properties of ligands and kinetics was published. This lack of knowledge complicates modification of lead structures towards favourable kinetic properties. Currently, measuring kinetics only provides the possibility to differentiate between e.g. slow and fast dissociating leads.

The topic of the thesis was to implement surface plasmon resonance (SPR) based biosensors to determine equilibrium binding constants, kinetic rate constants and enthalpic/entropic contributions of ligands binding to the myelin-associated glycoprotein (MAG). In an interdisciplinary environment with chemists, biologists,

NMR and molecular modelling specialists, interaction data was required to support the finding of new leads and ligands exhibiting advanced binding properties.

The SPR-based biosensor was validated on a model system for carbohydrate/protein interactions. A diagnostic anti-sialyl Lewis^a (sLe^a) antibody (GSLA-2) used in tumor diagnostic was investigated. High selectivity of GSLA-2 towards the sLe^a epitope was found and a close interaction with STD-NMR finally enabled an exact description of the binding epitope. Additionally, the influence on interactions caused by hydrophobic labels attached to a ligand was described.

For the myelin-associated glycoprotein, comparison of several immobilization approaches displayed specific differences important for the characterization of drug/target interactions. On all surfaces, reproducible results were obtained in good agreement with data from a hapten inhibition assay. Interesting though unusual was the occurrence of negative sensorgrams on surfaces with oriented immobilization (capturing and enzymatic). These were only observed for sialic acid derivatives, a certain class of MAG ligands. Larger molecules like the ganglioside GT_{1b} or second-site ligands displayed positive signals. Supporting experiments proved the negative signals to be specifically derived from ligand binding. The most reasonable explanation was a ligand-induced conformational change caused by sialic acid derivatives.

Whereas capturing led to a baseline drift, enzymatic immobilization improved the assay format significantly. Implementation of enzymatic immobilization provided a highly reliable technique. Practicability for very low protein concentrations (4 µg/ml) facilitated a direct immobilization of secreted proteins out of cell culture supernatant delivering a gentle procedure.

All sialic acid-based ligands displayed fast association and dissociation rate constants with a complex half-life in the range of 1-2 seconds. Therefore, future search for new leads exhibiting slower dissociation appears promising. Interactions of sialic acid derivatives with MAG were found to be mainly enthalpy driven. A decent correlation between structural modifications and their enthalpic/entropic contribution was found. Furthermore, it was possible to support and even expand data published on signal deviations related to drug-like molecules.

The non-availability of the crystal structure of the myelin-associated glycoprotein complicated rational ligand design but was successfully compensated by a combination of SPR-based biosensor data, STD-NMR and homology modeling. Even though a crystal structure would significantly simplify ligand design, a detailed picture of the interaction process including important kinetic data could be obtained.

ABBREVIATIONS

ADMET	Absorption, Distribution, Metabolism, Elimination, Toxicity
ASGP-R	Asialoglycoprotein receptor
AUC	Analytical ultracentrifugation
BIA	Biomolecular Interaction Analysis
BSA	Bovine serum albumin
cAMP	cyclic adenosine monophosphate
CD	Circular dichroism
CMD	Carboxymethyl dextran
DMSO	Dimethyl sulfoxide
CNS	Central nervous system
DRG	Dorsal root ganglia
DTT	Dithiothreitol
EC50	50% effective concentration
FDA	Food and drug administration (U.S.)
FPLC	Fast protein liquid chromatography
FTIR	Fourier transform infrared spectroscopy
GDP	Guanosine diphosphate
GTP	Guanosine triphosphate
hAGT	O^6-alkylguanine-DNA-alkyltransferase
HIV	Human immunodeficiency virus
HTS	High-throughput screening
IC_{50}	50% inhibition concentration
ITC	Isothermal titration calorimetry
K_A	Equilibrium association constant
K_D	Equilibrium dissociation constant
K_i	Inhibition constant
k_{on}	Association rate constant
k_{off}	Dissociation rate constant
Lem	Lemieux spacer

MAG	Myelin-associated glycoprotein
MDI	Myelin-derived inhibitor
MW	Molecular weight
NC	Nitrocellulose
NCE	New chemical entity
NgR	Nogo receptor
NME	New molecular entity
NMR	Nuclear magnetic resonance
Omgp	Oligodendrocyte myelin glycoprotein
P20	Polysorbate-20 (Tween-20)
PAGE	Polyacrlyamide gel electrophoresis
PBS	Phosphate buffered saline
PCR	Polymerase chain reaction
PND	Post-natal day
PNS	Peripheral nervous system
PTM	Post-translational modifications
ROCK	Rho Kinase
RT	Room temperature
RU	Resonance units
R_{eq}	Equilibrium response
R_{max}	Maximum response
rIP	Relative inhibitory potency
SAR	Structure-activity relationship
SCI	Spinal cord injury
SDS	Sodium dodecylsulfate
Siglec	Sialic acid binding Ig-like lectin
SKR	Structure-kinetics relationship
sLe^a	Sialyl Lewis^a
sLe^x	Sialyl Lewis^x
SNAP	hAGT mutant
SPR	Surface plasmon resonance

STD	Saturation transfer difference
TIR	Total internal reflection
TNF	Tumor-necrosis factor

1 INTRODUCTION

1.1 Drug discovery

Drug discovery is a challenging and extensive process. In the development of a successful drug, specialists from numerous areas (pharmacology, biology, chemistry, medicine, computational sciences, system engineering, marketing,...) are involved. In a multidisciplinary process, they all have to focus on one goal, a potent and safe drug that finally creates a return on investment. Pharmaceutical companies worldwide spend $ 50 billion per year on the drug discovery process.[1] The entire development for one final drug costs approximately $ 800 million. Lately, especially safety issues requested by the regulatory authorities have substantially grown.[2] If successful, the drug turns out to be a blockbuster, representing a yearly turnover of $ 1 billion.
Considering the human body with all of its still unknown biochemical pathways, construction of a drug that fulfils today's safety guidelines provides an explanation for such high cost. Furthermore, pharmaceutical companies try to avoid unexpected side effects in the post-marketing phase to prevent huge compensation payments and a loss of image by voluntary safety efforts. Due to the relation "the safer, the costly" expenditures on drugs continue to rise to estimated worldwide drug sales of US $570 billion in 2007.[3]

Traditional drug discovery can be structured in 5 major steps (*figure 1*).

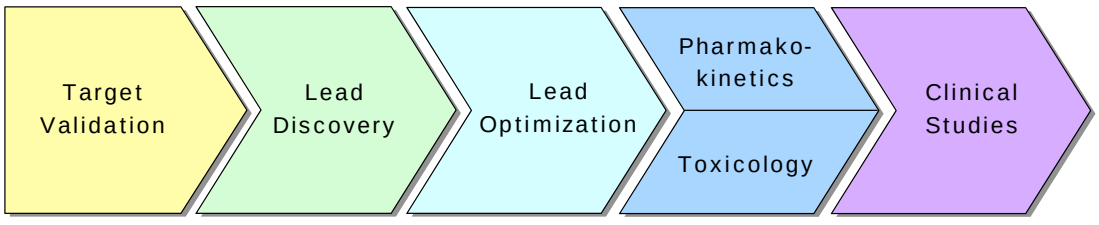

Figure 1. The drug discovery process on a progression scale from early target finding to clinical trials in men. The process is rather circular then linear where failure leads to a return to an earlier step.

First a target is identified and validated. Targets are considered defined mediators of biochemical processes that influence pathophysiological functions like proteins, nucleic acids, lipids or carbohydrates.

Key questions for target validation include:

- Is there a medical need?
- Is there a market worth the investment?
- Is the target fundamental for the pathological outcome?
- Is the target drugable? Druggability can be described as the existance of protein folds that favour interactions with drug-like chemical compounds.[4,5]
- Who are the competitors and how far are their projects developed?

After target validation, small molecules are explored. Usually, high-throughput methods are applied to screen huge libraries.[6] In a subsequent optimization process medicinal chemists modulate leads towards higher binding affinity and drug-like properties.[7-9] Along with affinity, selectivity for the target is a major task. To avoid unwanted drug actions, the compound should only affect the target at clinically relevant concentrations. Finally, after pharmacokinetic and toxicological studies, clinical trials are conducted in men. These steps are not defined sharply and the process between target validation and clinical trials is rather iterative than linear.
As indicated, reliable information on *in vivo* efficacy and safety are of huge interest already at early stages. Therefore, today's lead selection criteria should include safety as much as potency and efficacy. In order to prevent failure in later steps *e.g.* clinical trials an accurate prediction of these parameters is needed.
When planning a new drug discovery project, success is most likely with a G-protein-coupled receptor (GPCR), a nuclear receptor or an ion channel as a target. More than 50% of all FDA approved drugs act on these classes even though there are many other protein families (*figure 2*).[1]

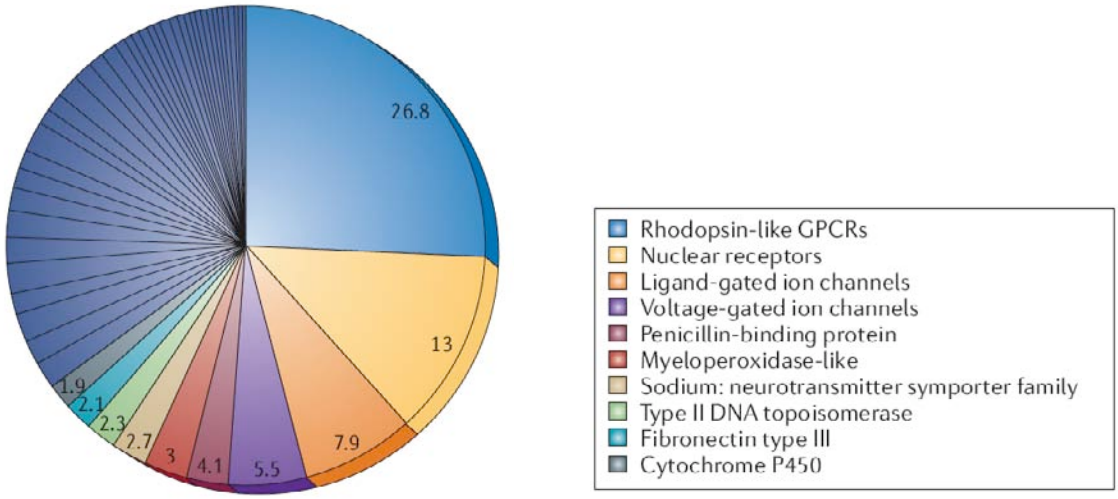

Figure 2. Analysis of the gene-family distribution of current drugs per drug target.[1]

But why is that? One interesting hypothesis focuses on current methods of interaction analysis. The major statement is that the binary ligand/target residence time influences drug success significantly. A detailed explanation is provided in *1.3.1*.

Summing up, the major challenge of drug discovery is to discover potent drugs against relevant targets that exhibit no or, in comparison to the benefit, tolerable adverse effects on the health of patients. Early safety and efficacy predictions for drug candidates are a major concern of pharmaceutical companies.

1.2 Myelin-associated glycoprotein (MAG) as drug target

1.2.1 Signal transmission by neurons

Neurons are a major class of cells in the nervous system. Their main role is to process and transmit information. Morphologically, a prototypical neuron is composed of a cell body, a dendritic tree and an axon *(figure 3)*. In the classical view of the neuron, the cell body and dendritic tree receive inputs from other neurons, and the axon transmits output signals.

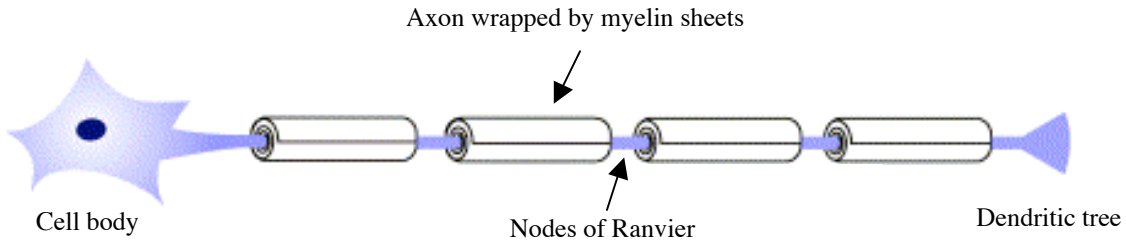

Figure 3. Shape of a neuron containing myelin sheets wrapped around the axon allowing rapid signal transduction

In the central nervous system (CNS) and peripheral nervous system (PNS), many axons are wrapped concentrically and tightly by a multilamellar sheath of myelin (*figure 3 and 4*), which is produced by oligodendrocytes in the CNS and Schwann cell in the PNS.[10] The myelin behaves as an insulator and is essential for rapid nerve conduction, as evidenced by debilitating demyelinating diseases in the CNS and PNS such as multiple sclerosis and the Guillain Barré syndrome.[11] The myelin sheath is interrupted regularly by the nodes of Ranvier that are small, unmyelinated regions of axons (*figure 4*).

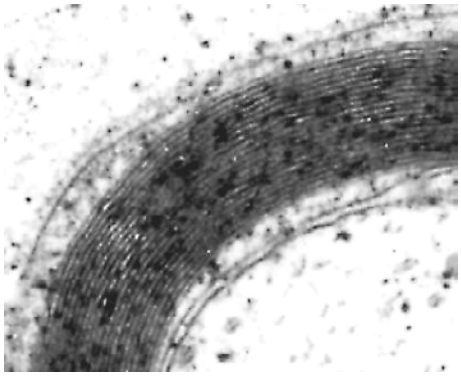

Figure 4. Axon wrapped with myelin sheets.

In the axonal membrane at these nodes, voltage-gated sodium channels are highly concentrated, thus allowing for the saltatory propagation of the action potential down the length of myelinated axons (*figure 5-A*).[12] The rapid impulse conduction that results from the focal position of sodium channels along the axon has facilitated the evolution of complex nervous system.

1.2.2 Failure of axonal regeneration in adult mammalian CNS

In contrast to the PNS and the embryonic CNS, regeneration of the adult brain and spinal cord after lesions is extremely limited. Damage to the CNS of higher vertebrates, including humans, often results in devastating and persistent functional deficits. Therefore, patients with spinal cord injuries (SCI) or neurodegenerative diseases like Alzheimer and multiple sclerosis suffer permanently from the loss in, *e.g.* movement, body functions, sensation, and thinking. In the case of SCI, only a controversial option of pharmacotherapeutic treatment is available and the need for effective drugs is obvious.[13] According to the American Association of Neurological Surgeons, approximately 34,000 new spinal cord injuries in the major pharmaceutical markets occur each year. In the U.S., related costs are estimated to $14.5 billion per year.[14]

Although injured axons can sprout spontaneously, this regeneration attempt is transitory and no significant re-growth occurs over long distances.[15] However, this failure is not due to an intrinsic or irreversible lack of the ability of the CNS neurons

to regenerate, but rather to the non-permissive nature of the CNS environment.[16] This was demonstrated by studies where many types of CNS neurons extended long axons either by grafting pieces of peripheral nerves onto a lesion site,[17,18] or by isolating neurons and growing them in culture.[19] Furthermore, neurons such as dorsal root ganglia (DRG) possess axons in both the CNS and PNS, but can only regenerate peripheral damage. Unlike the Schwann cells in the PNS, oligodendrocytes continue to express myelin proteins, including inhibitors, after injury and they do not engulf myelin debris. Such an inhibitory environment is considered being a summary of several factors. A lack of neurotrophic factors, a glial scar and inhibitory proteins within myelin debris were described to play a significant role.

The glial scar appears as a physical barrier against axon outgrowth that is formed by reactive astrocytes and extracellular matrix molecules such as chondroitine sulphate proteoglycans (*figure 5-C*).[20] In addition, these scar-associated proteoglycans were revealed to be potent inhibitors of axon growth *in vitro* themselves.[21] The glial scar was found to mature within weeks depending on location but can be regarded as the final step in prohibiting nerve regeneration.[22-24] Nevertheless, directly after a lesion, lack of neurotrophic factors and presence of myelin-derived inhibitors (MDIs) seem to be accountable for the major impediment of neurite outgrowth (*figure 5-B*). Therefore, inhibition of MDIs and/or administration of neurotrophic factors are assumed to induce neurite outgrowth *in vivo* before maturation of the glial scar. Combination therapies for successful treatment of SCI and neurodegenerative diseases appear promising.

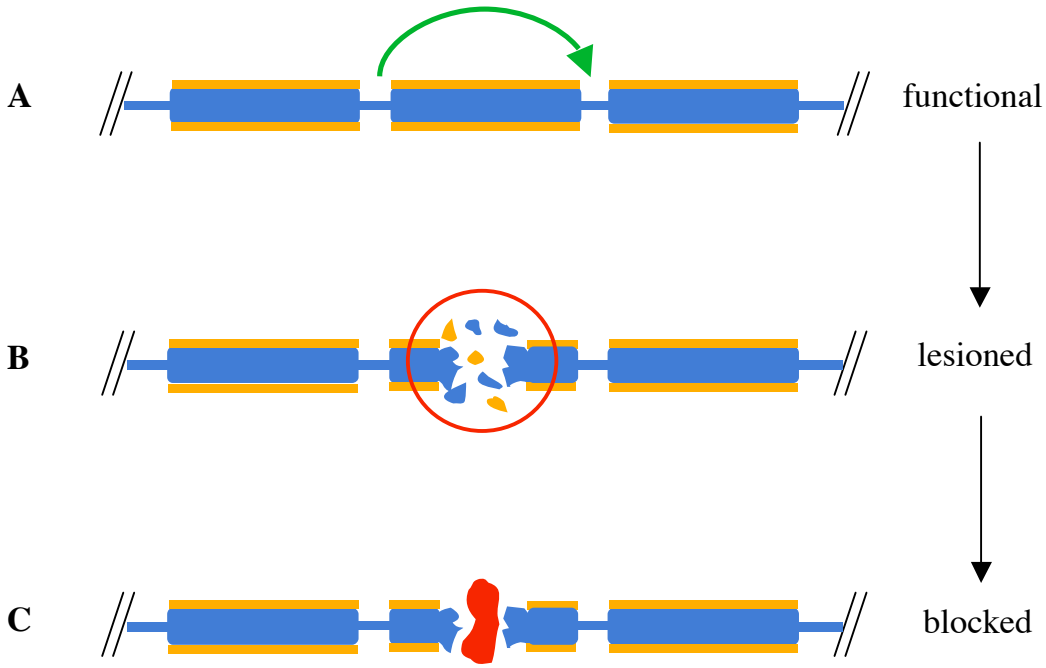

Figure 5. Lesion of a functional neuron and its subsequent inhibition states that are responsible for neurite outgrowth inhibition: A functional neuron transmits the signal via its nodes of Ranvier (A). After lesion, an inhibitory environment at the site of the rupture limits neurite outgrowth (B). Finally, reactive astrocytes create a physical barrier that prohibits any future outgrowth (C).

1.2.3 Myelin derived inhibitors (MDI)

The three major MDIs were described to be the myelin-associated glycoprotein (MAG), the oligodendrocyte myelin glycoprotein (Omgp) and Nogo (*table 1*).

Table 1. Myelin derived inhibitors (MDI) present at the site of lesion.

MDI	Source	Axonal receptor
NogoA	Residual myelin	NgR family
Omgp	Residual myelin	NgR family
MAG	Residual myelin	NgR family Gangliosides

Nogo was the first MDI reported in literature. It was identified as an antigen to an antibody (IN-1) that was isolated due to its ability to neutralize myelin based neurite outgrowth inhibition *in vivo*.[15,25-27] Three isoforms of Nogo (Nogo-A, -B and -C) are generated by alternative splicing and promoter usage. Nogo consists of two inhibitory domains: a unique amino-terminal region (amino-Nogo) on Nogo-A and a 66 amino acid loop (Nogo-66) that is common to all three variants.[28]

The second inhibitor, *oligodendrocyte myelin glycoprotein* (Omgp), is a glycosyl phosphatidylinositol GPI-anchored protein that contains a leucine-rich repeat (LRR) domain.[29] Omgp is found in the CNS as well as in the PNS.[30]

The third MDI is the *myelin-associated glycoprotein* (MAG) that is located in both CNS and PNS like Omgp.

1.2.4 Structure and function of MAG

MAG belongs to the family of the I-type lectins. These are carbohydrate-binding proteins within the immunoglobulin superfamily that are determined by their IgSF-like amino acid sequence.[31,32] The selective binding of sialylated carbohydrate structures by MAG further places it into the Siglec (sialic acid binding Ig-like lectin) subfamily.[33] A few other IgSF member lectins have been identified that recognize non-sialylated carbohydrate structures like PECAM, ICAM-1, N-CAM and CD48.

Within the group of Siglecs, several members have been depicted and numbered sequentially (*table 2*).[34] All Siglecs share common features like an *N*-terminal variable type domain (v-type) and one or more constant type domains (c-type) that are located extracellularly and a transmembrane domain. Most Siglecs function as signal transduction molecules and occur predominately within the immune system.

Table 2. Human siglecs with its alternative names and the tissue distribution.[34]

Siglec	Alternative name	Tissue/Cell type distribution
Siglec-1	Sialoadhesin	Macrophages in spleen, lymph nodes, and bone marrow
Siglec-2	CD22	B cells
Siglec-3	CD33	Myeloid cell lineage
Siglec-4	MAG	Peripheral and central nerve system
Siglec-5	CD33-related	Granulocytes and monocytes
Siglec-6	CD33-related	B cells
Siglec-7	CD33-related	NK cells and monocytes
Siglec-8	CD33-related	Eosinophils
Siglec-9	CD33-related	Granulocytes and monocytes
Siglec-10	CD33-related	B cells, eosinophiles and monocytes
Siglec-11	CD33-related	Macrophages

The cluster of differentiation (CD) is used for the identification of cell surface molecules on leukocytes. CD33-related Siglecs share two conserved immunoreceptor tyrosine-based inhibitory motif.

MAG is a 100 kDa integral membrane protein comprising five extracellular Ig-like domains with 8 or 9 potential glycosylation sites.[35,36] The carbohydrate moiety represents approximately 30% of the entire molecular weight of MAG.[37] The first *N*-terminal Ig domain is of a variable (v)-type and domains 2-5 are of homologous constant (c)-type (*figure 6*). MAG represents 1% and 0.1% of the total myelin protein in the CNS and PNS, respectively, and it is mostly located in the inner loop in the CNS.[38,39] As the result of alternative splicing, two isoforms of MAG, S- and L-MAG, are produced, differing only by their cytoplasmatic domain.[40]

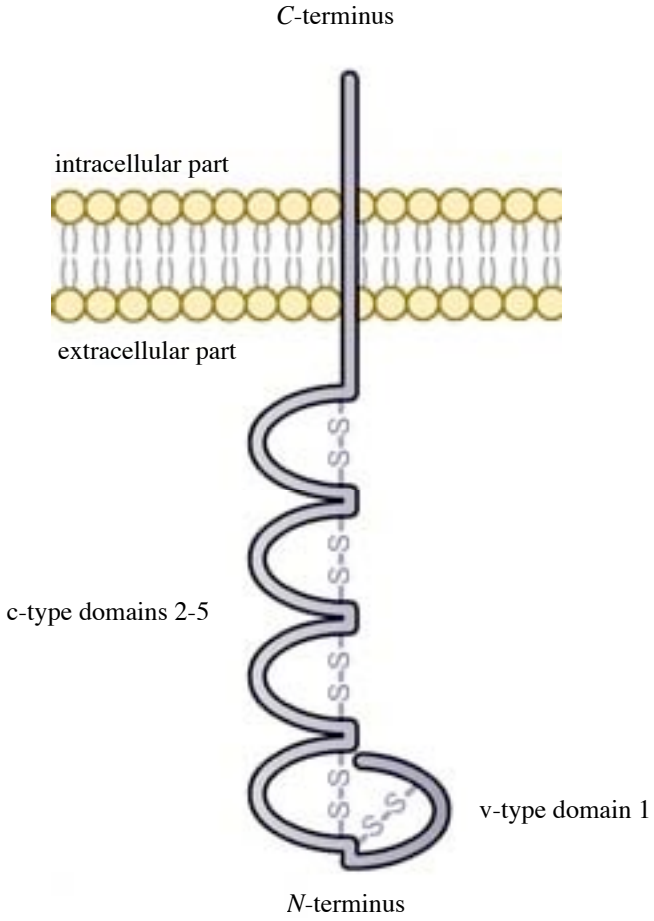

Figure 6. Structure of MAG with the extracellular *N*-terminal v-type domain and the subsequent four c-type domains. The first two *N*-terminal domains fold towards each other building an interdomain disulfide bridge.

Recent studies have shed light on the function and structure of the cytoplasmatic domains of MAG (MAGct). The S-MAGct has a random coil structure in solution.[41] It binds zinc, which induces a change in the surface hydrophobicity of the protein,[42] but apparently, no folding occurs upon Zn binding.[41] It is likely that the main function of the S-MAGct is related to interactions with the Schwann cell microtubular cytoskeleton, and that an unfolded structure is essential for these interactions. Secondary structure predictions and circular dichroism measurements of synthetic peptides indicate that the L-MAGct, on the other hand, probably folds into a structure containing both helices and sheets.[43] Evidence also exists on a tendency of L-MAGct to homodimerise, which may be important in myelin-related signal transduction

events. MAG is exclusively expressed by myelinating glial cells specifically oligodendrocytes in the CNS and Schwann cells in the PNS.[44]

One interesting feature of MAG is its bi-functionality that is similar to other axon guidance molecules.[45,46] When cultured on MAG-expressing DRG neurons older than post-natal day 4 (PND4), neurites extended shorter than when cultured on control cells. In contrast, MAG promoted neurite outgrowth from DRG neurons from animals younger than PND4. The response switch, which is also observed in retinal ganglia and Raphe nucleus neurons, is concomitant with a development decrease in the endogenous neuronal cAMP levels.[47] It was shown, that artificially increased cAMP levels in older neurons before spinal cut can alter their growth-state and induce axonal growth even in the presence of MDIs. Both cAMP analogous and priming with neurotropic factors to increase cAMP levels promoted axonal regeneration after lesion.[48,49]

For MAG, a subsequent signalling cascade needed to be involved to transfer the outgrowth inhibition signal into the neuron. In search for such a cascade, it was found that neurons from a $p75^{NTR}$-knockout mouse displayed no inhibition of neurite outgrowth even though a direct interaction between MAG and $p75^{NTR}$ was absent.[50] The $p75^{NTR}$ is a member of the tumor-necrosis factor (TNF) receptor family involved in apoptosis. In additional experiments, $p75^{NTR}$ was precipitated by all three MDIs (MAG, Nogo-66 and Omgp) and the Nogo receptor (NgR) was present in the precipitate of each.[51,52] It was concluded that all MDIs interact with the glycosyl-phosphatidylinositol-anchored (GPI-anchored) NgR to elicit inhibition of neurite outgrowth. Because NgR contains no transmembrane domain, signal-transduction is elicited via the co-receptor $p75^{NTR}$. Additionally, stimulation of the Rho-ROCK pathway by such formed trimeric receptor complexes was described.[50,52]

Even before these receptor complexes were known, members of the Rho family of small GTPas proteins had been implicated in myelin's inhibitory effects.[53] RhoGTPases, a subfamily of the Ras superfamily of GTPases, function as molecular devices that control multiple signalling pathways in a very precise and coordinated way by switching between a biochemically inactive (GDP-bound) and a active (GTP-

bound) state.[54,55] In the active, GTP-bound state, RhoGTPases activate numerous downstream effectors like the Rho Kinase (ROCK).

ROCK is a serine/threonine (Ser/Thr) protein kinase that was identified about ten years ago as a RhoGTP-binding protein.[56,57] A variety of evidence indicated that injury to brain and spinal cord results in a strongly activated RhoA-ROCK pathway.[58-61] Inhibition of ROCK by three different molecules (fasudil, Y-27632 and $p21^{CIP1/WAF1}$) enhanced nerve-fibre growth in mouse and rat spinal-cord injury models.[62-66].

1.2.5 Sialic acid specificity of MAG

MAG was depicted to specifically bind to sialo-glycoproteins and sialo-glycolipids (gangliosides), preferably when the sialic acid residue is attached by a α(2,3)-O linkage.[33] Nerve cell surface gangliosides like G_{D1a} and G_{T1b} were identified as such specific ligands (*figure 7*).[67-70]

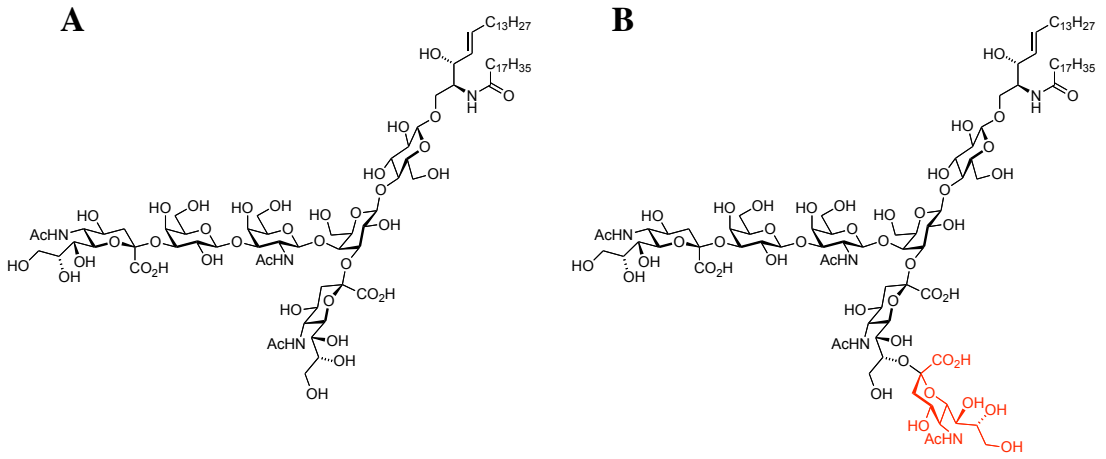

Figure 7: Molecular structure of the major two brain gangliosides G_{D1a} (A) and G_{T1b} (B).

Interestingly, MAG-mediated neurite outgrowth inhibition was reversed by blocking ganglioside biosynthesis.[67] In addition, nerve cells from mice lacking complex gangliosides weren't inhibited by MAG. This was strong evidence for an additional inhibitory cascade based on such a ganglioside/MAG interaction.

The sialic acid binding site on MAG was mapped to Arg118 by mutation studies.[71] In a soluble form of mutated MAG, sialic acid binding capacity as well as its ability to inhibit neurite outgrowth was completely lost (*figure 8-B*). Hence, the ganglioside binding site must be located in the *N*-teminal (Ig)-like v-domain of MAG.

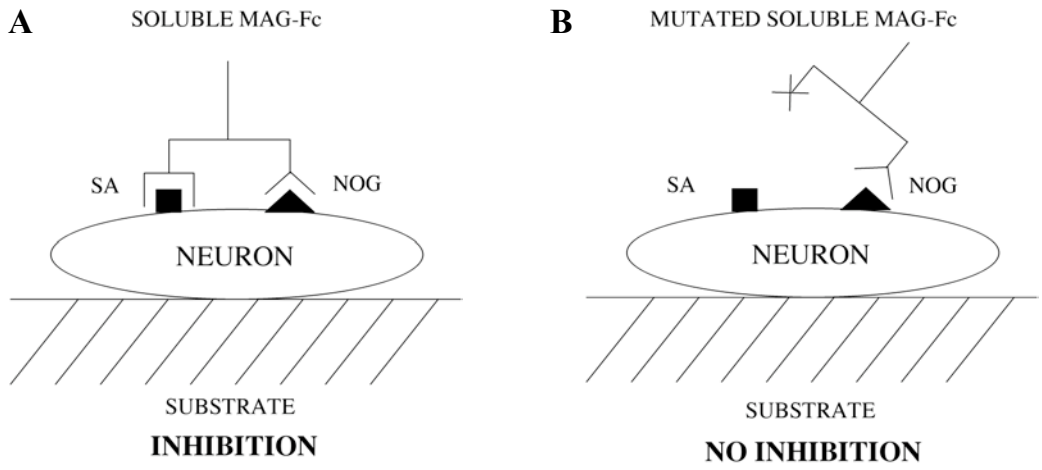

Figure 8. Neurons were grown on a neurite promoting substrate and soluble wild-type or mutated Fc-MAG was added. Soluble Fc-MAG(d1-3) inhibited outgrowth by 50% (A). Mutation of Arg118 to alanine or aspartic acid (B) abolished inhibition completely.[71]

Interestingly, Arg118-mutated MAG presented to neurons through expression on CHO cells showed no loss of inhibitory potential (*figure 9-B*). These contradictory results where explained by compensation of lost sialic acid binding activity by other cell adhesion molecules (CAMs) on the cell surface.[16]

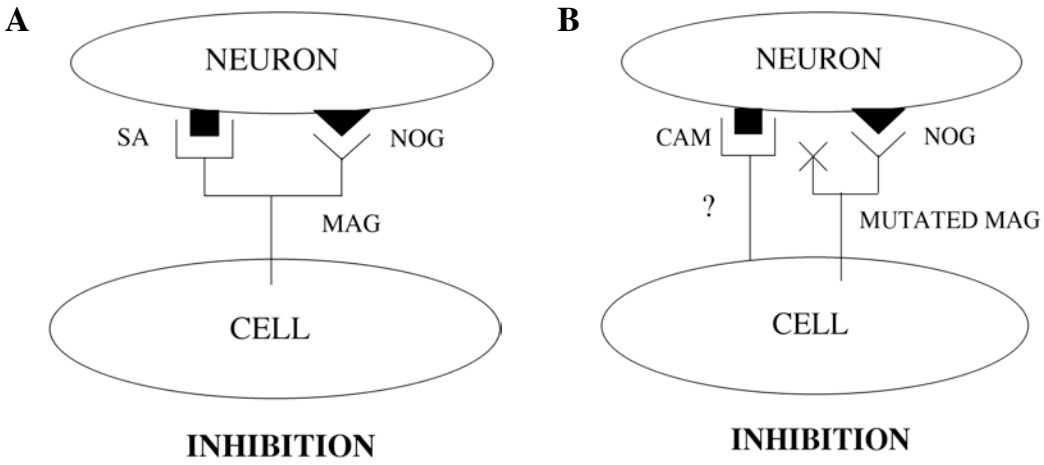

Figure 9: MAG was expressed on CHO cells as wild-type or mutated (R118A, R118D). Neurite outgrowth was inhibited though the sialic acid binding site was absent in the mutated MAG.[71]

Surprisingly, other experiments showed that clustering of gangliosides by antibodies led to activation of Rho and subsequent outgrowth inhibition even without

involvement of MAG or NgR.[50,67,72,73] Probably this was due to a direct interaction of G_{T1b} and $p75^{NTR}$. Binding to gangliosides like G_{D1a} and G_{T1b} is likely to potentate and augment the inhibitory effects of MAG by inducing clustering of the signalling molecules.[16] It is possible that gangliosides clusters act as MAG receptors where direct MAG/ganglioside interaction finally activates the Rho-ROCK cascade.[74] In general, such clusters of carbohydrate epitopes were shown to mediate cell adhesion and/or signal transduction and are referred to as glycosynapses.[75]

Moreover, the found neurite outgrowth inhibition of Arg118-mutated MAG led to the conclusion that an additional inhibition site must be present. This observation was in agreement with the discovered NgR inhibition cascade.[76,77]

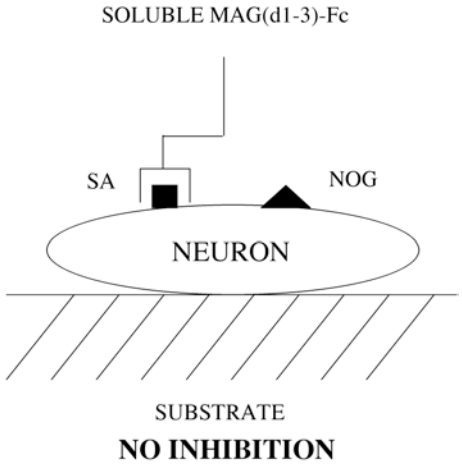

Figure 10. Absence of the extracellular domains 4 and 5 resulted in complete elimination of the inhibitory potency of MAG. Therefore, the sialic acid independent inhibition site must be located in these domains.[71]

Due to the fact that soluble truncated MAG (*N*-terminal domains 1-3) bound to neurons in a sialic acid–dependent manner, but only full-length MAG inhibited neurite outgrowth, the NgR binding site on MAG must be located on the 4th and 5th Ig-like domain (*figure 10*).

The importance of gangliosides for neurite outgrowth inhibition was further underlined by *in vivo* experiments. Treatment with a sialidase enhanced spinal axon outgrowth into implanted peripheral nerve grafts in a rat model of brachial plexus avulsion.[78] Besides, it was noticed that cleavage of Omgp and Nogo receptors did not result in beneficial regeneration. Outgrowth inhibition was therefore stated to be

primarily MAG mediated. Gangliosides were also shown to contribute to the long-term axon-myelin stability.[79] An exact picture of the function of MAG and the physiological importance of ganglioside binding is still missing. High affinity inhibitors for the sialic acid binding site are required to clarify the function and pharmacological relevance of MAG.

The entire inhibition cascade of MDIs including both the NgR and the ganglioside cascade is summarized in *figure 11*.

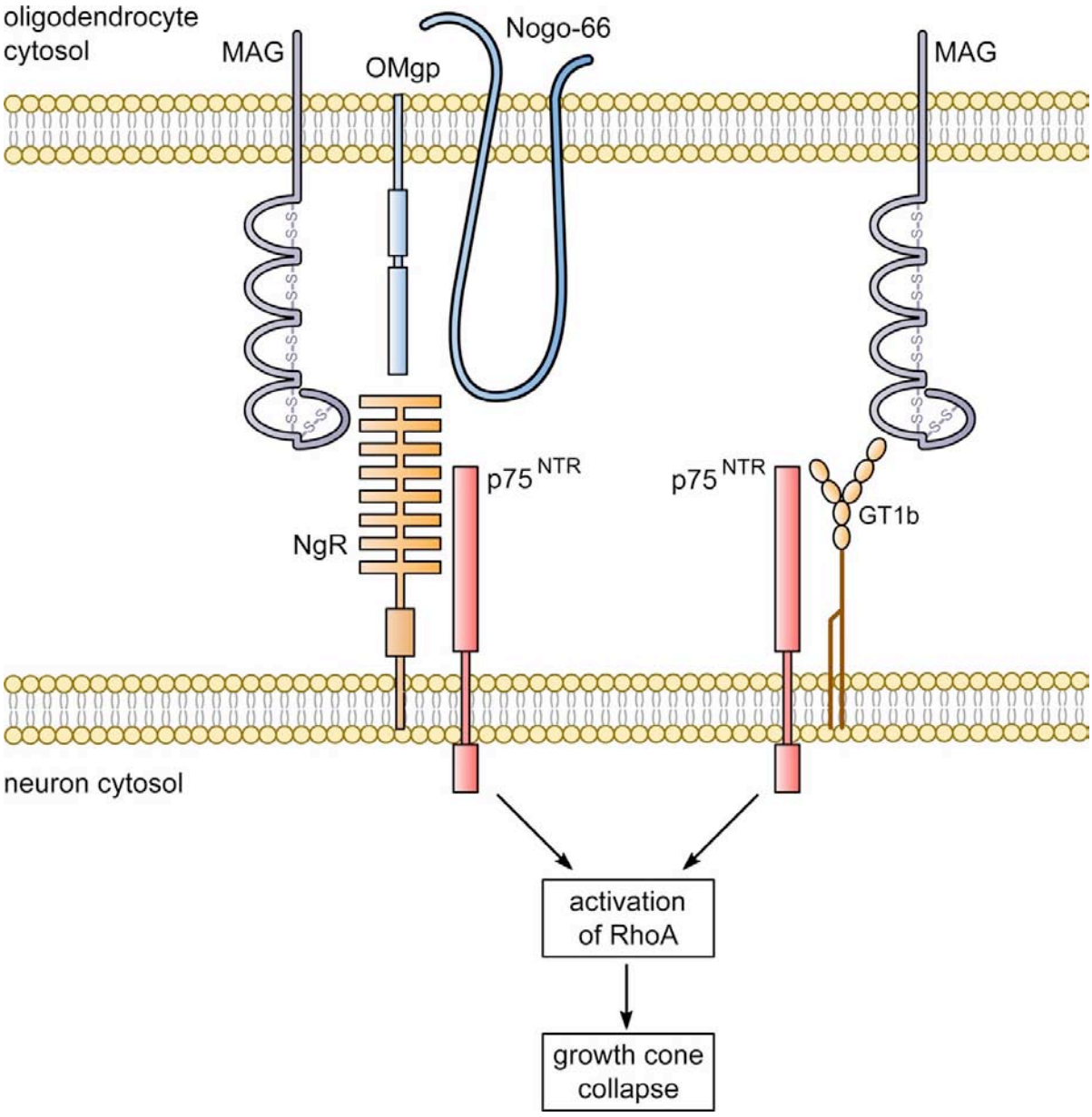

Figure 11 (by courtesy of A. Vögtli): Simplified cascade of neurite outgrowth inhibition caused by myelin-derived inhibitors. Activation of two different pathways joins up into a final growth cone collapse.

The specificity of MAG towards different gangliosides was analyzed at an early stage.[70,80] Adhesion of MAG transfected COS cells to wells coated with different gangliosides were studied. In these experiments it was found that the Chol-1 ganglioside $G_{Q1b\alpha}$ exhibited the highest affinity followed by the two major brain gangliosides G_{D1a} and G_{T1b} (*figure 12*). Chol-1 gangliosides are quantitatively minor structures that are expressed exclusively on cholinergic neurons.[81,82] The functional significance of $G_{Q1b\alpha}$ for MAG is still unclear.

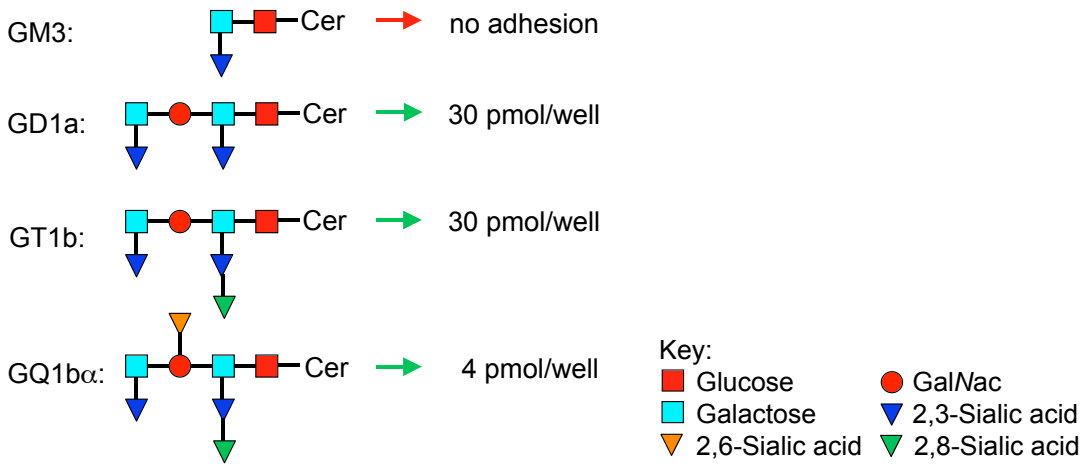

Figure 12. Ganglioside binding specificity of MAG. High affinity is observed for the major brain gangliosides G_{T1b} and G_{D1a}.

The higher affinity of $G_{Q1b\alpha}$ compared to G_{T1b} or G_{D1a} must be derived from the α(2,6)-O-linked sialic acid moiety. The structure activity relationship (SAR) profile was further refined by numerous synthetic contributions dealing with neuraminic acid derivatives and ganglioside fragments.[68,83-85] These results led to the identification of Neu5Ac-α(2→3)Gal-β(1→3)[Neu5Ac-α(2→6)]Gal*N*Ac as the major carbohydrate binding epitope (*figure 13-A*). Moreover, the terminal α(2,3)-linked sialic acid was described to contribute significantly to binding to MAG. Several important functional groups were identified (*figure 13-B*) *e.g.* the carboxylic group that was known to interact with Arg118 on MAG.

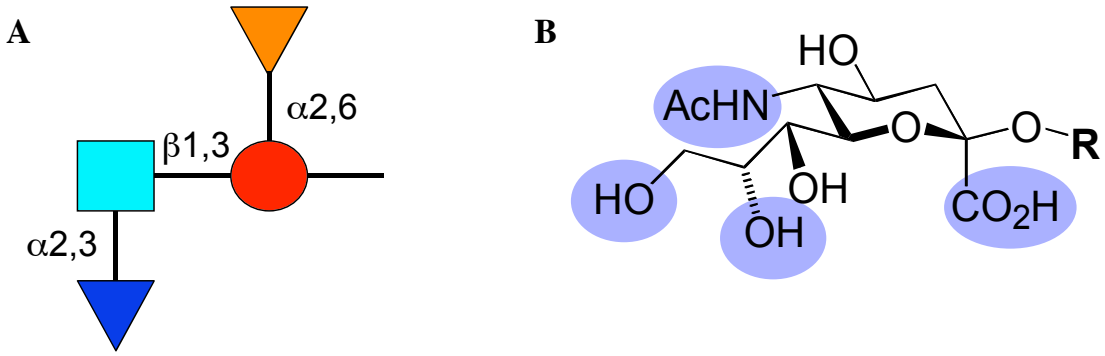

Figure 13. Carbohydrate binding epitope of MAG (A) and the α(2,3)-linked sialic acid with its contributing functional groups highlighted in purple (B).

In *figure 14* the α(2,3)-linked sialic acid of G_{T1b} that was found to contribute significantly to binding is highlighted in red.

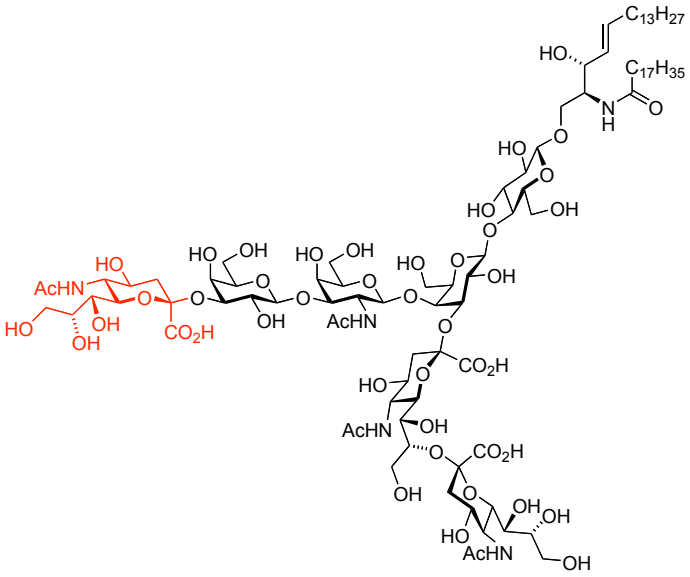

Figure 14: G_{T1b} with its terminal α(2,3)-linked sialic acid highlighted in red. This sialic acid moiety is mainly responsible for MAG binding.

On the carbohydrate epitope, STD-NMR experiments revealed a number of hydrophobic contacts (*figure 15*). A strong interaction was found for the methyl moiety on *N*-Ac of the α(2,3)-linked sialic acid.

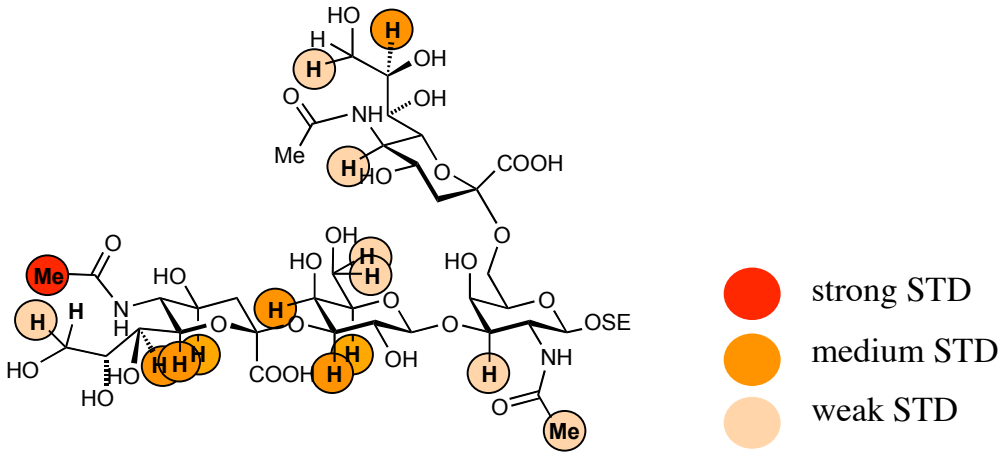

Figure 15. STD-NMR signals obtained for the carbohydrate binding epitope of MAG (unpublished results).

Structure-activity relationship (SAR) studies were aggravated by the fact that no crystal structure of MAG was available. For analysis of the binding mode a homology model based on sialoadhesin (Siglec-1) co-crystallized with methyl 9-benzamido-9-deoxy-Neu5Ac was available (unpublished results).

Recently, ligands based on the described carbohydrate epitope were tested for their ability to reverse MAG mediated inhibition of axon outgrowth from rat cerebellar granule neurons *in vitro*. Interestingly, these ligands enhanced axon regeneration in proportion to their MAG binding affinities.[86] Axon outgrowth was significantly enhanced after addition of high affinity ligands (*figure 16-B*) compared to untreated neurons (*figure 16-A*). The highest inhibition potency was found for the binding epitope Neu5Ac-α(2,3)Gal-β(1,3)[Neu5Ac-α(2,6)]Gal*N*Ac (*table 3*).

Table 3. Correlation of axon outgrowth with MAG binding affinity.[86]

	Glycan	MAG binding[a]	Axon outgrowth[b]
1	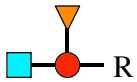	+	-
2	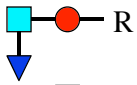	++	+
3	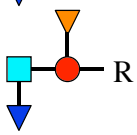	+++	++

R=OThr(*N*Ac,OCH_3)
[a]inhibition of solid phase binding
[b]inhibition of axon outgrowth inhibition

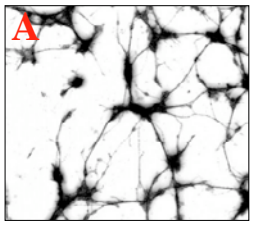

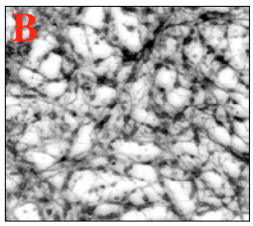

Figure 16. Axon outgrowth monitored for neurons without addition of MAG ligands (A) and with 10 µM ligand 3 present (B).

These findings encourage further exploration of carbohydrate mimics as potential MAG inhibitors. Especially the α(2,3)-linked sialic acid seemed to be optimal as lead structure due to its low molecular weight (262.47 g/mol) and the structure activity relationship (SAR) revealed. Unfortunately, no *in vivo* results for such mimetics were available.

1.2.6 Overview of neurite outgrowth inhibition targets

After revealing parts of the inhibition cascade, the range of possible therapeutic strategies for the treatment of spinal cord injury and related diseases broadened significantly (*table 4*). On several targets promising progresses were achieved whereas others have drawn little interest.

A first success story is Cethrin, a rho GTPase antagonist invented by BioAxone Therapeutic. In December 2005, Cethrin was approved orphan drug status by the FDA for treatment of acute thoracic and cervical spinal cord injuries.

Table 4. Overview of potential targets for the development of a spinal cord injury treatment.

Target	Strategy	Company (compound)	Ref
MAG	Block interaction with NgR	GlaxoSmithKline (mAB)	[87,88]
Nogo	Block interaction with NgR	Novartis (mAB IN-1)	[15,89,90]
Omgp	Block interaction with NgR	-	-
NgR	Block interaction with MDIs	Biogen	[91]
Rho	Inhibit GTPase activity	BioAxone (Cethrin)	FDA approval
ROCK	Inhibit Kinase activity	Asahi Kasei (Fasudil)	[62-65,66]
cAMP level	Block Phosphodiesterase 4	Meiji Seika Kaisha (Rolipram)	see below
cAMP level	cAMP analogues		see below
cAMP level	adenylyl cyclase activator	forskolin	see below

As described, elevation of cAMP levels was shown to overcome inhibition of MAG and myelin. An increase is either achieved by injection of cAMP analogues, adenylyl cyclase activator (forskolin), phosphodiesterase inhibitors or neurotrophines.[48,49]

Rolipram, a phosphodiesterase 4 (PDE4) inhibitor was shown to surmount inhibition by MAG and myelin in culture. Additionally, neurons from animals treated with rolipram were nott inhibited for various periods by MAG or myelin, indicating a post-lesion effect. Importantly, when rolipram was delivered 2 weeks after a hemisection lesion, along with embryonic spinal cord tissue implanted at the injury site at the time of lesion, there was not only a significant increase in axon growth and in functional recovery, but also an attenuation of the glial scar.

Rolipram was developed as an antidepressant and was used in clinical trials but because of side effects (emesis, nausea) in some patients, the trials were stopped. It has also been shown to exhibit immunosuppressive and anti-inflammatory effects. However, treatment of depression requires long-term administration. For spinal cord injuries, rolipram may only need to be delivered for a limited period of time, during which time side effects would be tolerable. A further attraction of rolipram for treating spinal cord injury is that it readily crosses the blood-brain barrier. Therefore, subcutaneous delivery would avoid intervention at the site of injury.[92]

1.2.7 Hapten inhibition assay for ligand screening

The affinity of MAG ligands was predominately determined in a hapten inhibition assay.[68] A microtiter plate, pre-coated with sialic acid (*figure 18-A*), is incubated with a ligand (*figure 18-B*). In general, an Fc-MAG(d1-3) construct (*figure 17-B*) containing the three *N*-terminal extracellular domains of MAG was employed. The crystallizable fragment (Fc region) is part of an antibody composed of two heavy chains that each contributes two to three constant domains, depending on the class of the antibody (*figure 17-A*).[93]

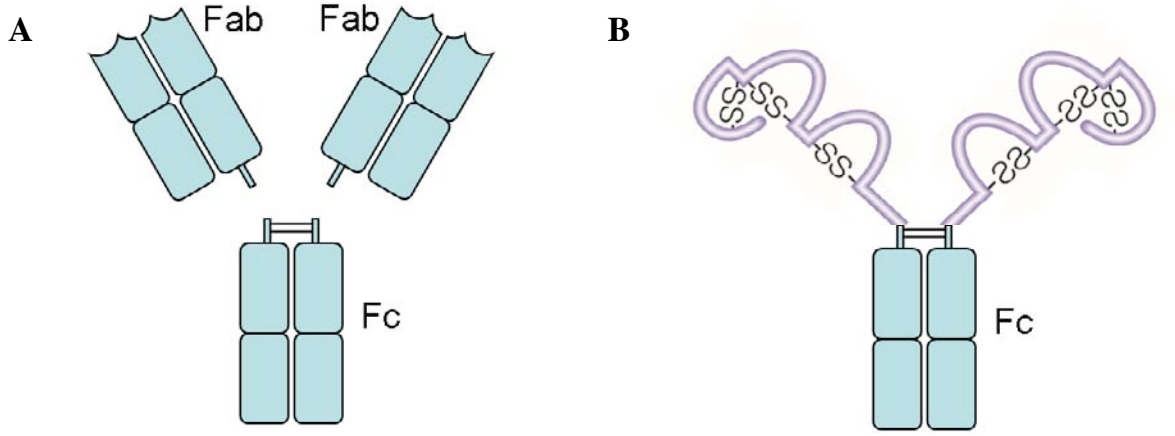

Figure 17. The Fc and Fab fragments of antibodies (A). The Fc-MAG(d1-3) construct is composed by the Fc fragment and two MAG(d1-3) domains (B).

Fc-MAG(d1-3) (*figure 17-B*) and a polyclonal goat anti-human IgG antibody coupled to an alkaline phosphatase are added to the wells. The Fc-MAG(d1-3) and the polyclonal antibody form a complex as indicated in *figure 18-C*. Binding of the ligand to MAG will inhibit binding of Fc-MAG(d1-3) to the sialic acids on the plate competitively (*figure 18-D*). Ligand affinity will therefore be correlated with the amount of Fc-MAG(d1-3) bound to the plate. Afterwards, unbound Fc-MAG(d1-3) is removed by washing (*figure 18-E*). The amount of Fc-MAG(d1-3) is then detected by addition of substrate for the alkaline phosphatase to the wells.

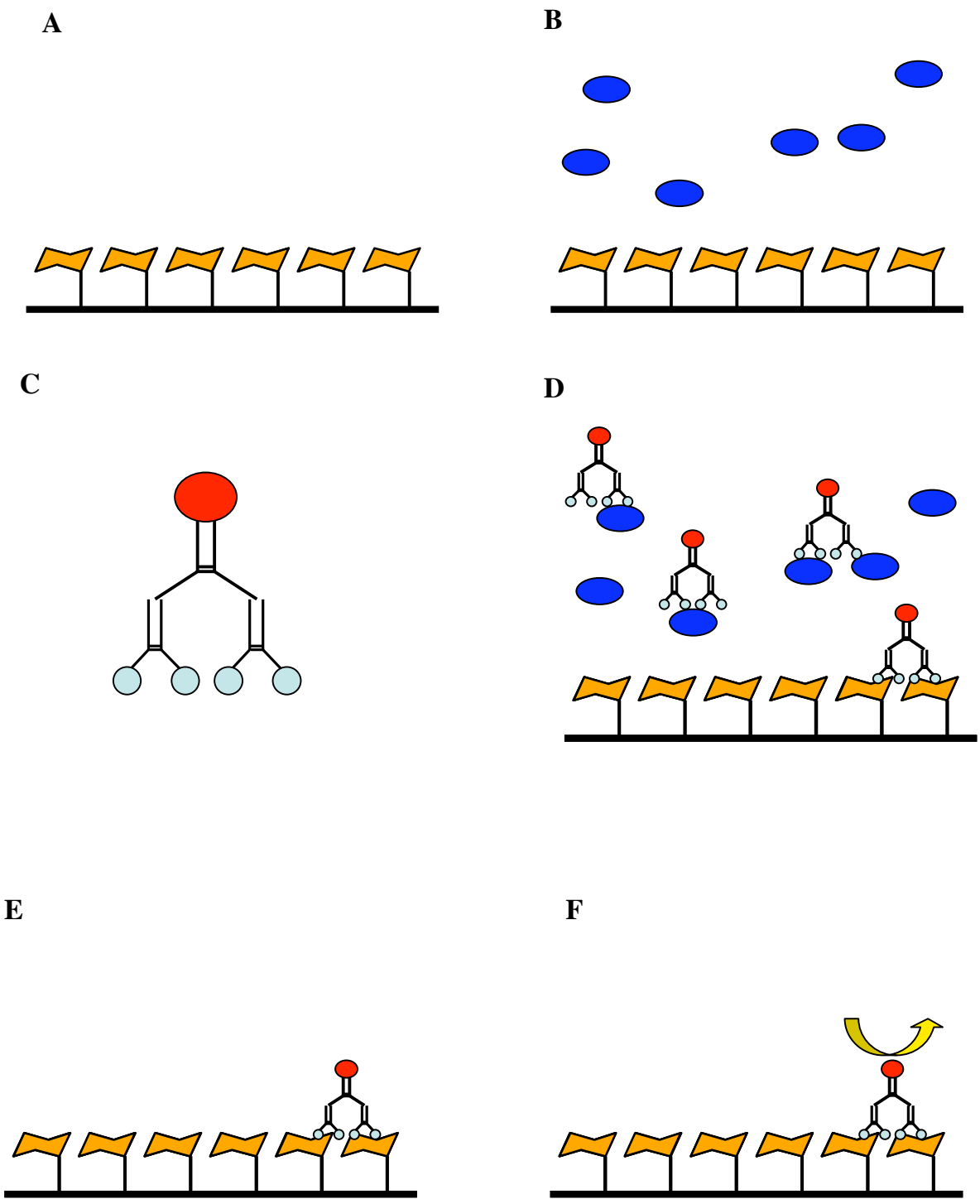

Figure 18. Setup of the hapten inhibition assay: Sialic acids bound to the surface are displayed in orange (A) and the ligand measured in blue (B). The Fc-MAG(d1-3) and a polyclonal goat anti-human IgG antibody coupled to an alkaline phosphatase are added to the wells (C). The higher the ligand affinity the less Fc-MAG(d1-3) binds to the surface (D). After washing (E), a fluorescent substrate is added to the wells and the amount of bound MAG is determined (F).

1.3 Biacore biosensors for advanced interaction analysis

1.3.1 Measuring biomolecular interactions in drug discovery

For pharmaceutical companies it is fundamental to understand pharmacological as well as toxicological properties of potential drug candidates at early stages of development. Besides, such molecules should preferably be orally available. In general, the later task is partly accomplished by taking the Lipinski rules of five into account.[9,94] This finally allows administration of the drug as a solid formulation like a tablet what is considered economically beneficial due to simple administration and storage.

To cope with the demand for potent drugs without adverse effects no general rule is applicable. At least in the case of toxicity, problematic chemical structures *e.g.* nitro-group are known and can be avoided. In a traditional drug discovery process, a large set of small molecules (300 Da) is screened against a validated target to discover new leads compounds. The process is well known as high throughput screening (HTS) and is carried out in a static assay format.[6] High affinity is employed as selection criteria for new lead structures.[95] Unfortunately, testing increasing numbers of compounds at faster and faster rates did not turn out to be as productive as anticipated.[96]

Lead compounds should preferably be of lower molecular complexity[97], have a smaller number of rings and rotatable bonds[98], a lower MW and be more polar[99] than actual drugs. Afterwards, medicinal chemists increase affinity by adding and/or exchanging functional groups on such lead molecules based on 3-dimensional informations on the target *e.g.* x-ray based. The process is known as structure-based drug-design.[100] Finally, *in vivo* experiments and clinical trials are carried out with drug candidates. Failure at this late state is economically undesired and much effort is conducted to avoid such loses.

In biological systems representing open systems, levels of physiological ligands change within milliseconds via rapid release and clearance. Consequently, equilibrium with receptors or enzymes is often not reached. Besides, drug

concentrations vary over time if not applied intravenously. In such an environment, the kinetics of interactions ought to play an important role.

Structure-based drug design is typically developed in a competitive mode were a molecule has to compete with a physiological ligand or substrate. Unfortunately, accumulation of substrate or ligand can diminish efficacy and potency of competitive inhibitors or antagonists.[101] Based on this finding, David C. Swinney stated that the biochemical mechanism of drug action has to be taken into account to avoid failure. His hypothesis was that most effective drugs utilize non-equilibrium transitions to enhance activity (*table 5*). These can either be based on the drug (covalent bond formation, very slow dissociation) or the target (two-step model). In a two-step model, an initial equilibrium binding event is followed by a transition to an non-equilibrium system. Receptors displaying such a mechanism include GPCRs, ion channels and nuclear receptors that are targets for 50% of all drugs approved by the U.S. food and drug administration (FDA).[1] The success of drug research seems to be dependent on the mentioned biochemical mechanism and the ability to select based on the mechanisms.

The importance of the biochemical mechanism of drug action can already be derived from two famous statements. Paul Ehrlich stated that a substance would not work unless it is bound *"Corpora non agunt nisi fixata"*. This is in close agreement with the above mentioned biochemical mechanism. Even earlier, Paracelsus postulated that alone dosage makes the poison *"Sola dosis facit venenum"*. Prolonged drug-target dissociation times enable dosage reduction what is an effective gain for drug safety.

Swinneys hypothesis was further supported by biosensor studies where biological potency was better described by the dissociation rate constant than by equilibrium binding affinity.[102,103]

Table 5. Successful drugs and its non-equilibrium mechanisms of drug action.[101]

Drug	Target	Mechanism	k_{off}
Aspirin	COX-1	Irreversible	Irreversible
Omeprazole	H^+, K^+ ATPase	Irreversible	Irreversible
Clavulanic acid	β-lactamase	Irreversible	Irreversible
Rivastigmine	Acetylcholinesterase	Pseudo-Irreversible	> 48 h
Candesartane	AT-2-receptor	Insurmountable	112 min
Deslortadine	H_1 receptor	Insurmountable	> 6 h
Verapamil	Ca^{2+} channel	Use-dependent	0.25 s
Casodex	Androgen Receptor	Induced degradation	-

Copeland *et al*. further discussed the biochemical mechanism with an emphasis on kinetic behaviour of drugs.[104] They proposed that one of the most crucial factors for sustained drug efficacy *in vivo* is not the apparent affinity of the drug for its target *per se*, but rather the residence time of the drug molecule on its molecular target. The residence time is defined as the binary complex residence time meaning the period for which the receptor is occupied by the drug. It is only dependent on the drug/target complex dissociation. Therefore, they agreed with Swinney on the importance of including kinetic data, especially on the residence time, into drug discovery decisions.

On the other hand, safety issues were elucidated by kinetic data of drugs. In the case of roxifian, slow dissociation was shown to be the reason for severe thrombocytopaenia.[105,106] In some cases, however, there might be a temporal distinction between desired effect and toxicity, such that rapid binding and dissociation of a ligand results in the desired pharmacology, whereas sustained residence leads to adverse effects. This has been suggested for D_2 receptor blockers that act as atypical antipsychotics.[107] It was found that a rapid dissociation rate was the only feature to distinguish between typical and atypical antipsychotic drugs.

Concluding, high affinity in a static assay as a validation tool for drug candidates might therefore not be sufficient to predict potency and safety. Hence, techniques that provide information about biochemical mechanisms *e.g.* kinetics have great potential for drug discovery.

SPR-based biosensors enable determination of kinetic parameters and have been in use for over 20 years. The technique is mainly provided by Biacore AB (GE healthcare) and has revolutionized the field of binding analysis. It is nowadays commonly applied in research and pharmaceutical industry.[108] In the pharmaceutical industry it is mostly used as a secondary screen for validation of HTS hits.

The technique is surface-based, meaning that one interaction partner is immobilized on a solid support. For drug discovery, a target protein usually has to be immobilized to screen ligands. A disadvantage is that immobilization could lead to restrictions in rotational freedom and accessibility of the protein, which can finally influence binding parameters *e.g.* affinity and kinetics.[109] Even though many HTS assays are surface-based, this led to scepticism against the biosensor technique at first. Therefore, several attempts were conducted to prove its comparability to solution-based assay formats. It was demonstrated that kinetic, binding equilibrium and thermodynamic results were in close agreement with methods like isothermal titration calorimetry (ITC), analytical ultracentrifugation (AUC) and stopped-flow fluorescence (SFF).[110-112] Moreover, a high degree of reproducibility was observed in studies with multiple users.[112,113] Although these comparison studies led to positive results, the most critical step for surface-based techniques remains to be immobilization. All comparison studies where performed with carbonic anhydrase II and results are likely to deviate for other proteins. Hence, the assay setup has to be designed properly for all surface-based methods.

To finally implement kinetic data into the drug development process, the influence of structural properties on kinetics, structure kinetics relationship (SKR), has to be elucidated. Rules, how to retard dissociation, would simplify a yet iterative process. Unfortunately, no such general rules are available though attempts were conducted to clarify the situation.[114,115] Probably, the relative importance of the association and dissociation rates is a unique property of a certain drug target. Nevertheless, a

selection of human immunodeficiency virus (HIV) 1 protease inhibitors displayed kinetic differences (*figure 19*) based on their core structures.[103,116,117] While a slow association rate could be compensated by higher concentrations, slow dissociation rates must be achieved by optimizing the ligand. For drug development, these findings are of substantial importance. Kinetic data obtained in a first screening would allow lead selection based on dissociation behaviour.

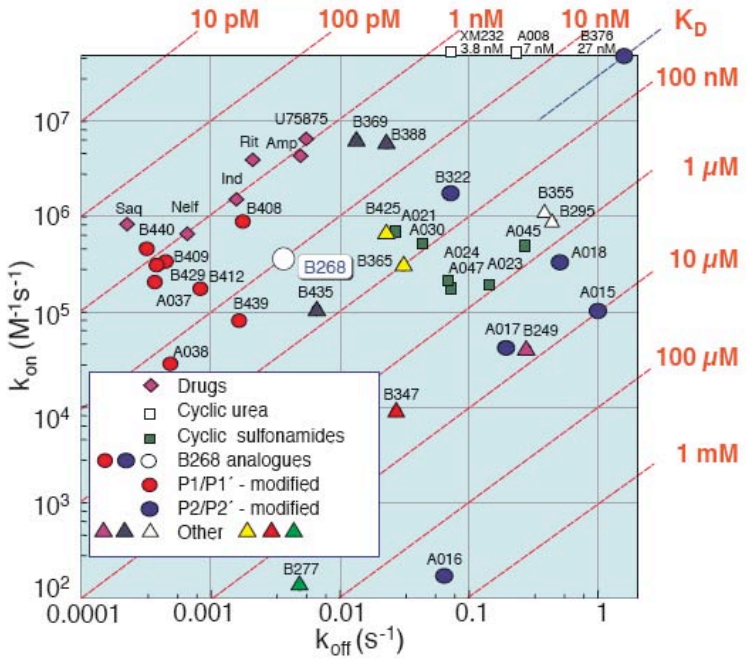

Figure 19. A k_{on}, k_{off} scatter plot of HIV protease inhibitors displaying the clustering of core structures.

Additional biosensor studies with HIV-1 protease inhibitors revealed fascinating details on the interaction processes and underlined its specific advantages. Thermodynamic analyses were performed with selected compounds.[118] It was possible to disclose the entropic and enthalpic influence on the association as well as the dissociation rate. In this case, the energy barrier for complex formation was dominated by large association enthalpy changes whereas for dissociation equal contributions were found. Experiments with HIV-1 protease mutants, known to mediate clinical drug resistance, revealed that resistance correlated with faster complex dissociation.[119,120] Other experiments indicated that association and dissociation rates were influenced differently by *pH* changes.[121] Combining these results increases the understanding of the interaction process between HIV-1 protease

and its inhibitors significantly. Knowledge about energy barriers of association and dissociation phases and drug resistance are likely to become of great value for pharmaceutical companies.

Analyses of conformational changes of proteins were reported as an additional feature of SPR-based biosensors. It was found that unfolding or a change from compact helical to extended structures like β–sheets decreased the signal intensity.[122,123] For ligand-induced conformational changes, a decrease of signal intensity for maltose binding protein and an increase for human cytomegalovirus protease were described.[124,125] In the case of receptors, transduction of a physiological signal upon ligand binding is predominately elicited via a conformational change. The possibility to screen for such conformational changes would allow differentiating between agonists (appropriate changes) and antagonists (no or inappropriate changes).

Beside the SPR-based biosensor technique, a wide range of methods is available to determine parameters like affinity, kinetics and thermodynamics of biomolecular interactions (*table 6*). They all possess their specific advantages and disadvantages. Technique specific artefacts might occur and therefore validation of obtained results with other methods is highly recommended. Hence, other techniques should not be considered competitive but rather complementary to such biosensors. Only a combination of results from different methods will provide an accurate description of the interaction process.

Table 6. Techniques to characterize lead or drug/target interactions.

	Affinity	Kinetics	ΔH, ΔS	Stochio-metry	Conf. changes	Label free	Epitope mapping
SPR	√	√	√	(√)	(√)	√	
CD	√				√	√	
ITC	√		√	√		√	
MPA	√		(√)				
NMR	√					√	√
MS	√			(√)		√	√
SFS	√	√			√		
AUC	√			√	√	√	
DPI	√	√		√	√	√	

CD: circular dichroism, ITC: isothermal titration calorimetry, MPA: microtiter plate assay, SFS: stopped-flow spectroscopy, AUC: analytical ultra-centrifugation, AFM: atomic force microscopy, DPI: dual polarization interferometry

1.3.2 Biacore technology

The detection principle of Biacore is based on a phenomenon called surface plasmon resonance (SPR). It arises as an electron charge density wave that was first described in the late 1950s.[126] Around 30 years later Pharmacia Biosensor AB launched a commercially available SPR detection system. The company had a close relation to the pharmaceutical industry what was represented in the company name. In 1996, the the name was changed into Biacore AB and finally it was merged with GE healthcare in 2006.

The SPR-phenomenon is based on total internal reflection (TIR), an evanescence electric field (E), and surface plasmon waves. A light beam that propagates through two non-absorbing media of different refractive index will be totally reflected at the interface when exceeding a critical incidence angle (Θ). The reflected light beam keeps its net energy upon reflection but an electric field intensity called evanescence wave (E) leaks into the medium of lower refractive index. The amplitude of the evanescent wave decreases exponentially with distance from the surface, and the effective penetration depth is about half the wavelength of the incident light.[127] By usage of a thin metal film at the interface, surface plasmons are excited when the p-polarized component of the evanescence field penetrates this layer. This results in an enhancing of the evanescent wave. Surface plasmons are waves of oscillating surface charge densities in a conducting metal and are equivalent to photons in the case of light. A non-magnetic metal like gold is normally used for these layers.[128-130]

Since both photons and surface plasmons are a form of electromagnetic energy, they can be fully described only by quantum physics. However, their properties can be explained in a simplified manner as vector quantities. The light photon momentum at the interface can be resolved into two vector components (parallel and perpendicular to the interface). The magnitude of these incident light vectors (ilv) directly depends on the light angle. The surface plasmon wave can be similarly described as a vector, which depends on a number of factors (metal properties, layer thickness, surrounding media). Resonance occurs only when the energy and momentum of the incident light vector corresponds to the one of the surface plasmon vector (spv). In this case, the

energy is converted from photons into plasmons what consequently leads to a drop in the intensity of the reflected light (*figure 20-D)*. Under non-resonance conditions no such conversion arises and the light is fully reflected (*figure 20-C*).

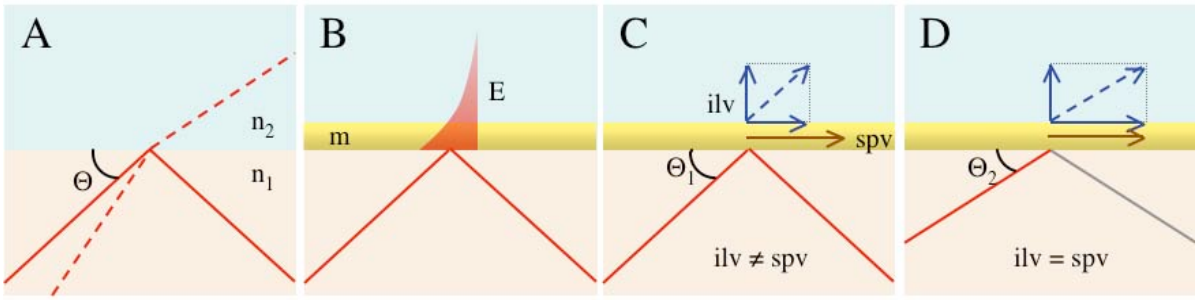

Figure 20 (by courtesy of D. Ricklin). Principles of SPR. **A:** Total internal reflection (solid line) and refraction (dashed line) of a light beam in dependence of the incidence angle Θ at the interface of two different media (n_1, n_2). **B**: Evanescence field wave (E) leaking through a thin metal film (m). **C, D:** SPR in the gold surface. If the incident light vectors (ilv) have another value than the surface plasmon vector (spv) light is fully reflected (**C**). Only a specific angle leads to a matching of the two vectors and a resulting resonance (**D**).

In an experimental setup, metal nature and thickness as well as the properties of one medium are kept constant. Resonance conditions are therefore only dependent of the angle of the incident light and the refractive index of the second medium. Therefore, refractive index changes in the second medium can be monitored by adjusting the incident light angle until a dip in light intensity (resonance) is detectable.[128-130]

For Biacore experiments, sensor chips that carry a thin gold layer (50 nm) on a glass support are applied. The gold surface is in direct contact with a flow cell and a prism follows the glass side. A monochromatic, p-polarized light beam at a wavelength of 760 nm is focused in a wedge on the gold surface and the total internal reflection for all angles is monitored on a diode array. The described evanescence field wave penetrates into the flow cell and enables detection of the refractive index to a distance of about 700 nm from the surface.

Biomolecular interaction measurements with SPR are based on the fact that binding of molecules to the surface alters the refractive index. Such a change is recorded as a change in the incidence light angle and converted into a response signal (*figure 21*). The response signal is measured in resonance units (RU) that correspond to a shift in

the resonance angle of approximately 10^{-4} °.[129] Since the mass of the molecules directly influences the refractive index, SPR biosensors are often referred to as mass detectors. Such a correlation between sensor signal and mass increase was experimentally determined for proteins (*Equation* 1).[131]

$$1\ RU = 1\ pg/mm^2 \qquad \text{Equation 1}$$

This correlation is almost constant for molecules with high protein and low lipid and carbohydrate content.[129] The relationship can be extrapolated to other molecules such as nucleic acids, carbohydrates, lipids or conjugate molecules. Hence, binding of nearly all molecules to the sensor chip can be detected though sensitivity is likely to vary for different types of ligands.[130] On the other side, sensitivity is dependent on the distance from the surface due to the exponential decay of the evanescent wave. Consequently, distribution of the molecules within the matrix will influence signal intensity. Additional, effects occurring around the interface, *e.g.* electrostatic attraction or conformational changes, will further influence signals.[132]

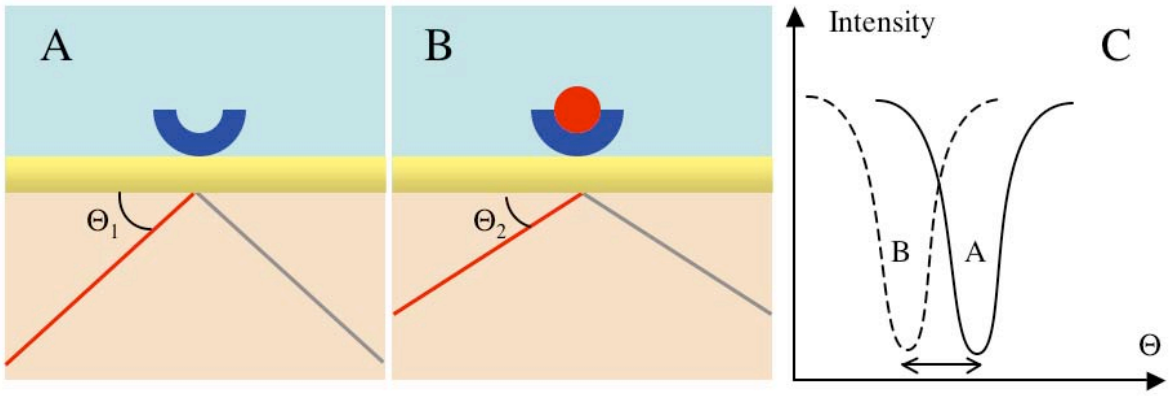

Figure 21 (by courtesy of D. Ricklin). Detection of biomolecular interaction by SPR. **A, B:** Sensor surface before and after interaction of two molecules. **C**: Shift of light intensity dip upon interaction.

In a typical Biacore experiment, one binding partner *e.g.* a receptor is immobilized on the sensor chip and the other is injected. A direct surface-attachment of *e.g.* proteins to a solid (gold) support often leads to loss in biological activity and a potential for unspecific binding events. To overcome this problem, a special surface chemistry was

developed involving a 'protecting polymer', which carries functional groups to simplify immobilization. On commercially available biosensor chips, thiolated carboxymethyl dextran chains are directly attached to the gold surface via the sulfur atom. This provides a hydrophilic environment and immobilized biomolecules are kept in a quasi-solvent environment.[133] Especially for labile proteins such physiological conditions increase stability. Inclusion of carboxyl groups in the dextran matrix enables immobilization via well-defined chemistry. To suppress electrostatic artefacts in experiments caused by remaining carboxyl groups and sample contaminants routine addition of salts *e.g.* 150 mM NaCl to the buffer is performed.[129] Other reagents such as EDTA or polysorbate are highly recommended to further limit non-specific signals. A schematic overview of the entire experimental setup is visualized in *figure* 22.

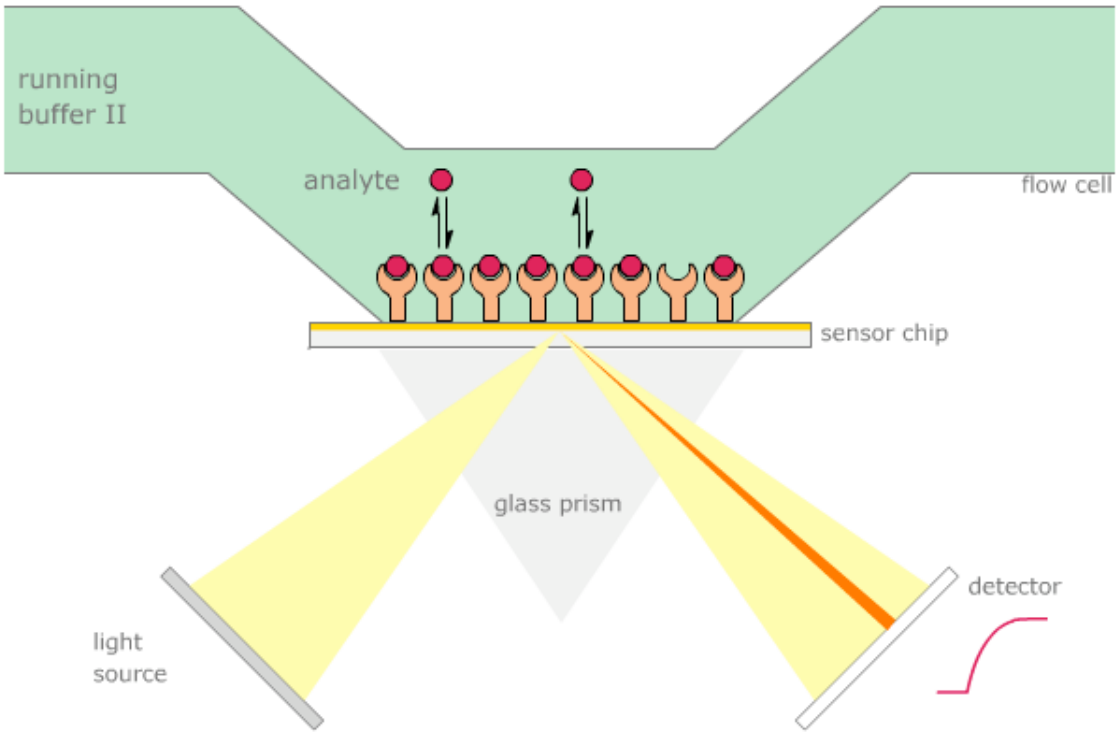

Figure 22 (by courtesy of A. Vögtli). Schematic overview of the experimental setup of the Biacore 3000. Precise sample delivery is conducted by the integrated fluidic cartridge (IFC). Binding of a ligand to an immobilized target is monitored in real-time by the SPR-based detection system.

In stationary systems, mass transport of molecules to the surface is governed by diffusion and convection processes. To ensure reliable results, incubation times of several hours are necessary, which is not suitable for real-time systems. A flow

system in a micro-flow cell offers a continuous transport of sample to and from the surface, what minimizes diffusion and convection effects. Therefore, an integrated fluidic cartridge was developed which reduced sample consumption and sample plug dispersion after injection.[129]

As described, the shift in resonance angle is monitored in real-time and plotted in dependence of time. In such a signal *versus* time plot, called sensorgram, the different stages of a binding event are visualized (*figure 23*). Running buffer flowing over the surface leads to a stable baseline. During continuous injection of sample, ligand binds to the target in a distinct association phase (*figure 23-A*). Already at that stage, dissociation occurs and influences the shape of the curve. Depending on the ligand, steady state is reached after a specific injection time, where binding and dissociating molecules are in equilibrium (*figure 23-B*). As soon as the injection is stopped, running buffer flows over the surface and the pure dissociation phase becomes visible (*figure 23-C*). In case of very slow dissociation, a regeneration step might be required to remove all ligand and reach the baseline (*figure 23-D*).

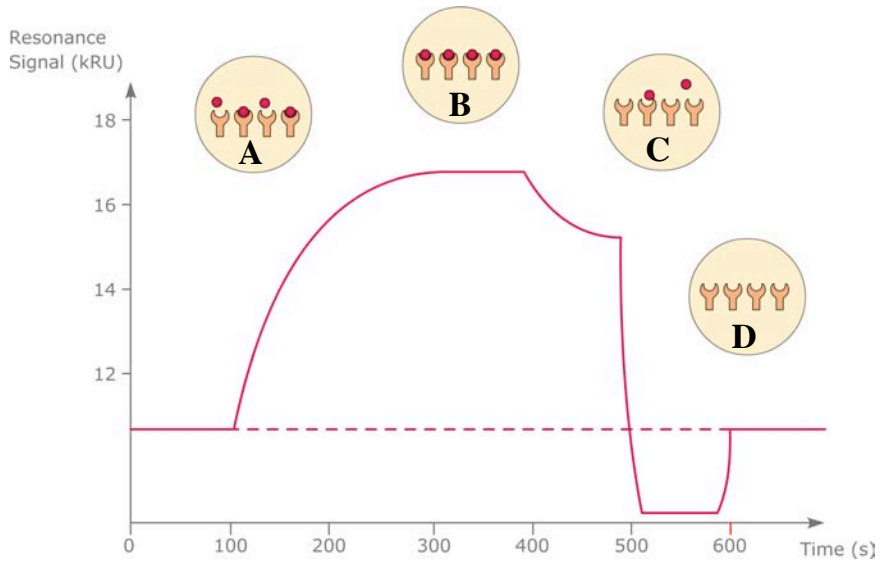

Figure 23 (by courtesy of A. Vögtli). A typical sensorgram obtained for a standard interaction measurement. Ligand from a sample starts to bind to the target (A) until a steady state is reached (B). After changing to pure buffer, dissociation of the ligand is visible (C). In case of remaining ligand a subsequent regeneration step is required (D)

Kinetic parameters like the association and dissociation rate constants (k_{on}, k_{off}) are derived from the sensorgram. The equilibrium dissociation constant (K_D) can be directly calculated from the kinetic rate constants using *equation 2* or from steady state signals at different concentrations using a saturation binding plot. Steady state affinity is calculated based on *equation 3*, where R_{eq} is the equilibrium response signal, K_A is the equilibrium association constant, C the concentration, R_{max} the maximum possible response, and n a steric interference factor.

$$K_D = \frac{k_{off}}{k_{on}} \text{ [M] and } K_A = \frac{k_{on}}{k_{off}} \text{ [M}^{-1}\text{]} \qquad \text{[Equation 2]}$$

$$R_{eq} = \frac{K_A \cdot C \cdot R_{\max}}{1 + K_A \cdot C \cdot n} \text{ [RU]} \qquad \text{[Equation 3]}$$

The effect of different kinetics on sensorgrams can easily be displayed by an *in silico* experiment where eight concentrations (200 – 0.25 μM) of four virtual compounds (A-D) are injected. Even though the affinity (K_D) is identical (*table 7*), a clear kinetic difference is visible in the sensorgrams (*figure 24*).

Table 7. Data describing the virtual compounds A, B, C and D.

Compound	K_D (μM)	k_{on} ($M^{-1} \cdot s^{-1}$)	k_{off} (s^{-1})
A	10	10000	0.1
B	10	1000	0.01
C	10	500	0.005
D	10	100	0.001

For compound B, C and D, a steady state affinity analysis is already complicated because steady state for the lower concentrations is not reached within injection time.

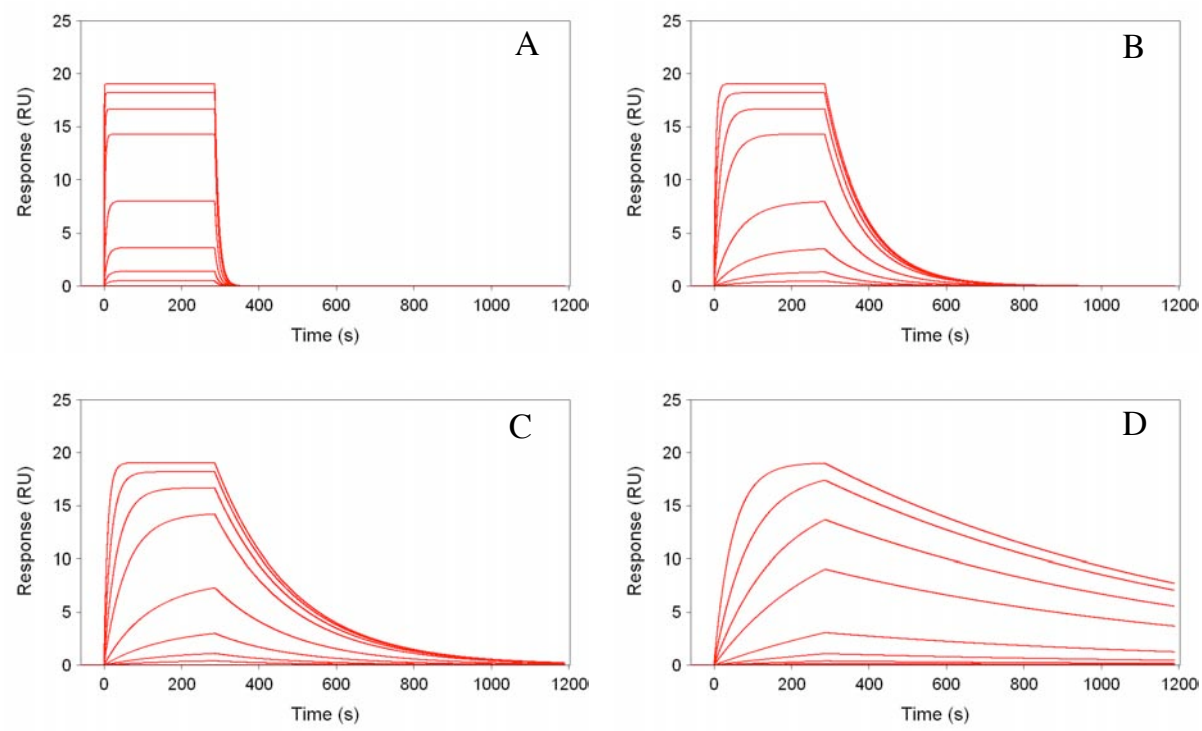

Figure 24. Importance of kinetics demonstrated by a simulation with four virtual compounds (A, B, C and D) all displaying a K_D of 10 μM.

1.3.3 Experimental setup

As mentioned, one of the interacting molecules has to be fixed on a sensor chip surface. The immobilized molecule is named target and the free one is referred to as ligand (*figure 25*). This nomenclature deviates from the original one introduced by Biacore but is convenient for pharmaceutical purposes, where different compounds (ligands) are screened against a defined target.

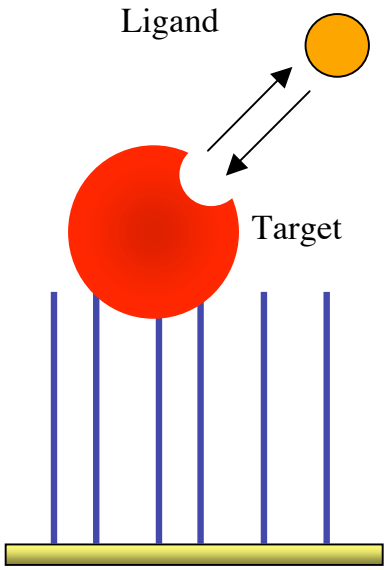

Figure 25. Experimental setup of a Biacore experiment. A target is immobilized onto a biosensor chip and a ligand is injected.

In general, it is recommended to plan experiments in a way that a simple 1:1-binding event is obtained. Therefore, multivalent binding partners should preferably be immobilized on the chip. A careful selection of the immobilization method is necessary and comparison of several strategies might be beneficial (*see p. 58*). In the case of proteins, the immobilized amount can be estimated by the relationship that 1 RU corresponds approximately to a surface concentration of 1 pg/mm$_2$.

For binding studies, the maximum response for a SPR signal can be approximated using *equation 4*. Because the relation is only exact for proteins, calculated R_{max} values for other molecules *e.g.* carbohydrates or drug-like molecules will deviate.

$$R_{\max} = \frac{MW_{analyte}}{MW_{target}} \cdot density_{target} \cdot valency \qquad \text{[Equation 4]}$$

Drug discovery applications often require immobilization of the larger molecule (receptor, enzyme, etc.). Small ligands (300-500 Da) are then screened resulting in low signal intensity due to the somehow mass dependency. Several 1000 RU of immobilized target protein result in R_{max} values of around 10-100 RU and partial deactivation further decreases the intensity. Molecules down to a molecular weight of 100 Da and a R_{max} value of 1 RU were measured on Biacore S51 successfully.[134] Even binding of Ca^{2+} was determined under special circumstances where potential conformational changes were involved.[125] If necessary, signal intensity problems with small ligands can be circumvented by several approaches.

- By attaching the low molecular weight molecule to the surface, the protein itself can be injected resulting in large signals. Unfortunately, protein consumption is high and for each ligand a new surface has to be prepared. To immobilize such molecules, a clear picture of the binding mode is needed to define the attachment site.
- A competitive assay format provides another solution. First, usage of a high molecular weight competitor can enhance the signal.[135] Second, a standard competitor can be immobilized and the small molecule is injected together with the protein. Again high protein consumption complicates its usage.[136] Nevertheless, both formats allow screening of several small molecules on the same surface. For competition experiments, determination of association and dissociation rate constants is complicated due to overlaying kinetics. A competitor with a slow association rate needs longer injection times to establish equilibrium.

Both the direct and the competition assays are sensitive to non-specific binding due to the detection principle. While all three formats are suitable for ranking experiments, only the direct assay can provide equilibrium and kinetic data of high-quality.[133]

As with all surface-based analysis methods, mass transport is a complicating factor.[137] This phenomenon might occur when the interaction between ligand and target is comparable or faster than the diffusion of ligand from bulk solution to the surface.

Mass transport is dependent on the flow rate, cell dimensions, diffusion coefficient and surface capacity.[138,139] For a given ligand, only the variation of flow rate and the surface capacity is possible. High flow rates (50-100 μl/min) at low surface densities are recommended for the reduction of mass transport limitation. However, the flow rate is often limited by the sample consumption or the required injection time. In addition, the influence is relatively small since k_m is proportional to the square root of the flow rate.[127] Experimental series with variation of surface density and flow rate could therefore be helpful for the detection of such effects and for finding a suitable compromise between sample consumption, signal intensity and mass transport.[140]

The Biacore 3000 allows precise temperature variation between 4 and 40 °C. Hence, determination of entropy and enthalpy by applying a van't Hoff plot is possible.[118] Furthermore, DMSO is tolerated up to 8% in a continuous experiment. This is especially important when dealing with drug-like molecules where lipophilicity (logP) is in the range of 2-5. In contrast to other buffer systems does the addition of DMSO require a special calibration.[141]

In order to clean all parts of the injection system and to equilibrate the surface, a series of pure buffer should be injected before each experiment.[142] Injections of such buffer blanks before and within binding experiment, inclusion of positive and negative controls, washing steps, as well as a proper maintenance further increase the accuracy and quality of the binding data.[143] Sample injection should be done in a randomized way and in replicates to eliminate the total experimental noise.

Regeneration is a critical step in a binding assay, especially when dealing with proteins. While too soft conditions might lead to remaining ligand, too harsh conditions can denature the protein. For strong interactions, a cocktail of different regeneration solutions might be necessary. Approaches for the development of proper regeneration conditions are described in literature.[144]

Evaluation and interpretation of obtained sensorgrams is another critical step. A huge amount of published data is unreliable due to poor quality and processing.[145] Proper data treatment is especially important when measuring low molecular weight ligands. Deviations from an expected binding model are often caused by poor experimental design, low purity of ligands and/or target heterogeneity. Unfortunately, such data can often be fitted to a more complex binding model.[140] Therefore, critical parameters

like sample purity should be verified before claiming a new binding mode or an additional binding pocket.

Because every sample solution will cause a signal in comparison to the running buffer, subtraction of a proper reference flow cell is needed. A reference flow cell should mimic the target flow cell as close as possible. Equal amounts of target with an inactivated binding site would represent an optimal reference. In general, equal amounts of inert proteins or just a blank surface are employed. In addition, injections of buffer blanks over the target flow cell cause small deviations from the reference and should be included. Subtraction of blanks and a reference flow cell assure high data quality and is termed double referencing.[142]

As explained, assay design should be kept easy and data should first be fitted to a simple 1:1-binding model (*Equation 5*). Since some targets possess more than one binding site, the equation has to be extended to a two independent binding site model. If mass transport effects are suspected or reported, a mass transport coefficient (k_m) might be introduced (*Equation 6*).

$$A + B \underset{k_{off}}{\overset{k_{on}}{\rightleftharpoons}} AB \qquad \text{[Equation 5]}$$

$$A_0 \underset{k_m}{\overset{k_m}{\rightleftharpoons}} A + B \underset{k_{off}}{\overset{k_{on}}{\rightleftharpoons}} AB \qquad \text{[Equation 6]}$$

A proper data processing is especially important for fitting kinetic data. Initially, different algorithms using curve transformation[146] or nonlinear least squares analysis[147] were used to evaluate binding kinetics. These methods only fitted single binding curves (or even portions thereof) and were found to be insufficient to distinguish between different binding mechanisms.[140] In the global analysis approach, the association and dissociation phases of the entire data set are fitted to a model simultaneously, resulting in very accurate and robust data.[148] Therefore, this method is implemented in the current evaluation software tools and should always be used for kinetic fits.

Software for data treatment and evaluation is available from Biacore (Biaevaluation). As a major drawback only a limited number of sensorgrams (24) can be fitted with older versions (Version 4.1) and handling is rather user-unfriendly. This gap was filled by Scrubber (BioLogic Software), a tool for the determination of affinity and, in the recent version 2.0, even kinetics. Data treatment is straightforward and larger numbers of curves *e.g.* from triplicate measurements can be fitted directly. Therefore, Scrubber is highly recommended where no newer software is available. For kinetic evaluations a software named Clamp is another possibility but rather difficult to handle.[149]

1.3.4 Immobilization of protein on biosensor surfaces

Protein immobilization is one of the most crucial steps in a Biacore experiment. Loss of partial or entire target activity, changes in ligand affinity and many other artefacts are directly related to unfavourable immobilization. The standard CM5 sensor chip from Biacore contains a glass slide with a thin gold layer (50 nm) that is covered with a carboxymethylated dextran with a dimension of 100 nm under physiological conditions. Introduced carboxy groups on the dextran chains permit covalent immobilization of proteins, oligosaccharides, nucleotides, or small molecules.
In general, immobilization strategies can be divided into four major groups[150] (*figure 26*) whereof A and D are typically applied in Biacore binding assays.

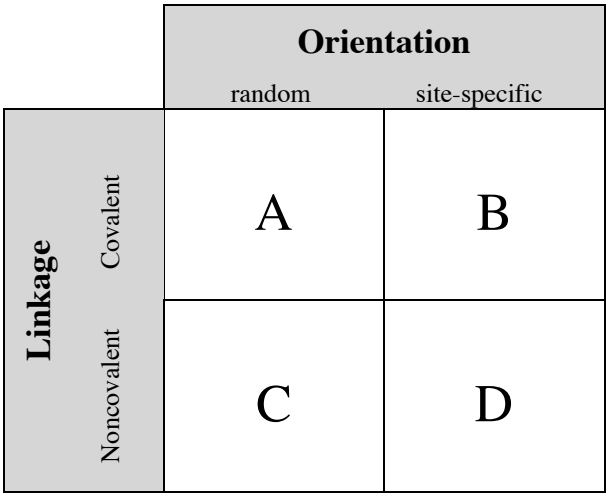

Figure. 26: Strategies for the immobilization of proteins onto solid supports. Differences are based on orientation and linkage.[150]

Random, non-covalent coupling approaches (C) are typically used in microtiter plate assays (MPA). Proteins are adsorbed randomly on coated surfaces via ionic or hydrophobic interaction. No control of protein orientation is possible and therefore these assays are susceptible to artefacts. In addition, such reactive surfaces need to be protected by "inert" proteins. Bovine serum albumin (BSA) is routinely applied but, as known by all pharmacologists, BSA is by far not inert.[151]

Random, covalent coupling approaches (A) usually generate stable surfaces with high density. Functional groups *e.g.* amine, hydroxy or carboxy groups present on targets

are utilised to form covalent bonds. Immobilization occurs at multiple attachment sites *e.g.* lysines and therefore lead to randomized attachment which might results in a loss of activity due to direct modification of residues in the binding site, steric hindrance, conformational changes or surface heterogeneity. However, if a specific functional group is available at a defined location of the target, site-specific coupling enables generation of an oriented, homogeneous surface.

Amine coupling is routinely applied for immobilization of proteins due to the high availability of amine groups. The amine coupling procedure makes use of the primary amine groups on the protein surface (lysine residues and the *N*-terminus). A direct reaction of amine groups with active esters generated by *N*-hydroxysuccinimide (NHS)/ 1-ethyl-3-(3-dimethylaminopropyl)carbodiimide (EDC) is the chemical basis (*figure 27*). In order to increase efficiency of the reaction, proteins are concentrated in the dextrane matrix. By lowering the *pH* of the immobilization buffer just below the *pI* of the protein, surface attraction is optimized. Amine groups become positively charged and get attracted by the negatively charged carboxyl group in the matrix. Because the reaction will only occur with uncharged amines, the immobilization *pH* should not be too low.[152] A careful evaluation of *pH* and protein concentration is needed to optimize the attraction.

Nearly all proteins and peptides possess multiple primary amine groups, which are often surface-exposed due to their hydrophilicity. Furthermore, amine groups are easily introduced artificially on molecules. In the case of proteins, lysines are often randomly distributed over the surface and amine coupling will result in a random and non-predictable immobilization of the protein (*figure 28-A*). It sometimes leads to a massive decrease of surface activity, *e.g.* more than 80% loss is reported for some antibodies, and this might also influence binding affinity and kinetics.[153] Analysis of the amino acid sequence, crystal structure and especially the binding site are recommended to avoid interference. Another drawback is the usage of acidic conditions for surface attraction. Acid labile proteins will result in inactive surfaces. Yoshitani *et al.* demonstrated that surface attraction can be circumvented by higher concentrations of target protein (2 mg/ml).[154]

Additionally, several popular buffer systems like Tris bearing primary amines are forbidden. Sodium azide, which is frequently used as a preservative in protein preparations, might also interfere and should consequently be removed.[155] Even

though there are several drawbacks, amine coupling still is the most frequent used immobilization technique.

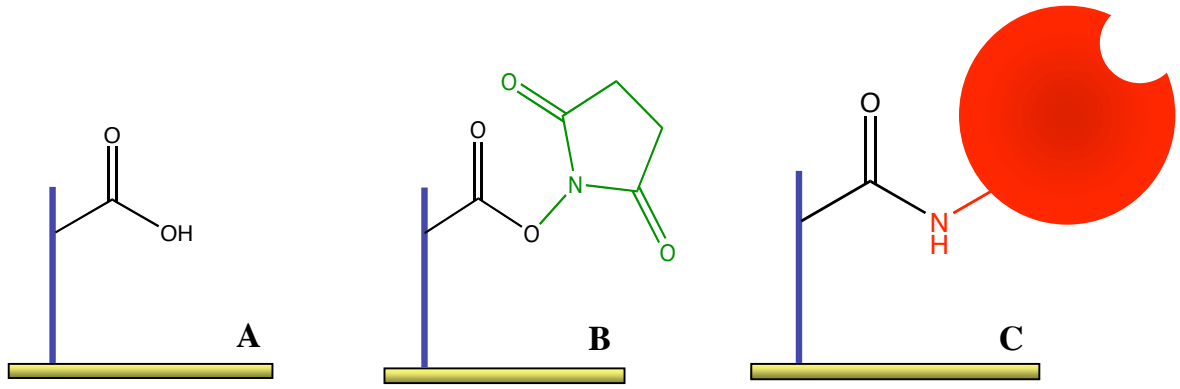

Figure 27: Coupling methods for Biacore sensor chip CM5. After activation of the matrix-based carboxyl groups (A) by NHS and EDC (B), targets can directly be immobilized via primary amine groups (C) or the surface can be functionalized for alternative strategies. (NHS = *N*-hydroxysuccinimide,, EDC = 1-ethyl-3-(3-dimethylaminopropyl)-carbodiimide.

Thiol groups and sugar moieties present on the target are additional possible sites for a linkage. Immobilization of thiol-bearing targets can be performed either by formation of disulfide bridges or by covalent reactions with maleimides. Thiol groups occur rarely compared to primary amines and therefore these approaches might lead to a more site-directed and oriented immobilization of the target. However, since the spontaneous formation of disulfides is thermodynamically not favoured, activation of the thiol group either on the chip surface or in the target is needed.[156] In the case of proteins, all kind of chemical treatments are a potential source for artefacts.

Capturing (D) approaches (*figure 28-B*) make use of a specific biomolecular interaction between the target and an immobilized capturing molecule. The approach is based on non-covalent protein/protein or protein/small molecule interactions. Such interaction systems are often utilized in biochemistry for affinity chromatography and are therefore frequently available.

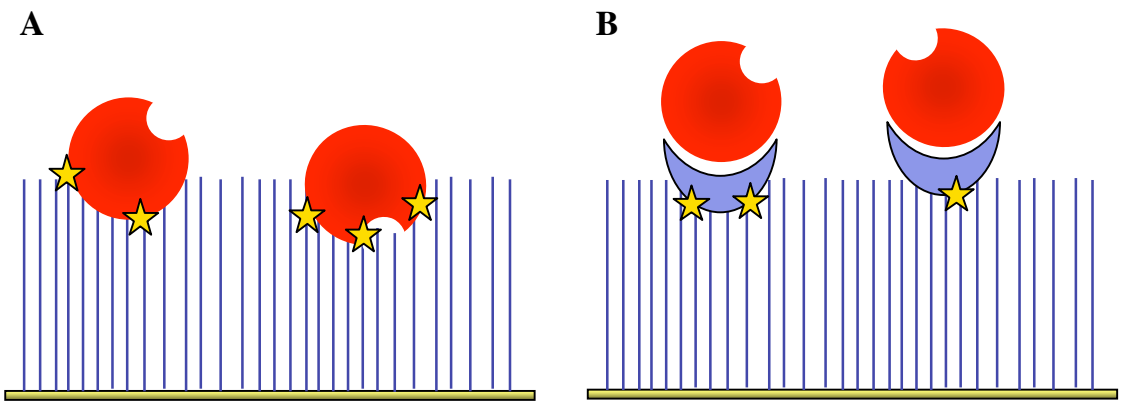

Figure 28: Target orientation after different coupling procedures. Randomized covalent immobilization (**A**) compared to a capturing approach (**B**). Sites of covalent attachment are marked with a star.

Capturing can be used for oriented coupling, since binding occurs at a well-defined site of the target. Three major coupling classes can be defined: antibody-antigen systems, interactions between proteins and naturally occurring binding sites *e.g.* Protein A/IgG and capturing of artificially introduced affinity tags *e.g.* FLAG-tag. Whereas naturally occurring binding sites are unproblematic, introduction of an artificial affinity tag has the potential to alter activity of the actual protein.

A common disadvantage of all capturing approaches is their non-covalent character. Whereas affinity purification is feasible in the µM range, creation of stable sensor surfaces is difficult. At least low nM affinity or a multivalent capturing system is needed for proper immobilization. Captured surfaces often show a certain degree of bleeding (surface decay). For ligands with low signal intensities, strong bleeding can significantly influence data quality. As an advantage, captured surface can be regenerated by direct elution of the target. Thus, capturing is an advantage for unstable target proteins on one side and ligands that are not regenerative on the other. The deactivated protein is eluted but the stable capturing systems (protein A, antibodies) can be re-used what will significantly reduce the amount of sensor chips needed.

Covalent and site-specific immobilization (B) is the optimal procedure for a Biacore experiment. Interesting new techniques were described based on bioengineering. One approach avails a small enzyme based on the human DNA repair protein O^6-alkylguanine-DNA-alkyltransferase (hAGT) and is commercially available as a mutant thereof (SNAP-tag).[157,158] A second attempt utilizes a trans-splicing mechanism of Split-Inteins.[159] For both strategies, target preparation includes cloning and expression to incorporate the actual immobilization system. Due to labour intense preparations, these applications are rarely observed.

The SNAP-tag is a novel tool for protein research, allowing the specific, covalent attachment of virtually any molecule to a protein of interest. The SNAP-tag is a small enzyme based on the human DNA repair protein O6-alkylguanine-DNA-alkyltransferase (hAGT). The hAGT is a suicide enzyme. It transfers the alkyl group from its substrate, O6-alkylguanine-DNA, to one of its cystein residues. After the reaction, the substrate remains covalently bound to the enzyme. For immobilization of a target protein via SNAP-tag, the target gene is cloned into a plasmid containing the SNAP-tag gene. For Biacore binding assays, the substrate BG-$(PEG)_3$-NH_2 is coupled to a CM5 sensor chip by standard amine coupling (*figure 29-A*). After expression, the fusion protein is immobilized enzymatically onto the derivatized surface via the active thiol group of the SNAP-tag (*figure 29-B*).

It was shown that surfaces displaying these substrates result in the selective immobilisation of hAGT fusion proteins.[157] No significant reactivity against proteins other than hAGT was observed. Immobilization was completely specific enabling immobilization without time-consuming purification steps. By using the SNAP-tag without the target protein, a perfect reference flow cell can be obtained.

SNAP-tag was shown to provide additional advantages for Biacore binding assays. Cyclophilin D as a fusion protein with hAGT was successfully immobilized onto such modified surfaces.[158] The method was compared to direct amine coupling. Immobilization of the cyclophilin D-hAGT was performed under physiological pH and ionic strength. High immobilization rates were obtained with higher density of immobilized substrate. At any immobilization level, the fusion protein exhibited higher relative binding activity than cyclophilin D immobilized via amine coupling.

A 100% relative activity was achieved at low immobilization levels of the cyclophilin D-hAGT. Only 70% relative activity was the maximum reached when coupling cyclophilin D directly via its amine groups. Even though the technique was shown to be advantageous and is commercially available, only two Biacore publications are available up to now.

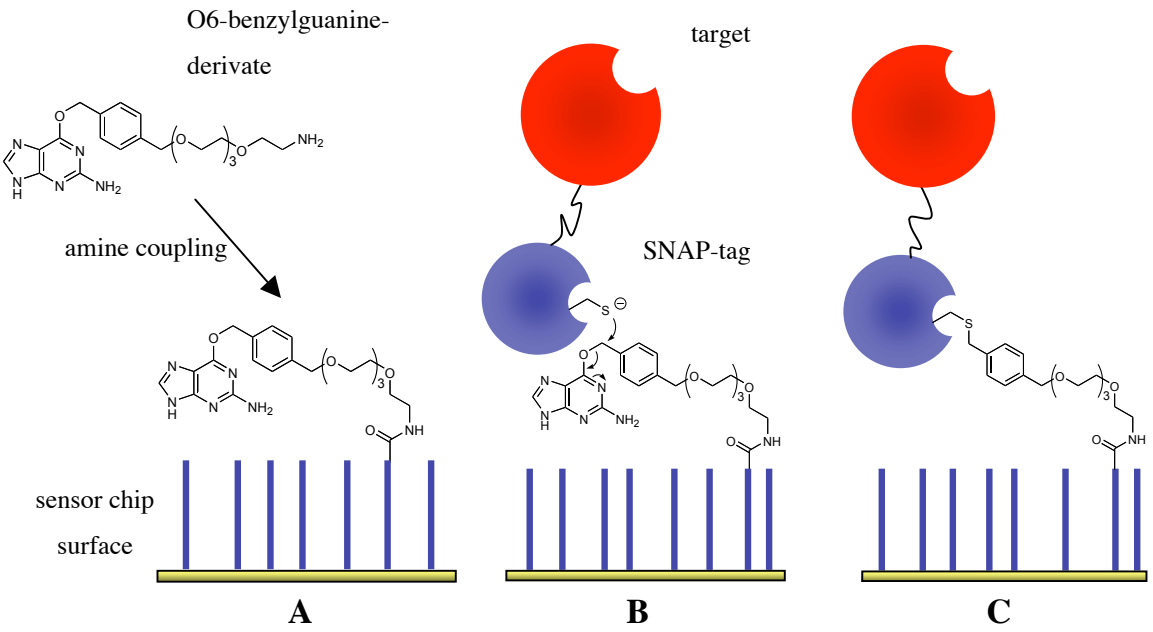

Figure 29. Enzymatic immobilization: First the substrate is immobilized via standard amine coupling (A). Afterwards the enzymatic reaction is performed (B) linking the target protein covalently to the sensor chip (C).

The SNAP-tag was successfully expressed in a variety of expression systems including bacteria, yeast, insect and mammalian cell lines. Beside immobilization, the SNAP-tag can be used for many other applications like FRET-assays, protein imaging (detection, internalization, translocation) and flow cytometry.

Recently, an approach based on protein trans-splicing was shown to be useful for immobilization on solid supports.[159] The naturally occurring DnaE intein from *synechocystis sp*., an intein self-processing domain that is split into two fragments (N-intein and C-intein), was used. The two intein fragments are inactive individually but under appropriate conditions they can bind to each other and form a functional protein-splicing domain. This leads to trans-splicing where the intein domains are cut

out and the ends are joined. For immobilization, the target DNA sequence is fused to the N-intein sequence. The C-intein fragment is coupled to the surface via a PEGylated peptide-linker and the N-intein construct is added. After trans-splicing, the target is directly immobilized via the linker. An advantage of the described technology, comparing to the SNAP-tag, is the absence of a remaining protein part needed for immobilization. Such a remaining part could be a source for non-specific binding. Because the technology has not yet been applied on Biacore, the suitability remains to be proven.

Concluding, every strategy possesses its specific advantages and disadvantages (*table 8*). For every target, the immobilization procedure should therefore be selected carefully.

Table 8. Comparison of strategies typically applied for biosensor experiments.

	A	B	D
Site-specific	No	Yes	Yes
Stable	Yes	Yes	No
Physiological conditions	No/Yes	Yes	Yes
Surface Capacity	High	Medium	Medium
Labour intensity	Low	High	Medium
Controllability	Low	High	Medium
Regenerative	No	No	Yes

While the standard CM5 sensor chip is suitable for most applications, some experiments require modifications of the matrix chemistry or a pre-coated capturing structure. Biacore therefore offers a selection of sensor chip with alternative surface coatings to extend the possible applications or to reduce experimental artefacts (*table 9*).

Table 9. Available sensor chip surfaces from Biacore with their surface modification and principal applications.[156]

Chip	Type	Application / Improvement
CM5	normal carboxymethyl dextran	general purpose
CM4	lower carboxymethylation	reduced non-specific binding
CM3	shorter dextran matrix	large molecules
C1	flat carboxyl (no dextran matrix)	dextran interference (e.g. lectins)
SA	immobilized streptavidin	biotinlyated molecules (e.g. RNA)
NTA	immobilized nitrilotriacetic acid	histidine-tagged proteins
L1	lipophilic groups on dextran	liposomes, bilayers
HPA	flat hydrophobic surface	lipid monolayers
Au	plain gold surface	custom design

In general, there are no restrictions for immobilization strategies as long as they do not interfere with the interaction mode. By using a plain gold surface a wide range of opportunities are available to create a chip of everybody's own imagination.

1.4 Expression of target proteins

For biomolecular interaction analyses the target proteins have to be available in high quantities. Today, expression of proteins has become a routine technique. This is mainly based on two Nobel Prices: 1978 Nobel Prize in Medicine for the discovery of restriction endonucleases (Werner Arber, Daniel Nathans and Hamilton Smith) and 1993 Nobel Prize in Chemistry for the discovery of the polymerase chain reaction (PCR) (Kary Mullis). Combination of those techniques enabled amplification and precise insertion of a gene of interest into a vector. Such vectors are used for transportation into a second organism for subsequent protein expression.[160] The entire process is referred to as cloning.

Often, proteins need to be tailored (truncated or mutated) to obtain solubility or to evaluate binding domains and active sites. Besides, recombinant proteins are produced where the original DNA sequence is fused with another sequence to obtain artificial proteins with special properties. To express wild type, truncated, mutated or recombinant proteins, a wide selection of different systems is available. Predominately used organisms are mammalian cells, baculovirus infected insect cells and bacterial cells like *E. coli* or yeast.[161] Very interesting developments are cell-free expression systems, where the production machinery of cells is used in an *in vitro* setup.[162]

Using eukaryotic cells for eukaryotic genes can be particularly important in obtaining biologically active proteins. Nevertheless, every system exhibits specific advantages and disadvantages that have to be assessed. An especially important process for protein expression is the posttranslational modification (PTM). Attachment of biochemical groups *e.g.* acetate, carbohydrates or enzymatic cleavage/folding functionalize proteins by modifying amino acids or by making structural changes *e.g.* disulfide bridges formation. Often, extensive PTM is required to obtain a functional protein.[161]

1.4.1 Baculovirus infected insect cells as expression system

The baculovirus infected insect cell expression system provides a eukaryotic environment that is generally conductive to the proper folding, disulfide bond formation, oligomerization, and post-translational modifications required for the biological activity of some eukaryotic proteins. Post-translational modifications that have been reported to occur in baculovirus-infected insect cells include signal cleavage, proteolytic cleavage, *N*-glycosylation, *O*-glycosylation, acylation, amidation, phosphorylation, prenylation and carboxylation. The sites of such modifications are usually at identical positions on the proteins produced in insect and mammalian cells. The precise nature of some of the post-translational modifications observed in insect cells, however, differs from those in mammalian cells, usually in subtle ways. Nevertheless, the insect baculovirus expression system mimics a vertebrate cell system quite remarkably with regard to protein post-translational modification. For genes encoding glycosylated and secreted proteins, there is a greater likelihood of obtaining biologically active products in the baculovirus expression vector system than in prokaryotic expression system.[163]

The most distinguishing feature of baculovirus expression vectors is the potential for very strong expression of a heterologous gene. Most heterologous proteins are produced at levels ranging from 10 mg to 100 mg per 10^9 cells. In the cases where different eukaryotic expression systems have been compared, the baculovirus system has usually outperformed the other expression systems in overall protein production. Insect cells are generally not anchorage dependent and can therefore be propagated in suspension culture as well as adherent. In addition, serum-free suspension culturing allows large-scale production with easy purification. Due to the above mentioned advantages, the use for recombinant protein production is rapidly growing.[164]

Different cells are used for infection and expression. The most common cell line is sf9, a clonal isolate, derived from *Spodoptera frugiperda* (fall armyworm) ovarian cells. It is used for transient or stable expression of recombinant proteins and for baculovirus propagation and is well characterized. For secreted proteins, High Five™ (H5) cells were described to be beneficial in terms of recovered protein amounts. H5

cells are a clonal isolate, derived from the parental *Trichopulsia ni* cell line and are commonly used for the expression of recombinant proteins using the Baculovirus Expression Vector System (BEVS).[163]

1.4.2 Mammalian cells as expression system

Expression in mammalian cells is considered the standard approach for human proteins, because only mammalian cells enable the entire spectrum of post-translational modifications.

The gene of interest is cloned into a suitable vector and transfected into appropriate cells to obtain transient protein expression. In such an approach the DNA is not incorporated into the genome but transcribed efficiently inside the cell. Transient expression usually leads to high amounts of protein in only short time. Obtained protein can then be examined in preliminary activity assays to evaluate the suitability of the expression system.[161]

In case of active protein, establishment of stable clones is needed. There the gene is incorporated into the genome and clones expressing the protein are selected via a specific selection marker (antibiotics or vital substrates). Usage of high concentrations of *e.g.* antibiotics allows selection of clones with superior incorporation of the gene and consequently high protein expression.

1.5 Aim of the thesis

The key goal of the MAG-project at the Institute of Molecular Pharmacy is to identify, synthesize and pharmacodynamically and pharmacokinetically characterize high affinity antagonists of MAG. Such antagonists would provide a tool to evaluate the still uncertain physiological function of MAG in *in vitro*/*in vivo* models. These antagonists could also be used as lead structures for a subsequent drug discovery effort. Therefore, work is focused on the synthesis and the elucidation of SAR of carbohydrate substructures and mimics binding to MAG.

For the characterization of drug/target interactions, assays are required that deliver accurate affinity data in reasonable time. Moreover, a detailed analysis including kinetic rate constants and entropy/enthalpy is needed to understand the process and predict potency. Gained knowledge allows the design of new structural modifications of ligands with advanced drug properties.

SPR-based biosensor technology provided by Biacore is a suitable tool for the mentioned tasks. Kinetic and thermodynamic data are acquired in a reproducible way without time-consuming and result-interfering labeling. Due to its surface-based nature, special considerations are necessary, particularly when immobilizing proteins.

Aim of the thesis was to implement Biacore technology into the ligand optimization process on MAG. Of great importance was the possibility to measure kinetics, enthalpy and entropy of interactions.

2 MATERIAL AND METHODS

2.1 GSLA-2 as a model system for carbohydrate-lectin interactions

2.1.1 Biacore instrumentation and materials

Biomolecular interaction analyses were performed on a Biacore 3000 surface plasmon resonance based optical biosensor (Biacore AB, Sweden). Sensor chips, immobilization kits, maintenance supply and standard buffers were purchased from Biacore AB. Standard buffers included HBS-N (10 mM HEPES, 150 mM NaCl, *pH* 7.4), HBS-P (HBS-N + 0.005% (v/v) polysorbate 20) and HBS-EP (HBS-P + 3 mM EDTA) and were ready-to-use (degassed and filtered). Proper maintenance included documented regular desorb and sanitize cycles and an annual check by a service technician. Sensor chips were preconditioned prior to usage by injecting a series of conditioning solutions. A flow rate of 50 ul/min was used and 2 times 20 ul of 50 mM NaOH, 10 mM HCl, 0.1% SDS and 100 mM H_3PO_4 was injected. After preconditioning the chip was used for immobilization within the next 4 hours.
Data processing and equilibrium binding constant determinations were accomplished with Scrubber© (BioLogic Software, Version 1.1g or 2.0a). Kinetic data were simultaneously fit using the non-linear regression program Clamp© or Scrubber 2.0a. Double referencing was applied to correct for bulk effects and other systematic artefacts.[165]

2.1.2 Biosensor experiments with GSLA-2

GSLA-2 was kindly obtained from John L. Magnani (GlycoTech Corporation, USA). The binding epitope was analyzed in detail using Biacore and STD-NMR in co-operation with the group of Prof. T. Peters (University of Lübeck, Germany)

2.1.2.1 Immobilization of GSLA-2 with amine coupling

Concentration and pH scouting for amine coupling of GSLA-2

Acetate buffers (10 mM, *pH* 4.0, 4.5, 5.0 and 5.5) were purchased from Biacore. For *pH* scouting, GSLA-2 was diluted to a 40 µg/ml concentration with different acetate buffers (*pH* 4.0, 4.5, 5.0, 5.5) or HBS-N (*pH* 7.4). These solutions were injected sequentially over a CM5 biosensor surface for 3 min at the flow rate of 10 µl/min. The surface was washed between each sample by injecting 50 mM NaOH for 30 s at a flow rate of 20 µl/min. Furthermore, 3 different concentrations (10, 20 and 40 µg/ml) were analyzed at *pH* 5.0 to evaluate the concentration dependency. The procedure was performed identical to *pH* scouting.

Amine coupling

The amine coupling kit was purchased from Biacore. The kit included all reagents needed for the immobilization procedure (*N*-hydroxysuccinimide (NHS), 3-(*N*,*N*-dimethylamino) propyl-*N*-ethylcarbo-di-imide (EDC), ethanolamine HCl).
The carboxy groups on the chip were activated for 10 minutes with a 1:1 mixture of 0.1 M *N*-hydroxysuccinimide (NHS) and 0.1 M 3-(*N*,*N*-dimethylamino) propyl-*N*-ethylcarbo-di-imide (EDC) at a flow rate of 10 µl/min. The GSLA-2 solution (3.9 mg/ml) was diluted to a 40 µg/ml concentration with acetate buffer *pH* 5.0. This solution was then injected over the activated surface at the flow rate of 10 µl/min. A high and a low capacity surface were established. Densities obtained were between 3'800 to 8'000 RU depending on the contact time. Afterwards the flow cell was blocked with a 10 min injection of 1 M ethanolamine, *pH* 8.0.

2.1.2.2 Binding assays with GSLA-2

The ligands sLe^a and Le^a were purchased from Sigma. sLe^a attached to a Lemieux spacer (sLe^a-Lem) was a kind gift from Prof. Ole Hindsgaul (Carlsberg Laboratory, Denmark). The sources of the compounds tested in the ranking experiments as well

as reagents required for NMR experiments are specified in Herfurth *et al.*.[166] Additional sLe^a and sLe^x mimetics were synthesized in house by Bea Wagner.

All experiments were performed in HBS-P buffer at a flow rate of 20 µl/min. For the binding assay, nine concentrations (0.25 µM–200 µM) of sLe^a-Lem and sLe^a were prepared and injected in a randomized order. Five blank buffer injections were performed before and one after each series. Association and dissociation were monitored for either 1 or 2 min, respectively. In the second experiment where binding of Le^a and sLe^x mimetics was tested, concentrations up to 2 mM were injected.

2.2 Myelin-associated glycoprotein (MAG) as drug target

The MAG project was conducted in close cooperation with the group of Prof. Sørge Kelm (University of Bremen, Germany). The Fc-chimera of MAG was expressed in a mutant CHO cell line synthesizing only high mannose glycans and purified as described previously.[33] The protein consisted of the Fc portion of human immunoglobulin IgG1 and the three *N*-terminal domains of murine MAG. This construct included the sialic acid binding site but the potential NgR binding site was absent.

For assay design it was either possible to immobilize the ligands or MAG itself. Because IC_{50} values were already available and kinetic data can only be derived precisely from a 1:1-binding event, the bivalent Fc-MAG(d1-3) construct was immobilized onto the dextran surface.

2.2.1 Immobilization of Fc-MAG(d1-3) with amine coupling

2.2.1.1 Amine coupling of Fc-MAG(d1-3)

A stock solution of Fc-MAG(d1-3) in 10 mM PBS (700 µg/ml) was a kind gift from Prof. Sørge Kelm.

Concentration and *pH* scouting were performed as described (*2.1.2*). The carboxy groups on the chip were activated for either 7 or 10 minutes with a 1:1 mixture of 0.1 M *N*-hydroxysuccinimide (NHS) and 0.1 M 3-(*N*,*N*-dimethylamino) propyl-*N*-ethylcarbo-di-imide (EDC) at a flow rate of 10 µl/min. For immobilizing MAG, the Fc-MAG(d1-3) solution was diluted with the appropriate buffer. To prevent deactivation of MAG at low *pH*, different conditions were tested. To obtain sufficient surface attraction at a higher *pH*, increased protein concentrations were required (*table 10*). These solutions were then injected over activated surfaces at a flow rate of 10 µl/min for the appropriate contact time. Afterwards the flow cell was blocked with either a 7 or 10 minutes injection of 1 M ethanolamine, *pH* 8.0.

Table 10. Immobilization conditions for amine coupling of Fc-MAG(d1-3)

pH	Concentration MAG (μg/ml)	Immobilization time (s)
4.0	40	120
4.5	70	360
5.0	70	360
5.5	140	600

2.2.1.2 Validation of coupled Fc-MAG(d1-3)

Compounds used were synthesized in-house by Dr. Sachin Shelke and Stefanie Mesch. A 20 mM stock solution was prepared in HBS-EP. Interaction experiments were performed in HBS-EP at a flow rate of 20 μl/min. The samples were injected in a randomized order. Five blank buffer injections were performed before and one after each experiment. Association and dissociation were monitored for 1 or 2 min, respectively.

2.2.2 Immobilization of Fc-MAG(d1-3) on a protein A surface

2.2.2.1 Immobilization of protein A with amine coupling

Protein A (P6031) was purchased from Sigma. Concentration and *pH* scouting was performed as described (*p. 71*). A sample and a reference surface were prepared sequentially or in parallel. The carboxy groups on the CM5 sensor chip were activated for 9 minutes with a 1:1 mixture of 0.1 M *N*-hydroxysuccinimide (NHS) and 0.1 M 3-(*N*,*N*-dimethylamino) propyl-*N*-ethylcarbo-di-imide (EDC) at a flow rate of 10 μl/min. For immobilizing protein A, a stock solution (1 mg/ml in 50 mM phosphate buffer, *pH* 7.0) was diluted in 10 mM sodium acetate, *pH* 5.0 to obtain a concentration of 30 μg/ml. This solution was then injected over the activated surface for 9 min at the flow rate of 10 μl/min. Protein A densities around 4'000 RU and

5'000 RU were achieved. Flow cells were blocked with a 9 min injection of 1 M ethanolamine, *pH* 8.0. After usage the chip was stored at 4 °C in HBS-EP buffer.

2.2.2.2 Capturing of Fc-MAG(d1-3) on the protein A surface

For capturing, the Fc-MAG(d1-3) solution was diluted to a 30-40 ug/ml concentration using HBS-EP. The protein A surface was regenerated by two sequential injections of glycine-HCl, *pH* 2.5 at a flow-rate of 60 µl/min for 5 sec. prior capturing. Afterwards the surface was equilibrated for at least 1 hour. Subsequently, Fc-MAG(d1-3) was injected at a flow-rate of 10 ul/min for 10 min. Stability of the surface was monitored for 30-60 min.

2.2.2.3 ***Validation of the capturing assay***

Trial experiments

Compounds were synthesized in-house by Dr. Sachin Shelke and a 20 mM stock solution in HBS-EP was prepared. The Triasialoganglioside G_{T1b} was purchased from Sigma.

The ligands used were chosen due to their difference in the rIC_{50} values by a factor of 70. Interaction experiments were performed in HBS-EP at a flow rate of 20 µl/min. First, several concentrations of both ligands (**SH-082** and **SH-035**) were injected over the surface to screen for binding affinity. To further proof the observed binding, 9 concentrations of a twofold dilution series of ligand **SH-082**, starting at 200 µM, were prepared. The samples were injected in triplicates in a randomized order. Five blank buffer injections were performed before and one after the experiment. Association and dissociation were monitored for 1 min. The entire experiment was repeated twice to check for reproducibility. Determination of the equilibrium dissociation constant K_D based on the dissociation signal was accomplished with GraphPad Prism (version 4.0a).

In a second attempt the physiological ligand G_{T1b} was measured to validate the assay. G_{T1b} was dissolved in HBS-EP by sonication to obtain a 20 mM stock solution. The

interaction experiment was performed in HBS-EP at a flow rate of 20 µl/min. For the experiment itself, 12 concentrations of a twofold dilution series, starting at 1 mM, were prepared. Samples were injected in a randomized order. Five blank buffer injections were performed before and one after the experiment. Association and dissociation were monitored for 1 min. Two pre-injections with a 200 µM solution of ligand **SH-082** were carried out.

Optimization of the surface stability

The compound was synthesized in-house by Stefanie Mesch. A 20 mM stock solution in HBS-EP was used. For capturing MAG, the Fc-MAG(d1-3) solution was diluted to a 40-70 µg/ml concentration with HBS-EP. Subsequently, the sample was injected at a flow-rate of 1 µl/min for 20-30 min. If needed the injection time was prolonged to increase the capturing level. Stability of the captured Fc-MAG(d1-3) was monitored for 30-60 min. For increased signal stability, the surface was equilibrated over night at 5 µl/min in HBS-EP.

Afterwards, 10 concentrations of a twofold dilution series of ligand **SM-m5**, starting at 200 µM, were prepared. All interaction experiments were performed in HBS-EP at a flow rate of 20 µl/min. The samples were injected in a randomized order. Five blank buffer injections were performed before and one after the experiment. Association and dissociation were monitored for 1 min. The first experiment was performed directly after capturing and two additional experiments 24 hours later.

2.2.2.4 Evaluation of negative sensorgrams

Carboxymethyl dextran (86524) and additional reagents utilized were obtained from Fluka.

Interaction experiments were performed in HBS-EP at a flow rate of 20 µl/min. A CM5 and a CM4 sensor chip were prepared as described in the optimized procedure. Buffers with the appropriate composition were filtered and degassed prior to usage.

For each experiment, 10 concentrations of a twofold dilution series of SH-136, starting at 400 µM, were prepared. The samples were injected in a randomized order. Five blank buffer injections were performed before and one after the experiment. Association and dissociation were monitored for 1 min. Afterwards, the surface on CM4 was regenerated by two injections of glycine-HCl, *pH* 2.5 at a flow-rate of 60 ul/min for 5 sec and equilibrated for at least 1 hour. As a negative control, the experiment was repeated on such a blank protein A surface using identical conditions.

2.2.2.5 DMSO tolerability

DMSO was purchased from Fluka and stored in a desiccator. Capturing was carried out as described (*2.2.2.3*). A stock solution (20 mM) of **SH-082** was prepared in DMSO. The stock solution was kept in a glass vial to eliminate contaminations by *e.g.* softeners. A running buffer containing the desired amount of DMSO (3 or 6%) in HBS-EP was prepared.

To eliminate the described influence of DMSO on signals, a calibration was necessary.[141] Two solutions were prepared (A = 1 ml running buffer + 50 µl HBS-EP, B = 1 ml running buffer + 1 µl DMSO). Solutions A and B were mixed as indicated in *table 11* and used for calibration. DMSO calibration solutions were injected after 5 blank injections and before the sample solutions.

Table 11. Solutions needed to calibrate for the influence of DMSO

A (µl)	400	300	200	100	0
B (µl)	0	100	200	300	400
Calibration	1	2	3	4	5

DMSO calibration was accomplished directly in Scrubber© (version 2.0a).

2.2.2.6 Sialic acid derivatives

After establishment of a stable biosensor assay, a set of in house sialic acid derivatives was measured. The K_D values were compared with the rIC_{50} values obtained from the hapten inhibition assay. Compounds were synthesized in-house by Dr. Sachin Shelke and Stefanie Mesch. Stock solutions (20 mM) were prepared in HBS-EP.

Interaction experiments were performed in HBS-EP at a flow rate of 20 µl/min. A CM5 sensor chip was prepared as described (*p. 77*). For each experiment, 10 concentrations of a twofold dilution series were done. Samples were injected in a randomized order. Five blank buffer injections were performed before and one after the experiment. Association and dissociation were monitored for either 1 or 2 min, respectively.

2.2.2.7 Detailed thermodynamic analysis

The interaction of sialic acid derivatives with MAG was further characterized by determining the entropic and enthalpic contributions to binding affinity. Three selected sialic acid derivatives **SH-164** (K_D=137 µM), **SH-136** (K_D=25.6 µM) and **SM-m6** (K_D=0.7 µM) were measured at various temperatures (5, 10, 15, 20, 25, 30 °C) and evaluated by applying a van't Hoff plot.[118] Ligand selection was based on structural properties and affinity. A distinct structural feature was required that influenced affinity by a factor of at least 5 (*figure 30-A, B and C*). A clear picture for the thermodynamic impact of such defined structural modifications was expected.

SH-164

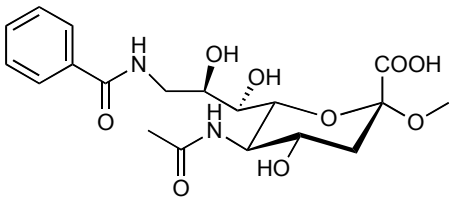

SH-136

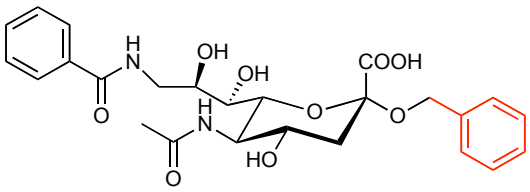

SM-m6

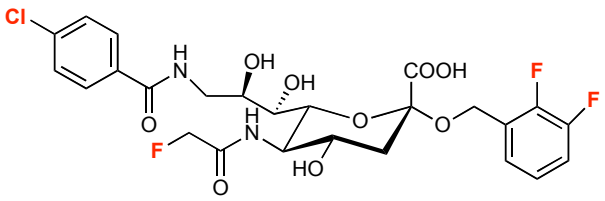

Figure 30: Ligands **SH-164**, **SH-136** and **SM-m6** selected for a detailed thermodynamic evaluation. Structural modifications are highlighted in red.

Capturing and interaction analyses were carried out as described (*p. 79*). The order of temperature variation for the measurements is indicated in *table 12*. First, each compound was measured at 25 °C. Subsequently, the Biacore 3000 was cooled down

to 5 °C over night. Afterwards each compound was measured with 5 °C increments in between. The utilized procedure eliminated a possible temperature dependent deviation based on a stepwise temperature change.

Table 12. The order of temperature variation was interrupted to eliminate a temperature dependent deviation.

Experiment	Temperature (°C)
1	25
2	5
3	10
4	15
5	20
6	30

2.2.3 Ligand optimization using second site screening

Described sialic acid derivatives were used for further optimization. A technique named second-site screening was applied in house by Dr. Brian Cutting and Dr. Sachin Shelke. Combination of *in-situ* click chemistry with second-site screening led to direct association of sialic acid derivative with a second site fragment out of a library.[167] Obtained SSC were identified, re-synthesized and subsequently analyzed on Biacore to proof higher affinity and to disclose the kinetic impact.

2.2.3.1 Characterization of second generation ligands

Capturing of MAG on the protein A surface and interaction measurements were carried out as described (*p. 79*).

In a first screening experiment, nine concentrations of a twofold dilution series of SSL, starting at 1 mM were prepared and injected in a randomized order. Five blank injections were performed before and one after each experiment. Association and dissociation were monitored for 1 min. In a second attempt, the concentration range was adjusted. Nine concentrations of a twofold dilution series, starting at 50 µM were prepared and injected in a randomized order. Five blank injections were performed before and one after each experiment. Association and dissociation were monitored for 1 min.

2.2.3.2 Competition experiments with sialic acid derivatives

Due to the observed two binding site model, a competition experiment was carried out to proof an identical binding site for both compound classes. A standard sialic acid derivative (**SH-082**) was used as competitor to verify binding of the second generation ligand to the sialic acid binding site.

Capturing of MAG on the protein A surface and interaction measurements were carried out as described (*p. 79*). Two experiments were performed were the competitor was used at 10 or 20 µM concentration, respectively For the experiments

itself, nine concentrations of a twofold dilution series, starting at 25 μM and containing an indicated amount of competitor, were prepared. The samples were injected in a randomized order. Five reference injections were performed before and one after each experiment. Reference injections were composed by either 10 or 20 μM competitor corresponding to the proper experiment.

2.3 Expression of MAG(d1-3)-SNAP

The mouse MAG(d1-3) gene (accesion number P20917, Swissprot database) was a obtained from Prof. S. Kelm. The SNAP gene was kindly donated by Covalys.

2.3.1 Insect cells as expression system

The Bac-to-Bac® baculovirus expression system provided a rapid and efficient method to generate recombinant baculoviruses for high-level expression of MAG-SNAP and SNAP in insect cells. The entire protein and DNA sequence of the SNAP and MAG(d1-3)-SNAP constructs are listed in *appendix II*.

2.3.1.1 Growth and culture of bacterial cells (E. coli)

E. coli strains

DH5α™ was used for plasmid amplification. DH5α increases insert stability and improves the quality of plasmid DNA prepared with mini-preps. The transformation efficacy in DH5α is high. Their background expression is minimal due to the lack of T7-RNA polymerase.
MAX Efficiency DH10Bac™ cells were used to produce recombinant baculovirus DNA. The bacmid propagates in DH10Bac as a large plasmid that confers resistance to kanamycin and can complement a lacZ deletion present on the chromosome to form colonies that are blue (Lac +) in the presence of a chromogenic substrate such as Bluo-gal or X-gal and the inducer IPTG. DH10Bac also contain a helper plasmid, which encodes the transposase and confers resistance to tetracycline.

Culture media for E. coli

Bacto Tryptone, Bacto Yeast extract and Bacto agar were obtained from Becton Dickinson and ampicillin sodium salt and X-Gal from Applichem. Gentamicin, Tetracyclin and Kanamycin from Gibco (Invitrogen).

LB-medium / LB agar plates

Table 13. Concentrations for LB-medium and plates

Reagent	Quantity
Bacto™ Tryptone	1.0%
Bacto™ Yeast Extract	0.5%
Sodium chloride	172 mM
Bacto™ Agar	1.5%

Tryptone, yeast extract and NaCl were dissolved in ddH_2O (*table 13*). The *pH* was adjusted to 7.5 and the solution was autoclaved.
For agar plates, agar was added before autoclaving the solution. After sterilization, the medium was cooled down to 50 °C and the appropriate antibiotics were added. The medium was poured into plates under laminar flow and after hardening, the plates were stored at +4 °C in a sealed plastic bag.

SOC –medium

Table 14. Composition of SOC-medium

Reagent	Quantity
LB medium	10 ml
2 M Magnesium chloride	50 µl
1 M D-Glucose	200 µl
LB medium	10 ml

A 2 M $MgCl_2$ solution was prepared and autoclaved. A 1 M *D*-Glucose solution was prepared and filtered (Minisart 0.2mm, Sartorius). Both solutions were added to the LB medium under laminar flow (*table 14*). SOC medium was prepared freshly for every usage.

SOB –medium

Table 15. Composition of SOB-medium

Reagent	Quantity
Bacto™ Tryptone	2.0%
Bacto™ Yeast Extract	0.5%
Sodium chloride	8.6 mM
Potassium chloride	2.5 mM

Tryptone, yeast extract, NaCl and KCl were dissolved in ddH_2O (*table 15*). The *pH* was adjusted to 7 and the solution was autoclaved. $MgCl_2$ was added just before usage.

Antibiotics

For clone selection after transformation ampicillin was used as antibiotic. For clone selection after transformation of pFastBac into DH10Bac cells, gentamicin, kanamycin and tetracycline were used.

IPTG and X-gal for Blue/White selection

β-Galactosidase is encoded by the bacterial gene lacZ. It cleaves the colorless substrate X-gal into galactose and a blue insoluble product. A common use of lacZ is for blue/white selection when cloning a DNA insert into a plasmid. If the insert is ligated into the polylinker, the lacZ gene will be disrupted and the colony will remain white.

Table 16. Final concentrations of additives added to culture media.

	Ampicillin	Gentamicin	Kanamycin	Tetra-cycline	X-gal	IPTG
Stock solution (mg/ml)	100	7	50	10	20	40
Liquid media (mg/ml)	100	7	50	10		
Agar plates (mg/ml)	150	7	50	10	40	40

The stocks (*table 16*) were prepared using ddH_2O. Obtained solutions were sterilized by filtration (Minisart 0.22 mm, Sartorius). Aliquots were stored at –20 °C. Tetracycline and X-gal were protected from light.

Clone picking and plasmid isolation

Incubation was carried out in a shaking incubator Innova 4000 (New Brunswick Scientific). LB-medium and agar plates were prepared as described (*p. 85*). Isolation of plasmid DNA was performed using the GenElute™ plasmid mini-prep kit from Sigma.

Using a sterile pipette-tip, a single colony was picked and inoculated in 3 ml of LB-medium containing an appropriate antibiotic. The culture was grown on a shaking incubator (300 rpm, 37 °C) until cells reached the stationary phase. Plasmid isolation was performed according to the procedure of the supplier for the mini-prep kit. The plasmid DNA out of 1 ml culture was finally eluted in 70 µl elution buffer.

2.3.1.2 Preparation of competent cells

Cells for electroporation

Agar plates and SOB–medium were used for outgrowth and prepared as described. For cultivation of cells an Incubator shaker Innova™ 4000 (New Brunswick Scientific) was used.

The *E.coli* strain was streaked out on agar plates and incubated at 37 °C overnight. Single clones were picked and incubated overnight at 37 °C in the incubator shaker in 5 ml SOB-medium without $MgCl_2$. Such overnight cultures were inoculated in 250 ml SOB-medium containing $MgCl_2$. During incubation, the optical density was measured at 600 nm (OD600) every one to two hours. After reaching an OD600 between 0.5 and 0.8 the cells were centrifuged at 5000 rpm and 4 °C for 10 min. Cells were washed in 250 ml glycerol solution (10%, 4 °C) by re-suspension. Afterwards they were centrifuged again at 5000 rpm and 4 °C for 10 min and re-suspended in 50 ml glycerol solution (10%, 4 °C). After an additional centrifugation step the cells were re-suspended in 1 ml glycerol solution (10%, 4 °C). Aliquotes were immediately frozen in liquid nitrogen and stored at –80 °C.

Cells for heat-shock transformation

The *E.coli* strain was streaked out on agar plates and incubated at 37 °C overnight. Two clones were picked and incubated overnight in 4 ml LB-medium at 37 °C in the incubator shaker. The OD600 was measured and 1 ml overnight culture was added to 100 ml LB -medium and incubated at 37 °C on the incubator shaker. The OD600 was measured after 1 hour and then every 20 min. until it reached a value between 0.4 and 0.5. Cultures were chilled on ice for 20 min. Subsequently the cells were aliquoted to 4 x 50 ml and centrifuged at 5000 rpm and 4 °C for 10 min.

Each pellet was re-suspended in 10 ml $CaCl_2$ solution (50 mM, 4 °C). Then cells were kept on ice for 40 min. Cells were centrifuged and re-suspended in 0.5 ml $CaCl_2$ solution (50 mM, 20% glycerol, 4 °C). Aliquotes were immediately frozen in a dry ice/ethanol bath and stored at –80 °C.

2.3.1.3 Transformation

Electroporation

Electroporation was performed using the Micro Pulser™ electroporation apparatus and Gene Pulser cuvettes 0.1 cm (Bio-Rad).
In 0.1 cm cuvettes, 50 µl cells were mixed with 5 µl mini-prep purified plasmid or 1 µl pSS26b from the clone saver punch. An electrical pulse with 1.80 kV was applied and immediately after the pulse 1 ml SOC medium was added to the cells. Afterwards, they were incubated at 37 °C and 550 rpm on the thermomixer for 40 min or 1.5 h. Subsequently, cell suspensions were streaked out on agar plates containing ampicillin.

Heat-shock transformation

Mini-prep purified plasmid (2 µl) was mixed with 100 µl DH10Bac cells and chilled on ice for 30 min. The cells were heat-shocked at 42 °C for 45 sec on the thermomixer and afterwards put on ice for 2 min. 900 µl SOC–medium was added and outgrowth was done for 4 hours at 300 rpm and 37 °C on the thermomixer. Afterwards cell suspensions were streaked out on agar plates containing kanamycin, gentamicin, tetracycline, IPTG and X-gal. After 48 hours white colonies were picked, re-streaked on plates and incubated at 37 °C for 15-17 hours.

2.3.1.4 Analyses for plasmid DNA

Agarose gel electrophoresis

Molecular biology grade agarose was purchased from Eurogentech. Ethidium bromide solution 1% was obtained from Applichem. Loading buffer as well as the perfectprep gel cleanup kit was purchased from Eppendorf. DNA molecular weight marker X was obtained from Roche Diagnostics. Visualization of the stained DNA was performed on a GelDoc2000 transilluminator (Bio-Rad).

A 1% Agarose solution in TBE-Buffer (44.6 mM Tris(hydroxymethyl)-aminomethan, 44.6 mM Boric acid, 1 mM Na2EDTA, pH 8), was heated in the microwave until the agarose was dissolved. The solution was cooled down for 2-3 min to ~ 50 °C and 2 µl ethidium bromide 1% was added. Subsequently, the mixture was poured into a gel tray containing an appropriate comb. After formation of the gel the comb was removed and TBE buffer was added to cover the gel.

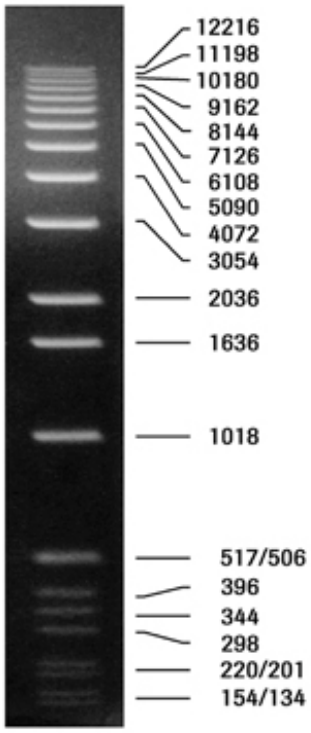

Figure 31. DNA marker x

DNA samples were diluted with ddH_2O if necessary and an appropriate amount of loading buffer was added to the samples. 2 µl DNA marker (*figure 31*) were included for size determination. The samples were loaded on the gel and an electric field was applied (80-85 V). Afterwards, DNA was visualised under UV light. For preparative use, the DNA fragments were isolated and purified using the Gel Cleanup Kit.

Storage of positive clones

For storage of positive clones, 30 µl overnight culture was inoculated in 3 ml LB–medium on an incubator shaker for 4-5 hours, until the cells reached the exponential phase of growing. Afterwards 850 µl culture were mixed with 150 µl glycerol solution and frozen directly in liquid nitrogen. Finally aliquots were stored at –80 °C.

2.3.1.5 Cloning of MAG(d1-3) into pSS26b

Recovery of plasmid DNA containing the SNAP-tag Gene

The plasmid containing the SNAP-tag gene was obtained from Covalys. A total of 100 µl TE buffer (10 mM mM Tris(hydroxymethyl)-aminomethan, 0.1 mM EDTA, pH 8.0, autoclaved) was added to the clone saver punch. After 15 min incubation at RT the solution was gently mixed by pipetting up and down, transferred to a sterile vial and stored at –20 °C.
For transformation into *E.coli* the DNA was diluted 10 fold with TE buffer. 0.5 and 1 µl diluted solution were used for transformation of pSS26b into DH5α by electroporation. Clones were picked and cultured overnight. The plasmid DNA was purified using the Genelute™ Plasmid Miniprep Kit and eluted in 70 µl elution buffer

Amplification of MAG(d1-3) out of pIgMAG(d1-3)

The plasmid pIgMAG(d1-3) containing the DNA sequence of the 3 *N*-terminal extracellular domains of MAG was obtained from Prof. Sørge Kelm. Primers were purchased from Microsynth if not indicated differently. Primers were dissolved in sterile ddH_20 to a 200 µM stock solution and further diluted to a 20 µM working solution. REDTaq™ DNA-polymerase from Sigma and pfu DNA-polymerase from Promega were used for PCR if no indicated differently. The pfu-polymerase exhibits proofreading activity and therefore ensures high fidelity. PCRs were performed on the thermal cycler icycler™ (Bio-Rad). PCR products were purified using a PCR clean-up kit ™ from Sigma.
For ligation into the pSS26b plasmid containing the SNAP-tag gene, a *N*-teminal Xho I and a *C*-terminal Hind III cleavage site were introduced in the primers. *N*-terminal primer extensions for higher cleavage activity were incorporated as proposed by New England Biolabs 2000/01 (presented in green).

Fw_MAG:

5’ CCGCTCGAGGGCCACTGGGGTGCCTGGAT 3’

CTCGAG Xho I cleavage site

Tm = (G + C) * 4 + (A + T) * 2 = 68 °C

Rw_MAG:

5’ CCCAAGCTTTGCATACATGACACTCAGCTCC 3’

AAGCTT Hind III cleavage site

Tm = (G + C) * 4 + (A + T) * 2 = 66 °C

First, a PCR was carried out using REDTaq DNA-polymerase to screen for optimal conditions (*table 17*).

Table 17. PCR with REDTaq™ DNA-polymerase to screen for optimal conditions

Reagent	Quantity (µl)	Temperature (°C)	Time (min)	N° of cycles
Sterile ddH_2O	39	Hold: 94	4	
10 mM PCR dNTP Mix	1	Denaturation: 94	0:30	30
5‘ primer	1	Annealing: Temperature graduation 59.3, 62.1, 63.9, 65	1	
3‘ primer	1			
Template (mini-prep)	1			
PCR buffer, 10x	5	Elongation	1	
Taq-polymerase	2	Final elongation: 72	5	

Two different template concentrations were used (1:10 and 1:100) and a blank was included missing the template.

To obtain a sequence suitable for cloning a second PCR was conducted with a pfu-polymerase that exhibits higher fidelity than the taq-polymerase (*table 18*).[168]

Table 18. PCR with Pfu DNA-polymerase for higher fidelity.

Reagent	Quantity (µl)	Temperature (°C)	Time (min)	N° of cycles
Sterile ddH_2O	40	Hold: 94	3	
10 mM PCR dNTP Mix	1	Denaturation: 94	1	30
5‘ primer	1	Annealing: Temperature graduation 59.3, 62.1, 63.9, 65	1:30	
3‘ primer	1			
Template	1			
PCR buffer, 10x	5	Elongation	2	
Pfu-polymerase	1	Final elongation: 72	10	

Double-Digest of MAG(d1-3) insert

All enzymes utilized for digestion were obtained from New England Biolabs except Hind III that was purchased from Roche Applied Science. Digestion of DNA was performed in an incubator overnight or in a thermomixer (eppendorf) for shorter incubation times.

Table 19. Mixture for a double-digest of MAG(d1-3)

Reagent	Quantity (µl)
PCR product table 18	100.0
Buffer 2 10x	14.0
BSA 10x	14.0
Xho I	4.0
Hind III	4.0
ddH_2O	4.0

The mixture (*table 19*) was incubated overnight at 37 °C.

Double-Digest of pSS26b vector

Table 20. Mixture for a double-digest of pSS26b

Reagent	Quantity (µl)
pSS26b mini prep	50.0
Buffer 2 10x	7.0
BSA 10x	7.0
Xho I	2.0
Hind III	2.0
ddH_2O	2.0

The mixture (*table 20*) was incubated overnight at 37 °C.

Dephosphorylation of digested pSS26b

Removing the 5' phosphate from both ends of a double-stranded DNA molecule (e.g. cloning vector) renders such molecules resistant to DNA ligase. However, phosphorylated experimental DNA can be ligated to dephosphorylated vector DNA. Thus, dephosphorylation provides a mechanism for reducing the potential background of re-circularized vectors in cloning experiments.[169] A suitable Shrimp alkaline phosphatase was purchased from Promega.

Table 21. Dephosphorylation of digested pSS26b

Reagent	Quantity (µl)
pSS26b (table 20)	70.0
Shrimp alkaline phosphatase (SAP)	1.5
SAP buffer	8.0
ddH_2O	0.5

The mixture (*table 21*) was incubated for 1 hour at 37 °C, then the enzyme was heat-inactivated at 65 °C for 15 min.

Ligation of MAG(d1-3) into pSS26b

The T4 DNA Ligase catalyzes the formation of a phosphodiester bond between juxtaposed 5' phosphate and 3' hydroxyl termini in duplex DNA/RNA. This enzyme will join blunt end and cohesive end termini as well as repair single stranded nicks in duplex DNA, RNA or DNA/RNA hybrids.[169] The T4 DNA ligase was obtained from NEB.

Table 22. Ligation of MAG(d1-3) into pSS26b

Reagent	Quantity (µl)
MAG(d1-3) digested (table 19)	2.0
pSS26b digested and dephos (table 21)	1.0
Buffer T4 DNA Ligase	1.0
10mM ATP	1.0
T4 DNA Ligase	1.0
ddH_2O	4.0

Ligation (*table 22*) was done overnight in a water bath which cooled slowly down from room temperature to 4 °C passing the optimal ligation temperature. To desalt the ligation product before electroporation, a dialysis was performed for 30 min using a 0.025 mm membrane. Afterwards, the plasmid was transformed into DH5α cells by electroporation (*p. 88*).

Digest analysis of pSS26b-MAG(d1-3)

Table 23. Ligation of MAG(d1-3) into pSS26b

Reagent	Quantity (µl)
pSS26b_MAG(d1-3) mini prep	10.0
Buffer 2 10x	2.0
BSA 10x	2.0
Xho I	1.0
Hind III	1.0
ddH_2O	4.0

The mixture (*table 23*) was incubated overnight at 37 °C. A blank was included missing the digestion enzymes.

2.3.1.6 Cloning of MAG(d1-3)-SNAP / SNAP into pFastBac-S

Amplification of MAG(d1-3)-SNAP and SNAP

For ligation into the pFastBacSS plasmid, a *N*-teminal Xba I and a *C*-terminal XhoI cleavage site were introduced in the primers. *N*-terminal primer extensions for higher cleavage activity were included as proposed in the product catalogue of New England Biolabs 2000/01 (presented in green).

Primer sequences:

Fw_MAG_XbaI:
5’GCTCTAGAGGCCACTGGGGTGCCTGGAT3’
TCTAGA (XbaI cleavage site)
Tm = (G + C)*4 + (A + T)*2 = 68 °C

FW_SNAP_XbaI:

5’ GCTCTAGAATGGACAAAGATTGCGAAATGA 3’

TCTAGA (Xba I cleavage site)

Tm = (G + C)*4 + (A + T)*2 = 66 °C

Rw_SNAP_FLAG_XhoI:

5’CCGCTCGAGCTATTACTTATCGTCATCGTCCTTGTAGTCTCCCAGACCCG GTTTACCCAG3’

CTCGAG (Xho I cleavage site)

CTATTA (stop codon)

CTTATCGTCATCGTCCTTGTAGTC (FLAG-tag)

Tm = (G + C)*4 + (A + T)*2 = 68 °C

Table 24. PCR setup for MAG(d1-3)-SNAP amplification

Reagent	**Quantity (µl)**	**Temperature (°C)**	**Time (min)**	**N° of cycles**
Sterile ddH_2O	40	Hold: 94	3	
10 mM PCR dNTP Mix	1	Denaturation: 95	1	35
5‘ primer: FW-MAG	1	Annealing Temperature: 55	1:30	
3‘ primer: RW-SNAP	1			
Template: clone 14	1			
PCR buffer, 10x	5	Elongation: 72	2	
pfu-polymerase	1	Final elongation: 72	10	

Table 25. PCR setup for SNAP amplification

Reagent	Quantity (µl)	Temperature (°C)	Time (min)	N° of cycles
Sterile ddH_2O	40	Hold: 94	3	
10 mM PCR dNTP Mix	1	Denaturation: 95	1	35
5‘ primer: FW-SNAP	1	Annealing Temperature: 55	1:30	
3‘ primer: RW-SNAP	1			
Template: clone 14	1			
PCR buffer, 10x	5	Elongation: 72	2	
pfu-polymerase	1	Final elongation: 72	10	

Both PCRs (*table 24 and 25*) were carried out using a hot start.

Double digest of pFastBac-S, MAG(d1-3)-SNAP and SNAP inserts

Table 26. Digest of MAG-SNAP and SNAP

Reagent	Quantity (µl)
MAG(d1-3)-SNAP or SNAP mini-prep	80.0
Buffer 2 10x	10.0
BSA 100x	1.0
Xho I	2.0
Xba I	2.0
Sterile ddH_2O	5.0

Table 27. Digest of pFastBac

Reagent	Quantity (µl)
pFastBac_S mini-prep	40.0
Buffer 2 10x	6.0
BSA 10x	6.0
Xho I	2.0
Xba I	2.0
ddH_2O	4.0

The mixtures (*table 26 and 27*) were incubated overnight at 37 °C.

Dephosphorylation of digested pFastBac-S

Table 28. Deposphorylation of pFastBac-S

Reagents	Quantity (µl)
pFastBac_S digested (table 27)	70.0
Shrimp alkaline phosphatase (SAP)	1.5
SAP buffer	8.0
ddH_2O	0.5

The mixture (*table 28*) was incubated for 1 hour at 37 °C, then the phosphatase was heat-inactivated at 65 °C for 15 min.

Ligation of MAG(d1-3)-SNAP and SNAP into pFastBac-S

Table 29. Mixtures for ligation of MAG(d1-3)-SNAP and SNAP into pFast-Bac-S

Reagents	Quantity (µl)
MAG(d1-3)_SNAP or SNAP	2.0
PFastBac-S (table 28)	0.5
Buffer T4 DNA Ligase	1.0
10mM ATP	1.0
T4 DNA Ligase	1.0
ddH_2O	4.5

Ligation (*table 29*) was done overnight in a water bath which cooled slowly down from room temperature to 4 °C passing the optimal ligation temperature. To desalt the ligation product, a dialysis was done for 1 h with a 0.025 mm membrane. Afterwards, the plasmid was transformed into DH5α cells by electroporation (*p. 88*).

Digest analysis of pFastBac-S-MAG(d1-3)-SNAP and -SNAP

Table 30. Successful ligation was checked by digest analysis.

Reagents	Quantity (µl)
MAG(d1-3)-SNAP or SNAP	10.0
Buffer 2 10x	2.0
BSA 100x	0.2
Xho I	1.0
Xba I	1.0
ddH_2O	6.0

The mixtures (*table 30*) were incubated overnight at 37 °C. 5 µl of digest product were mixed with 5 µl ddH_2O and 1 µl loading buffer. DNA analysis was carried out on an agarose gel.

2.3.1.7 Growth and culture of insect cells

Sf-900 II SFM with L-glutamine, Express Five SFM and all additives for culturing insect cells were purchased from Gibco (Invitrogen). Sf-900 II SFM is a protein-free medium which supports increased cell growth of a variety of insect cell lines as well as significantly increased production of recombinant protein using the baculovirus expression vector system (BEVS). Express Five is a protein-free medium, which supports increased cell growth of High Five insect cells as well as significantly increased production of recombinant protein using the BEVS. Cell cultures were propagated either as an adherent or a suspension culture in an Innova 4230 Incubater (New Brunswick Scientific). Cell culture grade DMSO was purchased from Sigma.
Shaker cultures of High Five™ and Sf9 cells were grown in sterile 250 ml Erlenmeyer flasks, covered with cotton and tin foil, in 30 ml medium on an incubator shaker maintained at 122 rpm and 27 °C. A viability test was done with trypan blue stain 0.4% and cells were sub-cultured to $4 \bullet 10^5$ cells/ml twice a week.

2.3.1.8 Isolation and analysis of bacmid DNA

Isolation and analysis of bacmid DNA out of DH10Bac

All chemicals used were purchased from Sigma except SDS that was obtained from Bio-Rad.

Bacmid DNA was isolated using a standard procedure given by the manufacturer.[170] 1.5 ml of bacterial culture were transferred to an eppendorf tube and centrifuged at 14'000 g for 1 minute to pellet the cells. The supernatant was removed and the pellets were re-suspended in 0.3 ml of Solution I (15 mM Tris, 10 mM EDTA, 100 μg/ml RNase A, pH 8.0, filter-sterilized) by gently pipetting up and down.

Afterwards, 0.3 ml of Solution II (0.2 M NaOH, 1% SDS, filter-sterilized) were added by mixing gently. The mixture was incubated at room temperature for 5 minutes. Subsequently, 0.3 ml of sterile 3 M potassium acetate pH 5.5 were added and gently mixed. A thick white precipitate of protein and *E. coli* genomic DNA was formed. The sample was placed on ice for 7 minutes and then centrifuged for 10 minutes at 14'000 g. The resulting supernatant (without any white precipitate) was transferred to an eppendorf tube containing 0.8 ml of isopropanol. The tube was inverted a few times to mix and placed on ice for 7 minutes. After centrifugation for 15 minutes at 14,000 g at room temperature the supernatant was removed. 0.5 ml of 70% ethanol was added and the tube was inverted several times and centrifuged for 5 minutes at 14,000 g at room temperature. The supernatant was removed and the pellet air-dried for 7 minutes at room temperature. The pellet was dissolved in 40 μl TE buffer by gentle tapping against the bottom. Finally the bacmid was stored at +4 °C

PCR analysis of bacmid DNA MAG(d1-3)-SNAP and SNAP

Table 31. PCR analysis of bacmid DNA

Reagent	Quantity (µl)	Temperature (°C)	Time (min)	N° of cycles
Sterile ddH_2O	39	Hold: 93	3	
10 mM PCR dNTP Mix	1	Denaturation: 94	0:45	30
5‘ primer:	1	Annealing Temperature: 55	0:45	
3‘ primer:	1			
Template: bacmid	1			
PCR buffer, 10x	5	Elongation: 72	5	
taq-polymerase	2	Final elongation: 72	7	

The PCR (*table 31*) was performed with a Hot-Start.

2.3.1.9 Transfection of bacmid DNA into insect cells

Transfection was carried out with common sf9 cells. The transfection reagent Cellfectin, a 1:1.5 (M/M) liposome formulation of the cationic lipid *N*, *N*I, *N*II, *N*III-Tetramethyl-*N*, *N*I, *N*II, *N*III-tetrapalmitylspermine (TM-TPS) and dioleoyl phosphatidylethanolamine (DOPE), was purchased from Invitrogen. 6-well tissue culture plates were used for transfection.

First $1 \bullet 10^6$ cells in 2 ml growth medium were seeded in a well and incubated for 2 hours at 27 °C to let the cells attach to the well. 30 µl bacmid DNA was mixed with 100 µl sf900 II SFM without antibiotics (solution A). Then 6 µl cellfectin reagent was mixed with 100 µl sf900 II SFM without antibiotics (solution B). Solution B was added to solution A and incubated for 30 min at RT (solution C). Afterwards 0.8 ml of sf900 II SFM (no antibiotics) was added to C (solution D). The medium was removed from the cells and solution D was added. After 5 hours of incubation at 27 °C, transfection mix was removed from the cells and replaced by 2 ml fresh sf900 II

SFM. Cells were checked for signs of infection till 5 days post-transfection. After 5 days the media was collected, centrifuged (500 g, 5 min., 4 °C) and stored at 4 °C. The obtained solution was referred to as the P1 viral stock. For protein expression the viral stock was amplified.

2.3.1.10 Amplification of P1 viral stock

For amplification of the P1 viral stock, 75 cm^2 culture flasks were used. A total of $3 \cdot 10^6$ sf9 cells were seeded in a 75 cm^2 culture flask with a final volume of 13 ml. After 1 h the cells had attached and 1 ml of P1 viral stock was added to the cells. After 5 days the medium was collected, centrifuged (500 g, 5 min., 4 °C) and stored at 4 °C.

2.3.1.11 Evaluation of insect cell lines for espression

Viral stocks from both MAG-SNAP and SNAP were used to infect sf9 and H5 cells. Expression was carried out in sf900 II SFM.
For expression of SNAP and MAG-SNAP, a 30 ml suspension culture at a density of $1 \cdot 10^6$ cells/ml was infected with 2 ml of P2 viral stock. Samples were taken after 24, 48 and 120 h for SNAP and 24, 48, 72 and 120 h for MAG-SNAP respectively. Analyses of obtained samples by SNAP-vista and western blot were conducted.

2.3.1.12 Purification of FLAG-tag Proteins

For affinity chromatography, ANTI-FLAG M2 Affinity gel from Sigma (Fluka) was filled into a 2 ml Bioscale MT-2 column (Bio-Rad). The entire purification of the FLAG-tag constructs was carried out on a BioLogic Chromatography system (Bio-Rad).
Purification steps were carried out at 4 °C. The supernatant obtained from expression in insect cells was cleared from cell debris by centrifugation at 22'000 rpm for 20 min. In addition, the centrifuged supernatant was filtered using a 0.20 μm Minisart

(Sartorius) prior to purification. The *pH* of the final filtrate was adjusted to 7.4 using 1 M Tris *pH* 8.0 to obtain optimal binding to the column. All purification steps were carried out at a flow-rate of 1 ml/min. The column was first equilibrated with PBS (50 mM phosphate, 150 mM NaCl, *pH* 7.4) for 20 minutes. The supernatant was loaded onto the column followed by a 60 min. wash step. Elution was performed with a 100 mM glycine buffer *pH* 3.5 during 15 minutes. Aliquots of 1 ml were collected and the pH was immediately corrected to neutral using 1 M Tris *pH* 8.0. Afterwards the column was immediately re-equilibrated to neutral *pH* using PBS. Fractions were checked for protein and purity on SDS-PAGE using enhanced coomassie staining.[171]
If the column was re-used within 24 h, equilibration in storage buffer (PBS, 0.02 % sodium azide) for 20 min. was conducted to avoid microbial growth and stored at 4°C. For long-term storage, 10 % glycerol was added to the storage buffer to protect the resin from degradation.

2.3.1.13 Buffer exchange and sample concentration

Due to known stability of MAG in 10 mM PBS, the buffer of both SNAP-tag and MAG-SNAP-tag was exchanged to PBS after purification. Additionally, the concentration was increased to allow testing different concentrations for immobilization.
PBS (10 mM sodium phosphate, *pH* 7.4, 150 mM NaCl) was prepared, filtered and stored at 4 °C. Buffer exchange and sample concentration was carried out with centrifugal filter devices Amicon Ultra-4 (Millipore). All centrifugation steps were performed at 4 °C using 4’000 g. First, the filter device was washed once with 4 ml of PBS. Then a maximum of 4 ml of sample was applied. The final concentrated sample was washed twice using 4 ml of PBS.

2.3.1.14 Western blot of FLAG-tagged proteins

The blotting was performed using the trans-blot SD semi-dry transfer cell (Bio-Rad). The nitrocellulose (NC) membrane as well as the whatman paper was purchased from Bio-Rad. The primary antibody ANTI-FLAG M2 and the secondary antibody Anti-Mouse IgG (Fc specific)-alkaline phosphatase were obtained from Sigma. The alkaline phosphatase substrate mixture 5-bromo-4-chloro-3-indolyl phosphate dipotassium (BCIP), nitrotetrazolium blue chloride (NBT) was purchased from Fluka. For blotting, eight pieces of whatman paper and one NC membrane were incubated in transfer buffer (25 mM Tris, 150 mM glycine, 20% (v/v) methanol). Four whatman papers were placed on the anode followed by the NC-membrane, the SDS-PAGE gel, additional 4 papers and the cathode. Transfer was carried out for 1 h applying 15 V.
After the transfer the membrane was stained with ponceau S solution to visualize the marker and verify transfer. Afterwards the membrane was washed with TBS (10 mM Tris, 150 mM NaCl, *pH* 7.5) for 10 min. Then the membrane was blocked for 15 min. with blocking buffer (2% BSA). Afterwards, 3 washing steps were done (2•TTBS (TBS with 0.05% Tween 20), 1•TBS) for 10 min. each. Subsequently, the membrane was incubated with the primary antibody (1:2'000 in TBS, 1% BSA, 0.1% sodium azide) for either 1 h at RT or over night at 4°C. Additional 3 washing steps were carried out before incubation with the secondary alkaline phosphatase coupled antibody (1:5'000 in TBS, 1% BSA, 0.1% sodium azide) for 1 h at RT. After additional 3 washing steps the complex was visualized with BCIP/NBT.

2.4 Mammalian cells as expression system

The entire DNA sequence of the MAG(d1-3)-SNAP construct is listed in *appendix II*.

Cloning of SNAP into pcDNAIII-Strep

The pcDNAIII-Strep plasmid containing a Strep-tag was kindly obtained from Dr. Frank Dietz. All cloning and expression were carried out in the Centre for Biomolecular Interactions Bremen. For cloning SNAP into the pDNAIII-Strep plasmid, an *N*-teminal Bam HI cleavage site including a 3C protease cleavage site and a *C*-terminal Eco RI cleavage site were introduced. Primer extensions for higher cleavage activity were included as proposed by New England Biolabs 2000/01.

OSK 1043:

5’CGGGATCCCTGGAGGTGCTGTTCCAGGGCCCCATGGACAAAGATTGCG AAATGA 3’

GGATCC Bam HI cleavage site

OSK 1044:

5’ CGGAATTCTCCCAGACCCGGTTTACCCAG 3’

AAGCTT Eco RI cleavage site

Table 32. PCR performed with pfu™ DNA-polymerase.

Reagent	**Quantity (µl)**	**Temperature (°C)**	**Time (min)**	**N° of cycles**
Sterile ddH_2O	41.0	Hold: 95	4	
10 mM PCR dNTP Mix	1.0	Denaturation: 95	0:30	30
5‘ primer (OSK 1043)	0.5	Annealing: 62	1	
3‘ primer (OSK 1044)	0.5			
pSS26b	1.0			
PCR buffer, 10x	5.0	Elongation: 72	1:20	
pfu-polymerase	1.0	Final elongation: 72	5	

The primer concentration was adjusted to 100 pmol/µl. A master mix was prepared for three samples and divided prior to PCR (*table 32*). pSS26b was used as template with a concentration of 2 µg/ml. A total of 50 µl plasmid solution with a concentration of 140 ng/µl was obtained.

Double-Digest of SNAP insert

Table 33. Digest of the amplified SNAP gene

Reagent	Quantity (µl)
PCR product (table 32)	45.0
Tango buffer 10x	14.0
Bam HI	2.0
Eco RI	1.5
ddH_2O	7.5

The mixture (*table 33*) was incubated overnight at 37°C.

Ligation of SNAP into pcDNAIII

Table 34. Ligation of the SNAP gene into pcDNAIII

Reagent	Quantity (µl)
pcDNAIII-Strep 10 ng/µl	2.0
SNAP insert 10 ng/µl (table 33)	1.5
Ligation buffer 5x	3.0
T4 ligase	1.0
ddH_2O	7.5

The ligation mixture (*table 34*) was incubated for 2 h at RT.

Colony PCR

Table 35. Colony PCR for positive clone selection

Reagent	**Quantity (µl)**	**Temperature (°C)**	**Time (min)**	**N° of cycles**
Sterile ddH_2O	19.9	Hold: 95	3	
10 mM PCR dNTP Mix	0.5	Denaturation: 95	0:30	30
5‘ primer T7 100 pM	0.25	Annealing: 56	1	
3‘ primer Sp6 100 pM	0.25			
Single clones picked				
PCR buffer, 10x	2.5	Elongation: 72	1:30	
$MgCl_2$	1.5	Final elongation: 72	3	
taq-polymerase	0.1			

DNA loading buffer (10 µl) was added to each finished PCR reaction (*table 35*). Marker (10 µl) and 20 µl of each sample were mixed and loaded onto an agarose gel.

Transfection of pcDNAIII-SNAP into Cos-7 cells

The transfection reagent Exgen 500 was purchased from fermentas.
A total of 1 µg of isolated plasmid from positive clones was added to 95 µl 150 mM NaCl and 2.2 µl Exgen 500. The mixture was incubated for 10 min at RT. A 24 well plate with 80% confluent Cos-7 cells in DMEM media containing 2% FCS was used and 1 well was transfected with each clone.

Harvest and analysis of transfected Cos-7 cells

The cells were harvested after 24 h and analyzed for protein production. The medium was removed and cells were washed twice with PBS. The cells were boiled in 50 µl sample buffer containing DTT at 95 °C for 10 min. The samples (20 µl) were run on

a SDS-PAGE and finally analyzed with western blot using a primary anti-Strep antibody with a secondary horseradish peroxidase labelled antibody (pierce).

2.4.1 Cloning of MAG(d1-3) into pcDNAIII-SNAP

Amplification of MAG(d1-3)

For cloning *MAG(d1-3)* into the pcDNAIII-SNAP plasmid, an *N*-teminal Hind III and a *C*-terminal Bam HI cleavage site were introduced. Primer design included the natural MAG signal sequence for secretion. At the *N*-terminus, an additional Xba I cleavage site was included to allow direct ligation into a pDEF vector for stable expressing clones.

OSK 1051:
5'CGAAGCTTATATCTAGAATGATATTCCTCGCCACCCT 3'
AAGCTT Hind III cleavage site
TCTAGA Xba I cleavage site

OSK 1052:
5' CGGGATCCTCCTGCATACATGACACTCAGCT 3'
GGATCC Bam HI cleavage site

Table 36. PCR setup for MAG(d1-3) amplifikation

Reagent	Quantity (µl)	Temperature (°C)	Time (min)	N° of cycles
Sterile ddH_2O	41	Hold: 95	4	
10 mM PCR dNTP Mix	1	Denaturation: 95	0:30	30
5‘ primer OSK 1051 100 pM	0.5	Annealing: 58	1	
3‘ primer OSK 1052 100 pM	0.5			
pigBos-MAG(d1-3) 100 ng/µl	1			
PCR buffer, 10x	5	Elongation: 72	1:20	
pfu-polymerase	1	Final elongation: 72	5	

PCR (*table 36*) was carried out using a hot-start.

Double-Digest of MAG insert and pcDNAIII-SNAP

Table 37: Digest of MAG(d1-3) insert

Reagent	Quantity (µl)
PCR product (table 36)	45.0
Bam HI buffer	6.0
Bam HI	1.5
Hind III	2.5
ddH_2O	5.0

Table 38. Digest of pcDNAIII-SNAP

Reagent	Quantity (µl)
pcDNAIII-SNAP	60.0
Bam HI buffer	8.0
Bam HI	2.5
Hind III	3.5
ddH_2O	6.0

The mixtures (*table 37 and 38*) were incubated overnight at 37°C.

Ligation of MAG(d1-3) into pcDNAIII-SNAP

Table 39. Ligation of MAG(d1-3) into pcDNAIII-SNAP

Reagent	Quantity (µl)
pcDNAIII-SNAP 10 ng/µl	2.0
MAG(d1-3) insert 10 ng/µl	2.0
Ligation buffer 5x	3.0
T4 ligase	1.0
ddH_2O	7.0

The ligation mixture (*table 39*) was incubated for 2 h at RT.

Colony PCR

Table 39. Colony PCR setup

Reagent	Quantity (µl)	Temperature (°C)	Time (min)	N° of cycles
Sterile ddH_2O	19.9	Hold: 95	3	
10 mM PCR dNTP Mix	0.5	Denaturation: 95	0:30	30
5‘ primer T7 100 pM	0.25	Annealing: 56	1	
3‘ primer Sp6 100 pM	0.25			
Clone x				
PCR buffer, 10x	2.5	Elongation: 72	1:30	
$MgCl_2$	1.5	Final elongation: 72	3	
taq-polymerase	0.1			

A total of 10 µl DNA loading buffer was added to each finished PCR reaction (*table 39*). Then, 10 µl marker and 20 µl of each sample were loaded onto an agarose gel.

Digest analysis of MAG(d1-3) plasmids

Table 40. Digest analysis of MAG(d1-3) plasmids

Reagent	Quantity (µl)
plasmid	5.0
Tango buffer	1.0
Xba I	0.5
ddH_2O	3.5

The mixture (*table 40*) was incubated overnight at 37 °C.

Transfection of pcDNAIII-MAG(d1-3)-SNAP into Cos-7 cells

Plates were prepared with 80 % confluent Cos-7 cells and 2 % FCS in DMEM media. A total of 10 µg of midi-prep plasmid DNA was added to 970 µl 150 mM NaCl and 20 µl Exgen 500. The mixture was incubated for 10 min at RT. A total of 5 plates with a diagonal of 10 cm were transfected with each clone.

Harvest and analysis of COS-7 supernatant

Strep-Tactin beads and Strep-tag antibody were purchased from IBA. The collected supernatant was incubated with such Strep-Tactin beads over night at 4 °C under constant rotation. The beads were centrifuged at 2'000 rpm and the supernatant was discarded. The beads were washed 4 times with cold PBS. Finally, the beads were heated for 10 min at 95 °C in non-reducing sample buffer to elute MAG-SNAP. The beads were centrifuged at 5'000 rpm and the supernatant was collected. The samples were analyzed under reducing and non-reducing conditions on a western-blot using an anti-Strep-tag antibody.

2.5 Enzymatic immobilization

2.5.1 Evaluation of immobilization conditions

2.5.1.1 Testing of different SNAP substrates

SNAP-tag protein expressed and purified as described with a concentration of 140 µg/ml and 340 µg/ml was used for screening a set of BG substrates. All substrates were obtained from Covalys and immobilized on standard CM5 sensor chips using amine coupling and HBS-N buffer. DMSO was purchased from Fluka.

A 33 mM stock solution in DMSO was prepared of all substrates. Additionally, a 5 mM carboxy-BG stock solution was prepared in a 30% DMSO 1 M $NaHCO_3$ mixture to evaluate described solubility problems. Experiments were carried out in HBS-N as running buffer. A CM5 sensor chip was preconditioned as described. The carboxy groups on the chip were activated for 10 minutes with a 1:1 mixture of 0.1 M *N*-hydroxysuccinimide (NHS) and 0.1 M 3-(*N*,*N*-dimethylamino) propyl-*N*-ethylcarbo-di-imide (EDC) at a flow rate of 10 µl/min. Stock solutions were diluted with HBS-N buffer to 1 or 2 mM concentration. These solutions were then injected over the activated surface for 10 or 20 min at the flow rate of 1 or 10 µl/min. Afterwards the flow cells were blocked with a 10 min injection of 1 M ethanolamine, *pH* 8.0.

After immobilization of the substrates the system was primed once before usage. SNAP-tag was injected over the modified surface at a flow rate of 1 µl/min. The velocity and the final level of immobilized protein were evaluated.

2.5.1.2 Testing of different SNAP concentrations

SNAP-tag protein with a concentration of 125 µg/ml was expressed and purified as described. The sample was used for screening different concentrations.

The influence of the concentration of SNAP-tag on immobilization velocity was tested. A 33 mM stock solution of **BG-PEG$_{12}$** in DMSO was used. Immobilization of the substrate was performed in parallel on all flow cells. Experiments were carried out in HBS-P as running buffer. A CM5 sensor chip was preconditioned as described.

The carboxy groups on the chip were activated for 10 minutes with a 1:1 mixture of 0.1 M *N*-hydroxysuccinimide (NHS) and 0.1 M 3-(*N*,*N*-dimethylamino) propyl-*N*-ethylcarbo-di-imide (EDC) at a flow rate of 10 µl/min. The DMSO stock solution was diluted with HBS-N buffer to a 1 mM concentration. This solution was then injected over the activated surface for 5 min at the flow rate of 10 µl/min. Afterwards the flow cells were blocked with a 10 min injection of 1 M ethanolamine, *pH* 8.0.
After immobilization of the substrate the system was primed once. The SNAP-tag sample was diluted twice 1:2 with 10 mM PBS to obtain two lower concentrations. The samples were injected sequentially for 150 min at a flow rate of 1 µl/min on the corresponding flow cell (Fc2: 62.5 µg/ml, Fc3: 31.25 µg/ml, Fc4: 125 µg/ml). The velocity and the final level of immobilized protein were evaluated.

2.5.1.3 Testing of different substrate immobilization times

SNAP-tag protein expressed and purified as described with a concentration of 40 µg/ml was used for screening different substrates immobilization times.
A 33 mM stock solution of **BG-PEG$_{12}$** in DMSO was used. Immobilization of the substrate was performed sequentially on flow cell 2 and 3. All experiments were carried out in HBS-P as running buffer. A CM5 sensor chip was preconditioned as described. The carboxy groups on the chip were activated for 10 minutes with a 1:1 mixture of 0.1 M *N*-hydroxysuccinimide (NHS) and 0.1 M 3-(*N*,*N*-dimethylamino) propyl-*N*-ethylcarbo-di-imide (EDC) at a flow rate of 10 µl/min. The DMSO stock solution was diluted with HBS-N buffer to a 1 mM concentration. This solution was then injected over the activated surface for 5 min (Fc2) or 20 min (Fc3) at the flow rate of 10 µl/min. Afterwards the flow cells were blocked with a 10 min injection of 1 M ethanolamine, *pH* 8.0.
After immobilization of the substrate the system was primed once before injection of the SNAP-tag. Two sequential injections for 150 min at the flow rate of 1 µl/min were performed. The velocity and the final level of immobilized protein were evaluated. In addition, the second injection was utilized to monitor a potential loss of enzyme activity during the 150 min injection time at 25 °C.

2.5.1.4 Preparation of a BG-PEG$_{12}$ sensor chip

Immobilization was carried out in HBS-P or HBS-N as running buffer. A CM5 sensor chip was preconditioned as described. If desired all flow cells were prepared in a single step. The carboxy groups on the chip were activated for 10 minutes with a 1:1 mixture of 0.1 M *N*-hydroxysuccinimide (NHS) and 0.1 M 3-(*N*,*N*-dimethylamino) propyl-*N*-ethylcarbo-di-imide (EDC) at a flow rate of 10 µl/min. The DMSO stock solution of **BG-PEG$_{12}$** was diluted with HBS-N buffer to a 2 mM concentration. This solution was then injected over the activated surface for 20 min at the flow rate of 1 µl/min. Afterwards the flow cells were blocked with a 10 min injection of 1 M ethanolamine, *pH* 8.0. After immobilization of the substrates the system was primed once before injection of the SNAP-tag.

2.5.1.5 Comparison of SNAP and MAG(d1-3)-SNAP

SNAP (170 µg/ml) and MAG(d1-3)-SNAP (290 µg/ml) expressed in insect cells and purified as described were used for immobilization. In addition, insect cell culture supernatant with an estimated SNAP concentration of 4 µg/ml was used for direct immobilization. The anti-FLAG M2 monoclonal antibody was purchased from Sigma.

A **BG-PEG$_{12}$** surface was prepared as described (*2.5.1.4*). Purified MAG(d1-3)-SNAP was injected for 150 min at a flow rate of 1 µl/min. To created equal molar surfaces SNAP was injected for 10 min. Insect cell culture supernatant containing SNAP was injected for 100 min at a flow rate of 1 µl/min.

To finally compare immobilization levels quantitatively, a monoclonal anti-FLAG antibody was utilized. A concentration of 290 nM was injected for 1 min and levels obtained were compared.

Additionally, the antibody was characterized to ensure saturation level at 290 nM. Interaction experiments were performed in HBS-EP at a flow rate of 20 µl/min. Starting at 290 nM, 8 concentrations of a twofold dilution series were prepared. To

remove the remaining antibody after binding a 15 sec. injection of glycine pH 1.5 was necessary. Association and dissociation were monitored for 1 min.

2.5.1.6 MAG(d1-3)-SNAP expressed in mammalian cells

The monoclonal anti-MAG antibody was a kind gift from Dr. Frank Dietz. Expression of MAG(d1-3)-SNAP was done in CHO cells on 10 cm plates. The supernatant was concentrated by a factor of 16. A **BG-PEG$_{12}$** surface was prepared as described (*p. 115*) and a direct immobilization was performed. A monoclonal anti-MAG antibody (0.6 mg/ml) was diluted 100 fold in running buffer and injected for 60 s at 20 µl/min.

Interaction experiments with **SH-136** were performed in HBS-EP at a flow rate of 20 µl/min. A total of 10 concentrations of a twofold dilution series, starting at 400 µM, were prepared. The samples were injected in triplicates in a randomized order. Five blank buffer injections were performed before and one after the experiment. Association and dissociation were monitored for 1 min.

3 RESULTS AND DISCUSSION

3.1 GSLA-2 as a model system for carbohydrate/lectin interactions

Antibodies were among the first proteins to be analyzed on SPR-based biosensors.[172] They have drawn increased interest in pharmaceutical companies where the market of therapeutic antibodies increased by 30% annually since 2000.[173] Therapeutic antibodies like Herceptin, Humera, Avastin and Xolair are among the most well known ones. Antibodies are extensively screened on SPR-based biosensors for their kinetic characterization and in 2005 a total of 151 papers were published.[145]

For SPR-based biosensors a clear advantage of antibodies as ligands are their high molecular weight that results in larger signals and the high affinity in the μM and nM range. Furthermore, immobilization of antibodies on biosensor chips was achieved with standard amine coupling. In general, antibodies are a straightforward system and can be used for training and validation.

GSLA-2 is a monoclonal antibody used for tumor diagnostics.[174] It recognizes the sialyl Lewis^a (sLe^a) epitope that has an increased occurrence on mucin type glycoproteins of patients with *e.g.* colon cancer.

3.1.1 Biosensor experiments with GSLA-2

3.1.1.1 Immobilization of GSLA-2 with amine coupling

pH and concentration scouting for amine coupling of GSLA-2

The first step for the coupling of proteins via their amine groups is the evaluation of immobilization conditions. By finding an optimal *pH*, a higher attraction to the carboxymethyl dextran matrix and, as a consequence, higher immobilization efficiency can be achieved (*p. 59*). In addition, an assessment of the optimal protein concentration allows the fine-tuning of the process. By adjusting concentration and *pH* the immobilization velocity can be optimized to permit a better controllability of the resulting immobilization level. Although the use of *pH* attraction is not a

necessity, it is usually applied to enable immobilization at lower protein concentrations, thus limiting sample consumption. Immobilization of a *pH* labile protein under physiological conditions (*pH* 7.4) was achieved with high concentrations (2 mg/ml).[154]

In general, proteins possess different conformations at different *pH* due to changes in intramolecular hydrogen bonding. The asialoglycoprotein for example elicits its physiological function via a *pH*-induced conformational change.[175,176] Although a protein can change back to its native state under physiological conditions, attachment to the carboxymethyl dextran matrix at several sites could diminish such rearrangements. Therefore one has to bear in mind that amine coupling could affect the proteins conformation.

Table 41. Surface attraction levels obtained for Fc-MAG(d1-3) at different pH values and concentrations.

pH	Response* (RU)
7.4	67
5.5	19'853
5.0	30'136
4.5	20'886
4.0	12'559

* at a concentration of 40 µg/ml

Concentration (µg/ml)	Response** (RU)
10	15'000
20	25'000
40	28'000

** at pH 5.0

The surface attraction was maximal at pH 5.0 (*table 41*). Higher concentrations led to an increased attraction, as expected. For lower concentrations, surface attraction decreased, but the velocity was slower what enables a better controllability of the final immobilization level. Nevertheless, a concentration of 40 µg/ml seemed to be optimal for sufficient attraction at *pH* 5.0 and was used for immobilization.

3.1.1.2 Binding assays with GSLA-2

For both sLe^a and sLe^a-Lem (Lem = $(CH_2)_8COOMe$) block signals were obtained displaying fast association and dissociation behaviour (*figure 32-A and C*). This is a typical kinetic for carbohydrate/protein interactions that are based on a fast recognition, but a weak interaction.[177,178] Injection of triplicates proved a high reproducibility and evaluation of the steady state demonstrated a perfect fit to a simple 1:1-binding site model (*saturation binding plot in figure 32-B and D*).

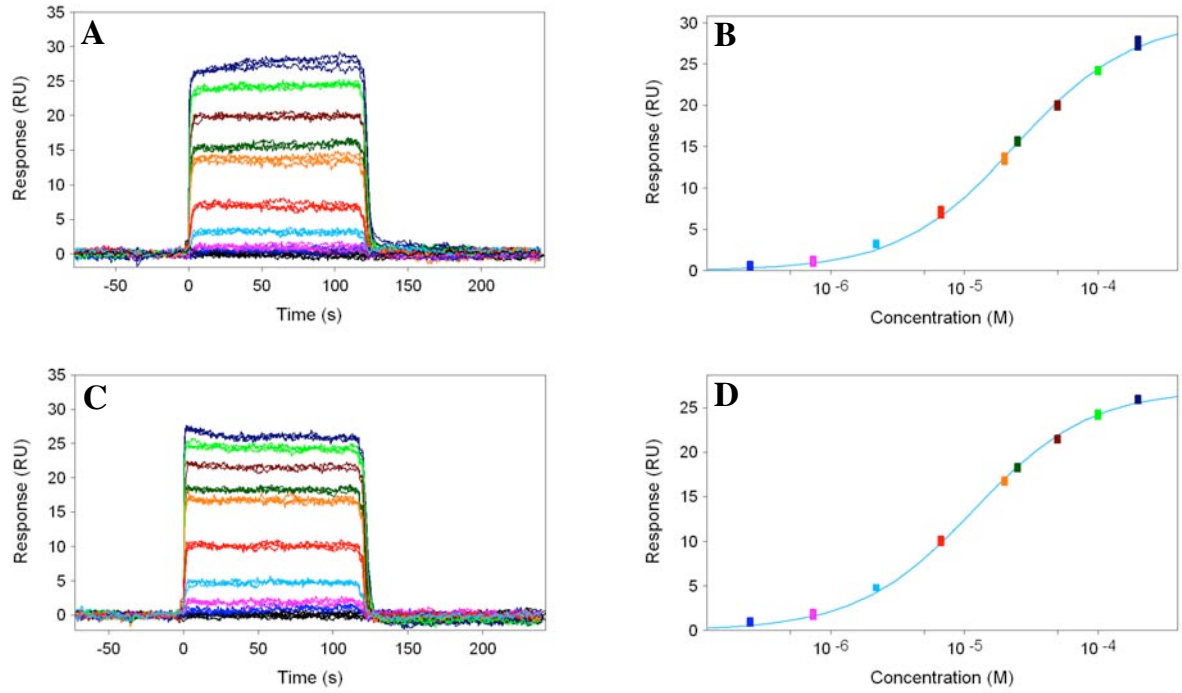

Figure 32. Sensorgrams and saturation binding plots for both sLe^a-Lem (A,B) and sLe^a (C,D).

A clear difference of the R_{max} values for the high (30 RU) and low (18 RU) capacity surface was observed that was consistent for both ligands (*table 42*). The surface capacity is referred to as the amount of protein immobilized. The calculated protein activity based on the R_{max} value displayed significant differences (*table 42*). The protein activity is calculated as the fraction of protein that is actually binding the ligand based on *equation 4 (p. 54)*. In both cases the activity was 10% higher for the low capacity (sLe^a-Lem: 36.4%, sLe^a 44.5%) than the high capacity surface (sLe^a-Lem: 25.6%, sLe^a 34.5%). The effect of higher activity on surfaces with lower amounts of protein was already described earlier.[179]

Even more interesting was the fact that signal intensity was in general 10% higher for sLe^a compared to sLe^a-Lem. Therefore, not only surface capacity but also the type of ligand had an influence on signal intensity. The observed phenomenon nicely highlighted that for small ligands the signal to molecular mass correlation is not exact. In the case of GSLA-2 a total deviation of approximately 20% was observed.

Table 42. Calculated activity for the high and low capacity surfaces.

Compound	Surface capacity (RU)	R_{max} (RU)	Activity (%)
sLe^a-Lem	8000	27.1	25.6
sLe^a-Lem	3800	18.1	36.2
sLe^a-Lem	3800	18.2	36.4
sLe^a	8000	30.4	34.5
sLe^a	3800	18.7	44.5
sLe^a	3800	18.4	43.8

Comparing K_D's derived from steady state and kinetic date evaluation proved consistency (*table 43*). Even for such fast interactions, determination of K_D values via kinetic data was feasible.

Table 43. Comparison of thermodynamic and kinetic data for sLe^a-Lem and sLe^a. Steady state saturation binding resulted in identical K_D values as calculated via the kinetic data.

Compound	K_D (μM)	R_{max} (RU)	k_{on} ($M^{-1}•s^{-1}$)	k_{off} (s^{-1})	$k_{on}•k_{off}^{-1}$ (μM)
sLe^a-Lem	11.8	27.1	$3.9•10^4$	0.46	12.4
sLe^a-Lem	10.4	18.1	$5.6•10^4$	0.59	10.5
sLe^a-Lem	9.5	18.2	$8.3•10^4$	0.79	10.4
sLe^a	24.2	30.4	$1.8•10^4$	0.42	23.9
sLe^a	20.6	18.7	$2.8•10^4$	0.55	19.9
sLe^a	24.5	18.4	$2.2•10^4$	0.57	25.4

Table 44. Calculated average values for thermodynamic and kinetic data of both sLe^a-Lem and sLe^a.

Compound	K_D (μM)	k_{on} ($M^{-1}•s^{-1}$)	k_{off} (s^{-1})	$t_{1/2}$ (s)
sLe^a-Lem	10.6 +/- 1.2	$5.9•10^4$	0.61	1.1
sLe^a	23.1 +/- 2.2	$2.3•10^4$	0.51	1.4

Comparison of the affinity for sLe^a (23.1 μM) and sLe^a-Lem (10.6 μM) underlined the impact of artificially added labels or linkers. The K_D values deviated by a factor of 2. Interestingly, sLe^a-Lem showed a higher affinity though a flexible chain was added. Either the hydrophobic chain established an additional hydrophobic contact or the higher lipophilicity forced the ligand out of the hydrophilic environment. The influence of such labels on affinity, specifically enzyme kinetics, was described before.[180] In the case of sLe^a-Lem, the label was added to enable easy purification of such hydrophilic molecules on RP-18 columns. In many other cases, the assay itself requires labeling for its detection system.

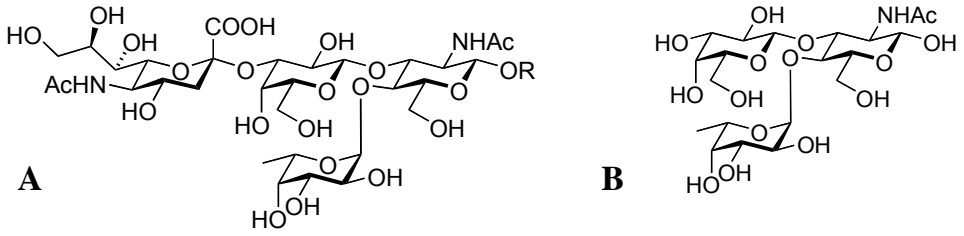

Figure 33. The antigen sLe^a (R = $(CH_2)_8COOMe$) (R = H) and the desialiylated Le^a measured.

The kinetic evaluation was more problematical because the data was close to the detection limit for the Biacore 3000 (k_{on} 10^2-10^7, k_{off} 10^{-1}-10^{-5}). Nevertheless, triplicate experiments allowed a consistent determination and values obtained were in good agreement with published data of carbohydrate/protein interactions.[178] Faster complex association was the driving force for higher affinity of sLe^a-Lem whereas complex dissociation behaviour remained roughly unaffected.

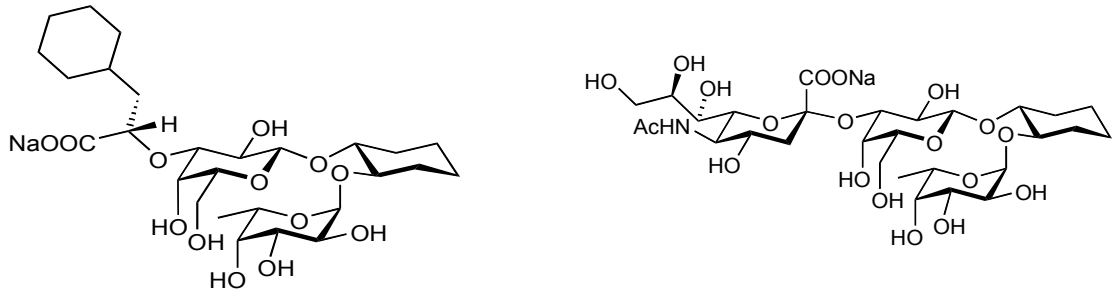

Figure 34. sLe^x mimics tested for binding to GSLA-2

To proof the high selectivity of GSLA-2 towards the sLe^a epitope, Le^a and two sLe^x derivatives were tested. In both sLe^x derivatives the Glc*N*Ac moiety was replaced by a cyclohexyl ring what removed the isomerism between sLe^a and sLe^x (*figure 34*). Desialydation of sLe^a completely prevented binding to GSLA-2 up to a 2 mM concentration. The importance of the sialic acid moiety for recognition was therefore nicely shown. Furthermore, none of the sLe^x mimetics bound to GSLA-2 up to a 2 mM concentration. Concluding, a specific interaction of the Glc*N*Ac moiety with GSLA-2 is needed.

Additionally, a set of sLe^a derivatives were analyzed by our collaborators in Lübeck using STD-NMR, transferred NOE analysis and surface plasmon resonance. The C6-methyl group of fucose and the *N*-acetyl group of the Glc*N*Ac residue were found to contribute significantly to binding.

Combination of NMR and surface plasmon resonance technologies permitted to describe the binding epitope of GSLA-2 in detail. The *N*-acetyl group of the Glc*N*Ac moiety as well as the sialic acid moiety were shown to be essential for binding. In addition, the C6-methyl group of the fucose residue contributed significantly to binding affinity (*figure 35*).

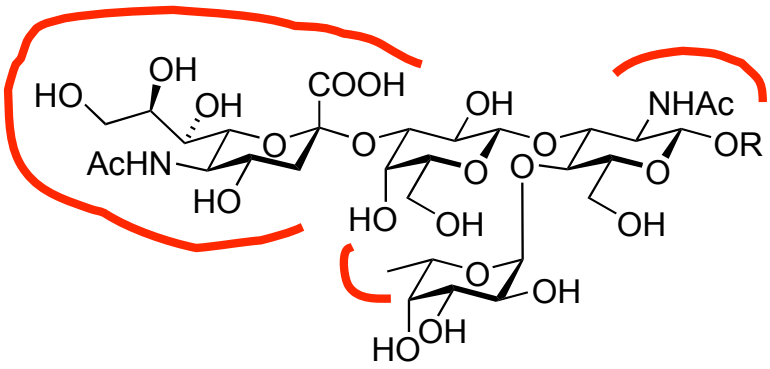

Figure 35. Binding epitope of GSLA-2 for the antigen sLe^a as determined by NMR and Biacore experiments.

The characterization of the GSLA-2/sLe^a interaction by the SPR-based biosensor and NMR was published in the J. Med. Chem.[166]

3.2 Myelin-associated glycoprotein (MAG) as drug target

The MAG project was conducted in close cooperation with the group of Prof. Sørge Kelm (University of Bremen, Germany). The protein consisted of the Fc portion of human immunoglobulin IgG1 and the three *N*-terminal domains of murine MAG (*figure 36-B*). The construct included the described sialic acid binding site in the v-domain but the potential NgR binding site in was absent.[33]

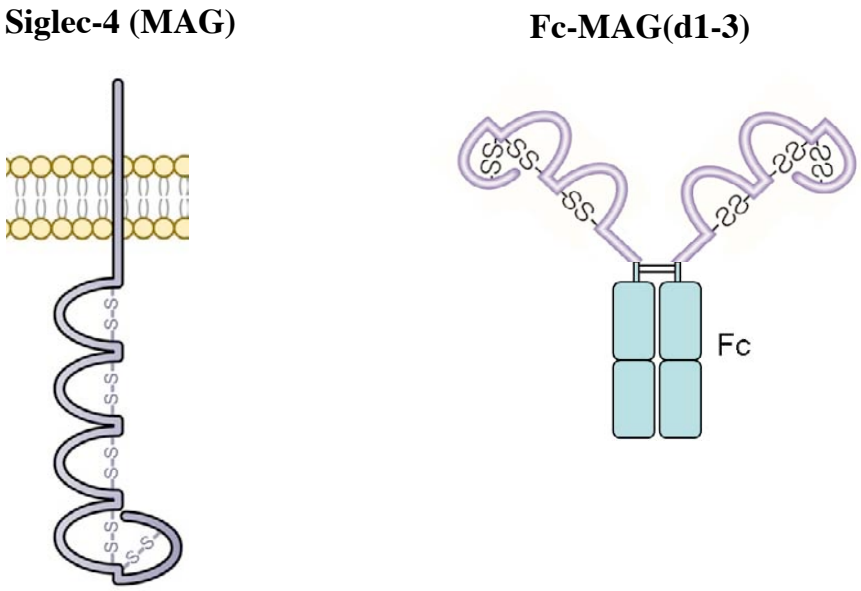

Figure 36. MAG including the five extracellular domains, the transmembrane and cytoplasmatic domain. The Fc-MAG(d1-3) construct composed by the three extracellular domains including the *N*-terminal v-type domain and the Fc portion of human immunoglobulin IgG1.

For the design of the Biacore assay there were to alternative approaches, either to immobilize the ligands or MAG itself. Because IC_{50} values were already available and kinetic data can only be derived precisely from a 1:1-binding event, the bivalent Fc-MAG(d1-3) construct was immobilized onto the dextran surface. Deviations of kinetic data for bivalent ligands were described before.[155] Coupling of MAG to the biosensor chip further provided the opportunity to measure several ligands on one surface leading to a reduced number of sensor chips needed. Additionally, also lower amounts of MAG were required. The major concerns were the activity of MAG after

immobilization with standard covalent immobilization strategies and the signal intensity for ligands with a molecular weights in the range of 500 Da.

All compounds synthesized at the Institute of Molecular Pharmacy were measured by our collaborators in a hapten inhibition assay using the same Fc-MAG(d1-3) construct (*p. 38*). Because no K_D reference values for MAG-ligands were available, relative IC_{50} values from the hapten inhibition assay were used for assay validation. Due to the oligovalent interaction and the weak competitor used in the hapten inhibition assay, only a qualitative validation was possible.

3.2.1 Amine coupling of Fc-MAG(d1-3)

A careful evaluation on a homology model was carried out to identify attachment sites. The homology model of the sialic acid binding v-domain is based on sialoadhesin (Siglec 1).[181] Lysines in the sialic acid binding site would prohibit amine coupling as immobilization strategy.

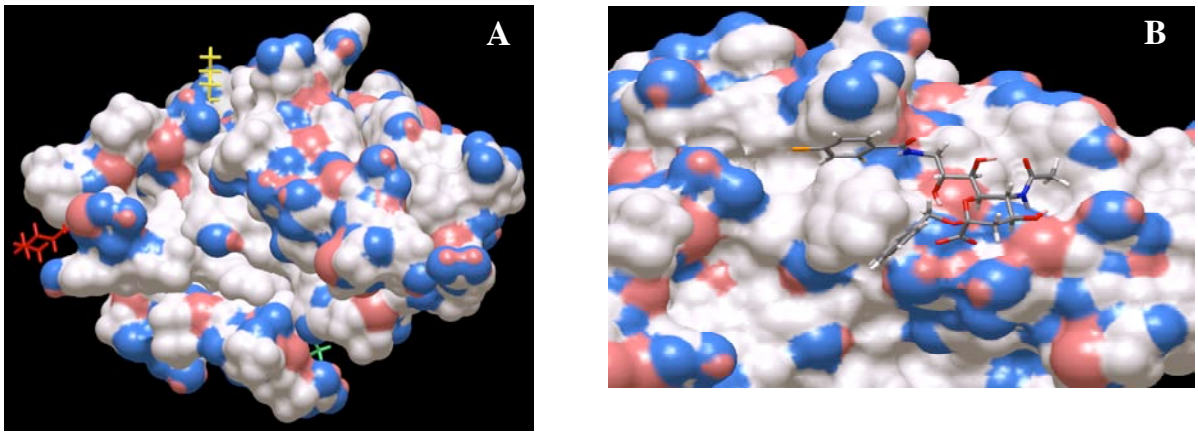

Figure 37. (A) Homology model of the *N*-terminal v-domain displaying all three lysines (Lys67, 85 and 114) as attachment sites for amine coupling. (B)

The potential sialic acid binding site (*figure 37-B*) was found to be in proximity of Lys114 (*figure 37-A, yellow*). The distance between Lys114 and the carboxyl group on the ligand is rather long (18 Å). Nevertheless, a disturbance of the binding site was

possible due to the flexibility of the lysine side chain and the orientation of the 9'-modification of the ligand towards that lysine.

3.2.1.1 Immobilization of Fc-MAG(d1-3)

Table 45. Immobilization conditions (*pH* and concentration tested.

pH	Response* (RU)
7.4	-8
5.5	200
5.0	400
4.5	6'981
4.0	19'095

*at a concentration of 40 μg/ml

Concentration (μg/ml)	Response** (RU)	Response*** (RU)
20	8'000	1'500
40	22'500	5'000
80	26'000	15'000

** at pH 4.0

*** at pH 4.5

A maximal attraction was obtained at pH 4.0 when injecting a 40 μg/ml concentration (*table 45*). Furthermore, three different concentrations (20, 40 and 80 μg/ml) for *pH* 4.0 and 4.5 were evaluated (*table 45*). A clear correlation between concentration and surface attraction was observed. The low attraction at pH 5.0 ad 5.5 was overcome by higher concentrations and enabled coupling at somewhat milder conditions. In the case of MAG, it was known that a low *pH* (around 3.0) is only tolerated for a short period as employed for affinity purification. In this case, exposure is limited to approximately 10 minutes. For *pH* 4.0 high surface densities were achieved easily with a protein concentration of 40 μg/ml. Unfortunately, fast surface attraction did complicate controllability of the final immobilization level. After stopping the immobilization, a drop was observed (*figure 38-A*).

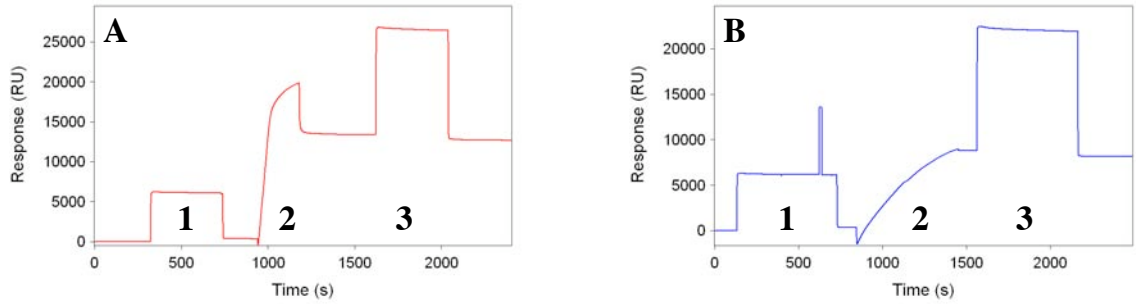

Figure 38. Amine coupling profile performed at *pH* 4.0 (A) and 5.5 (B): After activation of the surface with a mixture of EDC-NHS (1) the protein sample was injected (2). The procedure was finished by a deactivation step where all remaining activated carboxyl groups were capped by EA (3).

By increasing the concentration to 140 µg/ml, it was possible to immobilize sufficient Fc-MAG(d1-3) (6802 RU) at *pH* 5.5 within 10 minutes (*figure 38-B*). Levels achieved for other *pH* conditions are displayed in *table 46*.

Table 46. Immobilization levels at different *pH* values

pH	Immobilization level (RU)	Concentration (µg/ml)	Immobilization time (s)
4.0	7693	40	120
4.5	17184	70	360
5.0	3995	70	360
5.5	6802	140	600

3.2.1.2 Validation of coupled Fc-MAG(d1-3)

For all ligands measured, the chemical structure can be looked up in the *appendix I* via its specific label.

The validation process was performed with a set of sialic acid derivatives (**SH-082, SH-136, SM-I3** and **SM-I4)** for which the relative affinity (rIC_{50}) was known from the hapten inhibition assay. As described (*p.* 38), this assay is based on a multivalent interaction of MAG and a weak competitor and IC_{50} values were therefore likely to deviate from the K_D value. Additionally, the absolute values deviated significantly between different plates and were therefore normalized with a standard compound (**SH-019**). Nevertheless, the K_D for **SH-082, SH-136, SM-I3** and **SM-I4** was expected in the μM range.

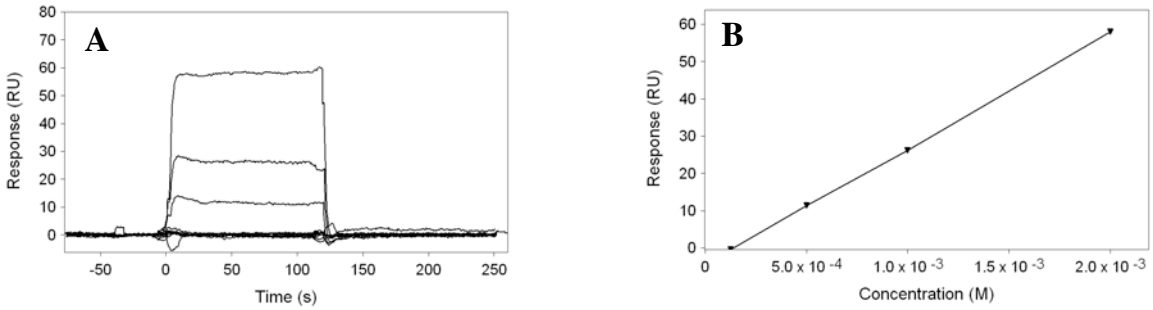

Figure 39. Sensorgrams (A) and saturation binding plot (B) for SH-082 measured on a surface that was created at *pH* 4.0.

For the Fc-MAG(d1-3) surface prepared at *pH* 4.0, no saturation of the binding was obtained for **SH-082** (*figure 39*). The surface appeared inactive due to the fact that concentrations up to 2 mM were used.

Immobilization at *pH* 5.5 resulted in an active surface and the equilibrium dissociation constants of all four ligands were in the expected range. A simple 1:1-binding model fitted best with the experimental data (*figure 40*). The fit and the sensorgrams were of inferior quality compared to the GSLA-2 results. This was most likely due to the overall lower signal intensity leading to a lower signal-to-noise ratio.

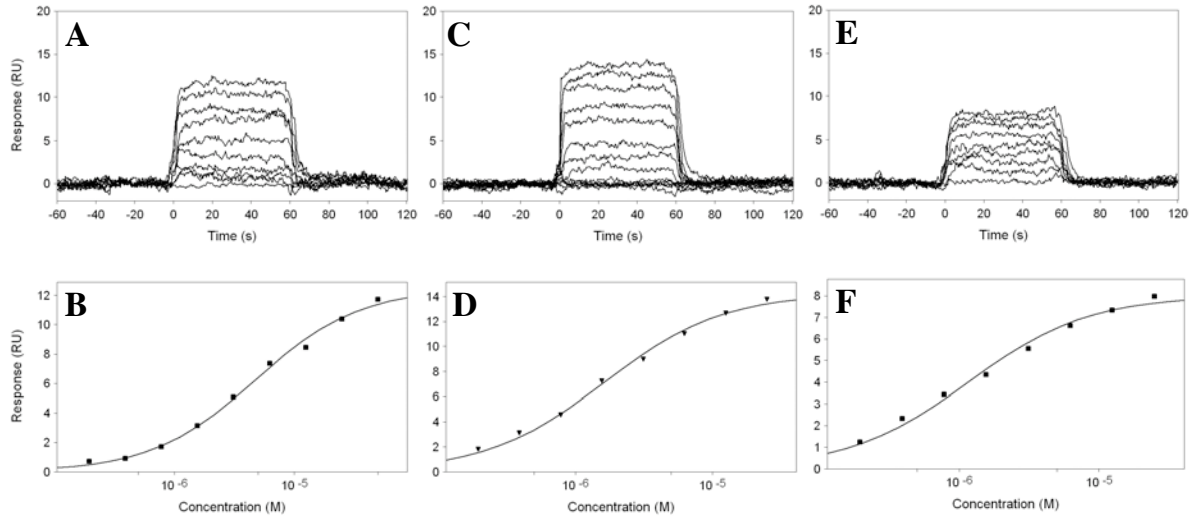

Figure 40. Sensorgrams and fitting curves for **SH-082** (A,B), **SM-I3** (C,D) and **SM-I4** (E,F).

Table 47. Equilibrium binding constants obtained on an amine-coupled surface at *pH* 5.5.

Analyte	K_D (μM)	rIC_{50}	R_{max} (RU)	MW (g/mol)	Activity (%)
SH-082	4.5	0.87	12.9	570#	15
SH-136	3.4	1.00	8.1	501*	13
SM-I3	1.9	0.29	13.4	626*	17
SM-I4	1.2	0.16	8.0	594*	11
SH-164	n.d.	10.00	4.0	425#	6

*measured on a surface with 7300 RU of Fc-MAG(d1-3)

#measured on a surface with 8400 RU of Fc-MAG(d1-3)

Maximal signal intensity observed was 17% what was rather low. The protein seemed to loose activity during immobilization. For **SH-164** no evaluation was possible due to an insufficient signal intensity (R_{max} = 4.0). Interestingly, **SH-019** that differed by only one benzyl group compared to **SH-164** displayed a doubled R_{max}. The increased signal intensity found was in good agreement with published data where a higher refractive index increment for aromatic groups was described.[182] Furthermore, a high influence of chlorides on the signal intensity was visible (*table 47*). Even though the molecular weight for a difluoro (**SM-I3**) and a dichloro (**SM-I4**) compound (*figure*

39) deviated only by 5 %, the R_{max} value for the dichloro compound was 35% larger. The highest activity was found for **SM-I4** containing the highest number of chlorides (3).

The deviations between the molecular weight and the SPR signal were similar to effects observed in the GSLA-2 project. Especially for low molecular weight ligands the nature of the ligand influences the signal intensity significantly. An extended study to correlate refractive indices of ligands with their signal intensity would provide a clearer picture. Nevertheless, such rules of thumb can provide an explanation for deviations.

3.2.2 Immobilization of Fc-MAG(d1-3) on a protein A surface

To evaluate a possible influence of amine coupling on MAG activity, a capturing approach was applied where no structures of MAG were involved in surface attachment. Due to the availability of a Fc fragment in the Fc-MAG(d1-3) construct, protein A was an obvious option. Usage of protein A to capture antibodies on sensor chips was described earlier.[183-185] Protein A was immobilized using standard amine coupling and Fc-MAG(d1-3) was captured on the prepared protein A surface.

3.2.2.1 Immobilization of protein A with amine coupling

High surface attraction was observed in the range of *pH* 4.0-5.0. This was in good agreement with a *pI* of 5.1 for protein A.

Table 48. Surface attraction obtained for the tested *pH* conditions.

pH	**Response (RU)**
7.4	n.d.
5.5	2’063
5.0	12’042
4.5	14’225
4.0	11’077

For immobilization, *pH* 5.0 (30 µg/ml) was chosen even though protein A should remain active at conditions below (*table 48*). Immobilization levels of 8’000-9’000 RU were obtained routinely on CM5 sensor chips. Parallel immobilization was carried out where two flow cells were prepared simultaneously. The protein A surface was stabilized over night at 5 µl/min in HBS-EP.

3.2.2.2 Capturing of Fc-MAG(d1-3) on the protein A surface

An injection at 10 µl/min for 10 minutes at a concentration of 40 µg/ml enabled capturing of sufficient Fc-MAG(d1-3) (4'500 RU) onto the protein A surface (*figure 41*). Two 5 s pulses of glycine pH 2.5 at a flow rate of 60 µl/min allowed complete removal of Fc-MAG(d1-3) (regeneration). Protein A maintained its activity after regeneration proven by a subsequent capturing of an equal amount of Fc-MAG(d1-3). As expected, a minor drift of baseline was observed that got stabilized after 30 to 60 minutes (*figure 41*).

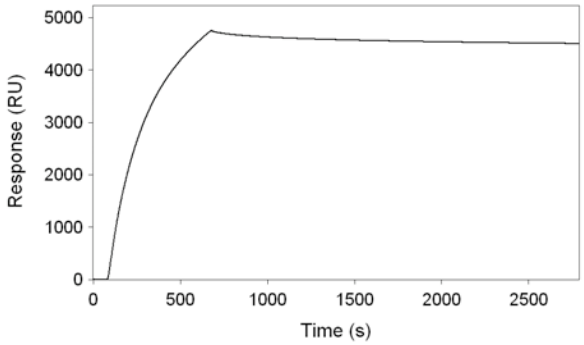

Figure 41. Capturing of Fc-MAG(d1-3) on protein A: After stopping the injection a drift of baseline was observed. This is due to the noncovalent bonding between the Fc part of Fc-MAG(d1-3) and protein A.

3.2.2.3 Validation of captured MAG)

For all ligands measured, the chemical structure can be looked up in the *appendix I* via its specific label.

Trial experiments on captured MAG

Ligand **SH-035** and **SH-082** were chosen for a first validation due to their difference in affinity (factor 100) found in the hapten inhibition assay. Injections of both compounds showed negative signals and a decaying baseline (*figure 42-A,B and figure 43*). The unstable baseline was expected but the negative sensorgrams were contradictory. In the simplified picture of a Biacore experiment were a positive signal

corresponds to a mass increase, such negative sensorgrams represented a mass reduction during the injection of the sample.

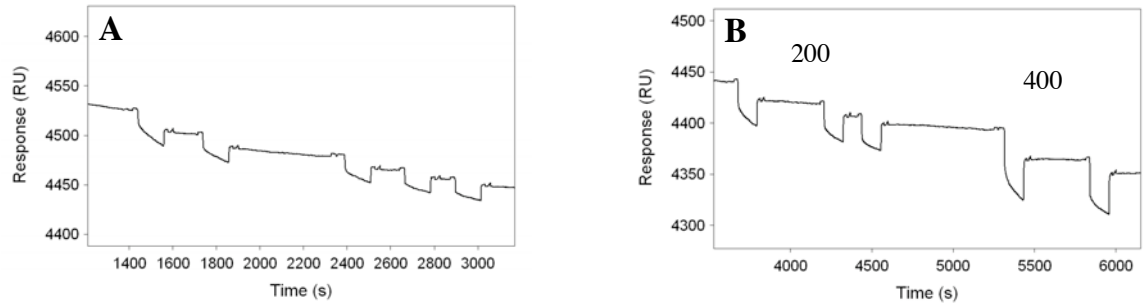

Figure 42. Trial experiments on the freshly captured surface: (A) Injections of **SH-035** (100 μM) and (B) Injections of **SH-035** (200 μM and 400 μM)

Beside the negative signals, a significant difference between the two ligands in respect to the dissociation signal was found (*table 49*). For **SH-035**, the major observation was that higher concentrations led to larger dissociation signals whereas for **SH-082** dissociation signals remained constant. This was a sign for saturation in the case of **SH-082** when accounting that the dissociation signal was independent of any baseline drift.

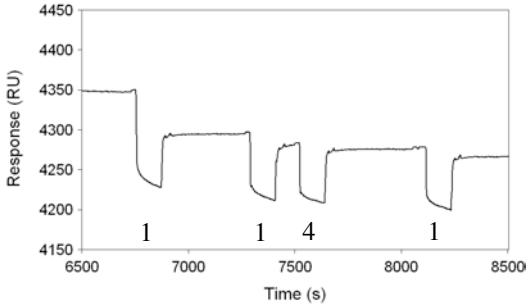

Figure 43. Injection of **SH-082** (100 μM = 1 and 400 μM = 4)

Table 49. Evaluation of dissociation signals

	SH-035	**SH-082**
rIC_{50}	0.01	1.15
100 μM	-13 RU	-66 RU
200 μM	-25 RU	
400 μM	-40 RU	-69 RU

The first injection of **SH-082** resulted in a larger drop during association compared to the following injections (*figure 43*). It appeared that the surface got further stabilized after a first injection.

The second trail experiment, where triplicate injections of nine concentrations of **SH-082** were carried out, further indicated the necessity of a pre-injection. The decay of

the surface (100 RU) for the first injection of a high concentration was clearly visible (*figure 44*). Afterwards, the drift of baseline was comparable to blank injections and subtraction of blank injections eliminated the drift in the experimental data.

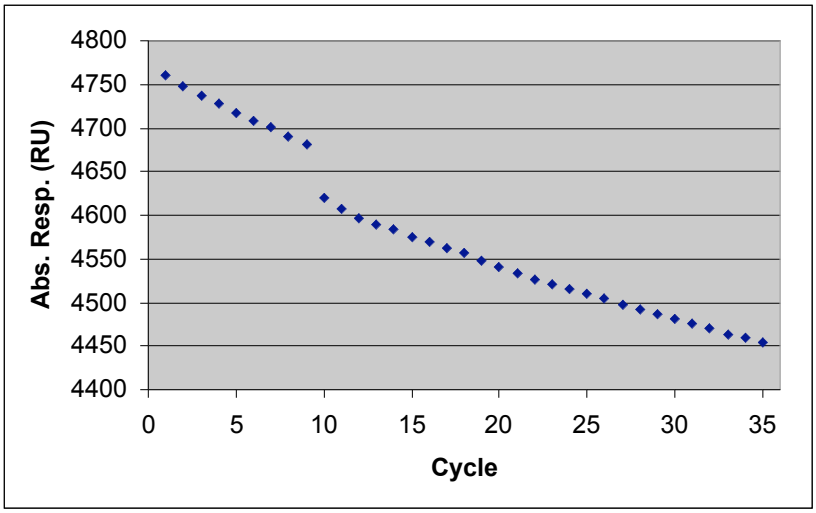

Figure 44. Evaluation of the drift of baseline in an experiment performed with triplicate injections. Each point marks the baseline (amount of MAG on the chip) before injection of a sample. The first injection of a saturation concentration led to a higher surface decay (injection 8). Before and after the mentioned injection no such drop is observed even for equal concentrations.

The data obtained was analyzed based on a saturation binding plot using two different approaches. The steady state signals were evaluated with scrubber (*figure 45*) and compared with the dissociation signals analyzed with GraphPad Prism (*figure 47*).

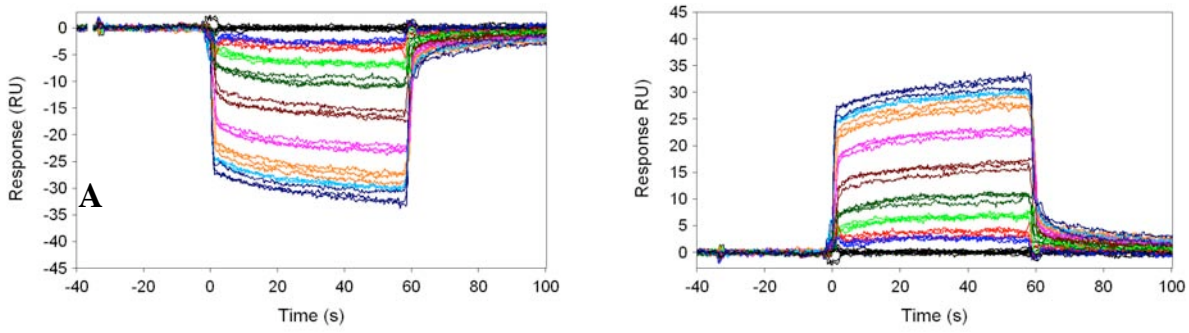

Figure 45. Original (A) and inverted sensorgrams (B) for **SH-082**. Sensorgrams were simply multiplied by –1, what can be done directly in the scrubber software.

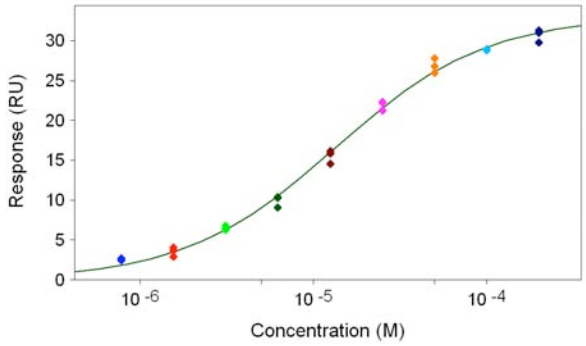

Figure 46. Saturation binding plot of data for **SH-082** displaying a perfect fit to a simple 1:1-binding model.

For standard evaluation in scrubber, the sensorgrams needed to be inverted (*figure 45-A,B*). High reproducibility was proven by almost overlaying curves for the triplicates. The surface decay was clearly visible during and after injection. Nevertheless, a perfect fit to a simple 1:1-binding model was obtained (*figure 46*).

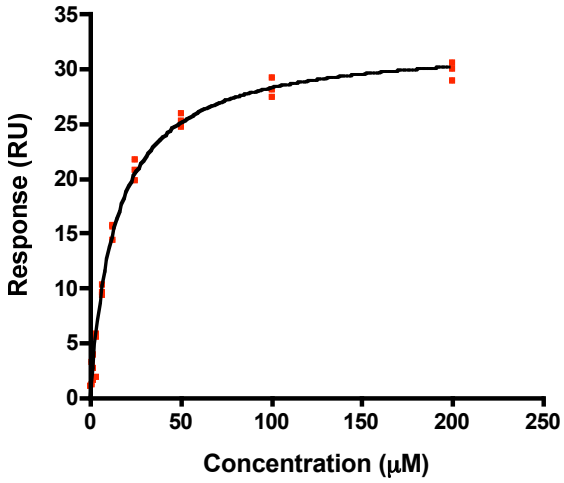

Figure 47. Fitting curve for the dissociation signals of SH-082 based on a simple 1:1 binding model.

During the entire first experiment the surface capacity was reduced by 200 RU (from 4650 to 4450 RU). This corresponded to approximately 5% of the captured Fc-MAG(d1-3). For the observed R_{max} value of 29 RU for this experiment the maximal calculated shift was only 1.45 RU. Such a small deviation can be neglected. As expected, the R_{max} value was lower in the second experiment (27.9 RU) in correlation to the reduced surface capacity. After regeneration and capturing of fresh MAG

(*experiment 3*), the R_{max} value was higher again (33.1 RU). Both approaches for data evaluation led to identical K_D values and a highly precise result was obtained when comparing all three experiments (*table 50*).

Table 50. Evaluation and comparison of triplicate experiments performed with **SH-082**. Highly reproducible equilibrium binding constants were obtained for both evaluation methods.

Experiment	K_D (µM) steady state	K_D (µM) dissociation signal	R_{max} (RU) steady state
1	13.4	13.4	29.2
2	14.4	14.75	27.9
3	13.4	14.8	33.1

For the physiological ligand G_{T1b}, a different picture was obtained. G_{T1b} most likely forms aggregates in aqueous solution. The higher molecular weight of G_{T1b} and the formed micelles were supposed to result in larger signals and therefore positive signals were expected.

Indeed, the sensorgrams of G_{T1b} were positive and showed slow association but faster dissociation (*figure 48-A*). Even though the steady state was not finally reached for all concentrations, steady state signals were evaluated.

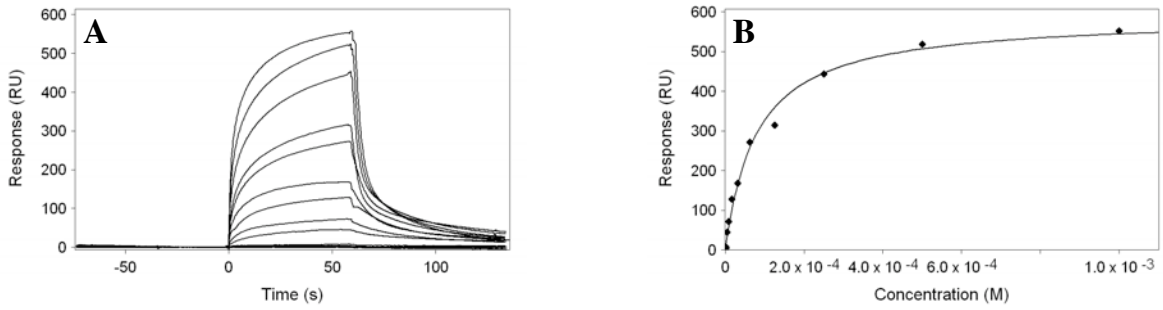

Figure 48. Positive sensorgrams obtained for **G_{T1b}** (A) and the fit of the steady state signals to a simple 1:1-binding model (B).

A decent fit was obtained as indicated in *figure 48-B*. The calculated K_D was 79.3 µM but had to be considered as an apparent K_D due to expected multivalency of micelles

and consequential concentration deviations. Nevertheless, positive sensorgrams and saturation binding somewhat supported the capturing assay.

An interesting direct immobilization of gangliosides on CM5 chips without usage of any immobilization chemistry was described in literature.[186] Several attempts were conducted to apply the setup for the MAG/G_{T1b} interaction but all failed. After referencing no reasonable signals were detectable. A possible reason is that G_{T1b} did not penetrate the matrix sufficiently due to its negative charges resulting in an ionic repulsion. On the other hand, immobilization without any real attachment was somehow not logical and, when accounting the fast dissociation of G_{T1b} in the experiment above, not very likely.

Optimization of the surface stability

In an optimized capturing procedure, the flow rate was adjusted to 1 µl/min what led to a reduced consumption of protein and increased stability of the surface. The ligand **SM-m5** was used to compare the stability of the surface directly after capturing and after over night equilibration.

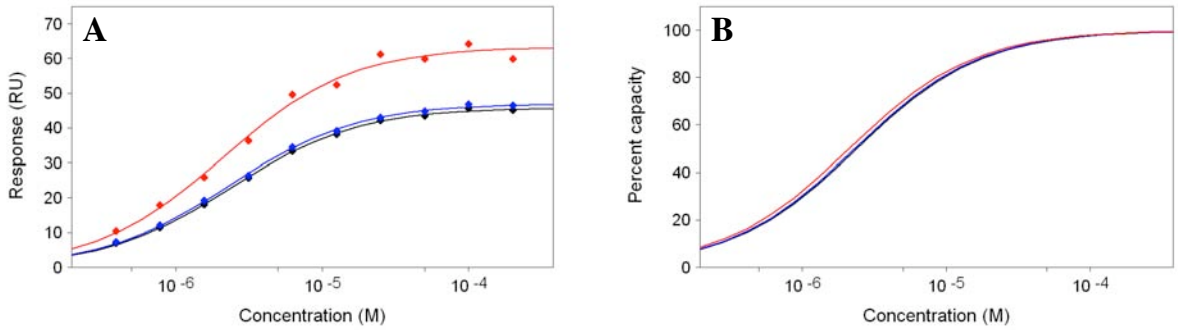

Figure 49. Results obtained for **SM-m5** (red = experiment performed directly after capturing, blue and black = experiment performed the next day after over night equilibration). Fitting curves based on a simple 1:1-binding model for the three different measurements (A) and normalized to 100 % capacity (B).

As expected, the loss of MAG (3%) and the deviation of the steady state signals compared to the fit were highest for the first experiment that was performed directly after capturing (*red curve, figure 49*). After 24 hours, the surface was stabilized and

the loss of MAG was significantly lower. Accordingly, the R_{max} values were lower in correspondence to the reduced amount of MAG on the surface (*table 51*).

Table 51. Results calculated for the three different experiments performed with **SM-m5**. A clear influence of over night equilibration after capturing is visible.

Experiment	K_D (μM)	R_{max} (RU)	MAG (RU)	Ratio (R_{max}/MAG)	Loss of MAG (%)
1	2.2	61.8	4628	0.13	3.0
2	2.2	47.5	3618	0.13	1.0
3	2.3	46.3	3548	0.13	0.6

3.2.2.4 Evaluation of negative sensorgrams

Evaluation of buffer conditions on negative signals and K_D values

Shifts of *pH* were already shown to influence the signal by far more than the small signals obtained for low molecular weight ligands.[179] Consequently, deviations of the *pH* between running buffer and sample should be avoided. Especially ligands containing acid or base functional groups bear potential to alter *pH* in a 10 mM buffer system. For that reason an experiment with an increased buffer capacity (50 mM instead of 10 mM HEPES) was carried out to prove the absence of such an effect. Beside, a non-specific interaction of either target or ligand with the matrix has the potential to influence the binding signal leading to negative sensorgrams.[179] An additional experiment where 1 mg/ml carboxymethyl dextran was added to the buffer system (HBS-EP) was conducted to eliminate such an effect. To further exclude an ionic repulsion effect on the sensorgrams, an attempt with an increased salt concentration (150 to 500 mM NaCl) was conducted. A higher ionic strength should prevent ionic interference to a certain degree. To explore carboxyl groups on the sensor chip as a source for negative sensorgrams, an additional assay on a surface with a reduced amount of carboxylic groups (CM4 sensor chip) was carried out.

All experiments were performed with **SH-019** as standard ligand. The chemical structure of **SH-019** can be looked up in the *appendix I.*

Table 52. Overview of all parameters tested including the obtained equilibrium binding constant for **SH-019**. No significantly different K_D was found and all sensorgrams remained negative.

Assay	K_D (μM)
HBS-EP*	21.8 +/- 0.2
HEPES 50 mM	17.6 +/- 0.1
NaCl 500 mM	14.9 +/- 0.1
CMD 1 mg/ml	17.8 +/- 0.1
CM4 chip	20.0 +/- 0.1
HBS-EP**	25.6 +/- 0.1

*10 mM HEPES *pH* 7.4, 150 mM NaCl, 3mM EDTA, 0.005% polysorbate 20

**exp. with a different stock solution

None of the parameters (buffer capacity, ionic strength or CMD) tested led to any significant shift of the K_D or influenced the negative signals considerably *(table 52*).
The negative signals were accounted to be independent of ionic attraction or repulsion, pH-dependent shifts or non-specific binding to the carboxymethyl dextran matrix. Comparing the K_D of identical experiments performed with different stock solutions (21.8 and 25.6 μM) accentuated a high reproducibility for the assay.
Furthermore, binding experiments on the CM4 sensor chip led to negative sensorgrams identical to those obtained on CM5 sensor chips. Evaluation of the data showed a perfect fit to a simple 1:1-binding model (*figure 50-A*) and a similar K_D (20.0 μM). Recapitulating, no differences were perceived compared to the standard CM5 sensor chip. Hence, the amount of carboxylic groups on the surface was excluded as source for negative signals.

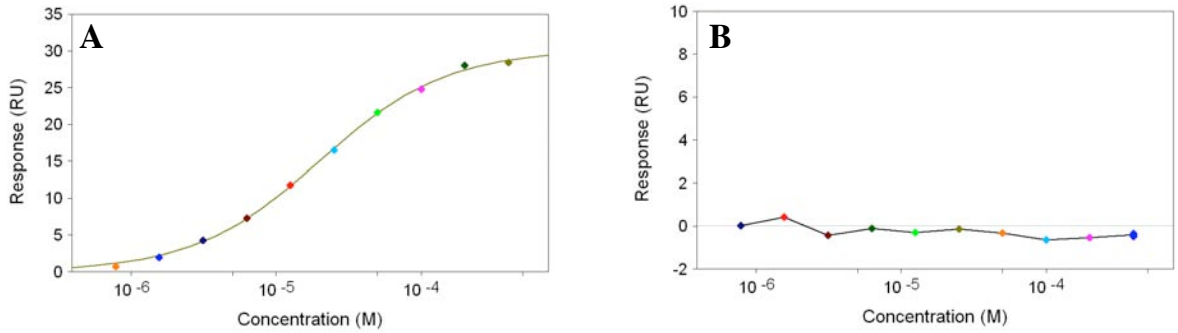

Figure 50. SH-019 measured on a CM4 sensor chip: A perfect fit to a simple 1:1-binding model was obtained (A). After removal of all Fc-MAG(d1-3) from the surface, the identical concentrations were injected but no binding was observed.

After successful measurements with **SH-019,** the surface was regenerated by injections of glycine buffer *pH* 2.5 as mentioned before. Subsequent experiments on the protein A surface within the identical concentration range showed no binding of **SH-019** (*figure 50-B*). This excluded an unspecific binding to the protein A surface as a source for negative signals. In addition, it was clarified that the obtained negative signals were not derived from matrix effects but from specific interaction with the captured Fc-MAG(d1-3).

The very careful validation of the capturing assay was necessary to proof absence of any artefacts causing the negative signals. One possible explanation was a conformational change upon ligand binding that compensates the small positive signal of the ligand. Extensive experiments with CD or FTIR would be required to proof such a change of radius upon ligand binding. An interesting finding was that negative sensorgrams for a carbohydrate/lectin interaction were already published but not evaluated in detail.[187] In this publication the binding of different monosaccharides to the asialoglycoprotein receptor (ASGP-R) was investigated. The investigators interpreted that no significant positive signal was obtained and therefore attached the monosaccharides to BSA what consequently led to positive signals. A closer look on the monosaccharide/ASGP-R interaction displayed that the negative signals were concentration-dependent and that affinity data was comparable to literature data.[179]
Usage of SPR for the detection of conformational changes was already described before.[124,125] It was found to be comparably sensitive to CD and FTIR.[122] In a

carbohydrate-lectin system, the influence of the hydrodynamic radius of proteins on SPR signals was described. The decrease of the protein radius correlated with a negative signal.[125] The hydrodynamic radius is the effective size of the molecule/protein as detected by its diffusion. Supporting experiments displayed that changes towards compact helical structures resulted in positive signals whereas β-sheets, turns or unordered structures led to negative signals.[123]
Unfortunately, an exact separation of a conformational change derived signal from a binding signal is likely to be difficult or even impossible in cases where kinetics for both processes are similar.

3.2.2.5 DMSO tolerability

To enable an analysis of water-insoluble compounds, the protein A based capture assay was validated for DMSO tolerability. The ligand **SH-082** was measured in HBS-EP containing 3% and 6% DMSO. This represented the usual DMSO range applied on Biacore 3000 though concentrations up to 8% are tolerated in a continuous flow. The chemical structure of **SH-082** can be looked up in the *appendix I*.

Table 53. Comparison of K_D values obtained for **SH-082** in a buffer system including DMSO.

	HBS-EP	**3% DMSO**	**6% DMSO**
K_D (μM)	19.2	19.6	19.2

For both 3 and 6% DMSO no deviation of the K_D was observed. Signals remained negative and the R_{max} values were slightly higher but still in the same region as observed for the standard assay. Furthermore, dissociation of the Fc-MAG(d1-3) protein A complex did not increase by addition of DMSO what was important for data quality and feasibility in general. Additionally, almost identical K_D values proved that no significant ligand agglomeration occurred in the water-based and the DMSO-based buffer system.

3.2.2.6 Sialic acid derivatives

Establishment of an accurate and precise assay setup with sufficient sensitivity enabled screening of ligands in respect to affinity, kinetics and thermodynamics. For all ligands measured, the chemical structure can be looked up in the *appendix I.*

The sialic acid core was chosen as scaffold for ligand development. Multiple options for modifications were possible in the side chains. The core included the selective ionic interaction of the carboxy group with Arg118.[71] In terms of molecular weight (309.27 g/mol) the scaffold fulfilled the Lipinski's rule of five (<500 g/mol).[9,94] On the other hand, too many H-bond acceptors (11) and H-bond donors (6) were present (Lipinski's: acceptors <10 and donors <5). Nevertheless, the core exhibited lead-likeness when accounting for the higher polarity what permitted extensive hydrophobic modifications.[95] Molecular flexibility is rather low for the core but the side chains are pretty flexible.

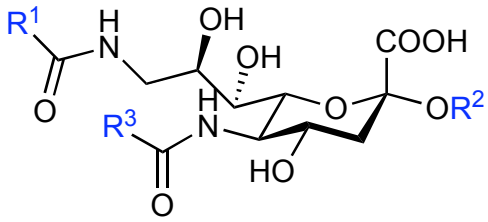

Figure 51. The core structure representing the minimal binding epitope with its modification sites R^1, R^2 and R^3. The carboxyl group forming an ionic interaction with MAG was included to maintain high specificity.

Three different positions on the core structure R^1, R^2 and R^3 (*figure 51*) were modified to increase affinity, improve kinetics and optimize drug-likeness.

In a first attempt, the focus was laid on the benzamido-group (R^1, R^2 and R^3) and the anomeric substituent R^4 (*figure 52*). The starting point was a patented structure (**SH-164**, R^1-R^3=H and R^4=Me) known to bind to MAG with a higher affinity than sialic acid. Synthetic work was done in-house by Dr. Sachin Shelke.

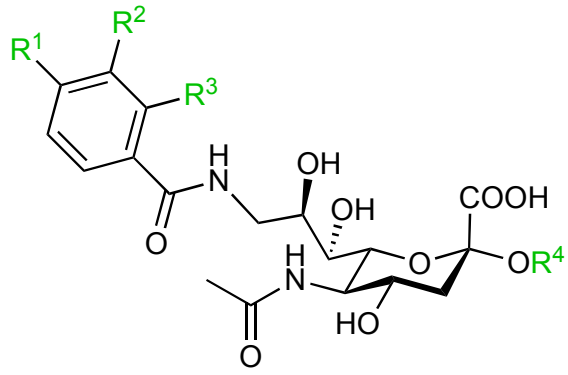

Figure 52. The starting point for the modifications was a patented structure (**SH-164**, R^1-R^3=H and R^4=Me) known to bind to MAG with a higher affinity than sialic acid. Modification sites R^1, R^2, R^3 and R^4 were used for the first optimization round.

Substitution of the OMe-group of **SH-164** at the anomeric centre with an OBn (**SH-019**) led to an increased affinity by a factor 5 (*table 54*). An even bigger effect was obtained for the incorporation of a triazole instead of the OMe (**SH-2-6**) where affinity increased by a factor of 2. A further enhancement was achieved by the introduction of a para-chloro at the 9'-position (**SH-081**). Halogens like chlorine or fluorine are regularly used in drug discovery.[188] Fluorines are often introduced for metabolic and pharmacokinetic reasons.

Table 54. First optimization round for the sialic acid scaffold with the K_D values determined.

Compound	R_1	R_2	R_3	R_4	K_D (μM)
SH-141	Cl	H	Cl	OBn	>300
SH-164*	H	H	H	OMe	137.0
SH-140	N_2O	H	H	OBn	59.6
SH-264	H	H	H	OCH_2CCH	76.4
SH-246	H	H	H	$O(CH_2)_4CCH$	39.6
SH-143	H	Cl	H	OBn	33.9
SH-019	H	H	H	OBn	25.6
SH-082	Cl	Cl	H	OBn	19.2
SH-081	Cl	H	H	OBn	17.1
SH-2-6	H	H	H	OTr	11.7

Bn = benzyl, Me = methyl, Tr = triazole

*the patented structure WO03/000709 A2 was resynthesized in-house.

Due to the lack of a crystal structure of MAG, a homology model was build up by Heiko Gaethje (University of Bremen, Germany) and Dr. Michele Porro based on sialoadhesin, a protein with high homology to MAG.[181] The homology model was employed to rationalize the Biacore data and propose future ligand modifications.

Ligand **SH-081** was docked onto the MAG-model (*figure 53*). The proposed docking mode displayed that the carboxylic group of the ligand generates a salt bridge with Arg118. Additionally, the hydrophobic modifications at the 2- and 9-position of the sialic acid scaffold found ideal partners for hydrophobic interactions in the side chains of Phe129 and Glu131. Especially the π-π interactions between Phe129 and the ligand are interesting. It provides an explanation for the increased affinity of the para-chloro modification in **SH-081** due to an enhanced interaction.[189] Moreover, a further hydrophobic contact between the acetate-group at position 5 and Trp22 as well as a hydrogen bond between the NH-group of the *N*-acetate and the backbone carbonyl group of Gln126 were observed. The important hydrogen bond between the

NH (donor) at the 9-position of the ligand and its protein partner, found to be the carbonyl backbone of Phe129, was identified. Indeed, the presented docking mode seemed to be very plausible, because of the similarity to the observed binding mode for methyl 9-benzamido-9-deoxy-Neu5Ac (**SH-164**) in the crystal structure of Sialoadhesin.

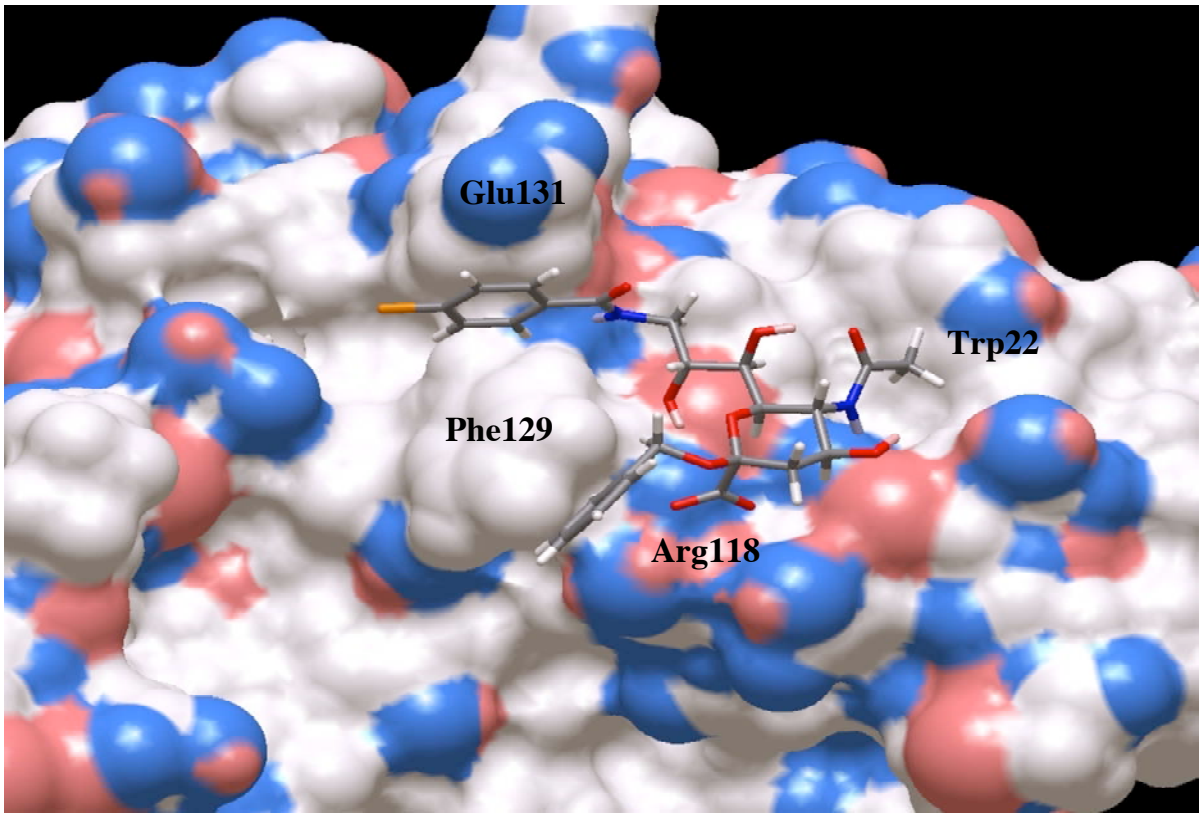

Figure 53. Docking of **SH-081** onto the homology model of MAG.

In the case of **SH-141**, **SH-143** and **SH-082**, a steric hindrance was possible to cause the reduced affinity. It seemed that only the para-position was modifiable. Furthermore did the extension at the anomeric centre by a hydrophobic chain (**SH-264** and **SH-246**) increase affinity in correlation to the length. Higher affinity due to an attached hydrophobic chain was already found in the GSLA-2 project.

Only **SH-081** was kinetically characterized in detail because all ligands exhibited a similar fast kinetic profile (*table 55*). The calculated on- and off-rate was in the same range as data from GSLA-2 ligands. The calculated complex half-life time was 1.4 s.

Table 55. Kinetic evaluation of the sensorgrams obtained for **SH-081**.

Compound	K_D (µM)	k_{on} ($M^{-1}•s^{-1}$)	k_{off} (s^{-1})	$t_{1/2}$ (s)
SH-081	17.1	$2.8•10^4$	0.48	1.4

In a next optimization round, the focus was shifted towards modifications at the anomeric centre and the *N*-acetyl side chain (*figure 54*). Ligand **SH-081** was chosen as new lead. Mostly electron withdrawing groups were incorporated to enhance the interaction of the OBn-group with Phe129 identical to effects observed for the benzamido group at the 9'-position. Additionally, known improvements on the *N*-acetate side chain were included to further enhance affinity.[68]

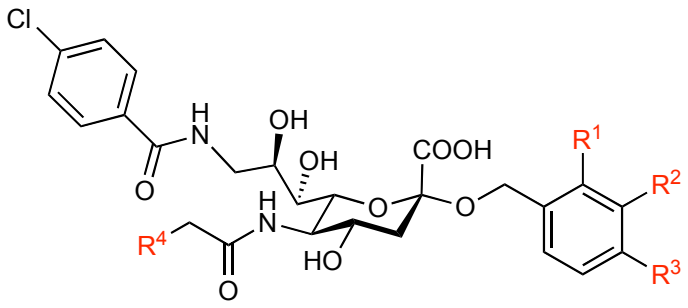

Figure 54. Modification sites R^1, R^2, R^3 and R^4 used for the optimization of the *N*-acetate side chain to enhance the π-π interaction between Phe129 and the OBn at the anomeric centre.

Table 56. Overview on all modifications done and the corresponding K_D values determined.

Compound	R_1	R_2	R_3	R_4	K_D (µM)
SH-081	H	H	H	H	17.1
SM-I4	F	F	H	H	4.4
SM-I3	Cl	Cl	H	H	4.3
SM-I6	H	H	F	H	12.4
SM-I5	H	H	Cl	H	15.0
SM-m6	F	F	H	F	0.7
SM-m4	F	F	H	Cl	2.0
SM-m5	F	F	H	OMe	2.2

As expected from the homology model, introduction of chlorines (**SM-I3**) and fluorines (**SM-I4**) in the ortho- and meta-position of the OBn further enhanced the π-π-interaction with the Phe129. Interestingly, no specific difference between chlorides and fluorides were observed. Compared to **SH-019**, affinity increased for both **SM-I3** and **SM-I4** by a factor of 4.

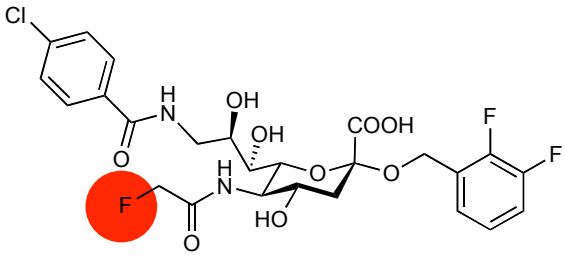

Figure 55. Chemical structure of the kinetically interesting compound **SM-m6**. Introduction of a fluorine (red) in the *N*-acetate side chain doubled complex half-life.

Introduction of a fluorine in the *N*-acetate side chain (**SM-m6**) further increased affinity by a factor of 6 (*figure 55*). This modification was already reported by Kelm *et al.* to enhance the interaction by a factor of 17.[68] Furthermore, complex half-life was doubled what was highly interesting but not explainable (*table 57*). Structure-kinetics relationship still remains a major challenge for kinetics-based ligand design. In addition, kinetic behaviour of ligands might be based on specific properties of the target protein *e.g.* the occurrence of a ideal binding pocket and therefore not universally applicable.

Table 57. Comparison of the kinetic data for the *N*-acetyl side chain modified with a fluoride.

Compound	k_{on} ($M^{-1} \bullet s^{-1}$)	k_{off} (s^{-1})	$t_{1/2}$ (s)	K_D (µM)
SH-081	$7.00 \bullet 10^4$	0.3000	2.3	4.4
SM-m6	$2.24 \bullet 10^5$	0.1638	4.2	0.7

Nevertheless, a selection of lead structures based on kinetics was proposed earlier.[114] Considering all data, it appeared that the sialic acid core resulted in a fast interaction profile. No significant progress towards slower complex dissociation was achieved

even though a large number of modifications were tested. A complete change of the core appeared promising to influence dissociation behaviour as long as the flat binding pocket does not favour fast dissociation in general. Modifications based on gained SAR would permit fast progress with a new core structure.

The large set of equilibrium dissociation constants determined by Biacore was correlated with the hapten inhibition assay data (*table 58*).

Table 58. All ligands, for which a rIC_{50} values from the hapten inhibition assay was available were compared to its K_D values determined by Biacore. A linear correlation analysis was carried out to prove qualitative agreement of the data. The reference ligand **SH-019** is highlighted in yellow.

Compound	K_D (µM)	rIC_{50}
SH-164*	137.0 +/- 0.5	10.00
SH-264	76.4 +/- 0.3	4.95
SH-140	59.6 +/- 0.4	1.67
SH-246	39.6 +/- 0.2	0.60
SH-143	33.9 +/- 0.1	1.43
SH-019	25.6 +/- 0.1	1.00
SH-082	19.2 +/- 0.1	0.87
SH-081	17.1 +/- 0.1	0.54
SH-2-6	11.7 +/- 0.1	0.43
SM-I4	4.4 +/- 0.1	0.16
SM-I3	4.3 +/- 0.1	0.29
SH-272	1.7	0.05

*Patent: S. Kelm, R. Brossmer, WO 03/000709 A2, 19.06.2001

A high linear correlation ($R^2 = 0.91$) between the equilibrium dissociation constants and the hapten inhibition assay based rIC_{50} values was obtained on a double-

logarithmic scale (*figure 56*). This supported the accuracy of the negative sensorgrams.

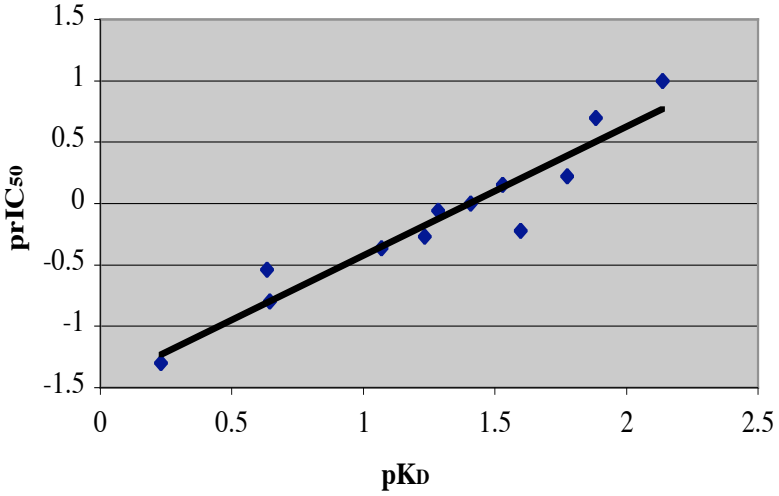

Figure 56. Linear correlation between K_D and rIC_{50} values on a double-logarithmic scale. High qualitative comparability between the Biacore and the hapten inhibition assay was proven by a R^2 factor of 0.91.

In terms of signal intensity, an interesting relation to the amine coupling assay was found. The R_{max} for **SM-I3** and **SM-I4** deviated considerably even though the molecular weight was almost identical (*table 59*). The negative signal of **SM-I3** was partially compensated by its higher signal intensity. The same effect of higher signal intensity for **SM-I3** was already found in the amine coupling assay (*p. 128*). The identical observation was made for **SH-019** and **SH-082**.

Already for the GSLA-2 characterization, such deviations enclosed a considerable influence on low molecular weight ligands (500 Da). These results further underlined that a direct correlation of signal intensity to mass is delusive. The impact of aromatic groups on signal intensity was already published in 2000 but needs to be extended by halogens.[182] Whenever dealing with low molecular weight ligands, deviations are likely to occur, what is especially important when comparing data from injections of only one concentration. In these cases, it might be that different signal intensities, normalized by the molecular weight, do still related to the same affinity.

Table 59. Comparison of results from amine-coupled and captured Fc-MAG(d1-3)

Analyte	R_{max} capt. (RU)	R_{max} amine (RU)
SH-082	-21.2	12.9
SH-136	-32.3	8.1
SM-I3	-24.5	13.4
SM-I4	-31.5	8.0

3.2.2.7 Detailed thermodynamic analysis

The interaction of sialic acid derivatives with MAG was further characterized by determining the entropic and enthalpic contributions to binding. A detailed entropy/enthalpy characterization of inhibitors binding to the HIV protease was done before with a Biacore 3000 and delivered interesting data about the interaction events.[118,190]

The selection focused on structural properties because only one class of ligands was available. A distinct structural feature was needed that influenced affinity by a factor of at least 5 (*figure 57*). The patented structure **SH-164** was used as starting point. Addition of a benzyl ring (**SH-019**) increased affinity by a factor of 5 that was proposed to be derived from an additional π-π interaction with Phe129. Incorporation of halogens (**SM-m6**) further enhanced the interaction by a factor of 25.

$$\ln(K_D) = \Delta H/R \bullet 1/T - \Delta S/R \qquad \text{Equation 7}$$

The three derivatives were measured at various temperatures (5, 10, 15, 20, 25, 30 °C) and evaluated by applying a van't Hoff plot. After linear regression, *equation 7* allowed to determine entropy and enthalpy via the slope (ΔH/R) and the y-intercept (ΔS/R).

SH-164 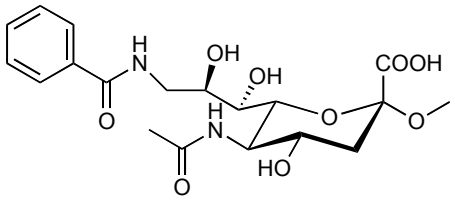 $K_D = 137\ \mu M$

SH-019 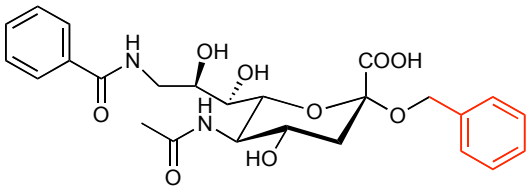 $K_D = 25.6\ \mu M$

SM-m6 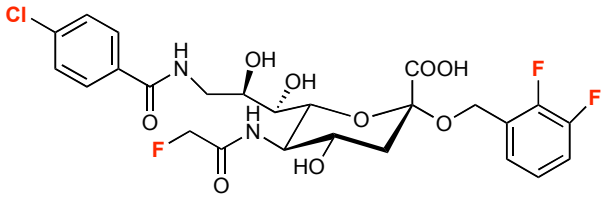 $K_D = 0.7\ \mu M$

Figure 57. Selected compounds (**SH-164**, **SH-019** and **SM-m6**) that were used for a closer thermodynamic description of the interaction between sialic acid derivatives and MAG. All chemical features introduced were meant to enhance the interaction and therefore augment the enthalpic contribution.

SH-164

Affinity of **SH-164** is based on a specific ionic interaction and hydrogen bridges as well as a π-π interaction. The core is rather rigid what should limit the entropic cost upon binding.[191] The side chain at the 9-position on the other hand is flexible. This forecast was in agreement with the obtained results. A 2-fold increase in affinity (132.3 to 64.5 µM) was observed over the range of 25 °C (*table 60*) what is characteristic for an enthalpy driven interaction.

Table 60. K_D values obtained for **SH-164** at different temperatures.

T (°C)	K_D (µM)
30	132.3
25	105.6
20	92.5
15	83.8
10	67.6
5	64.5

Affinity data were transferred into a van't Hoff plot and further analyzed (*figure 58*).

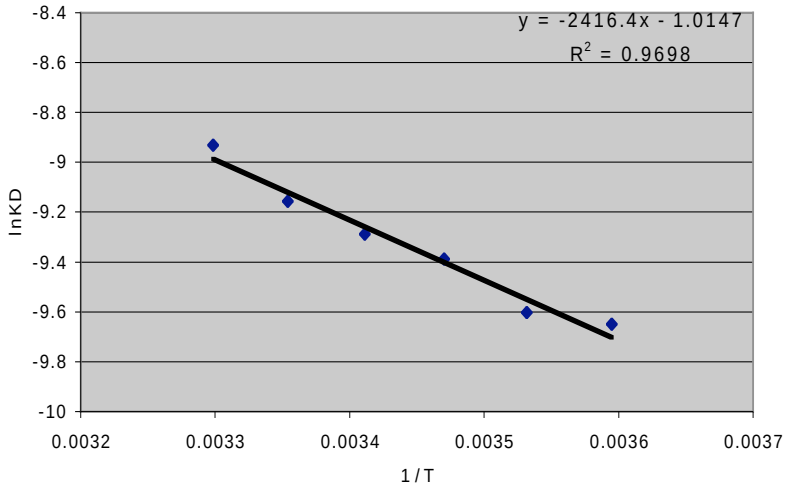

Figure 58: Van't Hoff plot for **SH-164** displaying a high correlation (0.97) for the linear regression.

Linear regression on the van't Hoff plot displayed a high correlation with a R^2 value of 0.97 (*table 61*). This confirmed a constant heat capacity within the temperature range applied what is a prerequisite for a proper van't Hoff analysis.[118] A clearly enthalpy driven interaction was found with a ΔH of -20.09 kJ•mol^{-1} and a $T\Delta S$ of –2.52 (*table 62*).

Table 61. Linear regression of **SH-164**

Slope	Intercept	R^2
-2416.4	-1.0147	0.9698

Table 62. Entropy and enthalpy calculated for 25 °C

ΔH ($kJ•mol^{-1}$)	ΔS ($kJ•mol^{-1}•K^{-1}$)	-TΔS ($kJ•mol^{-1}$)
-20.09	0.0084	-2.52

SH-019

Incorporation of an O-benzyl group at the anomeric centre was anticipated to create a π-π interaction with Phe129. An increased enthalpic contribution was expected due to the additionally introduced interaction.[192]

The K_D changed by a factor of 2 (9.8 to 21.8 µM) over the range of 20 °C. A higher affinity for lower temperatures was found (*table 63*) identical to **SH-164**, hence the interaction was enthalpy driven.

Table 63. K_D values obtained for **SH-019** at different temperatures.

T (°C)	K_D (µM)
25	21.8
20	17.7
15	15.5
10	12.8
5	9.7

Affinity data was transferred into a van't Hoff plot and further analyzed (*figure 59*).

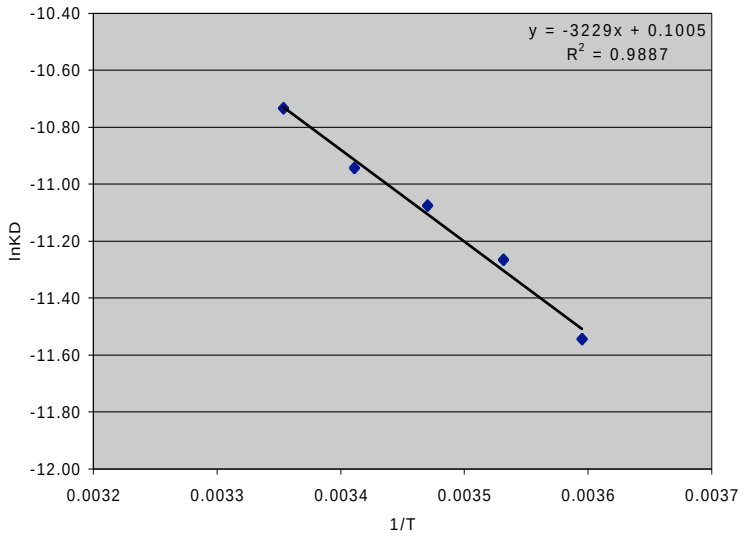

Figure 59: Van't Hoff plot for **SH-019** displaying a high correlation (0.99) for the linear regression.

Linear regression on the van't Hoff plot displayed a high correlation with a R^2 value of 0.99 (*table 64*). The heat capacity within the temperature range applied was constant and the plot was further analyzed to derive the entropy and enthalpy changes. A clearly enthalpy driven interaction was found with a ΔH of -26.85 kJ•mol^{-1} and a TΔS of 0.25 (*table 65*).

Table 64. Linear regression of **SH-019**

Slope	Intercept	R^2
-3229	0.1005	0.9887

Table 65. Entropy and enthalpy calculated for 25 °C

ΔH (kJ•mol^{-1})	ΔS (kJ•mol^{-1}•K^{-1})	-TΔS (kJ•mol^{-1})
-26.85	-0.00084	0.25

SM-m6

An enforcement of the π-π interactions was achieved by introducing electron withdrawing groups.[192] This was supposed to further increase the enthalpic contribution.

For **SM-m6** the K_D tripled from 0.277 to 0.807 μM over the entire temperature range (*table 66*) following the same enthalpic behaviour as observed for **SH-164** and **SH-019**.

Table 66. K_D values obtained for **SM-m6** at different temperatures.

T (°C)	K_D (μM)
30	0.999
25	0.807
20	0.557
15	0.440
10	0.333
5	0.277

Affinity data was transferred into a van't Hoff plot and further analyzed (*figure 60*).

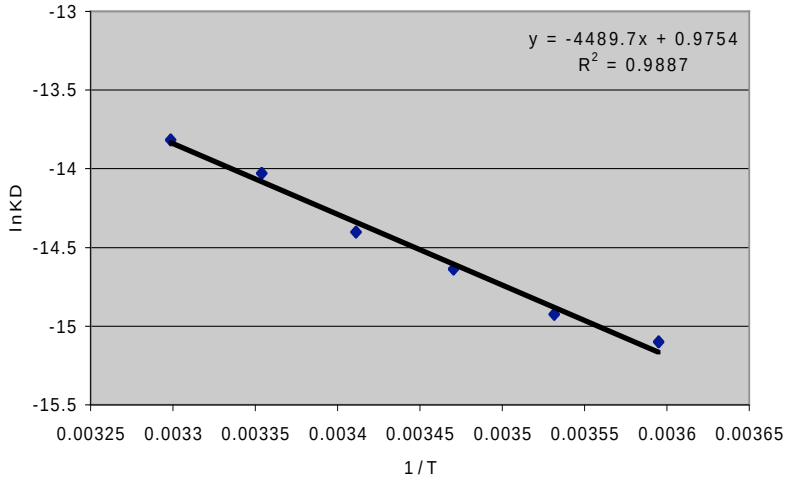

Figure 60: Van't Hoff plot for **SM-m6** displaying a high correlation (0.99) for the linear regression.

Linear regression on the van't Hoff plot displayed a high correlation with a R^2 value of 0.99 (*table 67*). The heat capacity within the temperature range applied was constant and the plot was further analyzed to derive the entropy and enthalpy changes. A clearly enthalpy driven interaction was seen with a ΔH of -37.33 kJ•mol^{-1} and a TΔS of 2.42 (*table 68*).

Table 67. Linear regression for **SM-m6**

Slope	Intercept	R^2
-4489.7	0.975	0.9887

Table 68. Entropy and enthalpy calculated for 25 °C

ΔH (kJ•mol^{-1})	ΔS (kJ•mol^{-1}•K^{-1})	-TΔS (kJ•mol^{-1})
-37.33	-0.00811	2.42

Recapitulating the results (*table 69*), introduction of an additional π-π interaction via an O-benzyl group led to an enthalpic gain by -6 kJ•mol^{-1}. This was in good agreement with published computational data.[189] In general, substitution of the O-methyl group by an O-benzyl improved ΔG at 25 °C by -3.99 kJ•mol^{-1}. Introduction of halogens to both aromatic rings and the *N*-acetate side chain was stated to further increase the enthalpic contribution by *e.g.* enhancing the π-π interaction potential.[192] Indeed, the evaluated results displayed such an increase (-10.48 kJ•mol^{-1}) compared to the unsubstituted ligand. The entropic penalty increased by 2.17 kJ•mol^{-1} at 25 °C. This could be the result of a disymmertization of the reducing end. Overall, ΔG improved at 25 °C by -8.31 kJ•mol^{-1}.

Table 69. Overview of thermodynamic data obtained for the selected sialic acid derivatives.

	ΔH (kJ•mol^{-1})	ΔS (kJ•mol^{-1}•K^{-1})	-T•ΔS* (kJ•mol^{-1})	ΔG* (kJ•mol^{-1})	K_D* (μM)
SH-164	-20.09	+ 0.00840	-2.52	-22.61	105.6
SH-019	-26.85	- 0.00084	0.25	-26.60	21.8
SM-m6	-37.33	- 0.00811	2.42	-34.91	0.8

*values calculated for 25 °C

Using the selected three ligands with distinct structural modifications and affinities spanning a range of two orders of magnitude enabled correlation of structural modifications to thermodynamic data. For planning such experiments, careful selection of ligands and access to interesting ligands is most important.

Additional information on kinetics was obtained for the measurements at the different temperatures. For the first time, a sialic acid derivative (**SM-m6**) displayed dissociation behaviour that was visible in the sensorgrams. At 5 °C, the impact was most distinct (*figure 61*). To determine the exact dissociation rate, a kinetic evaluation was performed for data measured at all temperatures. A decent kinetic fit to a simple 1:1 binding model was obtained.

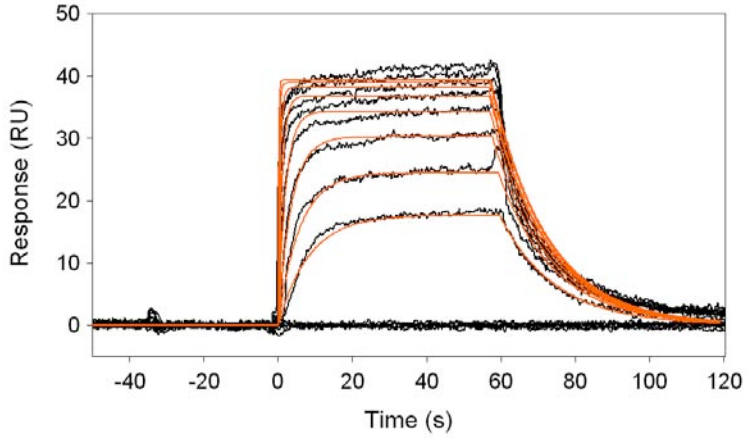

Figure 61. Kinetic fit to a simple 1:1-binding model on **SM-m6** sensorgrams acquired at 5 °C.

Over the measured temperature range, a trend of slower complex dissociation at lower temperatures was observed (*table 70*). At 25 °C the half-life time of the **SM-m6**/MAG complex was tripled (4.2 s) compared to **SH-081** (1.4 s). This was a clear kinetic advantage of **SM-m6** compared to all other ligands synthesized. Unfortunately, a coherent explanation for the kinetic improvement by incorporation of halogens is missing.

Table 70. Kinetic evaluation of data obtained for **SM-m6** at different temperatures.

T (°C)	k_{on} ($M^{-1} \bullet s^{-1}$)	k_{off} (s^{-1})	$t_{1/2}$ (s)	K_D (nM)
5	$2.75 \bullet 10^5$	0.0669	10.4	243
10	$3.05 \bullet 10^5$	0.0977	7.1	320
15	$2.30 \bullet 10^5$	0.0960	7.2	417
20	$2.73 \bullet 10^5$	0.1380	5.0	505
25	$2.24 \bullet 10^5$	0.1638	4.2	732
30	$1.98 \bullet 10^5$	0.1888	3.7	954

3.2.3 Ligand optimization using second site screening

In a pioneering technique termed "SAR by NMR", NMR screening was used to identify a ligand binding to the target through the use of an isotopically enriched protein and structural information.[193-195] At saturating concentrations of this first ligand, a second round of NMR screening was used to identify a second ligand that bound to the target simultaneously and in the vicinity to the first ligand ("second-site screening"). Later, an optimized procedure of second site screening through the use of a spin-labeled first site ligand was described.[196]

Second-site screening based on such a spin-labeled first site ligand was applied to MAG in-house by Dr. Brian Cutting and Dr. Sachin Shelke. By combination of *in-situ* click chemistry with second-site screening direct association of a first ligand with a second site fragment was achieved.[167] A nitro-indole was identified to bind in vicinity to the first site. By using spacers of different length, the first site ligand was coupled *in situ* to the nitro-indole in presence of MAG (*figure 62*). Such obtained second-site ligands were subsequently analyzed on Biacore to proof higher affinity.

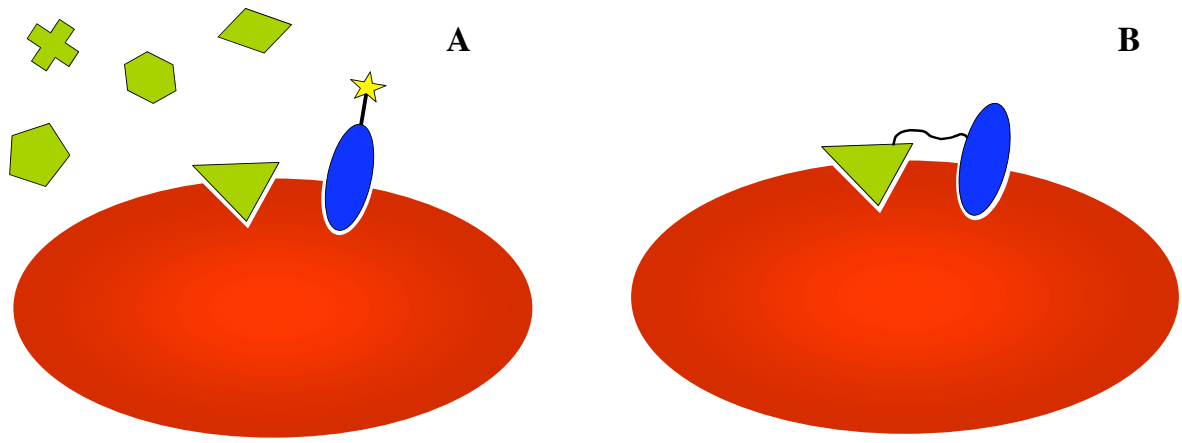

Figure 62. A molecular fragment (green) that binds close to the first site ligand (blue) is detected via a spin-label (yellow) attached to the ligand (A). After appropriate linkage of the found fragment to the first site ligand affinity should increase (B).

3.2.3.1 Characterization of second generation ligands

Second-site ligands were composed by a nitro-indole, the first-site sialic acid derivative and a triazole derived from linkage, differing only by spacer lengths (*figure 63*). First-site fragments as well as the nitro-indole were included in the measurements for comparison.

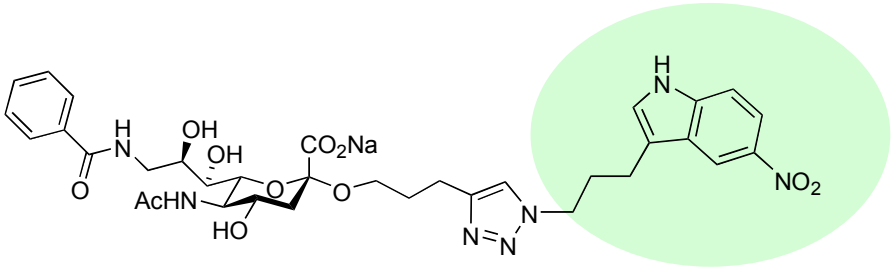

Figure 63: Chemical structure of the second generation ligand **SH-272** that was used for binding site evaluation. The second site fragment is highlighted in green.

Second generation ligands in general showed a different behaviour in the capturing assay compared to sialic acid derivatives. The main deviation was that all sensorgrams were positive. In a first evaluation on a low capacity surface using **SH-272** an increase was observed for concentrations above 125 µM and sensorgrams displayed fast interaction kinetics (*figure 64*).

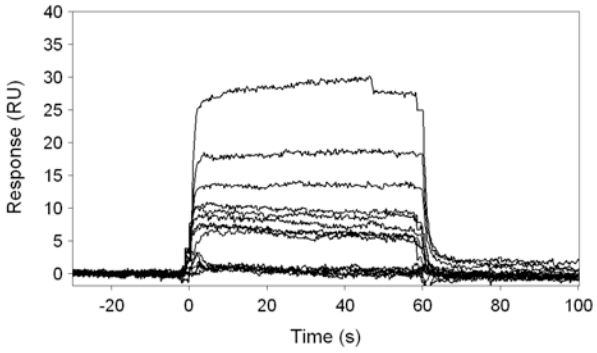

Figure 64. Sensorgrams obtained for **SH-272** starting at a 1 mM concentration. A liner increase was visible but signals went not properly back to baseline.

Interestingly, the steady state signal never went totally back to baseline for lower concentrations leading to a plateau on the level of 6-8 RU. Binding signals obtained

were perfectly fit to a two binding site model (*figure 65-B*) whereas the simple 1:1-binding site model failed (*figure 65-A*). The higher K_D was estimated in the range of unspecific binding events (6.2 mM) and for the first site a K_D of 1.3 µM was calculated. Therefore the concentration range was adjusted to the first binding site for additional experiments performed on a higher MAG density. A simple 1:1-binding site fit and an enhanced positive signal was expected.

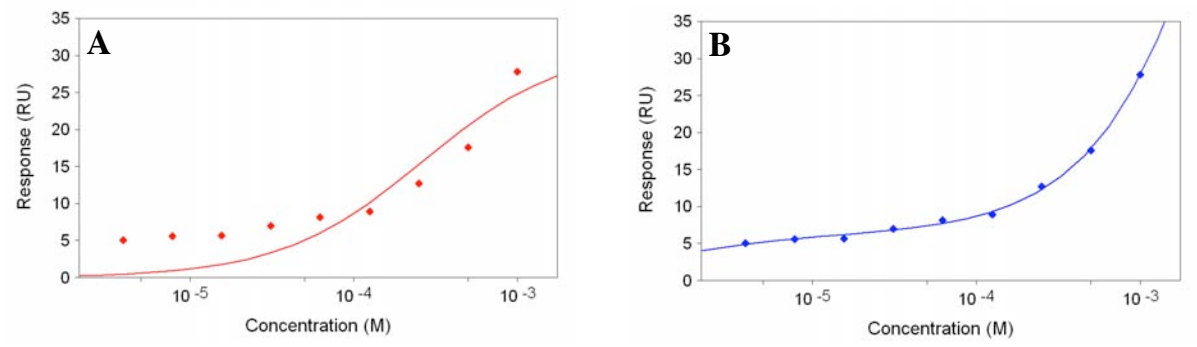

Figure 65. Fitting curves for **SH-272**: simple 1:1-binding site (A) and two-binding site model (B). A decent fit was obtained for the two binding site model.

To obtain larger signals, the surface was used directly after capturing of MAG. This led to a higher surface decay and broader signal distribution (*figure 66-A*). Nevertheless, signal intensity increased as expected. A clear drop of signal intensity during all injection was observed for triplicate measurements (*figure 66-B*). In an experiment performed 24 h later on a lower surface, the R_{max} value was back to 8 RU as seen in previous measurements (*figure 66-C*). Hence, second-site ligands had to be measured on a higher surface density to obtain sufficient signal intensity. A simple 1:1-binding event was observed with the indicated variation for the triplicates.

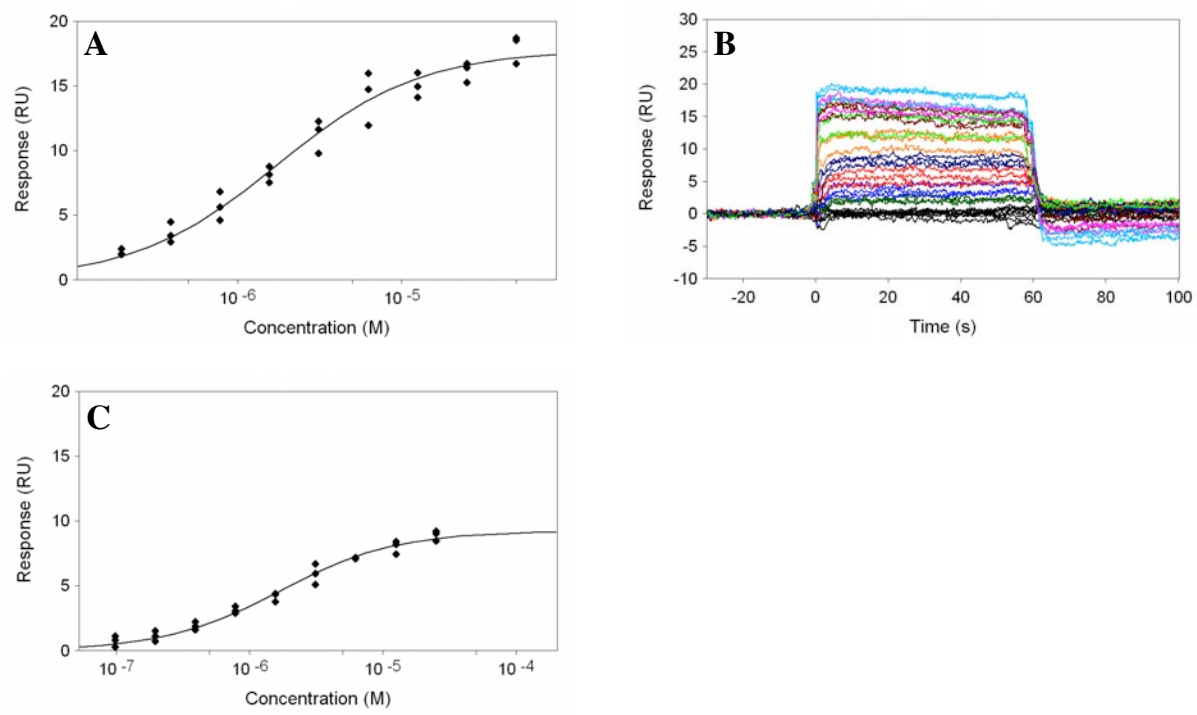

Figure 66. Sensorgrams and fitting curves for **SH-272** on a high (A, B) and low capacity surface (C).

All K_D values determined for **SH-272** on different surfaces and at different concentrations were in good agreement (*table 71*).

Table 71. Comparison of K_D's obtained for **SH-272** on different surfaces and concentrations.

Compound	Two binding-site model		High capacity surface	Low capacity surface
	site 1	site 2		
SH-272	1.30 μM	6.3 mM	1.74 μM	1.69 μM

Furthermore, **SH-272** was measured on an amine coupling surface to compare the data. A high correlation was found for both affinity as well as activity (*table 72*). This supported our hypothesis that negative sensorgrams were derived from a conformational change and that amine coupling did not alter protein activity, but limited its conformational freedom. Second-site ligands somehow acted differently and did not elicit a conformational change.

Table 72. Comparison of results for **SH-272** on capturing and amine coupling surfaces.

Assay	K_D capt. (μM)	R_{max} (RU)	Activity (%)
Capturing	1.74	17.7	23
Amine coupling	1.75	17.5	26

For the isolated nitro-indole (245.24 g/mol) no binding was observed up to a 600 μM concentration. This was most likely due to a combination of very low affinity and low molecular weight. The triazole derivative (**SH-2-6**) of the first-site ligand showed an affinity of 11.7 μM and negative signals. In general, negative signals were found for all first-site ligands. Furthermore, affinity increased with extension of the hydrophobic chain at the anomeric centre (*table 73*). An identical behaviour was already discussed for the GSLA-2 system and therefore appeared to be a general effect as long as no steric hindrance occurs. Either an additional hydrophobic interaction was established or the increased hydrophobicity pushed the ligand out of the hydrophilic buffer environment.

Table 73: First site fragments were analyzed to compare the exact gain of the second site fragment.

Compound	Chemical structure	K_D (μM)
SH-2-6	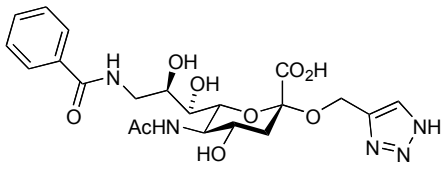	11.7
SH-264	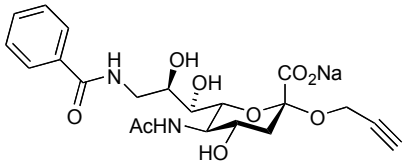	76.4
SH-218	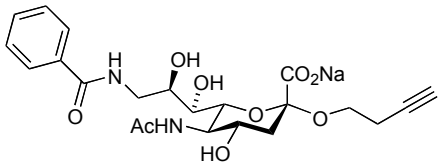	63.5
SH-192	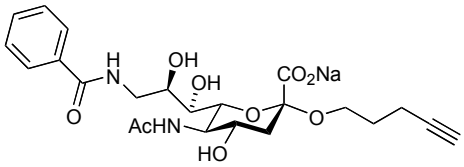	46.4
SH-246	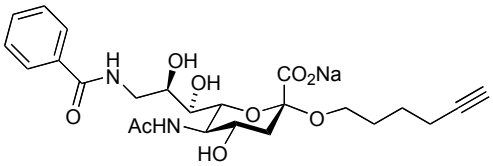	39.6
SH-267	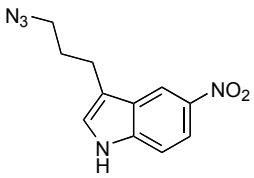	>600

3.2.3.2 Competition experiments with sialic acid derivatives

To evaluate the proposed competitive binding mode, a sialic acid derivative (**SH-082**) and a second-site ligand (**SH-272**) were used in a competition experiment. By including blanks that contained the specific competition molecule **SH-082**, it was possible to both clarify the crossing from negative to positive sensorgrams but also to perform a K_D determination by simply subtracting the blanks.

As expected, the binding of the **SH-272** compensated the negative signal of **SH-082**. Several observations proved the identical binding site. First, the R_{max} value displayed about the same positive value (*figure 67*). In case of a non-competitive binding, the negative signal would just have been compensated by the R_{max} value from **SH-272** (8-10 RU). Hence, crossing zero and the similar positive R_{max} value was a strong proof for a competition event.

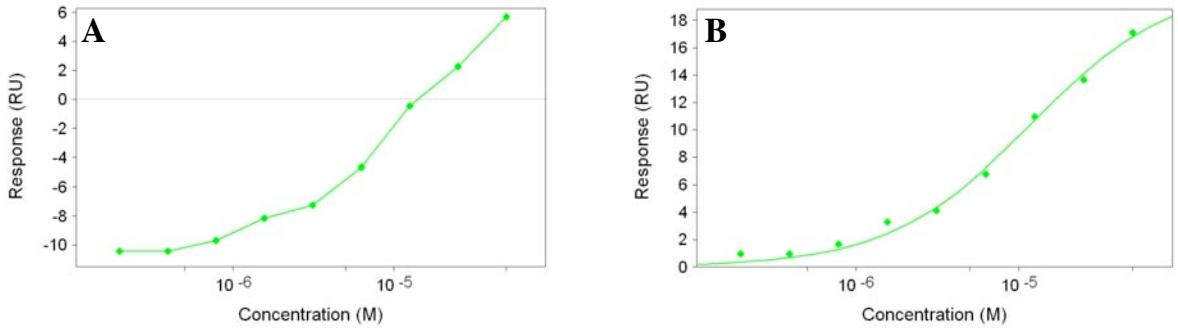

Figure 67. Compensation of the negative signal by binding of the second-site ligand to MAG (A). After subtraction of the blanks containing **SH-082**, it was possible to fit the data to a simple 1:1-binding model (B).

The experiments further revealed that a higher concentration of competitor led to a higher apparent K_D (*figure 68, table 74*). This represents the expected behaviour and further supported the identity of the binding site.

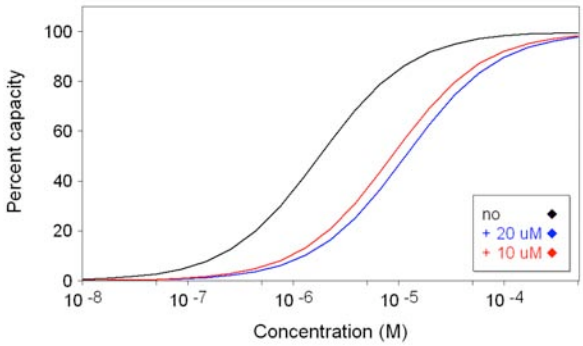

Figure 68. Normalized fitting curves obtained for All three competition experiments.

Table 74. Obtained K_D values for the competition experiment

Competitor (μM)	Apparent K_D (μM)
0	1.7
10	7.8
20	11.8

3.3 *Expression of MAG(d1-3)-SNAP*

Due to the discussed drawbacks, an additional immobilization strategy beside capturing and amine coupling was evaluated, with the focus on a gentle, oriented and covalent immobilization. A rather new technique (SNAP-tag) based on an enzymatic immobilization fulfilled all these requirements. The SNAP-tag is a mutant of the human DNA repair protein O^6-alkylguanine-DNA-alkyltransferase (hAGT) exhibiting advanced properties for immobilization. After attachment of its substrate to the sensor chip, the suizide enzyme links itself to the surface covalently (*figure 69*). Hence, a target protein that is genetically linked to the enzyme is immobilized onto the chip at physiological conditions (*pH* 7.4, 150 mM NaCl).

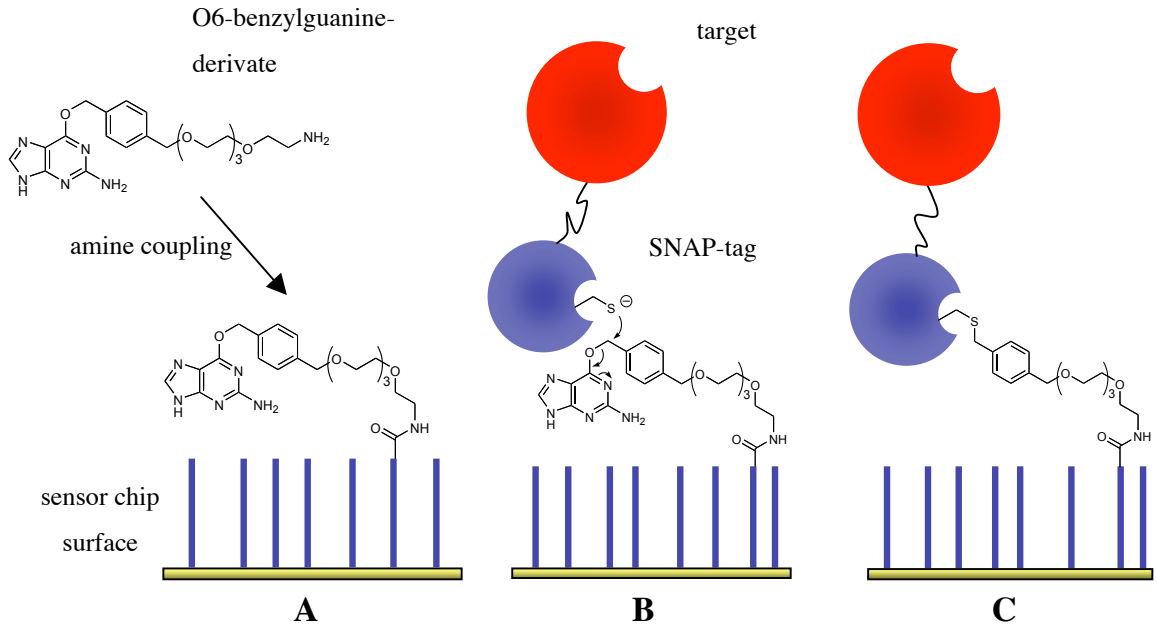

Figure 69. Enzymatic immobilization: First the substrate is immobilized via standard amine coupling (A). Afterwards, the enzymatic reaction of SNAP (blue) is performed (B) linking the target protein (red) covalently to the sensor chip (C).

In the case of MAG, it is known that glycosylation and post-translational modifications are important to obtain an active protein (unpublished results). Expression of active MAG was described in COS-7 and CHO cells. Therefore, *E.coli* and yeast were considered unsuitable. In contrast, mammalian or insect cells were applicable. Finally, due to its in-house availability, the baculovirus infected insect

cell expression system was applied for preliminary experiments. In a subsequent attempt, MAG(d1-3)-SNAP was expressed in COS-7 and CHO cells at the University of Bremen. The three different construct are described in *figure 70.*

Even though a direct enzymatic immobilization out of *E. coli* lysate was described earlier, insect cell media or the dilute sample for secreted protein could demand purification for proper immobilization. Therefore, an appropriate tag system was included. The His-tag was not applicable due to interference with the insect cell media. On the other hand, Invitrogen recommended the FLAG-tag. For the MAG(d1-3)-SNAP construct for the mammalian cell expression system a Strep-tag was applied.

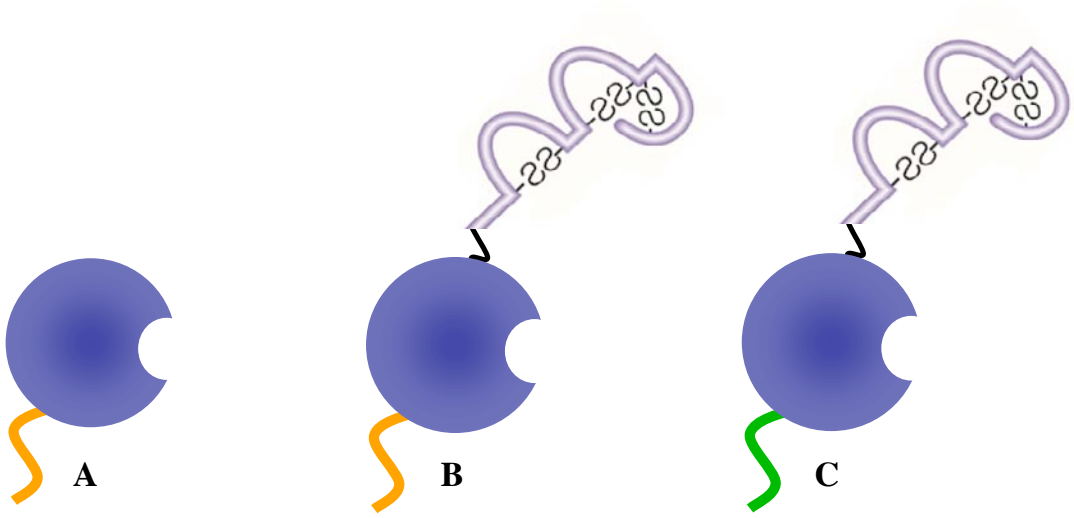

Figure 70. Overview of the constructs: In the first construct the SNAP-tag (blue) was fused to a FLAG-tag (orange) and expressed in insect cells (A). In the target construct the MAG(d1-3) sequence was fused to SNAP-FLAG and expressed in insect cells. For the expression in mammalian cells, the Strep-tag (green) was used for purification (C).

Several uncertainties complicated the usage of the SNAP-tag in insect cells. First, secretion of SNAP-tag from insect cells in its active form was not described yet. In addition, no information about stability of the SNAP-tag under low pH conditions (pH 3.5) was available. Stability at low *pH* was a prerequisite for FLAG-tag purification.

3.3.1 Insect cells as expression system

In a first attempt, PCR-integration was applied for cloning *MAG(d1-3)-SNAP* and *SNAP* into a pFastBac vector containing the acidic glycoprotein gp67 secretion signal.[197] PCR-integration results in a direct linkage of the secretion signal to the *N*-terminal MAG sequence. Unfortunately, no successful integration was obtained and a standard restriction-ligation approach was conducted instead. The major drawback was the incorporation of 2 *N*-terminal amino acids due to the restriction site. The *N*-terminal sequence was already known to be critical for the sialic acid binding site (unpublished results). The binding mode proposed based on the in the homology model displayed a potential problematic involvement of Trp22 that lies close to the *N*-terminus. Nevertheless, an evaluation of SNAP activity in such a construct was possible.

3.3.1.1 Cloning of MAG(d1-3) into pSS26b

Amplification of MAG(d1-3) out of pIgMAG(d1-3)

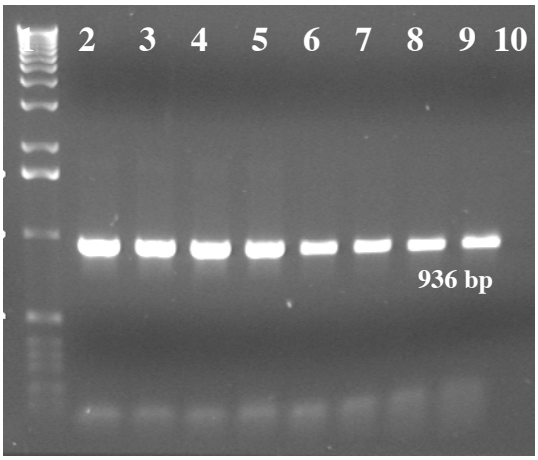

Lane 1: DNA marker X, 2 µl
Lane 2-5: vector conc. 1:10, 5 µl
Lane 2: 59.3°C , 5 µl
Lane 3: 62.1°C, 5 µl
Lane 4: 63.9, 5 µl
Lane 5: 65°C, 5 µl
Lane 6-9: vector conc. 1:100, temperature graduation as Lanes 2-5, 5 µl
Lane 10: Blank

Fig.ure 71. Screening for optimal temperature conditions. The correct size of the product was obtained for all PCRs (936 bp).

A single band was observed for all temperatures screened (*figure 71*). Because a temperature gradient led to no differences, future PCR reactions were done without

prior temperature evaluation but just based on primer melting temperature T_m. For higher template concentrations, a higher amount of PCR product was obtained.

Double-digest of pSS26b and MAG(d1-3) insert

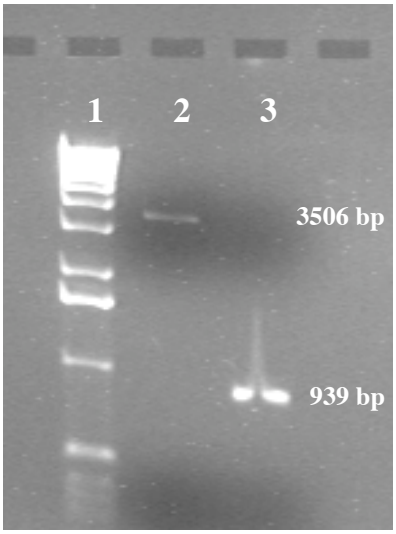

Lane 1: DNA marker X, 2 µl
Lane 2: digested pSS26b, 1 µl
Lane 3: digested MAG(d1-3) insert, 1 µl

Figure 72. Quantification of insert and vector after digest.

The pSS26b vector and the MAG(d1-3) PCR product were digested using XhoI and HindIII. The vector was clearly linearized (3506 bp) and the MAG(d1-3) insert still displayed the correct size (939 bp).

Digest analysis of pSS26b-MAG(d1-3)

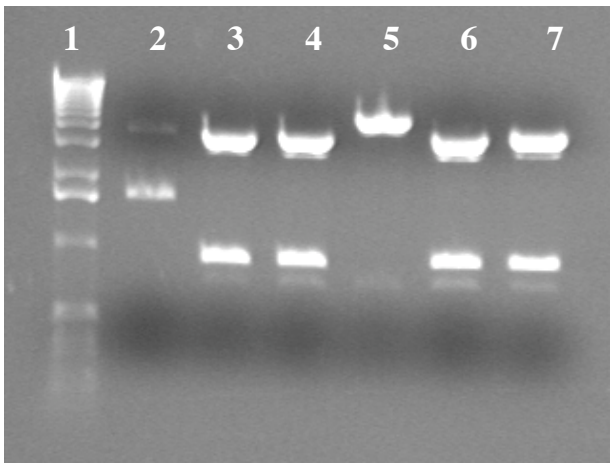

Lane 1: DNA marker X, 2 µl
Lane 2: Clone 1 MAG, 5 µl
Lane 3: Clone 2 MAG, 5 µl
Lane 4: Clone 3 MAG, 5 µl
Lane 5: Clone 4 MAG, 5 µl
Lane 6: Clone 5 MAG, 5 µl
Lane 7: Clone 6 MAG, 5 µl

Figure 73. Digest analysis of clones 2,3,5 and 6 displayed the correct fragment size of 936 bp.

Obtained mini-prep DNA was digested using XhoI and HindIII. Clones 2, 3, 5 and 6 were found to be positive (*figure 73*).

3.3.1.2 Cloning of MAG(d1-3)-SNAP / SNAP into pFastBac-S

Double digest of pFastBac-S, MAG(d1-3)-SNAP and SNAP inserts

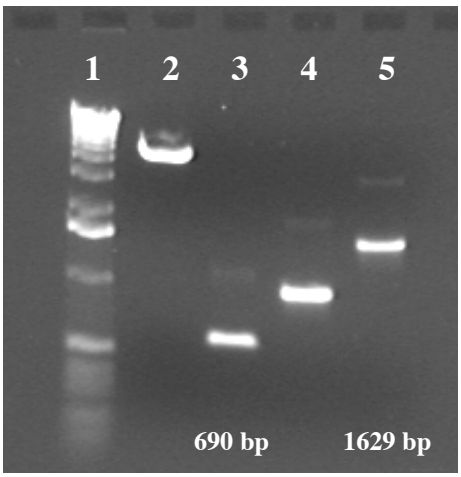

Lane 1: DNA marker X, 2 µl
Lane 2: pFastBac-S, 1 µl
Lane 3: SNAP-FLAG, 1 µl
Lane 4: (not relevant)
Lane 5: MAG-SNAP-FLAG, 1 µl

Figure 74. Quantification of inserts and vector after digestion with XhoI and XbaI.

After digestion with XhoI and XbaI, an equal amount of all inserts and vector was obtained (*figure 74*). For ligation, a ratio of 1: 4 (vector:inserts) was defined.

Digest analysis of pFastBac-MAG(d1-3)-SNAP and pFastBac-SNAP

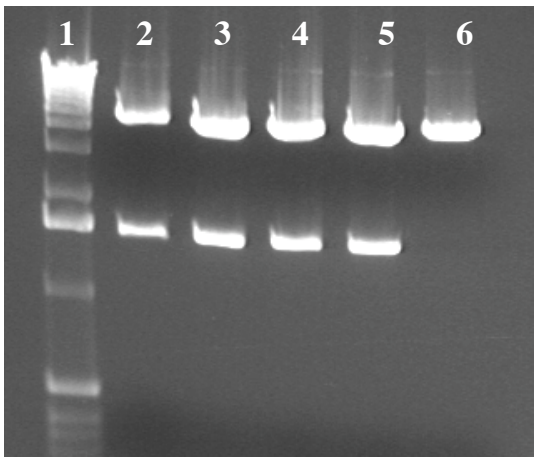

Lane 1: DNA marker X, 2 µl
Lane 2: Clone 1 MAG-SNAP, 5 µl
Lane 3: Clone 2 MAG-SNAP, 5 µl
Lane 4: Clone 3 MAG-SNAP, 5 µl
Lane 5: Clone 4 MAG-SNAP, 5 µl

Figure 75. Digest analysis of clones for MAG-SNAP using XhoI and XbaI.

After digestion of obtained mini-prep DNA with XhoI and XbaI clones 1-4 were found to be positive (*figure 75*).

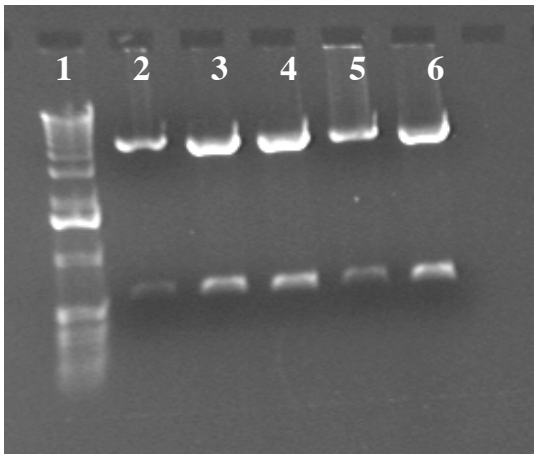

Lane 1: DNA marker X, 2 µl
Lane 2: Clone 1 SNAP, 5 µl
Lane 3: Clone 2 SNAP, 5 µl
Lane 4: Clone 3 SNAP, 5 µl
Lane 5: Clone 4 SNAP, 5 µl

Figure 76. Digest analysis of clones for MAG-SNAP using XhoI and XbaI.

After digestion of obtained mini-prep DNA with XhoI and XbaI clone 2, 3 and 5 were found to be positive (*figure 76*).

3.3.1.3 Isolation and analysis of bacmid DNA

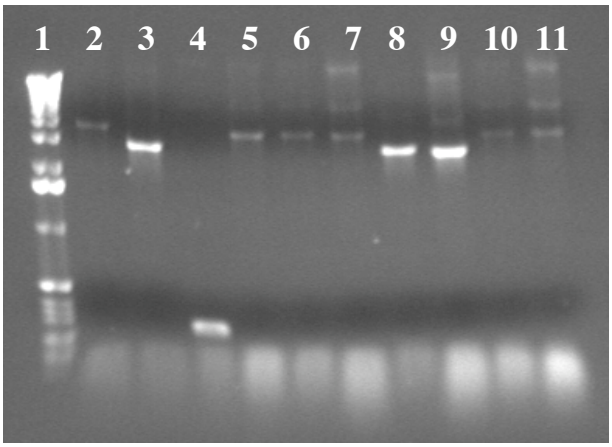

Figure 77: PCR analysis of isolated bacmid DNA. Incorporation of the genes of interest was checked before proceeding to transfection of sf9 cells.

Only one negative bacmid (300 bp) was found on lane 4 (*figure 77*). All other bacmids had successfully incorporated the gene.

3.3.1.4 Evaluation of insect cell lines for Expression

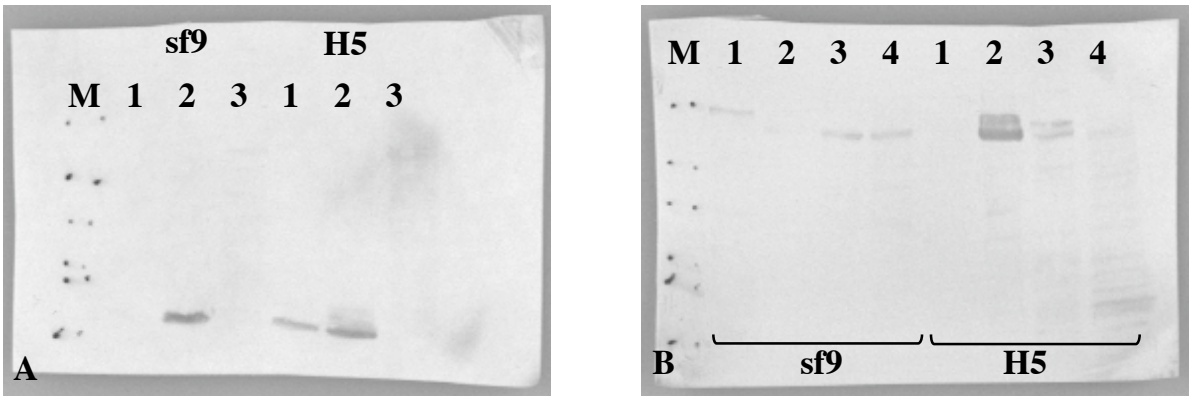

Figure 78. (A) Western blot of expressed SNAP-tag in either sf9 or H5 cells. Samples were taken after 24 (1), 48 (2) and 120 h (3). (B) Western blot of expressed MAG-SNAP-tag in either sf9 or H5 cells. Samples were taken after 24 (1), 48 (2), 72 (3) and 120 h (4).

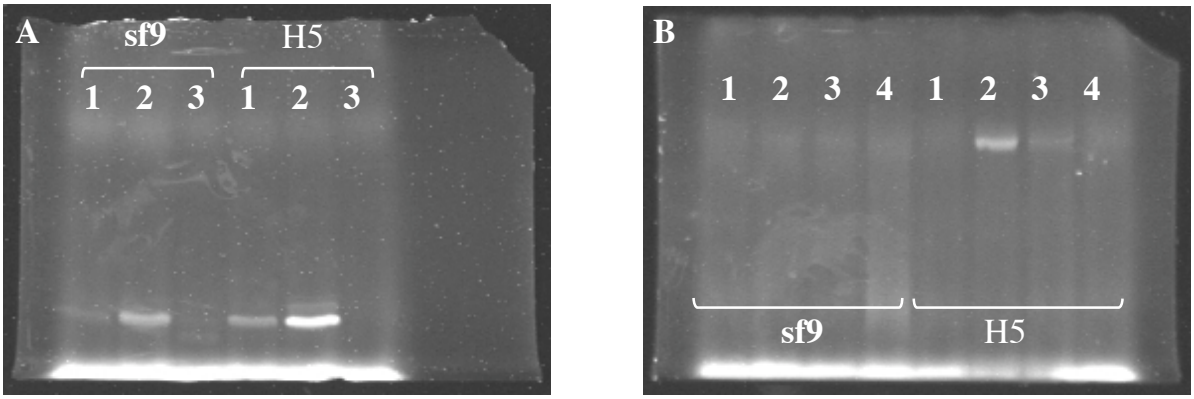

Figure 79. (A) Fluorescently labelled SNAP expressed in either sf9 or H5 cells. Samples were taken after 24 (1), 48 (2) and 120 h (3). (B) Fluorescently labeled MAG(d1-3)-SNAP expressed in either sf9 or H5 cells. Samples were taken after 24 (1), 48 (2), 72 (3) and 120 h (4).

The expression of SNAP (*figure 78-A*) and MAG-SNAP (*figure 78-B*) in insect cells was verified by western blot analysis using a anti-FLAG antibody. The band seen for SNAP (20.5 kDa) was in the range of 20 – 24 kDa and the one for MAG-SNAP (55 kDa) between 45 – 66 kDa. No additional bands were visible. For both constructs, an expression for 48 h was shown to be optimal. After 48 h, the protein bands disappeared probably due to cleavage by proteases present in the medium. For the MAG-SNAP construct, a benefit of H5 as expression system was observed.

The successful labeling of both constructs proved the enzymatic activity of the SNAP-tag after expression in insect cells (*figure 79-A and B*). Furthermore, the *N*- and *C*-terminal attachment of additional sequences did not disable enzyme activity. Unfortunately, the seen activity for the MAG-SNAP construct was lower even though the western blot showed as high expression as seen for SNAP. As a final consequence, all further expressions were carried out in H5 cells for 48 h.

3.3.1.5 Purification of FLAG-tag Proteins

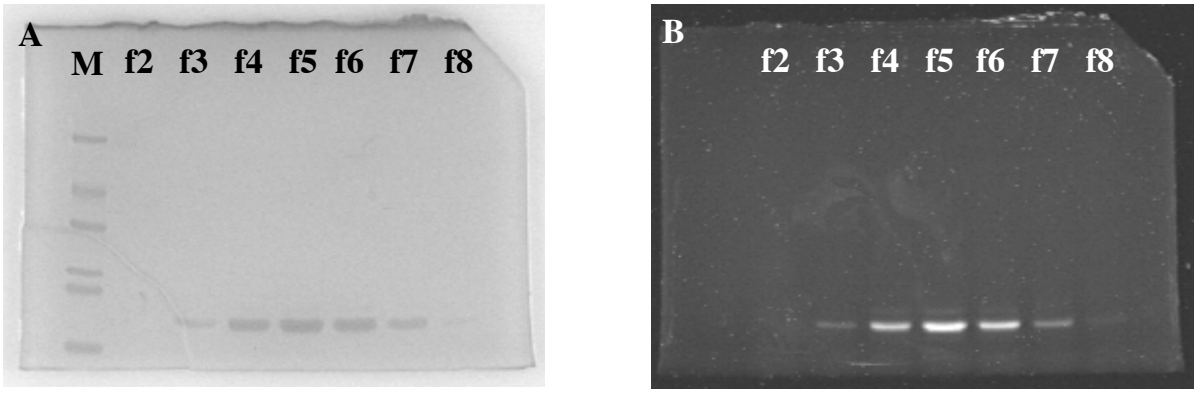

Figure 80. (A) SDS-PAGE of fractions 2 – 8 including a low molecular marker. Staining was performed with enhanced Coomassie. An even distribution of samples containing SNAP was observed as supposed. Visualization of active SNAP by using SNAP-vista blue after purification was possible (B).

The purification via the FLAG-tag was performed successfully resulting in pure protein (*figure 80-A*). The visualization of SNAP with a fluorescently labeled substrate proofed the resistance of SNAP against a *pH* of 3.5 during elution (*figure 80-B*). In addition, the observed intensity correlated to the amount of protein found in the coomassie-stained SDS-PAGE. Because MAG(d1-3) was known to withstand *pH* 3.5 in such a purification procedure, the FLAG-tag was proven to be suitable for the purification of MAG(d1-3)-SNAP.

3.3.2 Mammalian cells as expression system

Cloning and expression was performed at the Centre for Biomolecular Interactions, University of Bremen in the laboratory of Prof. Soerge Kelm, All enzymes used were purchased from Fermentas GmbH. The purification system was changed to Strep-tag/Streptactin that is routinely utilized in the group. In a first attempt, a transient expression was performed in COS-7 cells to check for expression of the construct. Afterwards a stable CHO cell line was established. Due to the use of the natural MAG secretion signal, no additional *N*-terminal amino acids were incorporated. The construct was build the way active MAG(d1-3) was produced earlier.

3.3.2.1 Cloning of SNAP into pcDNAIII-Strep

Colony PCR

Colony PCR is used as a fast and easy technique to screen for positive clones after ligation. Clones were picked from an agar plate and directly added to a prepared PCR mixture. Clones containing the correct gene resulted in a PCR product of the correct size.

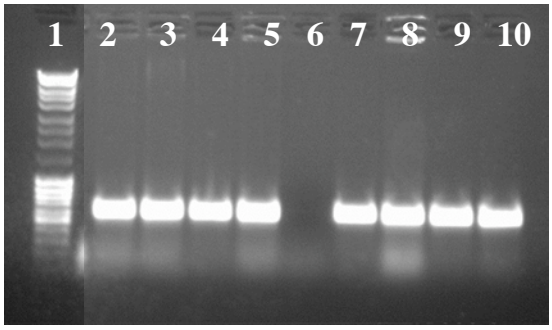

Lane 1: DNA marker, 10 µl
Lane 2-10: Colony PCR of clones 1-9, 10 µl

Figure 81. Colony PCR samples on agarose gel

All clones except clone 5 were positive (*figure 81*).

Harvest and analysis of transfected Cos-7 cells

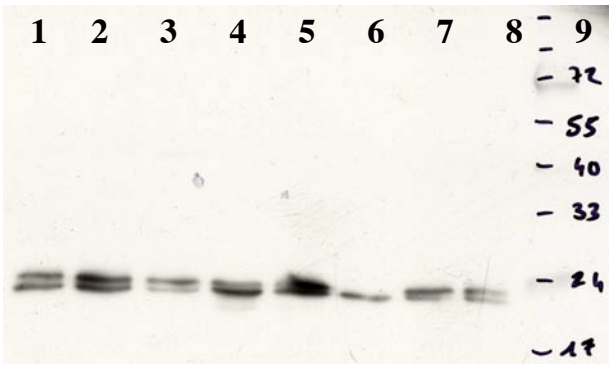

Lane 1-8: Lysate, 10 µl

Lane 9: MWM in kDa, 10 µl

Figure 82. Western blot with an anti-Strep antibody.

Harvested and lysed cells were checked for intracellular SNAP expression on a western blot using an anti-Strep antibody (*figure 82*). All eight positive clones showed expression of SNAP at the correct molecular weight (20.5 kDa).

3.3.2.2 Cloning of MAG(d1-3) into pcDNAIII-SNAP

Colony PCR

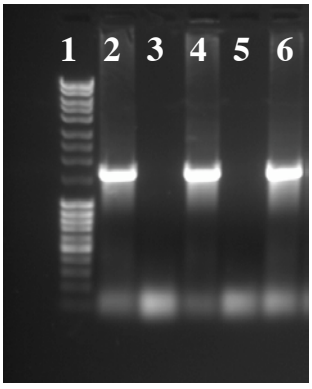

Lane 1: DNA marker, 10 µl

Lane 2-6: Colony PCR of clones 1-5, 10 µl

Figure 83. Colony PCR of five clones for MAG(d1-3).

Only three positive clones (clone 1, 3 and 5) were found in colony PCR (*figure 83*).

Digest analysis of MAG(d1-3) plasmids

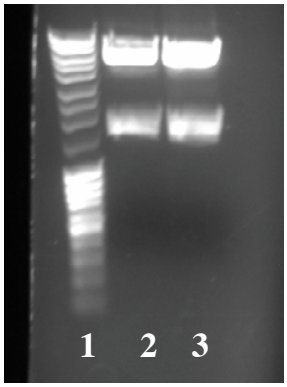

Lane 1: DNA marker, 10 µl
Lane 2: clone 1, 10 µl
Lane 3: clone 5, 10 µl

Figure 84. Digest analysis of clones 1 and 5.

Clone 1 and 5 showed the correct size (975 bp) for the insert (*figure 84*).

Harvest and analysis of COS-7 supernatant

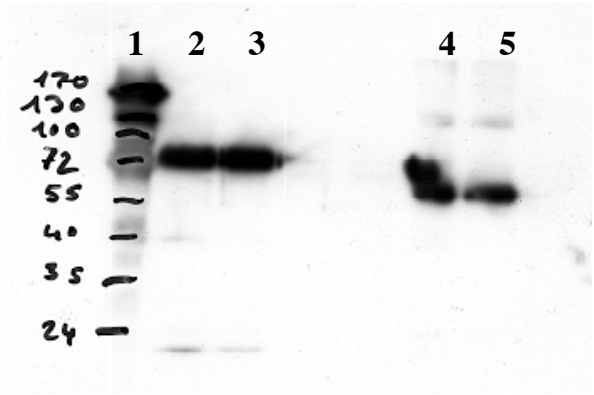

Lane 1: DNA marker, 10 µl
Lane 2: clone 1 red., 10 µl
Lane 3: clone 5 red., 10 µl
Lane 4: clone 1 non-red., 10 µl
Lane 5: clone 5 non-red., 10 µl

Fig.ure 85. Western blot of purified supernatant after transient expression with clone 1 and 5.

By both clone 1 and 5 MAG(d1-3)-SNAP was successfully expressed and secreted as observed by western blot (*figure 85*). The molecular weight was slightly higher for the reduced sample compared to the non-reduced sample. In addition, a low amount of dimer was observed under non-reducing conditions.
Furthermore, it was possible to recognize the MAG(d1-3)-SNAP construct with an anti-MAG antibody (*in-house, Bremen*) that required a native structure for binding (data not shown). The results were very promising and a stable CHO clone was to be produced.

3.4 Enzymatic immobilization

Enzymatic immobilization was already applied in surface plasmon resonance experiments successfully.[158] For the procedure itself, the substrate immobilization, time was known to have an influence on enzymatic immobilization.[157,158]

Investigations done included a set of modified substrates and the concentration dependency of the enzymatic immobilization. Screening of different substrates was interesting for the SNAP immobilization, but also for a general aspect where small molecules should be immobilized. Gained knowledge was used to develop a procedure for the immobilization of secreted proteins out of cell culture supernatants at low concentrations (1-10 µg/ml).

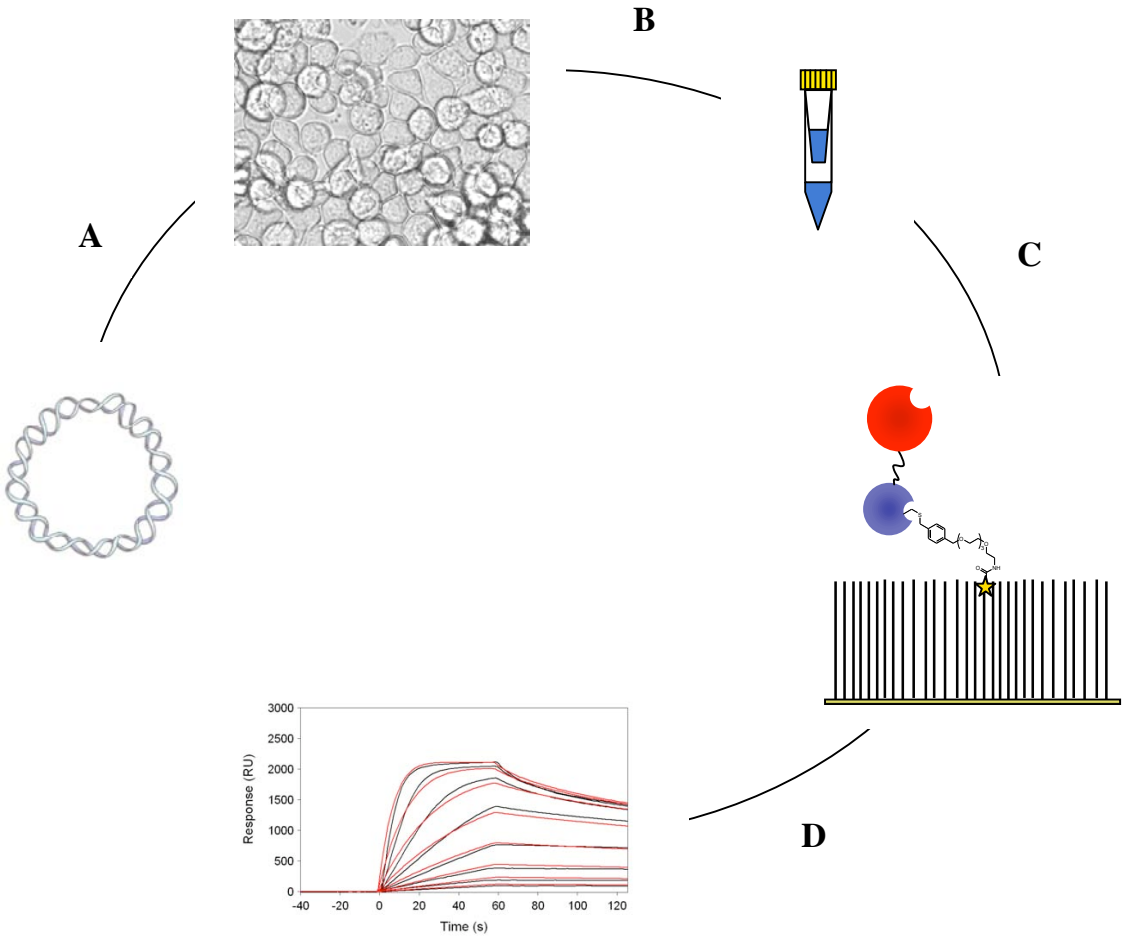

Figure 86. Final setup for a gentle production and immobilization of proteins. The gene of interest is cloned and transferred into a suitable expression system (A). After successful secretion, the protein is concentrated if necessary (B). Direct enzymatic immobilization of the target protein is performed on a modified biosensor chip (C). Interactions are measured on the highly active surface (D).

Refinement of the enzymatic immobilization procedure would enable a gentle generation of active biosensor surfaces (*figure 86*).

3.4.1 Evaluation of immobilization conditions

3.4.1.1 Testing of different SNAP substrates

To optimize SNAP immobilization, a set of different substrates was synthesized at Covalys (*table 75*). The original substrate (**BG-PEG$_3$**) was modified towards higher water solubility and better enzyme accessibility. Lower hydrophobicity was supposed to limit deposition in tubings and IFC, thus enable efficient *in situ* immobilization. Two strategies were followed: Extension of the hydrophilic chain between the amine group and the guanine (**BG-PEG$_{12}$**) as well as introduction of different hydrophilic groups at the C8 position of the guanine (**carboxy-BG, gluco-BG and sulfo-BG**).

Table 75. Set of substrates synthesized for generation of substrate surfaces with increased immobilization capacities and velocities. A red circle marks the amine coupling attachment site.

Substrate	Chemical structure
BG-PEG$_3$	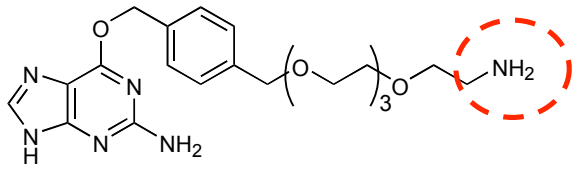
BG-PEG$_{12}$	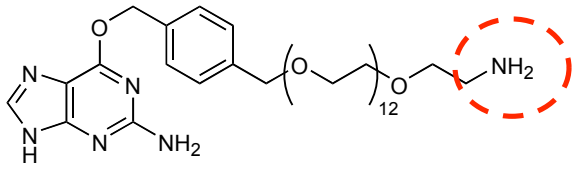
Carboxy-BG	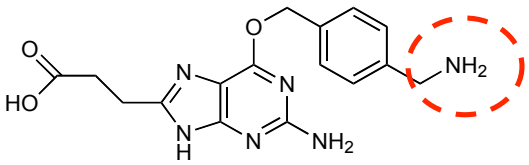
Sulfo-BG	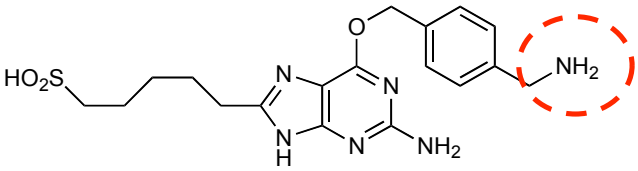
Gluco-BG	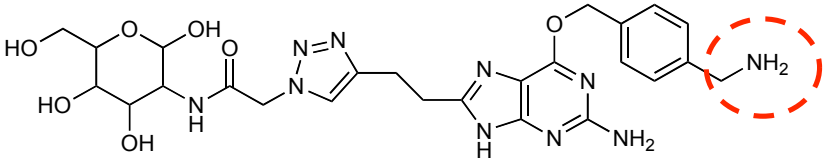

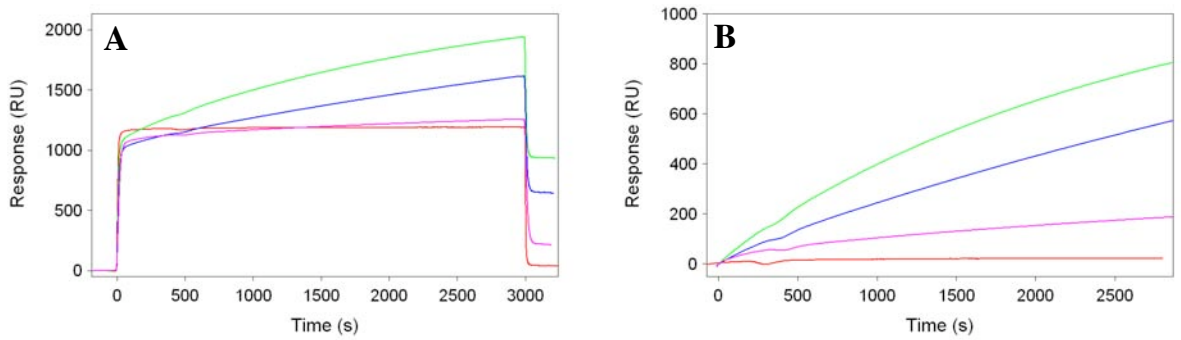

Figure 88. Immobilization of SNAP (140 µg/ml) using different substrates (green = **BG-PEG$_{12}$**, blue = **carboxy-BG**, pink = **gluco-BG**, red = reference) (A). After normalized to the start of injection the immobilization is clearly visible (B).

Since no immobilization of SNAP on the reference surface occurred (*figure 88-B, red sensorgram*), an unspecific binding to the surface could be excluded. Direct usage of concentrated fractions from purification led to a bulk signal due to differences in the buffer composition (100 mM glycine buffer and Tris) (*figure 88-A*). Buffer exchange to 10 mM PBS eliminated the bulk signal (*figure 90*). After normalization to the start of injection, immobilization could clearly be observed on all modified surfaces (*table 76).*

Table 76. Immobilization levels obtained for different substrates

Substrate	Immobilization of substrates	Immobilization level
BG-PEG$_{12}$	5 ul/min, 10 min, 1 mM	894 RU
Carboxy-BG	5 ul/min, 10 min, 1 mM	607 RU
Gluco-BG	5 ul/min, 10 min, 1 mM	178 RU

A clear advantage in respect to the immobilization level was observed for **BG-PEG$_{12}$**. Because **BG-PEG$_{12}$** was immobilized on flow cell 2, a lower SNAP concentration on the two sequential flow cells might have led to a lower result. Therefore, in a second experiment, **BG-PEG$_{12}$** was immobilized on flow cell 4 to exclude such an effect. Nevertheless, **BG-PEG$_{12}$** proved to be advantageous for SNAP immobilization. **Carboxy-BG** and **sulfo-BG** performed equally and the **gluco-BG** was inferior to the others (*figure 89*).

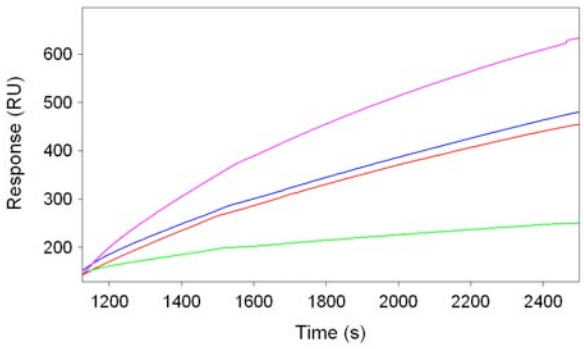

Figure 89. Immobilization of SNAP (140 µg/ml) using different substrates pink = **BG-PEG$_{12}$**, blue = **carboxy-BG**, red = **sulfo-BG**, green = **gluco-BG**

When **carboxy-BG** was dissolved in 30 % DMSO and 1 M $NaHCO_3$ pH 8.4, equal immobilization levels of **carboxy-BG** and **BG-PEG$_{12}$** were obtained (*figure 90*). Equal immobilization using a more hydrophilic substrate was possible but due to a more complex dissolution procedure **BG-PEG$_{12}$** was used for further experiments. In comparison to the original **BG-PEG$_3$**, immobilization was improved by a factor of 5 (*table 77*).

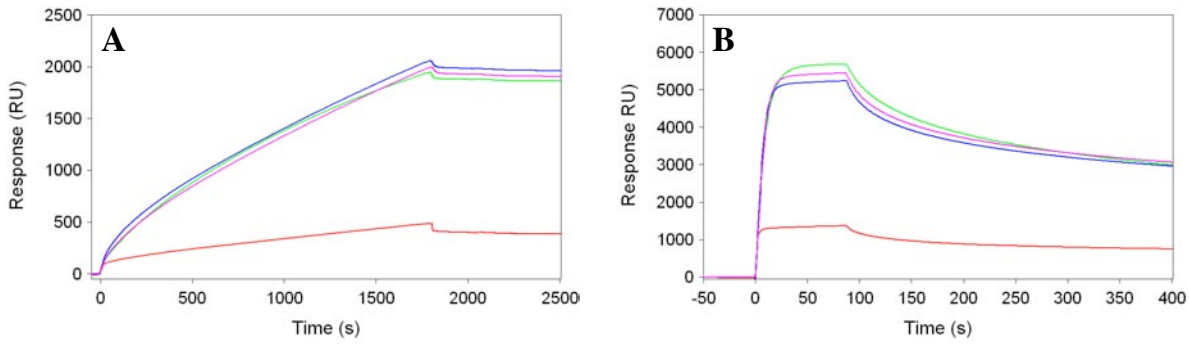

Figure 90. Immobilization of SNAP (340 µg/ml) on **BG-PEG$_3$** (red), **carboxy-BG** (blue, 10 µl/min), **carboxy-BG** (pink, 1 µl/min), **BG-PEG$_{12}$** (green). Binding of an anti-FLAG antibody proved the differences for the immobilization capacities (B). The antibody is described more in detail on p. xxx.

To reduce substrate consumption, immobilization of **carboxy-BG** was performed at 1 µl/min flow rate for 20 min. No significant deviation of the immobilization capacity or velocity was observed (*pink curve in figure 90*).

Table 77. Immobilization of SNAP on **BG-PEG$_3$**, **BG-PEG$_{12}$** and **carboxy-BG**.

Substrate	Immobillization level	anti-FLAG AB
BG-PEG$_3$	400 RU	1350 RU
BG-PEG$_{12}$	2000 RU	5700 RU
carboxy-BG	1950 RU	5450 RU

Faster immobilization and consequently higher immobilization levels obtained with **BG-PEG$_{12}$** was supposed to be derived from the longer spacer. A longer distance between the reactive amine group and the substrate might allow the substrate to be positioned further away from the dextrane matrix. Most likely this leads to an increased accession to the substrate. In contrast, **carboxy-BG** resulted in equal immobilization levels even though no such spacer was included. A beneficial effect of the introduced negative charge on substrate accessibility is a possible explanation.

3.4.1.2 Testing of different SNAP concentrations

The sensorgrams obtained showed a dependency of the SNAP concentration on the immobilization velocity (*figure 91*). Injection of 125 µg/ml SNAP resulted in a fast increase with signs of saturation towards the end. In contrast to 125 µg/ml, the injection of 31.3 µg/ml SNAP exhibited a rather linear increase.

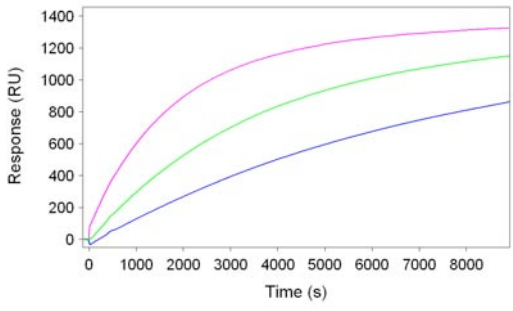

Figure 91. Sensorgrams of injections of three different SNAP concentrations over equal surfaces (magenta: 125 µg/ml, green: 62.5 µg/ml, blue: 31.3 µg/ml)

It seems that by longer injections of lower concentrations equal immobilization level can be achieved. An injection of 60 µg/ml allowed fast immobilization of high levels with the use of only 10 µg SNAP (*table 78*).

Table 78. Immobilization behaviour and total sample consumption for SNAP immobilization.

	Level (% max.) 50 min	**Level (% max.) 150 min**	**Total sample consumption**
125.0 µg/ml	1058 RU (80 %)	1324 RU (100 %)	18.8 µg
62.5 µg/ml	699 RU (53 %)	1149 RU (87 %)	9.4 µg
31.3 µg/ml	393 RU (30 %)	861 RU (65 %)	4.7 µg

On the created surfaces with low, mid and high SNAP capacity, **SH-019** and diazepam were tested for binding. Diazepam was evaluated because its binding to an earlier mutant of hAGT was described.[158] Interestingly, no binding of diazepam was observed (*figure 92-A*). Hence, efforts by Covalys to further optimize the hAGT to reduce unspecific binding appeared successful. In addition, **SH-019** did not bind to SNAP (*figure 92-B*) what was a prerequisite to use the technology for MAG.

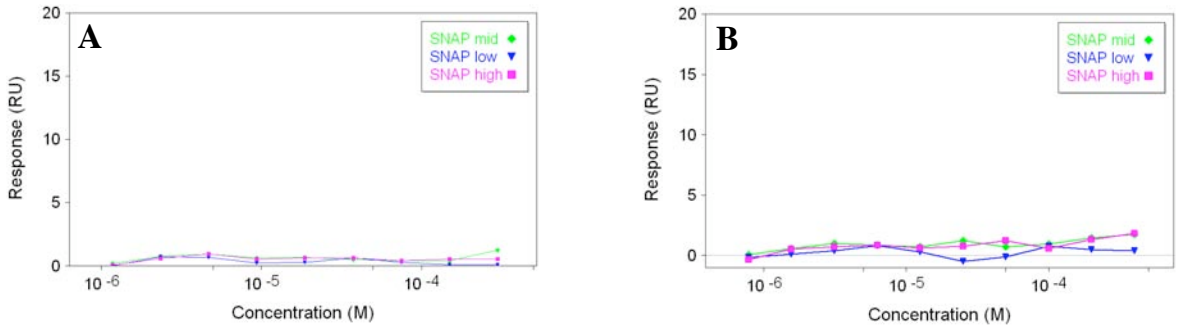

Figure 92. Steady state evaluation of binding experiments with Diazepam (A) and **SH-019** (B).

3.4.1.3 Testing of different substrate immobilization times

The difference between a substrate immobilization time of 5 and 20 minutes was analyzed using identical concentrations (1 mM) of **BG-PEG$_{12}$**. A SNAP sample (40 µg/ml) was injected over the surface and after 150 min, 53 % more SNAP (1967 RU)

was immobilized on the surface with 20 min substrate contact time then on the one with only 5 min (931 RU). After a second injection of a new SNAP sample, even more SNAP was immobilized but the ratio of the immobilization levels between the two surfaces did not change. This proved the reaction to be highly dependent on the substrate concentration on the sensor chip. The second injection of fresh SNAP led to the same slope what excluded a decreased velocity due to a denaturation of SNAP during the 150 min injection time (*figure 93*). Therefore, the saturation seemed to directly monitor the substrate level on the chip.

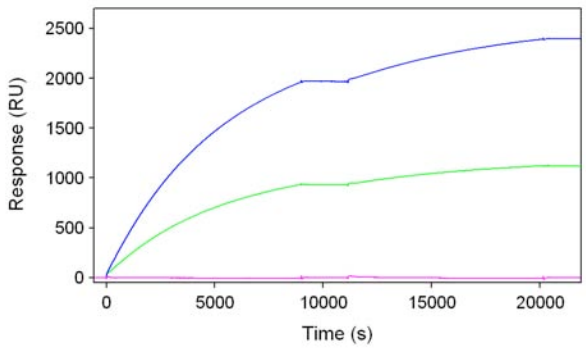

Figure 93. Sensorgrams of two sequential injections of SNAP over three different surfaces (magenta: reference, green: 5 min substrate contact time, blue: 20 min substrate contact time)

Comparing these results with earlier data using a SNAP concentration of 62.5 µg/ml (*table 79*) demonstrated that immobilization levels were highly controllable and reproducible by the substrate contact time and the actual SNAP concentration.

Table 79. Immobilization of SNAP obtained for surfaces with different substrate contact times.

	5 min contact time (40 µg/ml)	**20 min contact time (40 µg/ml)**	**5 min contact time (62.5 µg/ml)***
150 min	931 RU	1967 RU	1149 RU
300 min	1120 RU	2397 RU	

3.4.1.4 Comparison of SNAP and MAG(d1-3)-SNAP

The conditions discovered for an optimal enzymatic immobilization were used to immobilize purified MAG(d1-3)-SNAP (290 µg/ml) onto the sensor chip. Furthermore, a direct immobilization of insect cell culture supernatant containing SNAP (4 µg/ml) was examined.

Injection of supernatant led to a big bulk signal in contrast to purified SNAP and MAG-SNAP present in 10 mM PBS (*figure 94*).

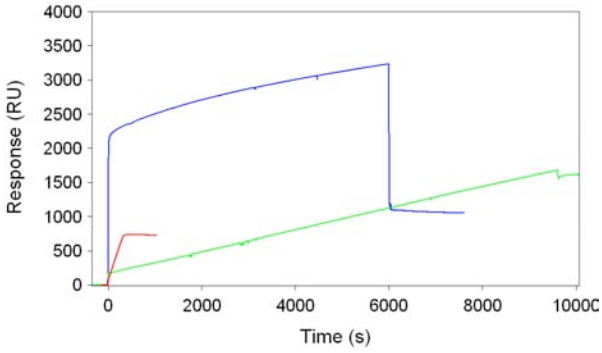

Figure 94. Immobilization of SNAP (red) and MAG-SNAP (green). In addition, a direct immobilization of SNAP (4 µg/ml) out of insect cell culture supernatant was carried out (blue).

Controllability for such an enzymatic immobilization was proven to be high when comparing levels that were normalized by the molecular weight (SNAP 36 RU, MAG(d1-3)-SNAP 30 RU).

Table 80. Immobilization of MAG(d1-3)-SNAP, SNAP and SNAP (supernatant)

Sample	Immobilization (RU)	Immobilization* (RU)
MAG(d1-3)-SNAP	1600	29
SNAP	730	36
SNAP (supernatant)	1050	52

*normalized by the MW

To compare protein levels quantitatively, a monoclonal anti-FLAG antibody was utilized. The antibody was characterized and then single injections at an adequate concentration (290 nM) were used to determine the protein level on the chip (*figure 94 and table 81*).

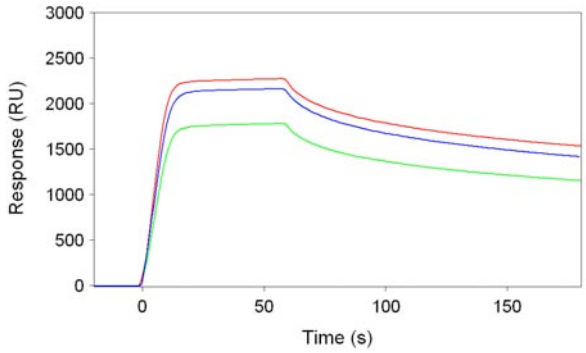

Figure 94:.Immobilization of SNAP (red) and MAG(d1-3)-SNAP (green). In addition, a direct immobilization of SNAP out of the supernatant was carried out (blue). An empty flow cell was used as reference.

Table 81. Responses obtained for the anti-FLAG antibody binding to immobilized SNAP/MAG(d1-3)-SNAP

Sample	anti-FLAG* (RU)	R_{max} (RU)	Response/R_{max}** (%)
MAG(d1-3)-SNAP	1770	4364	81.2
SNAP	2150	5341	80.6
SNAP (supernatant)	2250		

*injection of a 290 nM concentration

**Normalized to a bivalent ligand

A kinetic evaluation proved bivalent ligand behaviour as expected for an antibody (*figure 95*). The bivalent behaviour was in good agreement with the 40% binding observed. Therefore the antibody seemed to bind to more than 80% of the immobilized protein. A concentration of 290 nM seemed optimal to compare immobilization levels when considering the observed steady state signals for the two highest concentrations (290 and 145 nM).

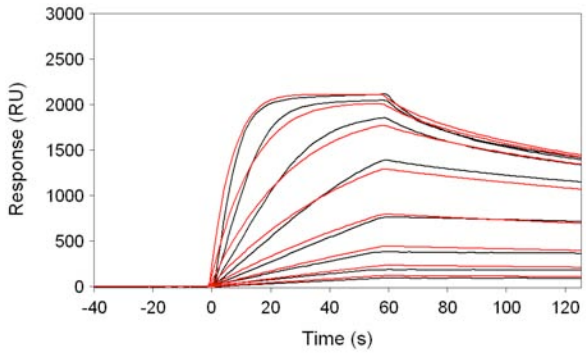

Figure 95. Injection series for determination of the apparent K_D of the anti-FLAG monoclonal antibody to SNAP-FLAG.

The anti-FLAG antibody provided a trivial tool to determine the actual amount of protein immobilized. In the case of direct immobilization of supernatant from insect cell cultures, the immobilization response was higher than the final corresponding antibody binding response. This pointed towards the fact that during immobilization, media reagents or other contaminants bound weakly to the surface leading to a slightly higher immobilization signal. The antibody allowed detecting such a deviation accurately.

The immobilization velocity was compared between SNAP and MAG(d1-3)-SNAP based on the molar protein concentration. A clear difference between immobilization of MAG(d1-3)-SNAP and SNAP was observed (*table 82*). For the MAG construct a slower immobilization velocity was found what could be derived from a reduced v_{max} of the enzyme or by the size of the protein. The amount of immobilized MAG(d1-3)-SNAP was 2311 RU and corresponded to a R_{max} value of 23 RU for a 500 Da ligand. Even though the amount of immobilized MAG was sufficient to measure low molecular weight ligands, higher protein concentrations should allow generating higher capacity surfaces. This was obvious when comparing results from SNAP where an increase of protein concentration by a factor of 8 resulted in a decrease of sample consumption by a factor of 5. On the other hand, injections of lower concentrations over night should result in saturation levels and increase capacity as well.

Table 82. Comparison of enzymatic immobilization of SNAP and MAG(d1-3)-SNAP.

Construct	Level* (RU)	Concentration (µg/ml) / (µM)	Injection (µl)	Chip# (substrate)
SNAP	96	40 / 2.0	150	20min, 1mM
SNAP	65	125 / 6.1	150	5min, 1mM
SNAP	56	63 / 3.1	150	5min, 1mM
SNAP	42	32 / 1.6	150	5min, 1mM
SNAP	98	340 / 16.6	30	20min, 2mM
MAG-SNAP	42	290 / 5.3	350	20min, 1mM

*The response was normalized with the molecular weight to be in relation to the immobilized molar amount of protein.

Immobilization of substrate on the sensor chip

3.4.1.5 MAG(d1-3)-SNAP expressed in mammalian cells

The entire enzymatic immobilization procedure for secreted proteins out of supernatant was applied to MAG(d1-3)-SNAP expressed in CHO cells.
A total of 1780 RU of MAG(d1-3)-SNAP was immobilized. An anti-MAG antibody (0.6 mg/ml) was diluted 100 fold in running buffer and injected for 60 s at 20 µl/min. A specific binding to MAG(d1-3) was observed whereas no binding to the reference surface occurred (*figure 96-A*). Removal of the anti-MAG antibody was only achieved using pH 1.5. Unfortunately, the MAG(d1-3) activity was diminished by more than 50% after regeneration. Such an acid instability was already known for MAG. Therefore, no repetitive experiments were possible to further characterize the interaction between the anti-MAG antibody and MAG.

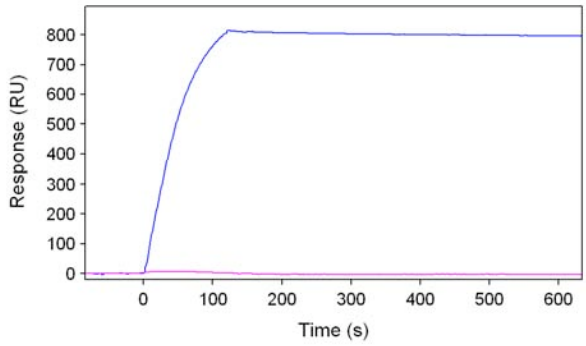

Figure 96. Binding of a specific anti-MAG antibody to immobilized MAG(d1-3)-SNAP (blue). No binding to the reference surface was seen (pink).

The reference ligand **SH-019** was used to compare MAG(d1-3)-SNAP with Fc-MAG(d1-3). A high reproducibility was observed for triplicate injections and sensorgrams displayed an identical kinetic profile compared to the capturing assay (*figure 97-A*). No baseline drift occurred what was expected due to the covalent immobilization. Sensorgrams remained negative what was congruent with the conformational change hypothesis. Beside the *C*-terminal SNAP-tag, no other attachment to MAG(d1-3) was needed what assured an entire conformational freedom.

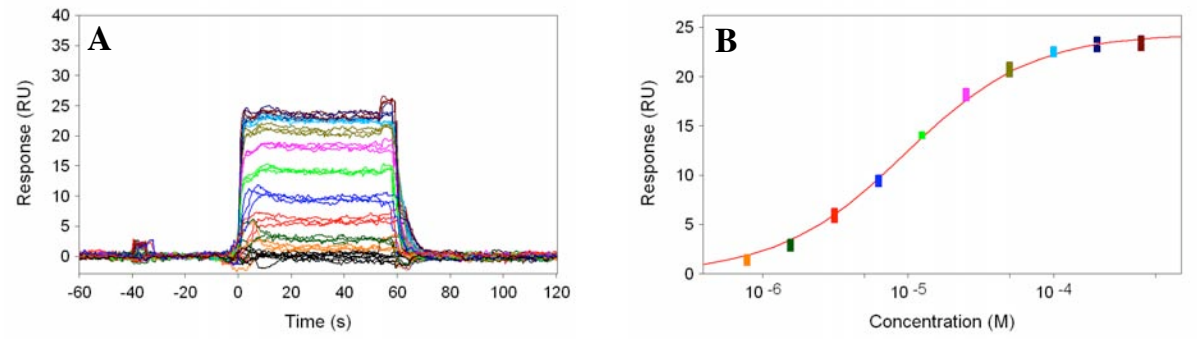

Figure 97. Sensorgrams (A) and fitting curve to a simple 1:1-binding model (B) obtained for SH-136.

The calculated K_D was 9.6 μM what was 2-fold lower than for the capturing assay. The fitting was of extraordinary good quality what further supported the usability of enzymatic immobilization (figure 97-B).

4 CONCLUSIONS AND OUTLOOK

GSLA-2

Preliminary experiments conducted with a diagnostic carbohydrate-binding antibody (GSLA-2) disclosed major advantages of the Biacore technology. Besides, a set of drawbacks and pitfalls were identified, specifically important for drug-like molecules of low molecular weight (<500 Da).

The antibody was coupled to the biosensor surface using a standard amine coupling procedure. A stable surface was generated on which the binding properties of its specific antigen sLe^a were characterized. Interaction of sLe^a with GSLA-2 displayed a fast kinetic profile with a complex half-life time in the range of 1.4 s and an equilibrium dissociation constant of 23.1 μM. Fast kinetics and μM affinity is a common attribute of monovalent carbohydrate/lectin interactions.

An interesting finding was that incorporation of a hydrophobic and flexible chain (Lem = $(CH_2)_8COOMe$) used for purification of sLe^a increased affinity by a factor of 2. The gain is based on a higher association rate constant. This can be explained by a higher drive to leave the buffer due to higher lipophilicity of the ligand. Lipophilic fluorescent or radioactive tags are often required for the investigation of ligand/receptor interactions. A label-free technique like Biacore possesses a vital advantage that is especially important for small compounds were any attachment is critical due to possible steric interference.

Real-time interaction measurements on Biacore result in a very detailed picture of the entire binding process. However, the highly sensitive detection system requires special carefulness for sample quality and signal interpretation. Not only the binding of the specific ligand but also conformational changes, matrix effects or unspecific binding are reflected in a sensorgram. This was specifically observed in the case of sLe^a, where an impure ligand led to a two-phase binding event. Upon a specific fast association a slow accumulation of potential impurities was observed. In this case, commercial availability of sLe^a enabled discrimination between specific signal and impurity.

Results obtained for the two ligands sLe^a and sLe^a-Lem further disclosed interesting phenomena in terms of signal interpretation. Comparison of the protein activity displayed differences between those ligands in the range of 20%. The protein activity is defined as the active part of the immobilized protein. A surface with a higher amount of immobilized GSLA-2 (8'000 RU) was 10% less active than a surface with only 3'800 RU. This was consistent for sLe^a and sLe^a-Lem. A possible explanation was the distribution of GSLA-2 inside the carboxymethyl matrix. Because sensitivity decreases linearly within the matrix (100nm), a change in distribution does influence the signal significantly. An additional 10% deviation was caused by the ligand itself. On both high and low capacity surfaces sLe^a displayed a 10% higher signal than sLe^a-Lem. This led to a final spectrum of the GSLA-2 activity between 26 and 44% for the different assays and ligands. At least for such small ligands a specific activity calculation seemed rather difficult.

In a co-operation with the University of Lübeck, Biacore data was combined with STD-NMR and a detailed description of the actual sLe^a binding site was attained. High specificity of GSLA-2 against the sLe^a epitope was confirmed by several experiments. Desialidation or exchange of the Glc*N*Ac moiety by a cyclohexyl ring prohibited binding completely. Hence, cross-reactivity for other carbohydrates was rather obnoxious. Kinetic and affinity data from Biacore were optimal complemented by the STD-NMR interaction profile. Such combination appeared highly promising for future projects.

Myelin-associated glycoprotein as drug target

The myelin-associated glycoprotein as target protein for spinal cord injury and myelination disorder treatment is well characterized. Gangliosides with their sialic acid moieties were depicted to be physiological ligands for MAG. *In-vitro* assays on isolated neurons supported a ganglioside mediated outgrowth inhibition beside a cascade activated by protein/protein interaction. Interestingly, downstream signalling was described to be identical for both activations. Several branches of the inhibition cascade still need to be elucidated but a first FDA approval for a drug influencing a downstream modulator (rho GTPase) in 2005 is highly promising.

While numerous publications are dealing with the biological pathway of MAG, important data required for a pharmaceutical approach are missing. Although efforts were conducted, no crystal structure is available complicating the rational design of ligands. A homology model was built in collaboration with Prof. Kelm based on Siglec 1 co-crystallized with methyl 9-benzamido-9-deoxy-Neu5Ac (**SH-164**).

Biacore assay development

For amine coupling, the analysis of the potential carbohydrate-binding domain based on the homology model was conducted. It exhibited three lysines in a distance of 10 Å to Arg118. In addition, the *N*-terminus is located in proximity of Trp22, which was found to be involved in carbohydrate binding. Though the distances between the binding site and the surface attachment sites were rather large, interference was possible.

Immobilization was performed successfully at *pH* 5.5 whereas *pH* 4.0 led to an inactive surface. The lower surface attraction at *pH* 5.5 was overcome by a 4-fold higher protein concentration. Instability of MAG at lower *pH* is known and might lead to immobilization of an inactive conformation or inactivated protein.

Signals obtained for the sialic acid derivatives were rather small (R_{max} < 15 RU), what diminished signal quality. For **SH-164** (425 g/mol) no data evaluation was possible due to the low signal intensity. Introduction of an aromatic group increased signal intensity by far more then the molecular weight, what enabled analysis of *e.g.* **SH-019** (501 g/mol). Besides, the introduction of two chlorides almost doubled the signal (**SH-082**). Such an impact was not described in literature but could occur for other low molecular weight ligands as well. Surface activity is often not published and therefore only little data is available.

To evaluate a possible deactivation of MAG after immobilization via its amine groups, a capturing approach was examined. The Fc fragment in the Fc-MAG(d1-3) construct offered a non-covalent immobilization via protein A. Immobilization of protein A via standard amine coupling was achieved easily and capturing of Fc-MAG(d1-3) led to optimal surface capacities. A steady baseline drift presented the major drawback. Nevertheless, a reduced flow rate for capturing and over night

stabilization facilitated triplicate measurements with an overall loss of only 0.6% of MAG per experiment.

Most astonishing was the fact that sensorgrams obtained were negative in a reproducible way. Such negative signals were only obtained for sialic acid derivatives. Larger molecules like G_{T1b} resulted in standard positive signals. The binding was saturable and after signal inversion a state of the art evaluation was possible. Signal intensity itself was higher compared to amine coupling and the evaluation of the SPR-experiment was possible for all ligands measured. Furthermore, a clear correlation between the MAG capacity and the R_{max} value was found and binding to protein A was ruled out. To specifically exclude a matrix effect as source for negative signals, a set of experiments was conducted with different buffer conditions. Higher ionic strength, increased buffer capacity, addition of DMSO or carboxymethyl dextrane and a sensor chip with a reduced amount of carboxyl groups were tested. None of the parameters influenced the negative signal or the K_D significantly. The remaining hypothesis was a ligand-induced conformational change that influenced the hydrodynamic radius of MAG. In this case, the negative signal derived from a conformational change was larger than the small positive signal of the ligand binding resulting in a net negative signal upon binding.

As described on the amine coupling surface, the same correlation of chlorides and higher signal intensity was found. These results further underlined that a direct correlation of signal intensity to mass was delusive for low molecular weight ligands. Biacore data compared with relative IC_{50} values from the hapten inhibition assay revealed a high correlation what further supported our interpretation of the negative signals.

Based on the established assay, a thermodynamic characterization of the interaction between MAG and the sialic acid derived ligands was performed. Selection of three compounds with distinct modifications enabled description of the exact impact of specific structural features. A general finding was that the interaction was enthalpy driven. Creation of a specific π-π interaction with Phe129 increased enthalpy by -6 $kJ \bullet mol^{-1}$ (1.4 $kcal \bullet mol^{-1}$). In contrast, the increased flexibility led to a small loss of entropy. Enforcement of the π-π interaction by halogens further fortified the

enthalpy. A detailed picture for the interaction was obtained which is in strong agreement with the docking mode of the ligands to the homology model.

Interestingly, all ligands measured displayed fast on- and off-rates. Only for **SM-m6** (K_D = 0.8 μM) a deceleration at lower temperatures (5 °C) was clearly visible in the sensorgrams. The sialic acid core structure and/or the flat binding site do most likely lead to such a fast interaction profile.

In a different ligand discovery approach, improved affinity was obtained by a so-called second-site approach. 5-Nitro-indole was found to bind in close proximity to the sialic acid binding site. Optimal linkage of the nitro-indole to the sialic acid core (= second generation ligand) increased binding affinity by a factor of 50. However, the kinetic behaviour remained fast what supported the core theory. Ligands obtained were of higher molecular weight (MW > 700 Da) and resulted in higher positive signals on the amine coupling surface. Interestingly, the capturing assay equally led to a positive signal. The identical binding site of sialic acid derivatives and the second generation ligands was verified by a competitive Biacore experiment.

Important is the fact that the sensorgrams turn positive after the attachment of the nitro-indole. Considering the conformational change hypothesis it seemed that second generation ligands did not elicit such changes. The nitro-indole might lock the conformation. Comparison of affinities of second generation ligand fragments disclosed a well-known circumstance. Affinity increased even though a longer hydrophobic chain with higher flexibility was introduced. This finding was consistent with results from the GSLA-2 project.

Enzymatic immobilization

For MAG, the importance of the protein immobilization strategy was clearly demonstrated. Either the surface was not stable or the attachment resulted in different binding properties. An enzymatic approach was considered to be a promising technique to circumvent difficult and/or doubtful immobilizations of proteins. The technique is based on the human suicide enzyme O^6-alkylguanine-DNA-alkyltransferase (hAGT) and referred to as SNAP-tag. After immobilization of its

substrate on a biosensor chip, the enzyme links itself to the surface via a specific enzymatic reaction. Hence, a genetically linked target protein can be immobilized covalently under physiological conditions. In the case of *pH* labile proteins, amine groups present in the binding site or conformational issues, the enzymatic immobilization approach would assure an active protein. Especially for non-characterized proteins or ligands, as it is often the case in drug discovery, a high fidelity is a prerequisite. Alteration of the target activity due to the linked enzyme represents the only drawback of the system.

For preliminary experiments, SNAP was expressed in insect cells in a secreted form. Expression levels were about 4 mg/L what represented an average value. Purification under low *pH* conditions (*pH* 3.5) did not diminish enzyme activity.

To enhance immobilization velocity, a set of modified substrates was tested for which substrate accessibility was optimized. A longer chain between the substrate and the amine group (attachment site) and the introduction of a carboxyl group on the substrate led to substantial improvements. A 4-fold increase was achieved allowing lower protein concentrations for the immobilization. This was especially needed for a direct immobilization of secreted protein out of cell culture supernatant at concentrations around 4 μg/ml.

For the enzymatic reaction, a clear protein concentration dependency and high stability at 25 °C was found. Immobilization levels obtained were optimal for the measurement of low molecular weight ligands and a high controllability of the immobilization level was achieved.

No unspecific binding of sialic acid derivatives to SNAP was detected what was a prerequisite for its usability. In comparison to SNAP (20.5 kDa), a slower immobilization velocity was observed for the MAG(d1-3)-SNAP construct (55 kDa). A decreased enzyme activity or the larger protein might have caused the deceleration.

Usability of the optimized procedure was evaluated with MAG(d1-3)-SNAP expressed in CHO cells. MAG was directly immobilized out of supernatant what was proved by a conformation-dependent anti-MAG antibody. To compare capturing with enzymatic immobilization, a sialic acid derivative was measured. A similar affinity and negative sensorgrams were observed. The negative sensorgrams were expected

due to the same conformational freedom as for captured MAG. Results further supported that the negative binding signals were directly related to MAG(d1-3). By combination of enzymatic immobilization and expression of the target in a secreted form, all harsh conditions for the protein were avoided.

Biosensors based on surface plasmon resonance proved its applicability for the characterization of drug-like ligands. Kinetic as well as thermodynamic data provided a detailed picture of the interactions and revealed possible directions for lead optimization. Especially the screening of compound libraries for a specific kinetic behaviour on a target protein adds a new dimension to drug development. Importance of this dimension is discussed extensively among pharmaceutical researchers nowadays and seems to be considered to a greater extent. Nevertheless, future success in predicting efficacy and safety by kinetic data will determine the spreading of technologies like Biacore within pharmaceutical companies.

Outlook

For the future of the MAG project, an *in vivo* assay or at least an *in vitro* neurite outgrowth assay is needed to test the available MAG ligands for their activity. Especially between sialic acid derivatives and second generation ligands a different impact is highly possible due to potential differences in ligand-induced conformational changes. Furthermore, supporting experiments on the potential ligand-induced conformational change with *e.g.* circular dichroism are required to support the hypothesis. Another aspect is the usability of the enzymatic immobilization. More proteins should be expressed and enzymatically immobilized on Biacore to prove its versatility.

5 LITERATURE

(1) Overington, J. P.; Al-Lazikani, B.; Hopkins, A. L. Opinion - How many drug targets are there? *Nature Reviews Drug Discovery* **2006**, *5*, 993-996.

(2) Greener, M. Drug safety on trial - Last year's withdrawal of the anti-arthritis drug Vioxx triggered a debate about how to better monitor drug safety even after approval. *Embo Reports* **2005**, *6*, 202-204.

(3) Reuters www.reuters.com, 2007.

(4) Russ, A. P.; Lampel, S. The druggable genome: an update. *Drug Discovery Today* **2005**, *10*, 1607-1610.

(5) Hopkins, A. L.; Groom, C. R. The druggable genome. *Nature Reviews Drug Discovery* **2002**, *1*, 727-730.

(6) Hertzberg, R. P.; Pope, A. J. High-throughput screening: new technology for the 21st century. *Current Opinion in Chemical Biology* **2000**, *4*, 445-451.

(7) Muegge, I.; Heald, S. L.; Brittelli, D. Simple selection criteria for drug-like chemical matter. *Journal of Medicinal Chemistry* **2001**, *44*, 1841-1846.

(8) Walters, W. P.; Murcko, A.; Murcko, M. A. Recognizing molecules with drug-like properties. *Current Opinion in Chemical Biology* **1999**, *3*, 384-387.

(9) Lipinski, C. A.; Lombardo, F.; Dominy, B. W.; Feeney, P. J. Experimental and computational approaches to estimate solubility and permeability in drug discovery and development settings. *Advanced Drug Delivery Reviews* **1997**, *23*, 3-25.

(10) Kandel, E. R. *Nerve cells and behavior*; McGraw-Hill, 2000; 19-35.

(11) Vyas, A. A.; Schnaar, R. L. Brain gangliosides: functional ligands for myelin stability and the control of nerve regeneration. *Biochimie* **2001**, *83*, 677-682.

(12) Salzer, J. L. Clustering sodium channels at the node of Ranvier: Close encounters of the axon-glia kind. *Neuron* **1997**, *18*, 843-846.

(13) Dobkin, B. H.; Havton, L. A. Basic advances and new avenues in therapy of spinal cord injury. *Annual Review of Medicine* **2004**, *55*, 255-282.

(14) Berkowitz, M.; O'Leary, P.; Kruse, D.; Harvey, C. Spinal cord injury: An analysis of medical and social costs. *New York: Demos Medical Publishing Inc*. **1998**.

(15) Schnell, L.; Schwab, M. E. Axonal Regeneration in the Rat Spinal-Cord Produced by an Antibody against Myelin-Associated Neurite Growth-Inhibitors. *Nature* **1990**, *343*, 269-272.

(16) Filbin, M. T. Myelin-associated inhibitors of axonal regeneration in the adult mammalian CNS. *Nat Rev Neurosci* **2003**, *4*, 703-713.

(17) David, S.; Aguayo, A. J. Axonal Elongation into Peripheral Nervous-System Bridges after Central Nervous-System Injury in Adult-Rats. *Science* **1981**, *214*, 931-933.

(18) Richardson, P. M.; McGuinness, U. M.; Aguayo, A. J. Axons from Cns Neurons Regenerate into Pns Grafts. *Nature* **1980**, *284*, 264-265.

(19) Bixby, J. L.; Harris, W. A. Molecular Mechanisms of Axon Growth and Guidance. *Annual Review of Cell Biology* **1991**, *7*, 117-159.

(20) Bovolenta, P.; Fernaud-Espinosa, I. Nervous system proteoglycans as modulators of neurite outgrowth. *Progress in Neurobiology* **2000**, *61*, 113-132.
(21) McKeon, R. J.; Hoke, A.; Silver, J. Injury-Induced Proteoglycans Inhibit the Potential for Laminin-Mediated Axon Growth on Astrocytic Scars. *Experimental Neurology* **1995**, *136*, 32-43.
(22) Davies, S. J. A.; Fitch, M. T.; Memberg, S. P.; Hall, A. K.; Raisman, G. et al. Regeneration of adult axons in white matter tracts of the central nervous system. *Nature* **1997**, *390*, 680-683.
(23) Davies, S. J. A.; Goucher, D. R.; Doller, C.; Silver, J. Robust regeneration of adult sensory axons in degenerating white matter of the adult rat spinal cord. *Journal of Neuroscience* **1999**, *19*, 5810-5822.
(24) Tang, X. F.; Davies, J. E.; Davies, S. J. A. Changes in distribution, cell associations, and protein expression levels of NG2, neurocan, phosphacan, brevican, versican V2, and tenascin-C during acute to chronic maturation of spinal cord scar tissue. *Journal of Neuroscience Research* **2003**, *71*, 427-444.
(25) Caroni, P.; Schwab, M. E. Antibody against Myelin-Associated Inhibitor of Neurite Growth Neutralizes Nonpermissive Substrate Properties of Cns White Matter. *Neuron* **1988**, *1*, 85-96.
(26) Chen, M. S.; Huber, A. B.; van der Haar, M. E.; Frank, M.; Schnell, L. et al. Nogo-A is a myelin-associated neurite outgrowth inhibitor and an antigen for monoclonal antibody IN-1. *Nature* **2000**, *403*, 434-439.
(27) GrandPre, T.; Nakamura, F.; Vartanian, T.; Strittmatter, S. M. Identification of the Nogo inhibitor of axon regeneration as a Reticulon protein. *Nature* **2000**, *403*, 439-444.
(28) Prinjha, R.; Moore, S. E.; Vinson, M.; Blake, S.; Morrow, R. et al. Neurobiology - Inhibitor of neurite outgrowth in humans. *Nature* **2000**, *403*, 383-384.
(29) Huang, J. K.; Phillips, G. R.; Roth, A. D.; Pedraza, L.; Shan, W. S. et al. Glial membranes at the node of Ranvier prevent neurite outgrowth. *Science* **2005**, *310*, 1813-1817.
(30) Mikol, D. D.; Gulcher, J. R.; Stefansson, K. The Oligodendrocyte Myelin Glycoprotein Belongs to a Distinct Family of Proteins and Contains the Hnk-1 Carbohydrate. *Journal of Cell Biology* **1990**, *110*, 471-479.
(31) Williams, A. F.; Davis, S. J.; He, Q.; Barclay, A. N. Structural Diversity in Domains of the Immunoglobulin Superfamily. *Cold Spring Harbor Symposia on Quantitative Biology* **1989**, *54*, 637-647.
(32) Williams, A. F.; Barclay, A. N. The Immunoglobulin Superfamily - Domains for Cell-Surface Recognition. *Annual Review of Immunology* **1988**, *6*, 381-405.
(33) Kelm, S.; Pelz, A.; Schauer, R.; Filbin, M. T.; Tang, S. et al. Sialoadhesin, myelin-associated glycoprotein and CD22 define a new family of sialic acid-dependent adhesion molecules of the immunoglobulin superfamily. *Curr Biol* **1994**, *4*, 965-972.
(34) Crocker, P. R. Siglecs: sialic-acid-binding immunoglobulin-like lectins in cell-cell interactions and signalling. *Curr Opin Struct Biol* **2002**, *12*, 609-615.

(35) Quarles, R. H.; Everly, J. L.; Brady, R. O. Demonstration of a Glycoprotein Which Is Associated with a Purified Myelin Fraction from Rat-Brain. *Biochemical and Biophysical Research Communications* **1972**, *47*, 491-&.
(36) Quarles, R. H.; Everly, J. L.; Brady, R. O. Evidence for Close Association of a Glycoprotein with Myelin in Rat-Brain. *Journal of Neurochemistry* **1973**, *21*, 1177-&.
(37) Frail, D. E.; Braun, P. E. 2 Developmentally Regulated Messenger-Rnas Differing in Their Coding Region May Exist for the Myelin-Associated Glycoprotein. *Journal of Biological Chemistry* **1984**, *259*, 4857-4862.
(38) Salzer, J. L.; Pedraza, L.; Brown, M.; Struyk, A.; Afar, D. et al. Structure and Function of the Myelin-Associated Glycoproteins. *Annals of the New York Academy of Sciences* **1990**, *605*, 302-312.
(39) Trapp, B. D. Myelin-Associated Glycoprotein - Location and Potential Functions. *Annals of the New York Academy of Sciences* **1990**, *605*, 29-43.
(40) Lai, C.; Brow, M. A.; Nave, K. A.; Noronha, A. B.; Quarles, R. H. et al. 2 Forms of 1b236 Myelin-Associated Glycoprotein, a Cell-Adhesion Molecule for Postnatal Neural Development, Are Produced by Alternative Splicing. *Proceedings of the National Academy of Sciences of the United States of America* **1987**, *84*, 4337-4341.
(41) Kursula, P.; Lehto, V. P.; Heape, A. M. The small myelin-associated glycoprotein binds to tubulin and microtubules. *Molecular Brain Research* **2001**, *87*, 22-30.
(42) Kursula, P.; Merilainen, G.; Lehto, V. P.; Heape, A. M. The small myelin-associated glycoprotein is a zinc-binding protein. *Journal of Neurochemistry* **1999**, *73*, 2110-2118.
(43) Kursula, P.; Tikkanen, G.; Lehto, V. P.; Nishikimi, M.; Heape, A. M. Calcium-dependent interaction between the large myelin-associated glycoprotein and S100 beta. *Journal of Neurochemistry* **1999**, *73*, 1724-1732.
(44) Schachner, M.; Bartsch, U. Multiple functions of the myelin-associated glycoprotein MAG (siglec-4a) in formation and maintenance of myelin. *Glia* **2000**, *29*, 154-165.
(45) Turnley, A. M.; Bartlett, P. F. MAG and MOG enhance neurite outgrowth of embryonic mouse spinal cord neurons. *Neuroreport* **1998**, *9*, 1987-1990.
(46) DeBellard, M. E.; Tang, S.; Mukhopadhyay, G.; Shen, Y. J.; Filbin, M. T. Myelin-associated glycoprotein inhibits axonal regeneration from a variety of neurons via interaction with a sialoglycoprotein. *Molecular and Cellular Neuroscience* **1996**, *7*, 89-101.
(47) Domeniconi, M.; Filbin, M. T. Overcoming inhibitors in myelin to promote axonal regeneration. *Journal of the Neurological Sciences* **2005**, *233*, 43-47.
(48) Bandtlow, C. E. Regeneration in the central nervous system. *Experimental Gerontology* **2003**, *38*, 79-86.
(49) Cai, D. M.; Shen, Y. J.; De Bellard, M.; Tang, S.; Filbin, M. T. Prior exposure to neurotrophins blocks inhibition of axonal regeneration by MAG and myelin via a cAMP-dependent mechanism. *Neuron* **1999**, *22*, 89-101.

(50) Yamashita, T.; Higuchi, H.; Tohyama, M. The p75 receptor transduces the signal from myelin-associated glycoprotein to Rho. *Journal of Cell Biology* **2002**, *157*, 565-570.
(51) Wong, S. T.; Henley, J. R.; Kanning, K. C.; Huang, K. H.; Bothwell, M. et al. A p75(NTR) and Nogo receptor complex mediates repulsive signaling by myelin-associated glycoprotein. *Nature Neuroscience* **2002**, *5*, 1302-1308.
(52) Wang, K. C.; Kim, J. A.; Sivasankaran, R.; Segal, R.; He, Z. p75 interacts with the Nogo receptor as a co-receptor for Nogo, MAG and OMgp. *Nature* **2002**, *420*, 74-78.
(53) Lehmann, M.; Fournier, A.; Selles-Navarro, I.; Dergham, P.; Sebok, A. et al. Inactivation of Rho signaling pathway promotes CNS axon regeneration. *Journal of Neuroscience* **1999**, *19*, 7537-7547.
(54) Burridge, K.; Wennerberg, K. Rho and Rac take center stage. *Cell* **2004**, *116*, 167-179.
(55) Bishop, A. L.; Hall, A. Rho GTPases and their effector proteins. *Biochemical Journal* **2000**, *348*, 241-255.
(56) Ishizaki, T.; Maekawa, M.; Fujisawa, K.; Okawa, K.; Iwamatsu, A. et al. The small GTP-binding protein Rho binds to and activates a 160 kDa Ser/Thr protein kinase homologous to myotonic dystrophy kinase. *Embo Journal* **1996**, *15*, 1885-1893.
(57) Leung, T.; Manser, E.; Tan, L.; Lim, L. A Novel Serine/Threonine Kinase Binding the Ras-Related Rhoa Gtpase Which Translocates the Kinase to Peripheral Membranes. *Journal of Biological Chemistry* **1995**, *270*, 29051-29054.
(58) Madura, T.; Yamashita, T.; Kubo, T.; Fujitani, M.; Hosokawa, K. et al. Activation of Rho in the injured axons following spinal cord injury. *Embo Reports* **2004**, *5*, 412-417.
(59) Aimone, J. B.; Leasure, J. L.; Perreau, V. M.; Thallmair, M. Spatial and temporal gene expression profiling of the contused rat spinal cord. *Experimental Neurology* **2004**, *189*, 204-221.
(60) Brabeck, C.; Beschorner, R.; Conrad, S.; Mittelbronn, M.; Bekure, K. et al. Lesional expression of RhoA and RhoB following traumatic brain injury in humans. *Journal of Neurotrauma* **2004**, *21*, 697-706.
(61) Dubreuil, C. I.; Winton, M. J.; McKerracher, L. Rho activation patterns after spinal cord injury and the role of activated Rho in apoptosis in the central nervous system. *Journal of Cell Biology* **2003**, *162*, 233-243.
(62) Tanaka, H.; Yamashita, T.; Yachi, K.; Fujiwara, T.; Yoshikawa, H. et al. Cytoplasmic p21(Cip1/WAF1) enhances axonal regeneration and functional recovery after spinal cord injury in rats. *Neuroscience* **2004**, *127*, 155-164.
(63) Sung, J. K.; Miao, L.; Calvert, J. W.; Huang, L. X.; Harkey, H. L. et al. A possible role of RhoA/Rho-kinase in experimental spinal cord injury in rat. *Brain Research* **2003**, *959*, 29-38.
(64) Dergham, P.; Ellezam, B.; Essagian, C.; Avedissian, H.; Lubell, W. D. et al. Rho signaling pathway targeted to promote spinal cord repair. *Journal of Neuroscience* **2002**, *22*, 6570-6577.

(65) Hara, M.; Takasu, M.; Watanabe, K.; Noda, A.; Takagi, T. et al. Protein kinase inhibition by fasudil hydrochloride promotes neurological recovery after spinal cord injury in rats. *Journal of Neurosurgery* **2000**, *93*, 94-101.
(66) Fournier, A. E.; Takizawa, B. T.; Strittmatter, S. M. Rho kinase inhibition enhances axonal regeneration in the injured CNS. *Journal of Neuroscience* **2003**, *23*, 1416-1423.
(67) Vyas, A. A.; Patel, H. V.; Fromholt, S. E.; Heffer-Lauc, M.; Vyas, K. A. et al. Gangliosides are functional nerve cell ligands for myelin-associated glycoprotein (MAG), an inhibitor of nerve regeneration. *Proc Natl Acad Sci U S A* **2002**, *99*, 8412-8417.
(68) Kelm, S.; Brossmer, R.; Isecke, R.; Gross, H. J.; Strenge, K. et al. Functional groups of sialic acids involved in binding to siglecs (sialoadhesins) deduced from interactions with synthetic analogues. *Eur J Biochem* **1998**, *255*, 663-672.
(69) Collins, B. E.; Yang, L. J.; Mukhopadhyay, G.; Filbin, M. T.; Kiso, M. et al. Sialic acid specificity of myelin-associated glycoprotein binding. *J Biol Chem* **1997**, *272*, 1248-1255.
(70) Yang, L. J.; Zeller, C. B.; Shaper, N. L.; Kiso, M.; Hasegawa, A. et al. Gangliosides are neuronal ligands for myelin-associated glycoprotein. *Proc Natl Acad Sci U S A* **1996**, *93*, 814-818.
(71) Tang, S.; Shen, Y. J.; DeBellard, M. E.; Mukhopadhyay, G.; Salzer, J. L. et al. Myelin-associated glycoprotein interacts with neurons via a sialic acid binding site at ARG118 and a distinct neurite inhibition site. *J Cell Biol* **1997**, *138*, 1355-1366.
(72) Niederost, B.; Oertle, T.; Fritsche, J.; McKinney, R. A.; Bandtlow, C. E. Nogo-A and myelin-associated glycoprotein mediate neurite growth inhibition by antagonistic regulation of RhoA and Rac1. *Journal of Neuroscience* **2002**, *22*, 10368-10376.
(73) Vinson, M.; Strijbos, P.; Rowles, A.; Facci, L.; Moore, S. E. et al. Myelin-associated glycoprotein interacts with ganglioside GT1b - A mechanism for neurite outgrowth inhibition. *Journal of Biological Chemistry* **2001**, *276*, 20280-20285.
(74) McKerracher, L. Ganglioside rafts as MAG receptors that mediate blockade of axon growth. *Proc Natl Acad Sci U S A* **2002**, *99*, 7811-7813.
(75) Hakomori, S. The glycosynapse (vol 99, pg 225, 2002). *Proceedings of the National Academy of Sciences of the United States of America* **2002**, *99*, 3356-3356.
(76) Liu, B. P.; Fournier, A.; GrandPre, T.; Strittmatter, S. M. Myelin-associated glycoprotein as a functional ligand for the Nogo-66 receptor. *Science* **2002**, *297*, 1190-1193.
(77) Domeniconi, M.; Cao, Z.; Spencer, T.; Sivasankaran, R.; Wang, K. C. et al. Myelin-associated glycoprotein interacts with the Nogo66 receptor to inhibit neurite outgrowth. *Neuron* **2002**, *35*, 283-290.
(78) Yang, L. J. S.; Lorenzini, I.; Vajn, K.; Mountney, A.; Schramm, L. P. et al. Sialidase enhances spinal axon outgrowth in vivo. *Proceedings of the National Academy of Sciences of the United States of America* **2006**, *103*, 11057-11062.

(79) Pan, B. H.; Fromholt, S. E.; Hess, E. J.; Crawford, T. O.; Griffin, J. W. et al. Myelin-associated glycoprotein and complementary axonal ligands, gangliosides, mediate axon stability in the CNS and PINS: Neuropathology and behavioral deficits in single- and double-null mice. *Experimental Neurology* **2005**, *195*, 208-217.

(80) Collins, B. E.; Kiso, M.; Hasegawa, A.; Tropak, M. B.; Roder, J. C. et al. Binding specificities of the sialoadhesin family of I-type lectins. Sialic acid linkage and substructure requirements for binding of myelin-associated glycoprotein, Schwann cell myelin protein, and sialoadhesin. *J Biol Chem* **1997**, *272*, 16889-16895.

(81) Derrington, E. A.; Masco, D.; Whittaker, V. P. Confirmation of the Cholinergic Specificity of the Chol-1 Gangliosides in Mammalian Brain Using Affinity-Purified Antisera and Lesions Affecting the Cholinergic Input to the Hippocampus. *Journal of Neurochemistry* **1989**, *53*, 1686-1692.

(82) Hirabayashi, Y.; Nakao, T.; Irie, F.; Whittaker, V. P.; Kon, K. et al. Structural Characterization of a Novel Cholinergic Neuron-Specific Ganglioside in Bovine Brain. *Journal of Biological Chemistry* **1992**, *267*, 12973-12978.

(83) Sawada, N.; Ishida, H.; Collins, B. E.; Schnaar, R. L.; Kiso, M. Ganglioside GD1 alpha analogues as high-affinity ligands for myelin-associated glycoprotein (MAG). *Carbohydr Res* **1999**, *316*, 1-5.

(84) Strenge, K.; Schauer, R.; Bovin, N.; Hasegawa, A.; Ishida, H. et al. Glycan specificity of myelin-associated glycoprotein and sialoadhesin deduced from interactions with synthetic oligosaccharides. *Eur J Biochem* **1998**, *258*, 677-685.

(85) Collins, B. E.; Ito, H.; Sawada, N.; Ishida, H.; Kiso, M. et al. Enhanced binding of the neural siglecs, myelin-associated glycoprotein and Schwann cell myelin protein, to Chol-1 (alpha-series) gangliosides and novel sulfated Chol-1 analogs. *J Biol Chem* **1999**, *274*, 37637-37643.

(86) Vyas, A. A.; Blixt, O.; Paulson, J. C.; Schnaar, R. L. Potent glycan inhibitors of myelin-associated glycoprotein enhance axon outgrowth in vitro. *J Biol Chem* **2005**, *280*, 16305-16310.

(87) Thompson, H. J.; Marklund, N.; LeBold, D. G.; Morales, D. M.; Keck, C. A. et al. Tissue sparing and functional recovery following experimental traumatic brain injury is provided by treatment with an anti-myelin-associated glycoprotein antibody. *European Journal of Neuroscience* **2006**, *24*, 3063-3072.

(88) Irving, E. A.; Vinson, M.; Rosin, C.; Roberts, J. C.; Chapman, D. M. et al. Identification of neuroprotective properties of anti-MAG antibody: a novel approach for the treatment of stroke? *Journal of Cerebral Blood Flow and Metabolism* **2005**, *25*, 98-107.

(89) Schnell, L.; Schwab, M. E. Sprouting and Regeneration of Lesioned Corticospinal Tract Fibers in the Adult-Rat Spinal-Cord. *European Journal of Neuroscience* **1993**, *5*, 1156-1171.

(90) Bregman, B. S.; Kunkelbagden, E.; Schnell, L.; Dai, H. N.; Gao, D. et al. Recovery from Spinal-Cord Injury Mediated by Antibodies to Neurite Growth-Inhibitors. *Nature* **1995**, *378*, 498-501.

(91) Li, W. W.; Walus, L.; Rabacchi, S. A.; Jirik, A.; Chang, E. et al. A neutralizing anti-Nogo66 receptor monoclonal antibody reverses inhibition of neurite outgrowth by central nervous system myelin. *Journal of Biological Chemistry* **2004**, *279*, 43780-43788.
(92) Nikulina, E.; Tidwell, J. L.; Dai, H. N.; Bregman, B. S.; Filbin, M. T. The phosphodiesterase inhibitor rolipram delivered after a spinal cord lesion promotes axonal regeneration and functional recovery. *Proc Natl Acad Sci U S A* **2004**, *101*, 8786-8790.
(93) Stryer, L. Biochemistry. **1999**.
(94) Lipinski, C. A.; Lombardo, F.; Dominy, B. W.; Feeney, P. J. Experimental and computational approaches to estimate solubility and permeability in drug discovery and development settings. *Advanced Drug Delivery Reviews* **2001**, *46*, 3-26.
(95) Hann, M. M.; Oprea, T. I. Pursuing the leadlikeness concept in pharmaceutical research. *Current Opinion in Chemical Biology* **2004**, *8*, 255-263.
(96) Chapman, T. Drug discovery - The leading edge. *Nature* **2004**, *430*, 109-+.
(97) Hann, M. M.; Leach, A. R.; Harper, G. Molecular complexity and its impact on the probability of finding leads for drug discovery. *Journal of Chemical Information and Computer Sciences* **2001**, *41*, 856-864.
(98) Oprea, T. I.; Davis, A. M.; Teague, S. J.; Leeson, P. D. Is there a difference between leads and drugs? A historical perspective. *Journal of Chemical Information and Computer Sciences* **2001**, *41*, 1308-1315.
(99) Teague, S. J.; Davis, A. M.; Leeson, P. D.; Oprea, T. The design of leadlike combinatorial libraries. *Angewandte Chemie-International Edition* **1999**, *38*, 3743-3748.
(100) Kubinyi, H. Structure-based design of enzyme inhibitors and receptor ligands. *Current Opinion in Drug Discovery and Development* **1998**, *1*.
(101) Swinney, D. C. Biochemical mechanisms of drug action: what does it take for success? *Nat Rev Drug Discov* **2004**, *3*, 801-808.
(102) Berezov, A.; Zhang, H. T.; Greene, M. I.; Murali, R. Disabling erbB receptors with rationally designed exocyclic mimetics of antibodies: structure-function analysis. *J Med Chem* **2001**, *44*, 2565-2574.
(103) Markgren, P. O.; Hamalainen, M.; Danielson, U. H. Kinetic analysis of the interaction between HIV-1 protease and inhibitors using optical biosensor technology. *Anal Biochem* **2000**, *279*, 71-78.
(104) Copeland, R. A.; Pompliano, D. L.; Meek, T. D. Opinion - Drug-target residence time and its implications for lead optimization. *Nature Reviews Drug Discovery* **2006**, *5*, 730-739.
(105) Billheimer, J. T.; Dicker, I. B.; Wynn, R.; Bradley, J. D.; Cromley, D. A. et al. Evidence that thrombocytopenia observed in humans treated with orally bioavailable glycoprotein IIb/IIIa antagonists is immune mediated. *Blood* **2002**, *99*, 3540-3546.
(106) Seiffert, D.; Stern, A. M.; Ebling, W.; Rossi, R. J.; Barrett, Y. C. et al. Prospective testing for drug-dependent antibodies reduces the incidence of thrombocytopenia observed with the small molecule glycoprotein IIb/IIIa

antagonist roxifiban: implications for the etiology of thrombocytopenia. *Blood* **2003**, *101*, 58-63.
(107) Kapur, S.; Seeman, P. Antipsychotic agents differ in how fast they come off the dopamine D-2 receptors. Implications for atypical antipsychotic action. *Journal of Psychiatry & Neuroscience* **2000**, *25*, 161-166.
(108) Huber, W. A new strategy for improved secondary screening and lead optimization using high-resolution SPR characterization of compound-target interactions. *Journal of Molecular Recognition* **2005**, *18*, 273-281.
(109) Myszka, D. G.; He, X.; Dembo, M.; Morton, T. A.; Goldstein, B. Extending the range of rate constants available from BIACORE: Interpreting mass transport-influenced binding data. *Biophysical Journal* **1998**, *75*, 583-594.
(110) Myszka, D. G.; Abdiche, Y. N.; Arisaka, F.; Byron, O.; Eisenstein, E. et al. The ABRF-MIRG'02 study: assembly state, thermodynamic, and kinetic analysis of an enzyme/inhibitor interaction. *J Biomol Tech* **2003**, *14*, 247-269.
(111) Day, Y. S.; Baird, C. L.; Rich, R. L.; Myszka, D. G. Direct comparison of binding equilibrium, thermodynamic, and rate constants determined by surface- and solution-based biophysical methods. *Protein Sci* **2002**, *11*, 1017-1025.
(112) Papalia, G. A.; Leavitt, S.; Bynum, M. A.; Katsamba, P. S.; Wilton, R. et al. Comparative analysis of 10 small molecules binding to carbonic anhydrase II by different investigators using Biacore technology. *Analytical Biochemistry* **2006**, *359*, 94-105.
(113) Cannon, M. J.; Papalia, G. A.; Navratilova, I.; Fisher, R. J.; Roberts, L. R. et al. Comparative analyses of a small molecule/enzyme interaction by multiple users of Biacore technology. *Anal Biochem* **2004**, *330*, 98-113.
(114) Markgren, P. O.; Schaal, W.; Hamalainen, M.; Karlen, A.; Hallberg, A. et al. Relationships between structure and interaction kinetics for HIV-1 protease inhibitors. *J Med Chem* **2002**, *45*, 5430-5439.
(115) Shuman, C. F.; Vrang, L.; Danielson, U. H. Improved structure-activity relationship analysis of HIV-1 protease inhibitors using interaction kinetic data. *J Med Chem* **2004**, *47*, 5953-5961.
(116) Markgren, P. O.; Lindgren, M. T.; Gertow, K.; Karlsson, R.; Hamalainen, M. et al. Determination of interaction kinetic constants for HIV-1 protease inhibitors using optical biosensor technology. *Anal Biochem* **2001**, *291*, 207-218.
(117) Markgren, P. O.; Hamalainen, M.; Danielson, U. H. Screening of compounds interacting with HIV-1 proteinase using optical biosensor technology. *Anal Biochem* **1998**, *265*, 340-350.
(118) Shuman, C. F.; Hamalainen, M. D.; Danielson, U. H. Kinetic and thermodynamic characterization of HIV-1 protease inhibitors. *J Mol Recognit* **2004**, *17*, 106-119.
(119) Maschera, B.; Darby, G.; Palu, G.; Wright, L. L.; Tisdale, M. et al. Human immunodeficiency virus - Mutations in the viral protease that confer resistance to saquinavir increase the dissociation rate constant of the protease-saquinavir complex. *Journal of Biological Chemistry* **1996**, *271*, 33231-33235.

(120) Shuman, C. F.; Markgren, P. O.; Hamalainen, M.; Danielson, U. H. Elucidation of HIV-1 protease resistance by characterization of interaction kinetics between inhibitors and enzyme variants. *Antiviral Res* **2003**, *58*, 235-242.
(121) Gossas, T.; Danielson, U. H. Analysis of the pH-dependencies of the association and dissociation kinetics of HIV-1 protease inhibitors. *Journal of Molecular Recognition* **2003**, *16*, 203-212.
(122) May, L. M.; Russell, D. A. The characterization of biomolecular secondary structures by surface plasmon resonance. *Analyst* **2002**, *127*, 1589-1595.
(123) Zako, T.; Harada, K.; Mannen, T.; Yamaguchi, S.; Kitayama, A. et al. Monitoring of the refolding process for immobilized firefly luciferase with a biosensor based on surface plasmon resonance. *Journal of Biochemistry* **2001**, *129*, 1-4.
(124) Geitmann, M.; Danielson, U. H. Studies of substrate-induced conformational changes in human cytomegalovirus protease using optical biosensor technology. *Analytical Biochemistry* **2004**, *332*, 203-214.
(125) Gestwicki, J. E.; Hsieh, H. V.; Pitner, J. B. Using receptor conformational change to detect low molecular weight analytes by surface plasmon resonance. *Anal Chem* **2001**, *73*, 5732-5737.
(126) Turbadar, T. Complete Absorption of Light by Thin Metal Films. *Proceedings of the Physical Society of London* **1959**, *73*, 40-44.
(127) Kaambhampati, D. *Protein Microarray Technology*; Wiley-VCH Verlag, 2003.
(128) *Surface Plasmon Resonance (Technology Note 1)*; Biacore AB, 2001; 1-4.
(129) Jonsson, U.; Fagerstam, L.; Ivarsson, B.; Johnsson, B.; Karlsson, R. et al. Real-time biospecific interaction analysis using surface plasmon resonance and a sensor chip technology. *Biotechniques* **1991**, *11*, 620-627.
(130) Nagata, K. H., H. *Real-Time Analysis of Biomolecular Interactions: Applications of BIACORE*; Springer: Japan, 2000.
(131) Stenberg, E.; Persson, B.; Roos, H.; Urbaniczky, C. Quantitative determination of surface concentration of protein with surface plasmon resonance using radiolabeled proteins. *J Colloid Interface Sci* **1991**, *143*, 513-526.
(132) Mannen, T.; Yamaguchi, S.; Honda, J.; Sugimoto, S.; Kitayama, A. et al. Observation of charge state and conformational change in immobilized protein using surface plasmon resonance sensor. *Anal Biochem* **2001**, *293*, 185-193.
(133) Lofas, S.; Johnson, B. A novel hydrogel matrix on gold surfaces in surface plasmon resonance sensors for fast and efficient covalent immobilization of ligands. *J Chem Soc Chem Commun* **1990**, 1526-1528.
(134) Myszka, D. G. Analysis of small-molecule interactions using Biacore S51 technology. *Anal Biochem* **2004**, *329*, 316-323.
(135) Halkes, K. M.; St Hilaire, P. M.; Crocker, P. R.; Meldal, M. Glycopeptides as oligosaccharide mimics: high affinity sialopeptide ligands for sialoadhesin from combinatorial libraries. *J Comb Chem* **2003**, *5*, 18-27.
(136) Kaila, N.; Somers, W. S.; Thomas, B. E.; Thakker, P.; Janz, K. et al. Quinic acid derivatives as sialyl Lewis(x)-mimicking selectin inhibitors: Design,

synthesis, and crystal structure in complex with E-selectin. *Journal of Medicinal Chemistry* **2005**, *48*, 4346-4357.
(137) Myszka, D. G.; Morton, T. A.; Doyle, M. L.; Chaiken, I. M. Kinetic analysis of a protein antigen-antibody interaction limited by mass transport on an optical biosensor. *Biophysical Chemistry* **1997**, *64*, 127-137.
(138) Glaser, R. W. Antigen-antibody binding and mass transport by convection and diffusion to a surface: a two-dimensional computer model of binding and dissociation kinetics. *Anal Biochem* **1993**, *213*, 152-161.
(139) Schuck, P. Kinetics of ligand binding to receptor immobilized in a polymer matrix, as detected with an evanescent wave biosensor. I. A computer simulation of the influence of mass transport. *Biophys J* **1996**, *70*, 1230-1249.
(140) Myszka, D. G. Kinetic analysis of macromolecular interactions using surface plasmon resonance biosensors. *Curr Opin Biotechnol* **1997**, *8*, 50-57.
(141) Frostell-Karlsson, A.; Remaeus, A.; Roos, H.; Andersson, K.; Borg, P. et al. Biosensor analysis of the interaction between immobilized human serum albumin and drug compounds for prediction of human serum albumin binding levels. *J Med Chem* **2000**, *43*, 1986-1992.
(142) Myszka, D. G. Improving biosensor analysis. *J Mol Recognit* **1999**, *12*, 279-284.
(143) *Biacore® 3000 Instrument Handbook*; March 1999 ed.; Biacore AB: Uppsala, 1999.
(144) Andersson, K.; Hamalainen, M.; Malmqvist, M. Identification and optimization of regeneration conditions for affinity- based biosensor assays. A multivariate cocktail approach. *Anal Chem* **1999**, *71*, 2475-2481.
(145) Rich, R. L.; Myszka, D. G. Survey of the year 2005 commercial optical biosensor literature. *Journal of Molecular Recognition* **2006**, *19*, 478-534.
(146) Karlsson, R.; Michaelsson, A.; Mattsson, L. Kinetic analysis of monoclonal antibody-antigen interactions with a new biosensor based analytical system. *J Immunol Methods* **1991**, *145*, 229-240.
(147) O'Shannessy, D. J.; Brigham-Burke, M.; Soneson, K. K.; Hensley, P.; Brooks, I. Determination of rate and equilibrium binding constants for macromolecular interactions using surface plasmon resonance: use of nonlinear least squares analysis methods. *Anal Biochem* **1993**, *212*, 457-468.
(148) Roden, L. D.; Myszka, D. G. Global analysis of a macromolecular interaction measured on BIAcore. *Biochem Biophys Res Commun* **1996**, *225*, 1073-1077.
(149) Myszka, D. G.; Morton, T. A. CLAMP: a biosensor kinetic data analysis program. *Trends Biochem Sci* **1998**, *23*, 149-150.
(150) Tomizaki, K. Y.; Usui, K.; Mihara, H. Protein-detecting microarrays: Current accomplishments and requirements. *Chembiochem* **2005**, *6*, 783-799.
(151) Austin, R. P.; Barton, P.; Mohmed, S.; Riley, R. J. The binding of drugs to hepatocytes and its relationship to physicochemical properties. *Drug Metabolism and Disposition* **2005**, *33*, 419-425.
(152) Johnsson, B.; Lofas, S.; Lindquist, G. Immobilization of proteins to a carboxymethyldextran-modified gold surface for biospecific interaction analysis in surface plasmon resonance sensors. *Anal Biochem* **1991**, *198*, 268-277.

(153) Kortt, A. A.; Oddie, G. W.; Iliades, P.; Gruen, L. C.; Hudson, P. J. Nonspecific amine immobilization of ligand can Be a potential source of error in BIAcore binding experiments and may reduce binding affinities. *Anal Biochem* **1997**, *253*, 103-111.
(154) Yoshitani, N.; Satou, K.; Saito, K.; Suzuki, S.; Hatanaka, H. et al. A structure-based strategy for discovery of small ligands binding to functionally unknown proteins: combination of in silico screening and surface plasmon resonance measurements. *Proteomics* **2005**, *5*, 1472-1480.
(155) Canziani, G. A.; Klakamp, S.; Myszka, D. G. Kinetic screening of antibodies from crude hybridoma samples using Biacore. *Anal Biochem* **2004**, *325*, 301-307.
(156) *Biacore Sensor Surface Handbook*; Biacore AB: Uppsala, 2003.
(157) Kindermann, M.; George, N.; Johnsson, N.; Johnsson, K. Covalent and selective immobilization of fusion proteins. *J Am Chem Soc* **2003**, *125*, 7810-7811.
(158) Huber, W.; Perspicace, S.; Kohler, J.; Muller, F.; Schlatter, D. SPR-based interaction studies with small molecular weight ligands using hAGT fusion proteins. *Anal Biochem* **2004**, *333*, 280-288.
(159) Kwon, Y.; Coleman, M. A.; Camarero, J. A. Selective immobilization of proteins onto solid supports through split-intein-mediated protein trans-splicing. *Angewandte Chemie-International Edition* **2006**, *45*, 1726-1729.
(160) Cohen, N. S.; Chang, A. C. Y.; Boyer, H. W.; B., H. R. Construction of Biologically Functional Bacterial Plasmids In Vitro. *PNAS* **1973**, *70*, 3240-3244.
(161) Glick, B.; Pasternack, J. *Molecular Biotechnology*; American Society for Microbiology, 1998.
(162) Liguori, L.; Marques, B.; Villegas-Mendez, A.; Rothe, R.; Lenormond, J. L. Production of membrane proteins using cell-free expression systems. *Expert Review of Proteomics* **2007**, *4*, 79-90.
(163) O'Reilly, D.; Miller, L.; Luckow, V. *Baculovirus Expression Vectors*; Oxford University Press, 1994.
(164) Kost, T. A.; Condreay, J. P.; Jarvis, D. L. Baculovirus as versatile vectors for protein expression in insect and mammalian cells. *Nature Biotechnology* **2005**, *23*, 567-575.
(165) Rich, R. L.; Myszka, D. G. Advances in surface plasmon resonance biosensor analysis. *Curr Opin Biotechnol* **2000**, *11*, 54-61.
(166) Herfurth, L.; Ernst, B.; Wagner, B.; Ricklin, D.; Strasser, D. S. et al. Comparative epitope mapping with saturation transfer difference NMR of sialyl Lewis(a) compounds and derivatives bound to a monoclonal antibody. *Journal of Medicinal Chemistry* **2005**, *48*, 6879-6886.
(167) Sachin, S. Exploring the carbohydrate-binding properties of myelin-associated glycoprotein (MAG) and its ligands by a dynamic integrated approach. In *Institute for Molecular Pharmacy*; University of Basel: Basel, 2006.
(168) Cline, J.; Braman, J. C.; Hogrefe, H. H. PCR fidelity of Pfu DNA polymerase and other thermostable DNA polymerases. *Nucleic Acids Research* **1996**, *24*, 3546-3551.

(169) Sambrook, J.; Frisch, E.; Maniatis, T. *Molecular Cloning: A Laboratory Manual*; Cold Spring Harbor Press: New York, 1989.
(170) Invitrogen Bac-to-Bac Baculovirus Expression System Instruction Manual. **2002**.
(171) Kang, D. H.; Gho, Y. S.; Suh, M. K.; Kang, C. H. Highly sensitive and fast protein detection with coomassie brilliant blue in sodium dodecyl sulfate-polyacrylamide gel electrophoresis. *Bulletin of the Korean Chemical Society* **2002**, *23*, 1511-1512.
(172) Malmqvist, M. Biospecific interaction analysis using biosensor technology. *Nature* **1993**, *361*, 186-187.
(173) (www.researchandmarkets.com/reportinfo.asp?report_id=75046).
(174) Rye, P. D.; Bovin, N. V.; Vlasova, E. V.; Molodyk, A. A.; Baryshnikov, A. et al. Summary report on the ISOBM TD-6 workshop: Analysis of 20 monoclonal antibodies against Sialyl Lewis(a) and related antigens - Montreux, Switzerland, September 19-24, 1997. *Tumor Biology* **1998**, *19*, 390-420.
(175) Geffen, I.; Spiess, M. Asialoglycoprotein receptor. *Int Rev Cytol* **1992**, *137B*, 181-219.
(176) Wragg, S.; Drickamer, K. Identification of amino acid residues that determine pH dependence of ligand binding to the asialoglycoprotein receptor during endocytosis. *Journal of Biological Chemistry* **1999**, *274*, 35400-35406.
(177) Toone, E. J. Structure and Energetics of Protein Carbohydrate Complexes. *Current Opinion in Structural Biology* **1994**, *4*, 719-728.
(178) Mehta, P.; Cummings, R. D.; McEver, R. P. Affinity and kinetic analysis of P-selectin binding to P-selectin glycoprotein ligand-1. *J Biol Chem* **1998**, *273*, 32506-32513.
(179) Ricklin, D. Surface plamon resonance applications in drug discovery. In *Institute for Molecular Pharmacy*; University of Basel: Basel, 2005.
(180) Miura, Y.; Kim, S.; Etchison, J. R.; Ding, Y. L.; Hindsgaul, O. et al. Aglycone structure influences alpha-fucosyltransferase III activity using N-acetyllactosamine glycoside acceptors. *Glycoconjugate Journal* **1999**, *16*, 725-730.
(181) Zaccai, N. R.; Maenaka, K.; Maenaka, T.; Crocker, P. R.; Brossmer, R. et al. Structure-guided design of sialic acid-based Siglec inhibitors and crystallographic analysis in complex with sialoadhesin. *Structure (Camb)* **2003**, *11*, 557-567.
(182) Davis, T. M.; Wilson, W. D. Determination of the refractive index increments of small molecules for correction of surface plasmon resonance data. *Analytical Biochemistry* **2000**, *284*, 348-353.
(183) Catimel, B.; Nerrie, M.; Lee, F. T.; Scott, A. M.; Ritter, G. et al. Kinetic analysis of the interaction between the monoclonal antibody A33 and its colonic epithelial antigen by the use of an optical biosensor. A comparison of immobilisation strategies. *J Chromatogr A* **1997**, *776*, 15-30.
(184) Darling, R. J.; Kuchibhotla, U.; Glaesner, W.; Micanovic, R.; Witcher, D. R. et al. Glycosylation of erythropoietin affects receptor binding kinetics: role of electrostatic interactions. *Biochemistry* **2002**, *41*, 14524-14531.

(185) Rich, R. L.; Myszka, D. G. BIACORE J: a new platform for routine biomolecular interaction analysis. *J Mol Recognit* **2001**, *14*, 223-228.
(186) Catimel, B.; Scott, A. M.; Lee, F. T.; Hanai, N.; Ritter, G. et al. Direct immobilization of gangliosides onto gold-carboxymethyldextran sensor surfaces by hydrophobic interaction: applications to antibody characterization. *Glycobiology* **1998**, *8*, 927-938.
(187) Terada, T.; Nishikawa, M.; Yamashita, F.; Hashida, M. Analysis of the molecular interaction of glycosylated proteins with rabbit liver asialoglycoprotein receptors using surface plasmon resonance spectroscopy. *Journal of Pharmaceutical and Biomedical Analysis* **2006**, *41*, 966-972.
(188) Bohm, H. J.; Banner, D.; Bendels, S.; Kansy, M.; Kuhn, B. et al. Fluorine in medicinal chemistry. *Chembiochem* **2004**, *5*, 637-643.
(189) Sinnokrot, M. O.; Sherrill, C. D. Substituent effects in pi-pi interactions: Sandwich and T-shaped configurations. *Journal of the American Chemical Society* **2004**, *126*, 7690-7697.
(190) Myszka, D. G.; Sweet, R. W.; Hensley, P.; Brigham-Burke, M.; Kwong, P. D. et al. Energetics of the HIV gp120-CD4 binding reaction. *Proceedings of the National Academy of Sciences of the United States of America* **2000**, *97*, 9026-9031.
(191) Ruben, A. J.; Kiso, Y.; Freire, E. Overcoming roadblocks in lead optimization: A thermodynamic perspective. *Chemical Biology & Drug Design* **2006**, *67*, 2-4.
(192) Ringer, A. L.; Sinnokrot, M. O.; Lively, R. P.; Sherrill, C. D. The effect of multiple substituents on sandwich and T-Shaped pi-pi interactions. *Chemistry-a European Journal* **2006**, *12*, 3821-3828.
(193) Hajduk, P. J.; Olejniczak, E. T.; Fesik, S. W. One-dimensional relaxation- and diffusion-edited NMR methods for screening compounds that bind to macromolecules. *Journal of the American Chemical Society* **1997**, *119*, 12257-12261.
(194) Fejzo, J.; Lepre, C. A.; Peng, J. W.; Bemis, G. W.; Ajay et al. The SHAPES strategy: an NMR-based approach for lead generation in drug discovery. *Chemistry & Biology* **1999**, *6*, 755-769.
(195) Meyer, B.; Weimar, T.; Peters, T. Screening mixtures for biological activity by NMR. *European Journal of Biochemistry* **1997**, *246*, 705-709.
(196) Jahnke, W.; Perez, L. B.; Paris, C. G.; Strauss, A.; Fendrich, G. et al. Second-site NMR screening with a spin-labeled first ligand. *Journal of the American Chemical Society* **2000**, *122*, 7394-7395.
(197) Geiser, M.; Cebe, R.; Drewello, D.; Schmitz, R. Integration of PCR fragments at any specific site within cloning vectors without the use of restriction enzymes and DNA ligase. *Biotechniques* **2001**, *31*, 88-90, 92.

APPENDIX

SH-019

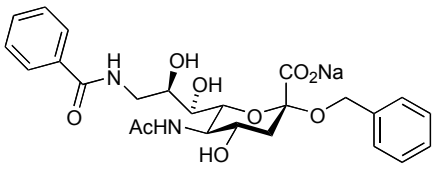

SH-164

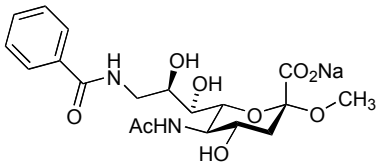

SH-081

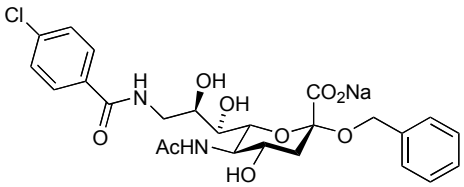

SH-082

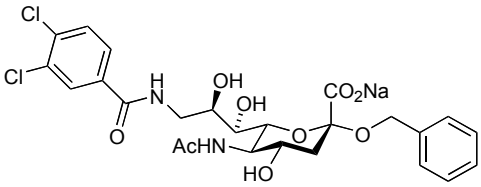

SH-035

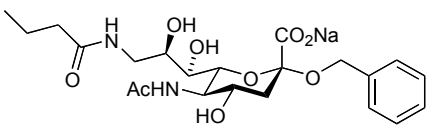

SH-140

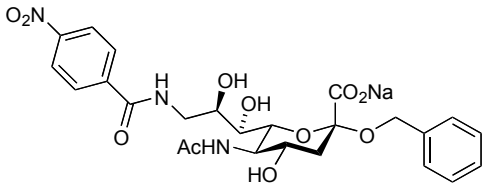

SH-141

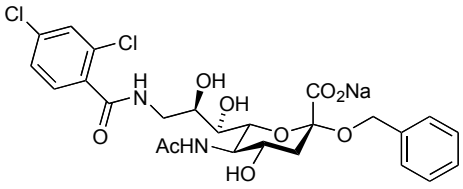

SH-142

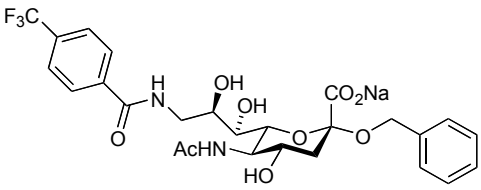

SH-143

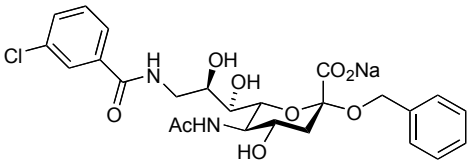

SM-I3

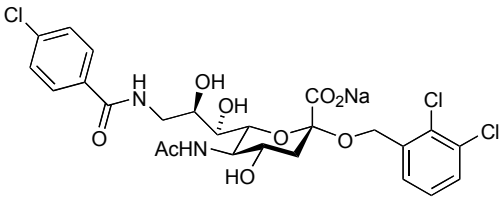

SM-I4

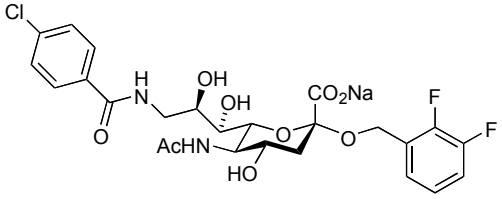

SH-264

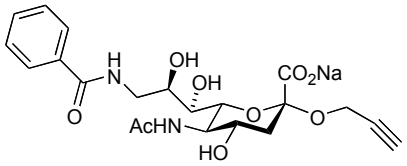

SH-218

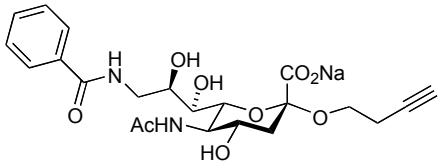

SH-192

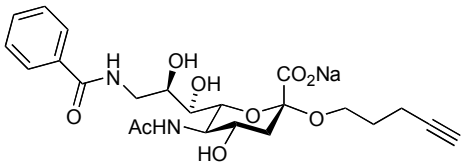

SH-246

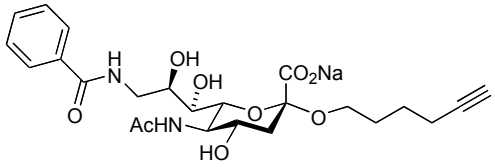

SH-2-6

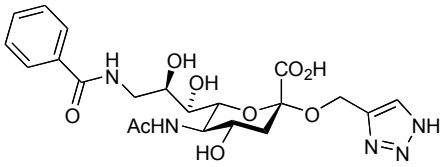

SH-272

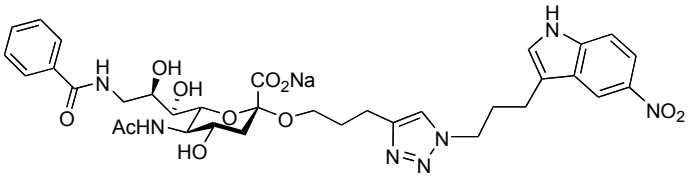

SH-281

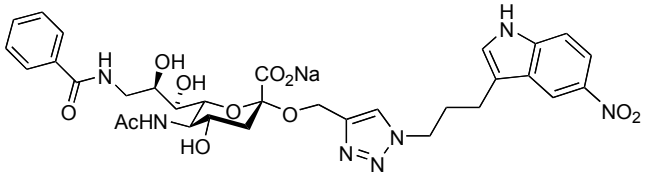

SH-267

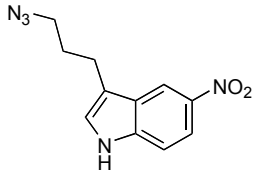

SM-m5

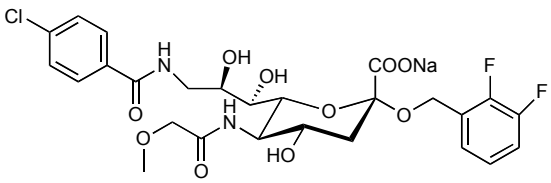

SM-m6

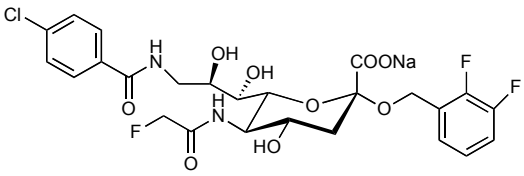

BG-PEG$_3$

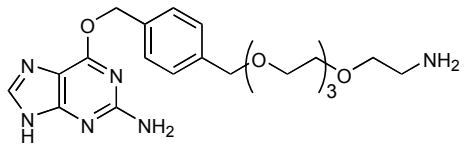

BG-PEG$_{12}$

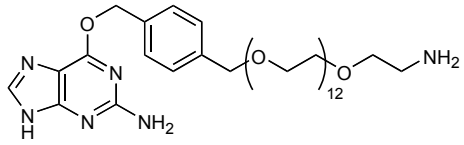

Carboxy-BG

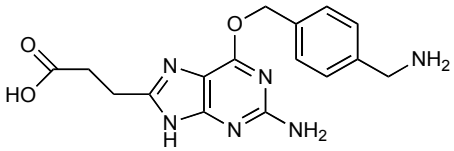

Sulfo-BG

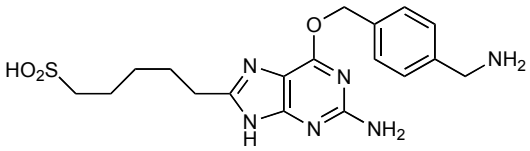

Gluco-BG

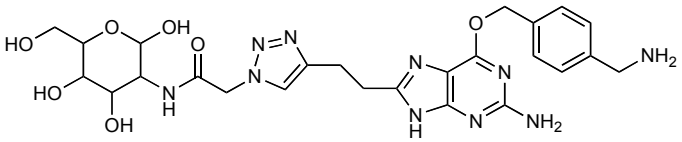

pSS26b

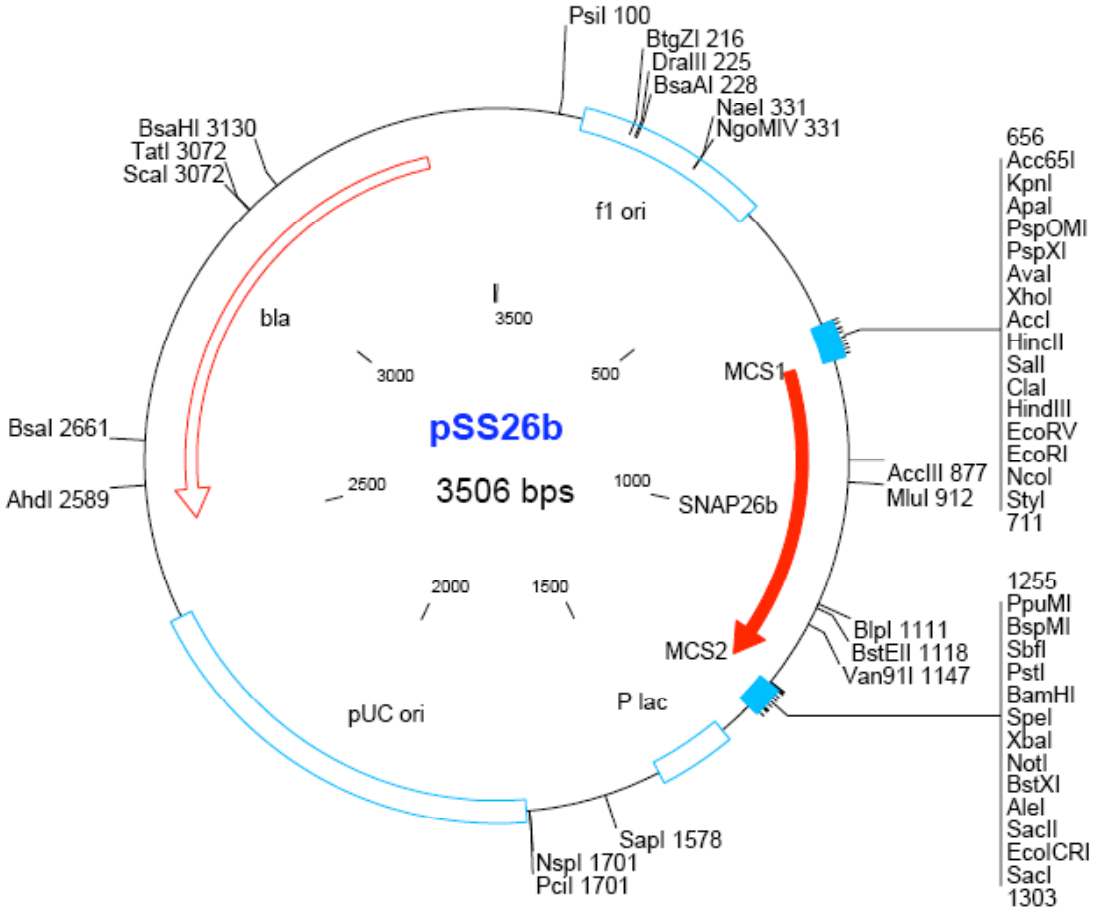
pSS26b
3506 bps
PsiI 100
BtgZI 216
DraIII 225
BsaAI 228
NaeI 331
NgoMIV 331
BsaHI 3130
TatI 3072
ScaI 3072
f1 ori
bla
MCS1
MCS2
SNAP26b
P lac
pUC ori
BsaI 2661
AhdI 2589
AccIII 877
MluI 912
BlpI 1111
BstEII 1118
Van91I 1147
SapI 1578
NspI 1701
PciI 1701
656
Acc65I
KpnI
ApaI
PspOMI
PspXI
AvaI
XhoI
AccI
HincII
SalI
ClaI
HindIII
EcoRV
EcoRI
NcoI
StyI
711
1255
PpuMI
BspMI
SbfI
PstI
BamHI
SpeI
XbaI
NotI
BstXI
AleI
SacII
EcoICRI
SacI
1303

SNAP expressed in insect cells

```
  1   ATGCTACTAG TAAATCAGTC ACACCAAGGC TTCAATAAGG AACACACAAG CAAGATGGTA
 61   AGCGCTATTG TTTTATATGT GCTTTTGGCG GCGGCGGCGC ATTCTGCCTT TGCGTCTAGA
121   ATGGACAAAG ATTGCGAAAT GAAACGTACC ACCCTGGATA GCCCGCTGGG CAAACTGGAA
181   CTGAGCGGCT GCGAACAGGG CCTGCATGAA ATTAAACTGC TGGGTAAAGG CACCAGCGCG
241   GCCGATGCGG TTGAAGTTCC GGCCCCGGCC GCCGTGCTGG GTGGTCCGGA ACCGCTGATG
301   CAGGCGACCG CGTGGCTGAA CGCGTATTTT CATCAGCCGG AAGCGATTGA AGAATTTCCG
361   GTTCCGGCGC TGCATCATCC GGTGTTTCAG CAGGAGAGCT TTACCCGTCA GGTGCTGTGG
421   AAACTGCTGA AAGTGGTTAA ATTTGGCGAA GTGATTAGCT ATCAGCAGCT GGCGGCCCTG
481   GCGGGTAATC CGGCGGCCAC CGCCGCCGTT AAAACCGCGC TGAGCGGTAA CCCGGTGCCG
541   ATTCTGATTC CGTGCCATCG TGTGGTTAGC TCTAGCGGTG CGGTTGGCGG TTATGAAGGT
601   GGTCTGGCGG TGAAAGAGTG GCTGCTGGCC CATGAAGGTC ATCGTCTGGG TAAACCGGGT
661   CTGGGAGACT ACAAGGACGA TGACGATAAG TAATAGCTCG AG
```

Signal sequence

SNAP

FLAG

Stop

Restriction sites

```
  1  SRMDKDCEMK   RTTLDSPLGK   LELSGCEQGL   HEIKLLGKGT   SAADAVEVPA
 51  PAAVLGGPEP   LMQATAWLNA   YFHQPEAIEE   FPVPALHHPV   FQQESFTRQV
101  LWKLLKVVKF   GEVISYQQLA   ALAGNPAATA   AVKTALSGNP   VPILIPCHRV
151  VSSSGAVGGY   EGGLAVKEWL   LAHEGHRLGK   PGLGDYKDDD   DK
```

MAG(d1-3)-SNAP expressed in insect cells

```
   1  ATGCTACTAG TAAATCAGTC ACACCAAGGC TTCAATAAGG AACACACAAG CAAGATGGTA
  61  AGCGCTATTG TTTTATATGT GCTTTTGGCG GCGGCGGCGC ATTCTGCCTT TGCGTCTAGA
 121  GGCCACTGGG GTGCCTGGAT GCCCTCGACC ATCTCAGCCT TCGAGGGCAC GTGTGTCTCC
 181  ATTCCCTGCC GTTTCGACTT CCCCGATGAG CTCAGACCGG CTGTGGTACA TGGCGTCTGG
 241  TATTTCAATA GTCCCTACCC CAAGAACTAC CCACCGGTGG TCTTCAAGTC CCGCACACAA
 301  GTGGTCCATG AGAGTTTCCA GGGCCGCAGC CGCCTATTGG GAGACCTGGG CCTACGAAAC
 361  TGTACCCTGC TTCTCAGCAC ACTGAGCCCC GAGCTGGGAG GCAAATACTA TTTCCGAGGC
 421  GACCTGGGTG GCTACAACCA GTACACCTTC TCGGAGCACA GCGTCCTGGA CATCGTCAAC
 481  ACCCCCAACA TTGTGGTTCC CCCGGAAGTG GTGGCAGGAA CGGAAGTGGA GGTCAGTTGT
 541  ATGGTGCCGG ACAACTGCCC AGAGCTGCGG CCAGAGCTGA GCTGGCTGGG CCACGAGGGG
 601  CTGGGAGAGC CCACTGTGCT GGGTCGGCTG CGTGAGGATG AAGGCACCTG GGTGCAGGTG
 661  TCGCTGCTAC ACTTCGTGCC TACTAGAGAG GCCAACGGCC ACCGTCTGGG CTGTCAGGCT
 721  GCCTTCCCCA ACACCACCTT GCAGTTCGAG GGTTACGCCA GTTTGGACGT CAAGTACCCC
 781  CCAGTGATTG TGGAGATGAA TTCCTCTGTG GAGGCCATTG AGGGCTCCCA TGTCAGCCTG
 841  CTCTGTGGGG CTGACAGCAA CCCGCCGCCG CTGCTGACTT GGATGCGGGA TGGGATGGTG
 901  TTGAGGGAGG CAGTTGCCAA GAGCCTGTAC CTGGATCTGG AGGAGGTGAC CCCAGGAGAG
 961  GACGGCGTCT ATGCTTGCCT AGCAGAGAAC GCCTATGGCC AGGACAACCG CACGGTGGAG
1021  CTGAGTGTCA TGTATGCAAA GCTTGATATC GAATTCCCCA TGGACAAAGA TTGCGAAATG
1081  AAACGTACCA CCCTGGATAG CCCGCTGGGC AAACTGGAAC TGAGCGGCTG CGAACAGGGC
1141  CTGCATGAAA TTAAACTGCT GGGTAAAGGC ACCAGCGCGG CCGATGCGGT TGAAGTTCCG
1201  GCCCCGGCCG CCGTGCTGGG TGGTCCGGAA CCGCTGATGC AGGCGACCGC GTGGCTGAAC
1261  GCGTATTTTC ATCAGCCGGA AGCGATTGAA GAATTTCCGG TTCCGGCGCT GCATCATCCG
1321  GTGTTTCAGC AGGAGAGCTT TACCCGTCAG GTGCTGTGGA AACTGCTGAA AGTGGTTAAA
1381  TTTGGCGAAG TGATTAGCTA TCAGCAGCTG GCGGCCCTGG CGGGTAATCC GGCGGCCACC
1441  GCCGCCGTTA AAACCGCGCT GAGCGGTAAC CCGGTGCCGA TTCTGATTCC GTGCCATCGT
1501  GTGGTTAGCT CTAGCGGTGC GGTTGGCGGT TATGAAGGTG GTCTGGCGGT GAAAGAGTGG
1561  CTGCTGGCCC ATGAAGGTCA TCGTCTGGGT AAACCGGGTC TGGGAGACTA CAAGGACGAT
1621  GACGATAAGT AATAGCTCGA G
```

Signal sequence

MAG

SNAP

Flag

Stop

Restriction sites

Proposed amino acids forming the active site are indicated in yellow (ref) and distribution of lysine within the v-domaine are highlighted in green.

```
1     SRGHWGAWMP  STISAFEGTC  VSIPCRFDFP  DELRPAVVHG  VWYFNSPYPK
51    NYPPVVFKSR  TQVVHESFQG  RSRLLGDLGL  RNCTLLLSTL  SPELGGKYYF
101   RGDLGGYNQY  TFSEHSVLDI  VNTPNIVVPP  EVVAGTEVEV  SCMVPDNCPE
151   LRPELSWLGH  EGLGEPTVLG  RLREDEGTWV  QVSLLHFVPT  REANGHRLGC
201   QAAFPNTTLQ  FEGYASLDVK  YPPVIVEMNS  SVEAIEGSHV  SLLCGADSNP
251   PPLLTWMRDG  MVLREAVAKS  LYLDLEEVTP  GEDGVYACLA  ENAYGQDNRT
301   VELSVMYAKL  DIEFPMDKDC  EMKRTTLDSP  LGKLELSGCE  QGLHEIKLLG
351   KGTSAADAVE  VPAPAAVLGG  PEPLMQATAW  LNAYFHQPEA  IEEFPVPALH
401   HPVFQQESFT  RQVLWKLLKV  VKFGEVISYQ  QLAALAGNPA  ATAAVKTALS
451   GNPVPILIPC  HRVVSSSGAV  GGYEGGLAVK  EWLLAHEGHR  LGKPGLGDYK
501   DDDDK
```

MAG(d1-3)-SNAP expressed in mammalian cells

```
        M  I  F  L  A  T  L  P  L  F  W  I  M  I  S ·
  1  TCTAGAATGA TATTCCTCGC CACCCTGCCG CTGTTTTGGA TAATGATTTC
   · A  S  R  G  G  H  W  G  A  W  M  P  S  T  I  S  A ·
 51  AGCTTCTCGA GGGGGCCACT GGGGTGCCTG GATGCCCTCG ACCATCTCAG
   ·  F  E  G  T  C  V  S  I  P  C  R  F  D  F  P  D
101  CCTTCGAGGG CACGTGTGTC TCCATTCCCT GCCGTTTCGA CTTCCCCGAT
    E  L  R  P  A  V  V  H  G  V  W  Y  F  N  S  P  Y ·
151  GAGCTCAGAC CGGCTGTGGT ACATGGCGTC TGGTATTTCA ATAGTCCCTA
   · P  K  N  Y  P  P  V  V  F  K  S  R  T  Q  V  V  H ·
201  CCCCAAGAAC TACCCACCGG TGGTCTTCAA GTCCCGCACA CAAGTGGTCC
   ·  E  S  F  Q  G  R  S  R  L  L  G  D  L  G  L  R
251  ATGAGAGTTT CCAGGGCCGC AGCCGCCTAT TGGGAGACCT GGGCCTACGA
    N  C  T  L  L  L  S  T  L  S  P  E  L  G  G  K  Y ·
301  AACTGTACCC TGCTTCTCAG CACACTGAGC CCCGAGCTGG GAGGCAAATA
   · Y  F  R  G  D  L  G  G  Y  N  Q  Y  T  F  S  E  H ·
351  CTATTTCCGA GGCGACCTGG GTGGCTACAA CCAGTACACC TTCTCGGAGC
   ·  S  V  L  D  I  V  N  T  P  N  I  V  V  P  P  E
401  ACAGCGTCCT GGACATCGTC AACACCCCCA ACATTGTGGT TCCCCCGGAA
    V  V  A  G  T  E  V  E  V  S  C  M  V  P  D  N  C ·
451  GTGGTGGCAG GAACGGAAGT GGAGGTCAGT TGTATGGTGC CGGACAACTG
   · P  E  L  R  P  E  L  S  W  L  G  H  E  G  L  G  E ·
501  CCCAGAGCTG CGGCCAGAGC TGAGCTGGCT GGGCCACGAG GGGCTGGGAG
   ·  P  T  V  L  G  R  L  R  E  D  E  G  T  W  V  Q
551  AGCCCACTGT GCTGGGTCGG CTGCGTGAGG ATGAAGGCAC CTGGGTGCAG
    V  S  L  L  H  F  V  P  T  R  E  A  N  G  H  R  L ·
601  GTGTCGCTGC TACACTTCGT GCCTACTAGA GAGGCCAACG GCCACCGTCT
   · G  C  Q  A  A  F  P  N  T  T  L  Q  F  E  G  Y  A ·
651  GGGCTGTCAG GCTGCCTTCC CCAACACCAC CTTGCAGTTC GAGGGTTACG
   ·  S  L  D  V  K  Y  P  P  V  I  V  E  M  N  S  S
701  CCAGTTTGGA CGTCAAGTAC CCCCCAGTGA TTGTGGAGAT GAATTCCTCT
    V  E  A  I  E  G  S  H  V  S  L  L  C  G  A  D  S ·
751  GTGGAGGCCA TTGAGGGCTC CCATGTCAGC CTGCTCTGTG GGGCTGACAG
   · N  P  P  P  L  L  T  W  M  R  D  G  M  V  L  R  E ·
801  CAACCCGCCG CCGCTGCTGA CTTGGATGCG GGATGGGATG GTGTTGAGGG
   ·  A  V  A  K  S  L  Y  L  D  L  E  E  V  T  P  G
851  AGGCAGTTGC CAAGAGCCTC TACCTGGATC TGGAGGAGGT GACCCCAGGA
    E  D  G  V  Y  A  C  L  A  E  N  A  Y  G  Q  D  N ·
901  GAGGACGGCG TCTATGCTTG CCTAGCAGAG AACGCCTATG GCCAGGACAA
```

```
    · R  T  V  E  L  S  V  M  Y  A        L  E  V  L  F ·
 951    CCGCACGGTG GAGCTGAGTG TCATGTATGC AGGATCCCTG GAGGTGCTGT
    ·  Q  G  P  M  D  K  D  C  E  M  K  R  T  T  L  D
1001    TCCAGGGCCC CATGGACAAA GATTGCGAAA TGAAACGTAC CACCCTGGAT
     S  P  L  G  K  L  E  L  S  G  C  E  Q  G  L  H  E ·
1051    AGCCCGCTGG GCAAACTGGA ACTGAGCGGC TGCGAACAGG GCCTGCATGA
    · I  K  L  L  G  K  G  T  S  A  A  D  A  V  E  V  P ·
1101    AATTAAACTG CTGGGTAAAG GCACCAGCGC GGCCGATGCG GTTGAAGTTC
    ·  A  P  A  A  V  L  G  G  P  E  P  L  M  Q  A  T
1151    CGGCCCCGGC CGCCGTGCTG GGTGGTCCGG AACCGCTGAT GCAGGCGACC
     A  W  L  N  A  Y  F  H  Q  P  E  A  I  E  E  F  P ·
1201    GCGTGGCTGA ACGCGTATTT TCATCAGCCG GAAGCGATTG AAGAATTTCC
    · V  P  A  L  H  H  P  V  F  Q  Q  E  S  F  T  R  Q ·
1251    GGTTCCGGCG CTGCATCATC CGGTGTTTCA GCAGGAGAGC TTTACCCGTC
    ·  V  L  W  K  L  L  K  V  V  K  F  G  E  V  I  S
1301    AGGTGCTGTG GAAACTGCTG AAAGTGGTTA AATTTGGCGA AGTGATTAGC
     Y  Q  Q  L  A  A  L  A  G  N  P  A  A  T  A  A  V ·
1351    TATCAGCAGC TGGCGGCCCT GGCGGGTAAT CCGGCGGCCA CCGCCGCCGT
    · K  T  A  L  S  G  N  P  V  P  I  L  I  P  C  H  R ·
1401    TAAAACCGCG CTGAGCGGTA ACCCGGTGCC GATTCTGATT CCGTGCCATC
    ·  V  V  S  S  S  G  A  V  G  G  Y  E  G  G  L  A
1451    GTGTGGTTAG CTCTAGCGGT GCGGTTGGCG GTTATGAAGG TGGTCTGGCG
     V  K  E  W  L  L  A  H  E  G  H  R  L  G  K  P  G ·
1501    GTGAAAGAGT GGCTGCTGGC CCATGAAGGT CATCGTCTGG GTAAACCGGG
    · L  G                    W  S  H  P  Q  F  E  K
1551    TCTGGGAGAA TTCGATATCG GTACCTGGAG CCACCCGCAG TTCGAAAAAT

1601    AACCCGGG
```

Name, Address:	Daniel Strasser Rosengartenweg 9 CH - 4058 Basel Phone: +41 (0)61 692 48 76 Mobile: +41 (0)79 778 79 93 daniel.strasser@unibas.ch
Date of birth:	February 19, 1978
Native place:	Gottlieben, Switzerland
Nationality:	Double citizen Swiss/ Swede
Martial status:	Single

EDUCATION

02/2004-06/2007	Dissertation, Institute for Molecular Pharmacy, Basel *Real-time drug discovery: Characterization of the myelin-associated glycoprotein/ligand interaction*
11/2005-02/2006	Entrepreneurship course «venture challenge», University of Basel
11/2003	eidg. dipl. Apotheker equivalent to M Sc Pharm (Grade 5.75/6)
03/2003-07/2003	Diploma thesis at F. Hoffmann–La Roche Ltd., Basel *Near-infrared spectroscopy: Determination of granule properties and their influence on liberation of active ingredient* (Grade 6/6)
10/1998-11/2003	Pharmaceutical Sciences, University of Basel
08/1993-02/1998	Grammar school, Matura Typus C, Kreuzlingen

PROFESSIONAL EXPERIENCE

12/2006-06/2007	Biacore Consultant, Actelion Pharmaceuticals Ltd., Basel
09/2001-01/2003	Lectures on Pharmacology, School of nursing, Aarberg
01/2002-12/2002	Substitute of pharmacy administrator, Pharmacy Aemisegger AG, Weinfelden
08/2000-08/2001	8 months practical: Pharmacy St. Clara, Basel 4 months practical: Institute for Clinical Pharmacy, Münsterlingen

LANGUAGES

German	native language
Swedish	fluent
English	fluent
French	fluent

9/2001 Intensive 30 course at LSI Bosten ME, USA (Level Advanced)

REFERENCES

Prof. Dr. Beat Ernst	Institute for Molecular Pharmacy, University of Basel
Dr. Walter Huber	Pharmaceutical Research, F. Hoffmann-La Roche Ltd., Basel
Dr. Lars Sukowski	Manufacturing Systems, F. Hoffmann-La Roche Ltd., Basel